THE INFLUENCE OF STRAIN RATE AND THE EFFECT OF FRICTION ON THE FORGING LOAD IN SIMPLE UPSETTING AND CLOSED DIE FORGING

Francis Bland Klemz
MPhil, CEng, MIMechE

A thesis submitted to the COUNCIL FOR NATIONAL ACADEMIC AWARDS in partial fulfilment for the degree of DOCTOR OF PHILOSOPHY

Department of Mechanical and Production Engineering
Sheffield City Polytechnic (Sponsoring Establishment)

The Drop Forging Research Association
Sheffield S3 7BA (Collaborating Establishment)

December 1984

ACKNOWLEDGEMENTS

The author wishes to express his gratitude to Dr M S J Hashmi, Director of Studies, for suggesting this research project, for his encouragement and helpful supervision.

Sincere thanks also to Dr A Thomas, Senior Scientific Officer, Drop Forging Research Association, Sheffield, for his very useful guidance, comments and continued interest in this project.

The encouragement given by Mr O Bardsley, former Head of Department, is much appreciated.

The assistance given by Mr R Teasdale, Mr D McKay, Mr R Wilkinson and colleagues, in the manufacture, construction and instrumentation of the experimental drop hammer and equipment was a valued contribution.

DECLARATION

The author declares that no part of this work has been submitted in support of another degree or qualification to this or any other establishment. The author further declares that he has not been a registered candidate or enrolled student for another award of the CNAA or other academic or professional institution during the course of the research programme.

F. B. Klemz.

F B Klemz

ABSTRACT

THE INFLUENCE OF STRAIN RATE AND THE EFFECT OF FRICTION ON THE FORGING LOAD IN SIMPLE UPSETTING AND CLOSED DIE FORGING.

F B Klemz

Forging provides an elegant solution to the problem of producing complicated shapes from heated metal. This study attempts to relate some of the important parameters involved when considering, simple upsetting, closed die forging and extrusion forging.

A literature survey showed some of the empirical graphical and statistical methods of load prediction together with analytical methods of estimating load and energy. Investigations of the effects of high strain rate and temperature on the stress-strain properties of materials are also evident.

In the present study special equipment including an experimental drop hammer and various die-sets have been designed and manufactured. Instrumentation to measure load/time and displacement/time behaviour, of the deformed metal, has been incorporated and calibrated. A high speed camera was used to record the behaviour mode of test pieces used in the simple upsetting tests.

Dynamic and quasi-static material properties for the test materials, lead and aluminium alloy, were measured using the drop hammer and a compression-test machine.

Analytically two separate mathematical solutions have been developed: A numerical technique using a lumped-mass model for the analysis of simple upsetting and closed-die forging and, for extrusion forging, an analysis which equates the shear and compression energy requirements to the work done by the forging load.

Cylindrical test pieces were used for all the experiments and both dry and lubricated test conditions were investigated. The static and dynamic tests provide data on Load, Energy and the Profile of the deformed billet. In addition for the Extrusion Forging, both single ended and double ended tests were conducted. Material dependency was also examined by a further series of tests on aluminium and copper.

Comparison of the experimental and theoretical results was made which shows clearly the effects of friction and high strain rate on load and energy requirements and the deformation mode of the billet. For the axisymmetric shapes considered, it was found that the load, energy requirement and profile could be predicted with reasonable accuracy.

CONTENTS

LIST OF FIGURES

CHAPTER 1

INTRODUCTION

1.1 Background

In recent years there has been an urgent need to increase the rate at which forgings can be produced in order to reduce manufacturing costs. This has led to a study of the dynamic behaviour of metals in order to exploit to the full the potential of high rate forming methods.

Manufacturers with existing forging equipment need reliable information regarding the load and energy needed to make particular forgings. It should be noted that the numerical technique, such as the finite element method and other techniques based on the upper bound method have successfully been employed to solve very complex forming processes. However these techniques require large computer facilities and are not easily accessible to everyday Engineers. Hence there would always be room for analytical solutions, for specific problems, based on simpler and easily understandable principles.

1.2 Literature Survey

1.2.1 Empirical Graphical and Statistical Methods of Load Prediction

A number of empirical methods have been formulated [1-5] to determine the forging load under dynamic conditions. However, these are applicable to a limited number of cases only.

Graphs relating the area of forging including flash to the forging load for different degrees of die complexity have been used. Examples are given in a

Drop Forging Research Association report[11].

BALOGUN[6] measured forging loads on presses to produce axisymmetric and plane strain forgings. Using multiple linear regression analysis, equations for estimating forging load were then developed.

NEUBERGER and PANNASCH[7] plotted values of mean effective yield strength vs mean height and deriving equations for the upper and lower curves which encompassed their experimental data, obtained expressions for the mean effective yield stress in terms of forging weight and forging area. They have also extended their analysis to produce nomograms for predicting load and energy requirements. Other investigators [8-10] have also compiled similar design nomograms.

In the Drop Forging Research Association report[11] on Load and Energy estimation in Forging, results calculated using Neuberger and Pannasch's[9] method were used to obtain equations for relative yield strength and forging load. The load equations were based on a multiple linear regression analysis of experimental results on completely axisymmetric forgings with external flash. The load equation is in terms of the area of forging including flash, the ratio of the flash land width to flash land thickness and the mean height of the forging including flash.

1.2.2 Analytical Methods for Estimating Load and Energy

SIEBEL[12] produced an analysis for the load estimation for the free upsetting of a cylinder or prism.

SCHROEDER and WEBSTER[13] have given a more detailed analysis of free upsetting in which they recognise a limiting value for frictional resistance. Once this resistance exceeds the material yield strength they argue that deformation proceeds by internal shearing of the deformed metal.

FOSTER[14] modified SIEBEL'S[12] analysis to extend to complex forging shapes. His method is to divide the forging into sections, and having found the stress required to induce metal flow in each section, determines the value of the load in each section by integration of the stress throughout the section.

DEAN[15], in a paper discussing the effect of flash land geometry on die stresses, evolved a method of calculating forging load based on an interpretation of the Schroeder-Webster[13] analysis.

Dean assumed that, in the final stage of forging, deformation is confined to a disc whose thickness is that of the flash gap. Within the body of the forging sticking friction is assumed, whilst the conditions in the flash land are decided by calculating the radius of the sticking region. The parameters involved in Dean's equations are: radius

to the entrance to the flash, radius to which sticking extends, radius to edge of flash land, coefficient of friction, normal stress on forging section, load, flash land width and mean yield strength.

DIETRICH and ANSELL[16] have considered the forging of plane symmetrical sections. As with the Siebel-Foster[14] method the forging is divided into sections and calculations begin with the flash and proceed towards the centre. Frictional resistance is accounted for by means of a 'back-pressure' term and the extrusion effect when metal flows into a reduced section is also allowed for.

BISWAS and ROOKS[17] have adapted an original analysis by ALTAN[18] to predict forming load and energy. In analysing the forging load for axisymmetric shapes they assumed that, free upsetting, extrusion into cavities and the formation of flash occur as three discrete forming stages.

McDERMOTT[19] has extended the upper bound elemental technique first suggested by KUDO[25] to calculate forging energy. In applying the method a forging is split into a number of regions and for each region an equation is set up relating the rate of energy dissipation to the strain rate of the forging in various principal directions. By developing admissible velocity fields for metal flow, the mean

yield strength in a section can be determined, allowing load and energy to be calculated.

1.2.3 Stress-Strain Properties at High Strain Rates

A number of workers have attempted to derive a single equation expressing the stress in terms of strain, strain rate and temperature. LUBAHN[20] obtained such an equation containing six constants from three empirical relationships. He assumed that for large strains the true stress/strain curve could be represented by a simple power law. This assumption was supported by tensile test data obtained on a number of materials by FUSFELD[21] and by LOW and GAROFALO[22] but was in poor agreement with the results of DORN et al.[23]

ALDER and PHILLIPS[24] used a cam plastometer to produce constant true strain rates in the range 1-40 sec^{-1} during compression to 50% reduction of height on (a) commercial-purity aluminium from -190°C to 550°C, (b) phosphorus-dioxidized copper from 18°C to 900°C and (c) a 0.17% carbon steel from 930°C to 1200°C. They found that of the three materials tested only aluminium, at room temperature, had a stress strain relationship that could be represented by a power law. This power law had an index of approximately 0.2. The effect of strain rate on the stress for a given strain was better expressed by a power law than by the semi-logarithmic formula of

LUDWIK[26].

SOKOLOV[27-31] also concluded from tests on lead, tin, zinc, aluminium, copper, nickel, brass and several steels, over a range of strain rates from 10^{-3} to 10^{2} sec^{-1} and at temperatures from 20°C to their respective melting points, that the power law provided a better interpretation of the effect of strain rate. However, a number of American workers[32-36] found from compression tests at 10^{2}-10^{3} sec^{-1} on copper at room temperature that the stress was proportional to the logarithm of the strain rate for a given strain (up to 25% compression).

Other workers who have been concerned with the effect of strain rate on the tensile properties are: GINNS[37], ELAM[38], JONES and MOORE[39], and MANJOINE and NADAI[40]. Nadai, working on aluminium, copper, and steel at strain rates of 10^{2}-10^{3} sec^{-1} and at elevated temperatures, found that the ultimate true stress varied approximately linearly with the logarithm of the strain rate, in agreement with the results of JONES and MOORE[39] on the yield strength of fourteen metals tested at room temperature and at strain rates up to 10^{-1} sec^{-1}.

SLATER, JOHNSON and AKU[40] derived approximate equations to account for the compressive engineering strain-time, dimensionless compressive engineering strain-rate, compressive engineering strain and

dynamic force-time characteristics for the fast compression of prismatic blocks of strain-hardening, strain-rate-sensitive material using a drop hammer. Within the limits of maximum strain rate of 250 sec^{-1}, maximum engineering compressive strain of 0.4 and a constant ambient temperature of approximately 20°C experimental and theoretical results were compared. Agreement between experimental and theoretical results was found, with the exception of the force-time relationship, where the theoretical prediction underestimates the maximum force by between 10 and 15 per cent. They concluded that lead at ambient temperature was not particularly strain-rate sensitive for strain rates of up to 250 sec^{-1}.

1.2.4 Use of a 'Model-Material' Technique

DANCKERT and WANHEIM[58] have used a model-material technique in the analysis of a rotational symmetrical forging. These results were then compared with an actual forging made from aluminium. This technique makes it possible to investigate the effect of different preforms and billet sizes on:

(a) the filling capacity of the final dies

(b) the flow pattern in the final product

(c) the extent of die wear quantitatively.

They demonstrated the use of 'the plane analogy' as

a means of using the material model to get an overall idea of material flow in the dies. More accurate information about the flow pattern was obtained by way of a "three-dimensional model-material experiment" in which the model is geometrically similar to the original process. To determine the stress distribution in the dies a special rubber model technique was used. In this technique the die to be investigated is made of transparent rubber which has a grid placed in its plane of symmetry. The transparent rubber die is placed in a liquid with the same refraction index as the rubber and the forging is carried out with the billet made of wax, simulating the metal billet. The distortion of the grid that occurs during forging is recorded photographically. By measuring the displacement of the grid points during the deformation of the wax billet it is possible to calculate stress values and to locate stress concentrations in the die.

1.2.5 Extrusion Forging

JAIN, BRAMLEY, LEE and SHIRO KOBAYASHI[61] looked at the effect of friction and die hole geometry on the total height of axisymmetric extrusion forgings, for a range of billet and hole sizes. These results were then compared with theoretical

predictions, which were based on an assumed velocity field. They concluded that to achieve a maximum amount of rise (extrusion) and minimum load and energy, a billet with a high aspect ratio should be used in conjunction with a radiused and drafted die hole. Their analysis did not take account of the taper in the flange profile.

NEWNHAM and ROWE[62] applied a slip-line field theory analysis to the problem of compound metal flow in a simple extrusion/forging process. They tested their predictions experimentally and confirmed the transition from simple forging to rigid-core forging and hence to extrusion with forging. Their analysis also did not take account of the taper in the flange profile.

1.3 Present Work

1.3.1 Simple Upsetting and Closed Die Forging

A theoretical and experimental study of the load requirements associated with the upsetting and closed die forging of cylindrical billets, which takes into account the effects of interface friction, axial

inertia, strain rate and strain hardening properties of the material, was made.

A theoretical analysis has been developed based on a numerical technique which enables the billet profile, the tup load and velocity to be determined at any stage during the in-process time. The stress and strain-time history at any point within the billet can also be determined. This method uses a lumped mass model for the actual cylindrical billet. Each mass was considered in turn and the associated dynamic force equilibrium equation was expressed in finite difference form. This related the displacement of each mass to the strain in the corresponding link after each time increment. The stress in each link, and hence the axial force, was then calculated from the material stress strain characteristics.

Various dies, to enable axisymmetrical shapes to be formed from lead cylinders, were made. These dies allow for radial expansion only and no provision was made for flash. Split dies were used for the more complicated shapes.

For the simple upsetting tests high speed photographs were taken of the billet as it was deformed. A Hi-cam high speed camera working at 2400 frames per second was used. The processed film was then projected on to a screen using a 16 mm cine-

projector with single frame movement facilities and analysed for instantaneous profiles and tup-displacement-time curves.

For the upsetting tests only, tests were also carried out on aluminium alloy billets heated to forging temperature.

1.3.2 Extrusion/Forging

As the flow of metal in this process is only partially radial the lumped-mass method outlined in Chapter 3 was found to be inapplicable and a different theoretical approach was developed. This approach considers the plastic work done in compression together with the work done in radial and circum-ferential shear. By equating the forces involved and assuming that the material deforms in a mode asso-ciated with the least work done, the shape of the profile during deformation can be predicted.

Dies with three different extrusion ratios were manufactured for experimental work in order to check the extrusion/forging theory. The majority of tests were carried out using lead billets. A few tests on aluminium and copper billets were also carried out to check for material dependency. Double-ended extrusion tests were also carried out using lead and copper billets.

A drop hammer was designed specifically for the

experimental work associated with this study. Its energy capacity enables lead billets to be deformed easily. The fact that lead is hot-worked at temperature means that it can be used to simulate the behaviour of other stronger materials that need to be heated to a suitable hot working temperature. The drop hammer incorporates instrumentation which enables load/time and displacement time behaviour to be measured and recorded.

CHAPTER 2

EXPERIMENTAL EQUIPMENT, INSTRUMENTATION AND BILLET MATERIAL PROPERTIES

2.1 Equipment

2.1.1 Drop Hammer

The drop hammer frame was made from 80 x 80 x 10 mm angle iron and is of welded construction. See Fig. 1.

The framework provides the upper support for the tup guide rails, and support for a motorised hoist which is used to raise the tup to the required height. A cord release mechanism allows the tup to be separated from its lifting cradle. The tup (see Fig. 2 and 3) has a mass of 15.64 kg with a maximum free fall height of 4.32 m. This is equivalent to a maximum impact velocity of 9.2 m/sec.

At the base of the drop hammer an inner framework made from 50 x 50 x 6 mm angle iron is used to contain the load cell unit and to provide support for the tup guide rails. The load cell housing is encased in concrete to provide an additional mass of material to absorb the shock load which occurs at impact.

In the interest of safety the lower 1 m of the drop hammer framework is encased in 3 mm thick duralumin plate. The remainder of the framework is encased in 25 x 25 mm wire mesh. Access for the removal of test pieces is by means of a hinged door which is pivoted in such a way that when in the open position

it will arrest the tup should it fall accidentally.

2.1.2 Displacement Measurement

The displacement/time behaviour of the material under test is measured using infra red light beams which are activated by means of a grid attached to the drop hammer tup (see Fig. 4). A complete layout of the instrumentation is shown in a photo-graph (Fig. 5).

2.2 Instrumentation

2.2.1 Load Cell

A schematic block diagram of the load cell instru-mentation is shown in Fig. 6. The signal from the load cell is fed into a Mini-balance and a Mini-amplifier unit, the strain gauges being activated by a 5 volt d.c. supply. The signal from the strain gauge is balanced so that its output will be zero at zero load.

Because the output voltage from the load cell was in milli-volts a Mini-amplifier was used to increase the signal strength by a gain of 200. This amplified signal was then fed to a Digital storage Oscilloscope OS4040. Later this stored signal was used to produce a load time trace on an X,Y plotter. The digital storage oscilloscope was also used to record and display simultaneously the signals from

the infra-red switch unit.

2.2.2 Calibration of Load Cell

Before the load cell was assembled, in the base of the drop hammer, it was calibrated using a 500 kN Denison Tensile testing machine. The calibration curve is shown in Fig. 7.

A further calibration was necessary when all the instrumentation was in place and a series of tests with the drop hammer were to be made. The calibration took the following form:

(a) The load-cell was disconnected

(b) A known voltage of 0.5 mV was applied to the load cell input terminals

(c) The resulting display on the oscilloscope was copied using the XY plotter (see Fig. 8).

The 'step' on the XY plotter print out is equivalent to 65.57 kN (Fig. 8). The size of the step can be changed by altering the 'Y' axis settings on either the oscilloscope or XY plotter. (A large 'step' size was used when low impact forces were measured.)

The 0.5 mV output from the load cell was amplified 200 times. With the digital storage oscilloscope set to display a step of 1 cm per 20 mV a 'step' of 50 mm would have been obtained if there were no errors in the instrumentation.

2.2.3 Infra-Red Switch Unit

The velocity of the falling tup just before impact was obtained by an electronic counter which was activated and stopped by an infra-red switch unit. See Fig. 4. The signals were generated from the switch unit by interrupting the passage of light passing between two light emitting and light sensitive heads, the interrupting device being a strip of clear plastic sheet on which there had been drawn a series of equally spaced black, parallel, horizontal lines of equal thickness.

This switch was also used to trigger the displacement/time display on the Digital storage oscilloscope OS4040, together with the load time display. A ten per cent pre-trigger was used.

Copies of the load/time, displacement/time traces were obtained from an XY plotter which had been connected directly to the digital storage oscilloscope.

2.3 Load and Displacement Recordings

2.3.1 Load Recordings

A typical load/time trace is shown in Fig. 9. It is possible to read off values of load and time direct from this trace (see page 31)

2.3.2 Displacement Recordings

For each test using the drop hammer three traces are required, see Fig. 10.

Fig. 10(a) is obtained by lowering the tup gently on to the test piece and the resulting trace provides a datum which indicates the point of impact.

Fig. 10(b) shows how the tup decelerates as the metal is deformed.

Fig. 10(c) is obtained by lowering the tup gently on to the deformed test piece. Its function is to identify the total extent of deformation and will show clearly if there has been any rebound incorporated in Fig. 10(b).

Fig. 10(b) is used to provide displacement/time data from which the deceleration of the tup can be calculated. Since the mass of the tup is known the associated force (which is the forging force) can be calculated simply as the product of the deceleration and the mass of the tup.

2.4 Determination of Material Properties

2.4.1 Quasi-Static Tests

The true stress/log strain relationships for the lead used to produce all the test pieces for this study were obtained using a Denison testing machine for

the static tests, and an Experimental Drop Hammer for the dynamic tests. The test pieces were cylinders 24 mm ± 0.13 mm diameter and 24 mm ± 0.13 mm high. In each case a paste of graphite in petroleum jelly was used to lubricate the surfaces in contact to reduce barrelling of the specimen.

In the quasi static test the Denison testing machine was set to compress the test piece at its slowest rate, a constant speed of 3.5 mm/min. The test was interrupted at each true strain interval of 0.1 in order that the surfaces in contact could be relubricated. Results from three identical tests were averaged.

2.4.2 Dynamic Tests

For the complete deformation to occur at a constant strain rate, using a drop hammer, it would be necessary for the ratio, tup velocity/height of test piece, to be constant. In practice the strain rate will usually decrease as the deformation progresses. To allow for this only the initial 10% of data associated with a particular load/time, displacement/time output was used to calculate strain rate. By altering the height through which the tup had to fall the impact velocity was accurately controlled. By precompressing the test piece to the required thickness a strain rate could be applied to the test piece where its initial strain condition was known.

In this way successive steps were used to obtain stress/strain data at constant strain rate.

A computer program was used to help analyse load/time and displacement/time data.

The relationship between stress and strain for different strain rates is shown in Fig. 11. These curves, based on experimental results were found to fit closely the strain rate sensitivity equation

$$\sigma = \sigma_1[1 + (\frac{\dot{e} + \dot{e}_1}{D})^{\frac{1}{p}}]$$

where σ is the dynamic flow stress corresponding to strain rates $\dot{e}$ of up to 500 per second and σ_1 is the flow stress corresponding to strain rate $\dot{e}_1$ equal to 1 per second. The constants of strain rate sensitivity D and p were found to be $1000s^{-1}$ and 0.65 respectively.

2.4.3 Quasi-static tests on lead and idealised diagram

From the quasi-statically obtained stress-strain characteristics shown in Fig. 11 it was found reasonable to assume that for direct comparison with quasi-static tests, the lead billets behaved as a bilinearly elastic-perfectly plastic material with a constant flow stress of 17 N/mm^2, after a strain of about 14%. This is shown in Fig. 12 and was incorporated in the numerical technique. For the

extrusion forging analysis outlined in Chapter 6 lead billets were assumed to be rigid-perfectly plastic with a yield stress of 17 N/mm^2.

2.4.4 Quasi-Static Tests on Aluminium Alloy and Idealised Diagram

The diagram shown in Fig. 13 was also obtained from quasi-static tests. In its idealised form it is suitable for analysis involving the finite difference numerical techniques used in this study.

ARRANGEMENT OF DROP HAMMER

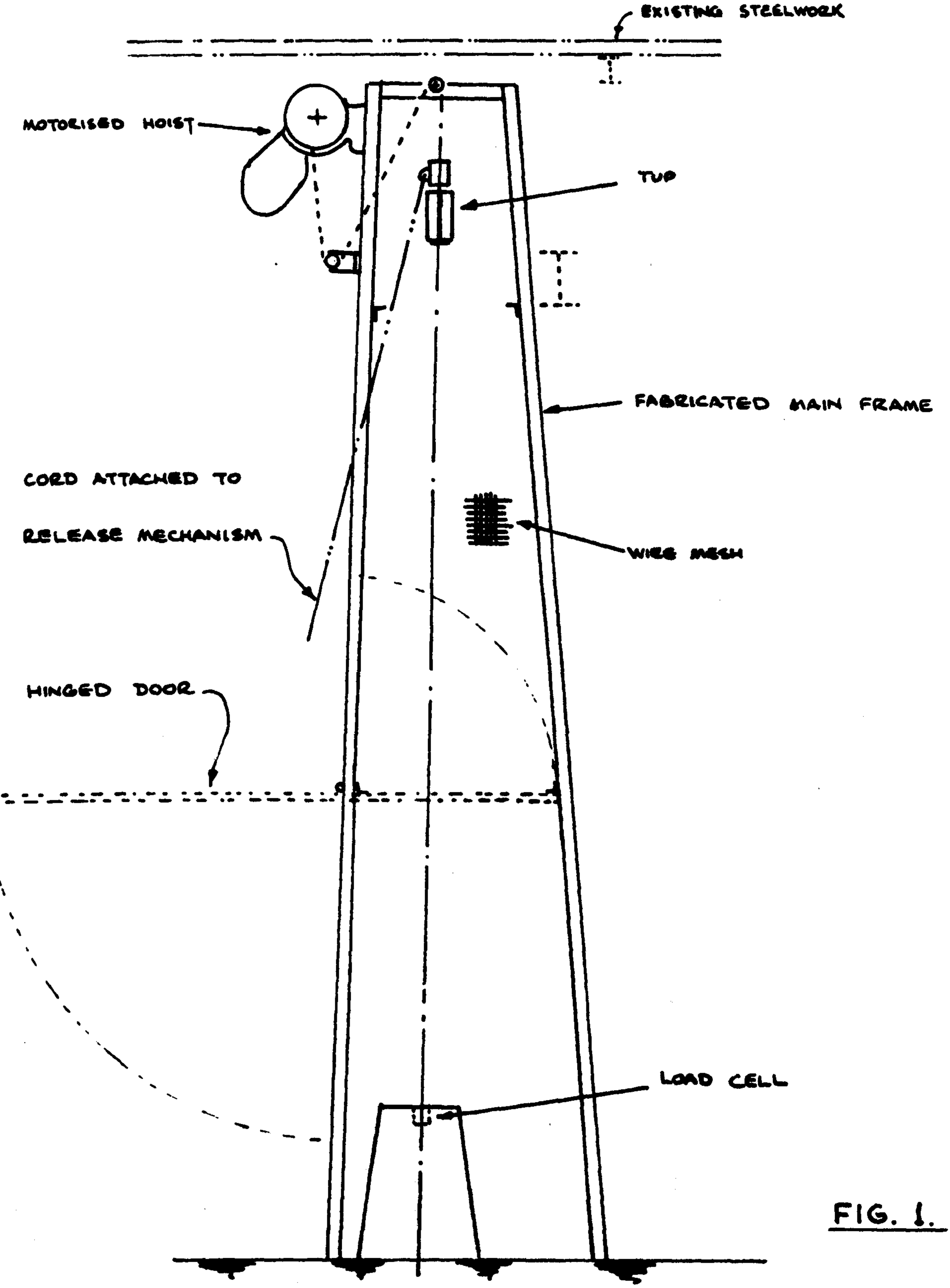

FIG. 1.

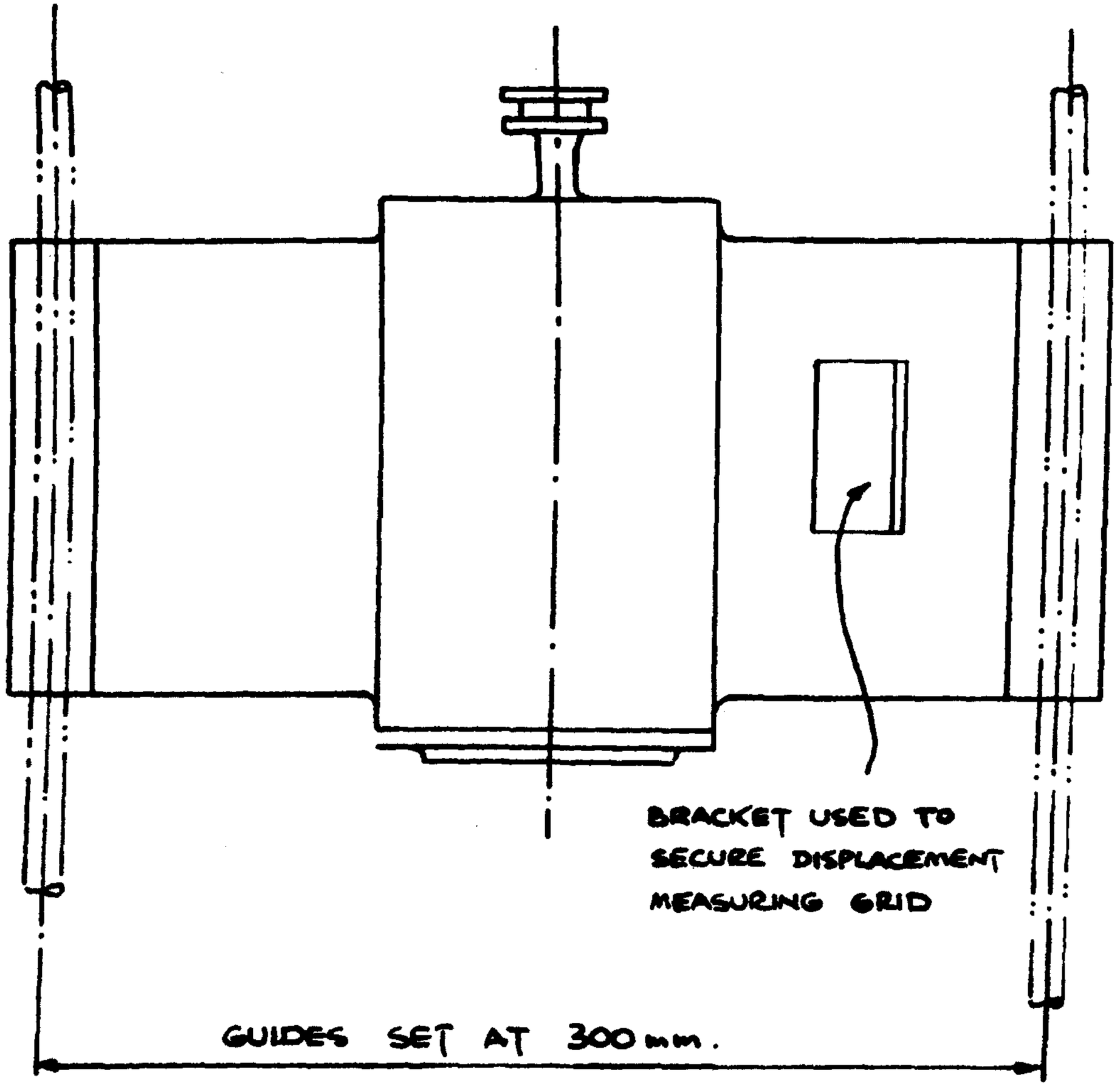

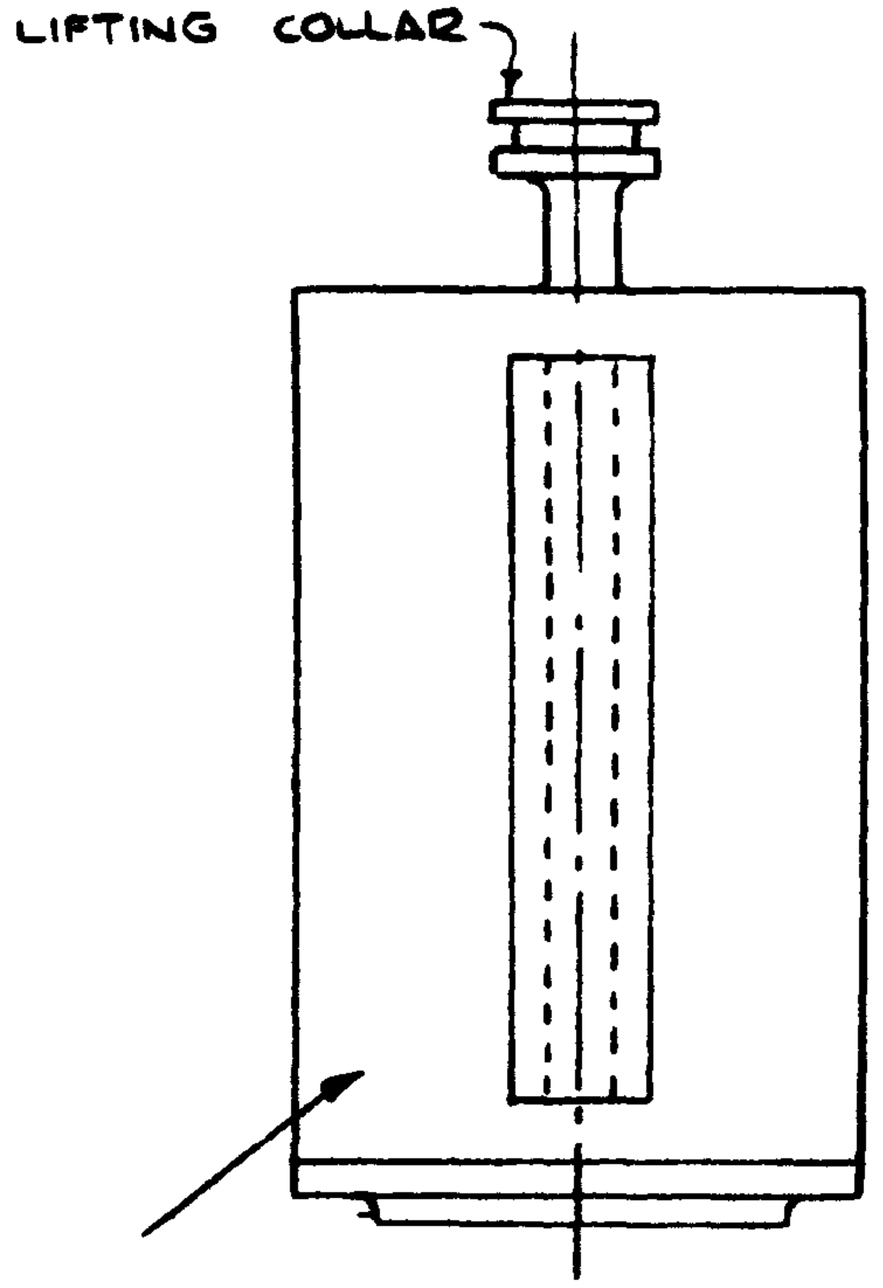

DROP HAMMER TUP

FIG. 2

moving grid
(attached to tup)

infra red
switching device

Moving grid/infra-red switch device

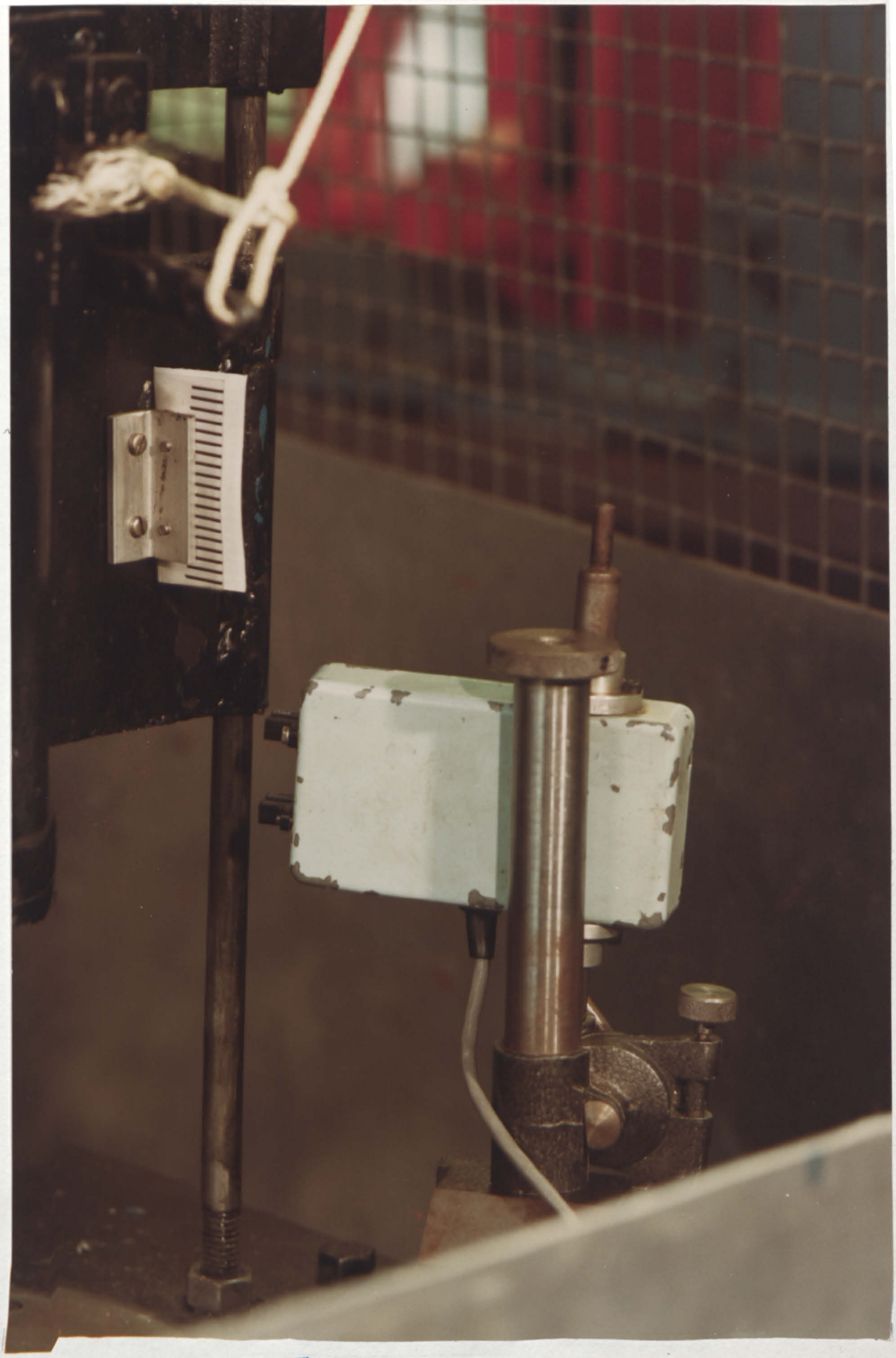

FIG. 3

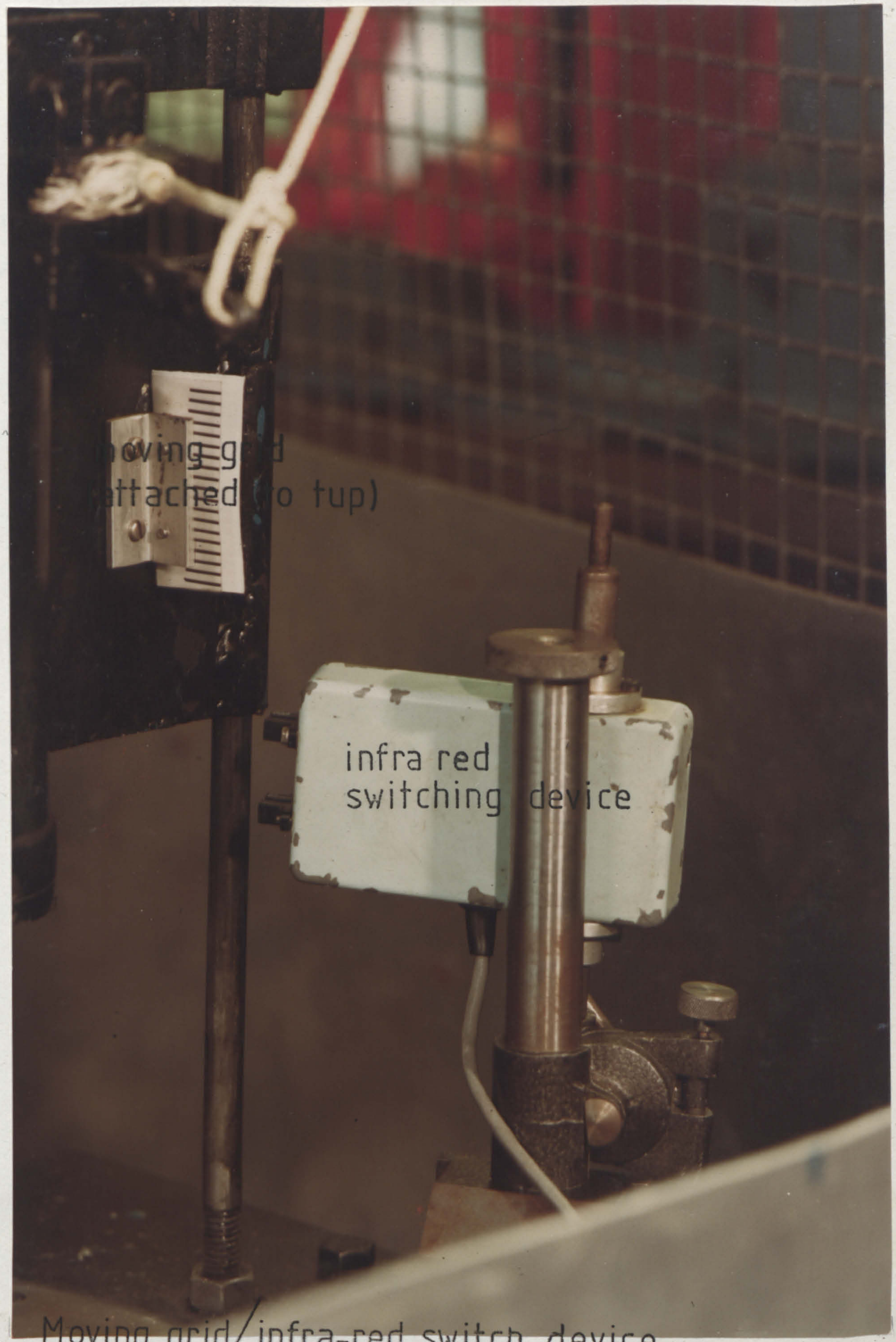

Moving grid/ infra-red switch device
FIG. 3

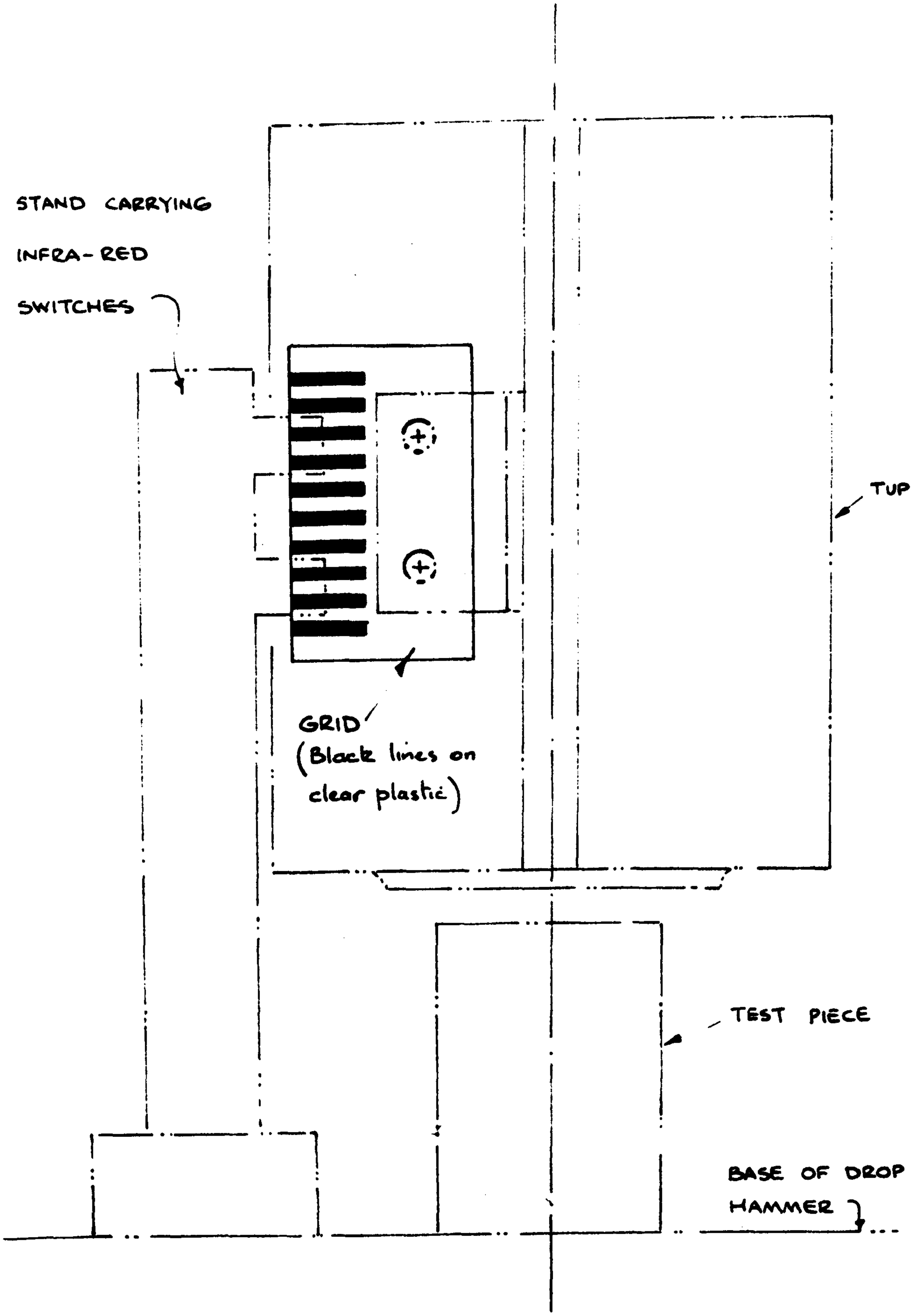

MEASUREMENT OF DEFORMATION

FIG. 4

Layout of Instrumentation

timer

stabilised
power supply

digital storage
oscilloscope

x,y plotter

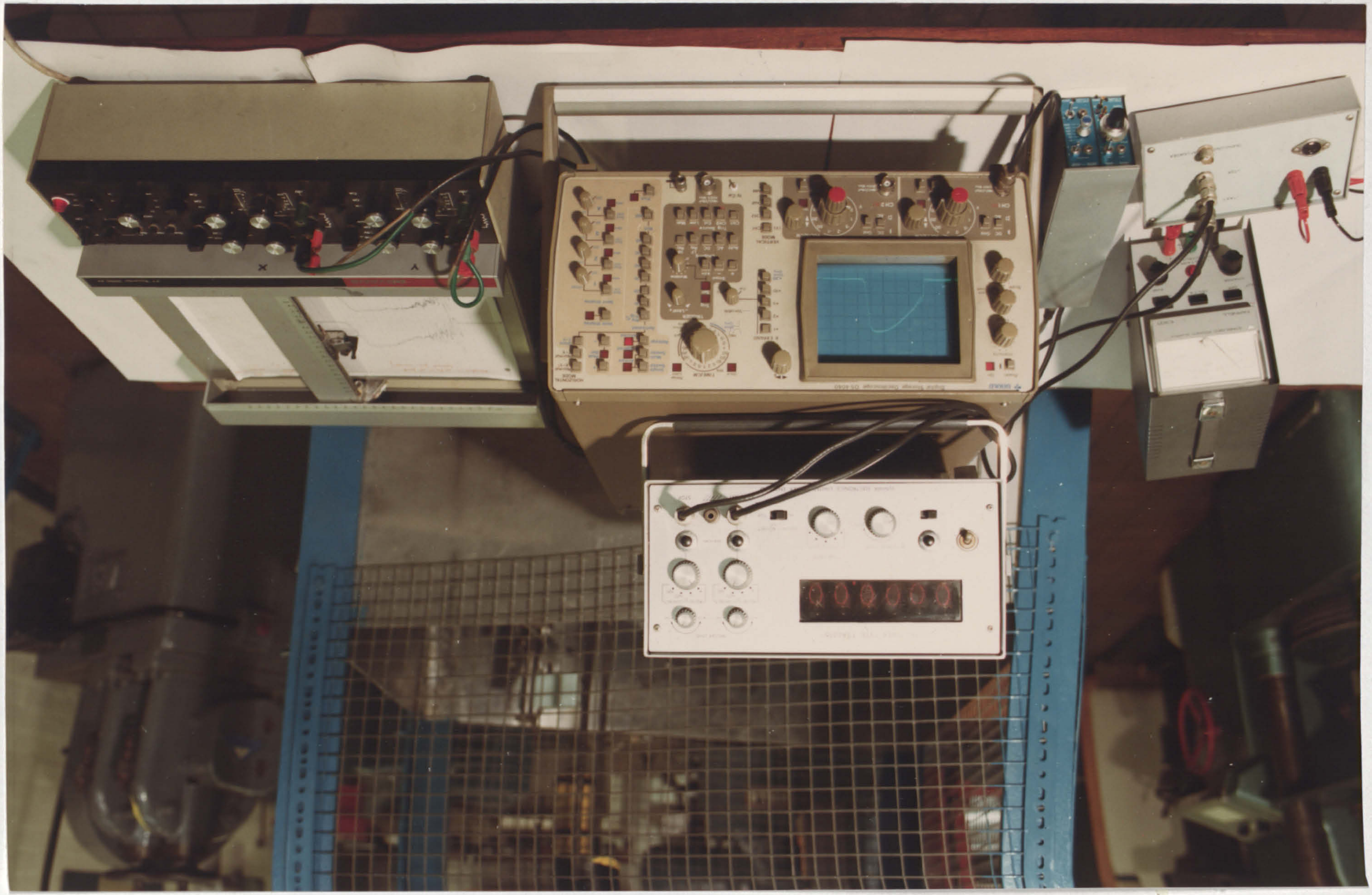

FIG. 5

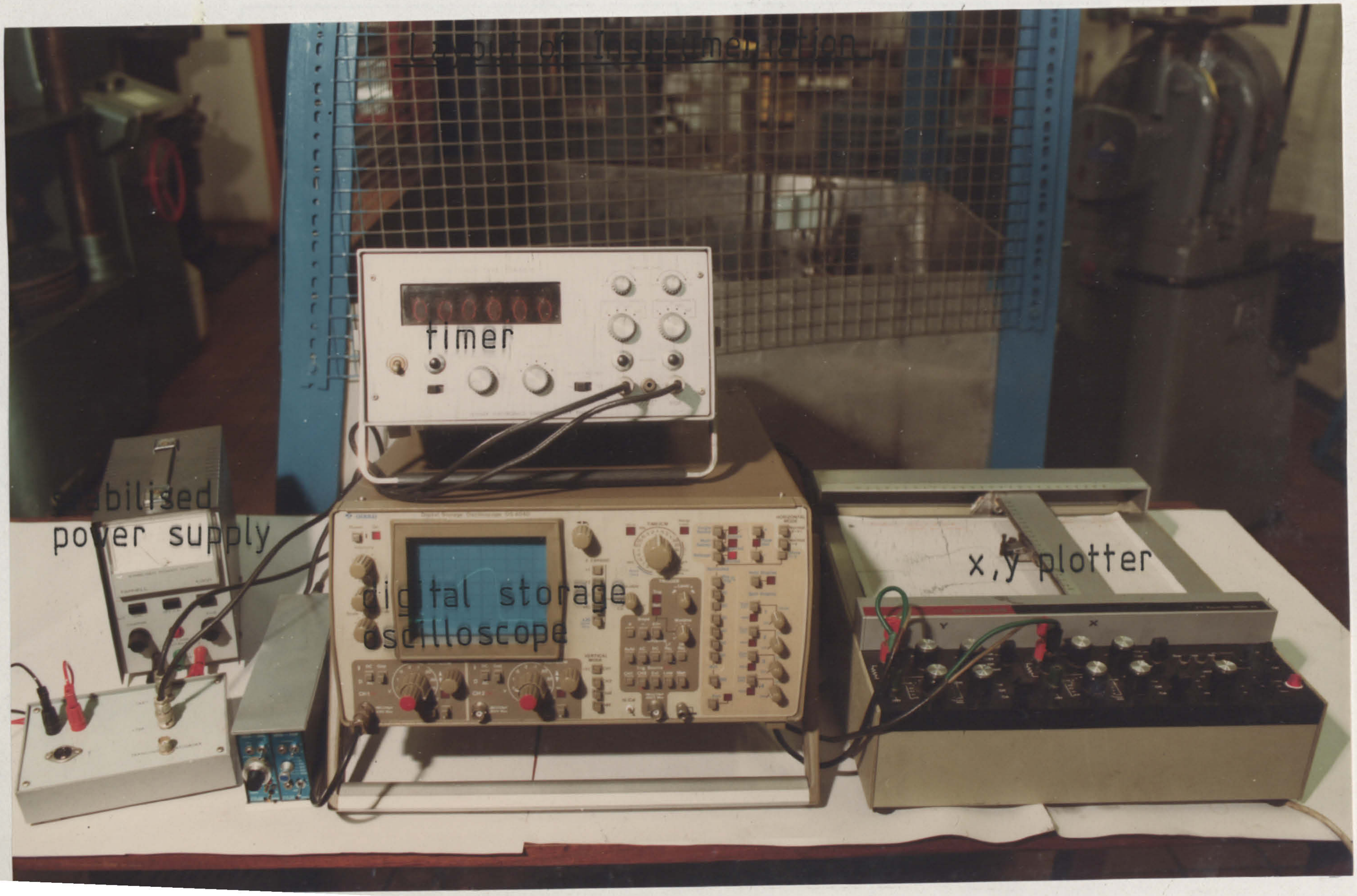
timer
stabilised
power supply
digital storage
oscilloscope
x,y plotter

FIG. 5

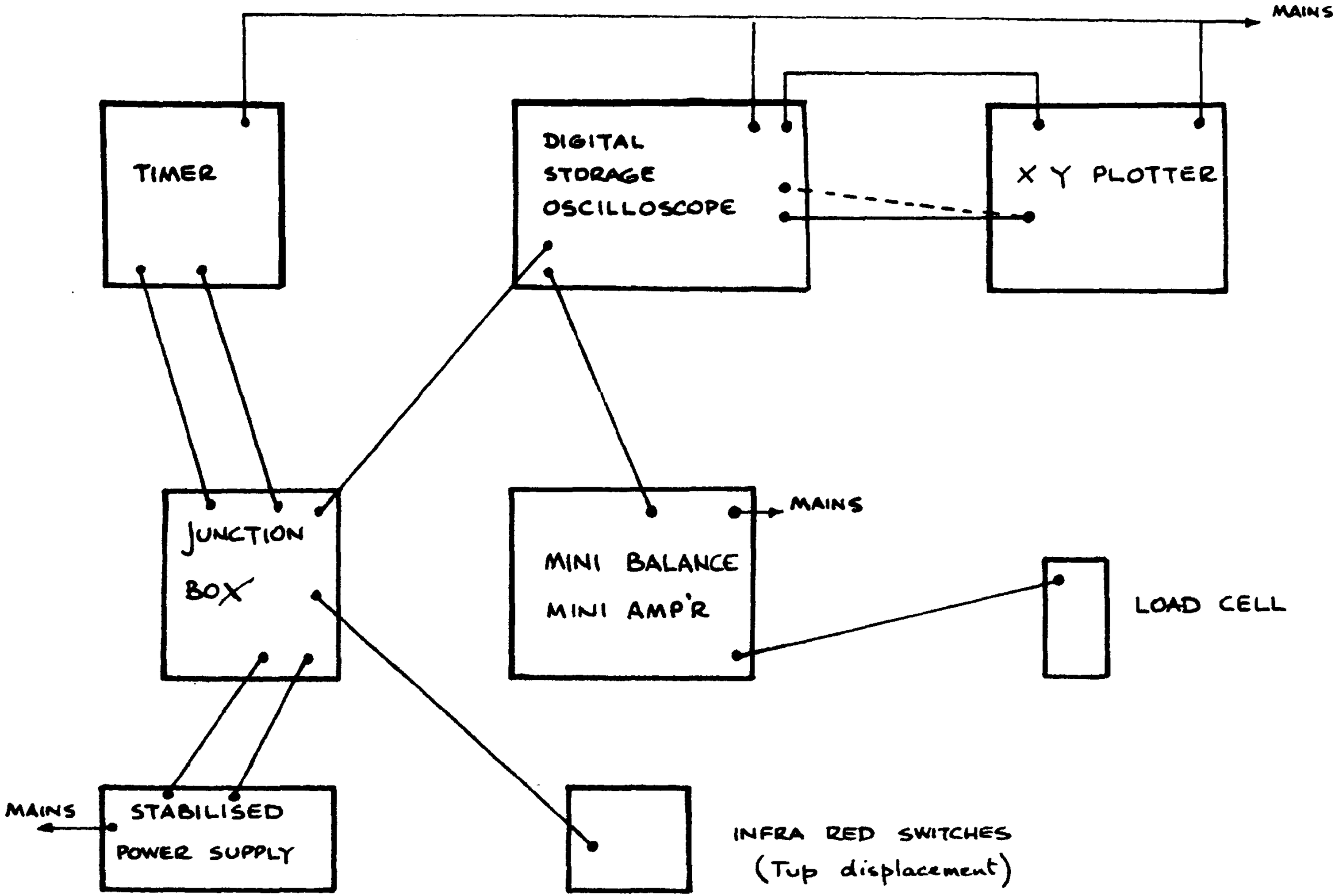

FIG. 6 SCHEMATIC BLOCK DIAGRAM OF INSTRUMENTATION

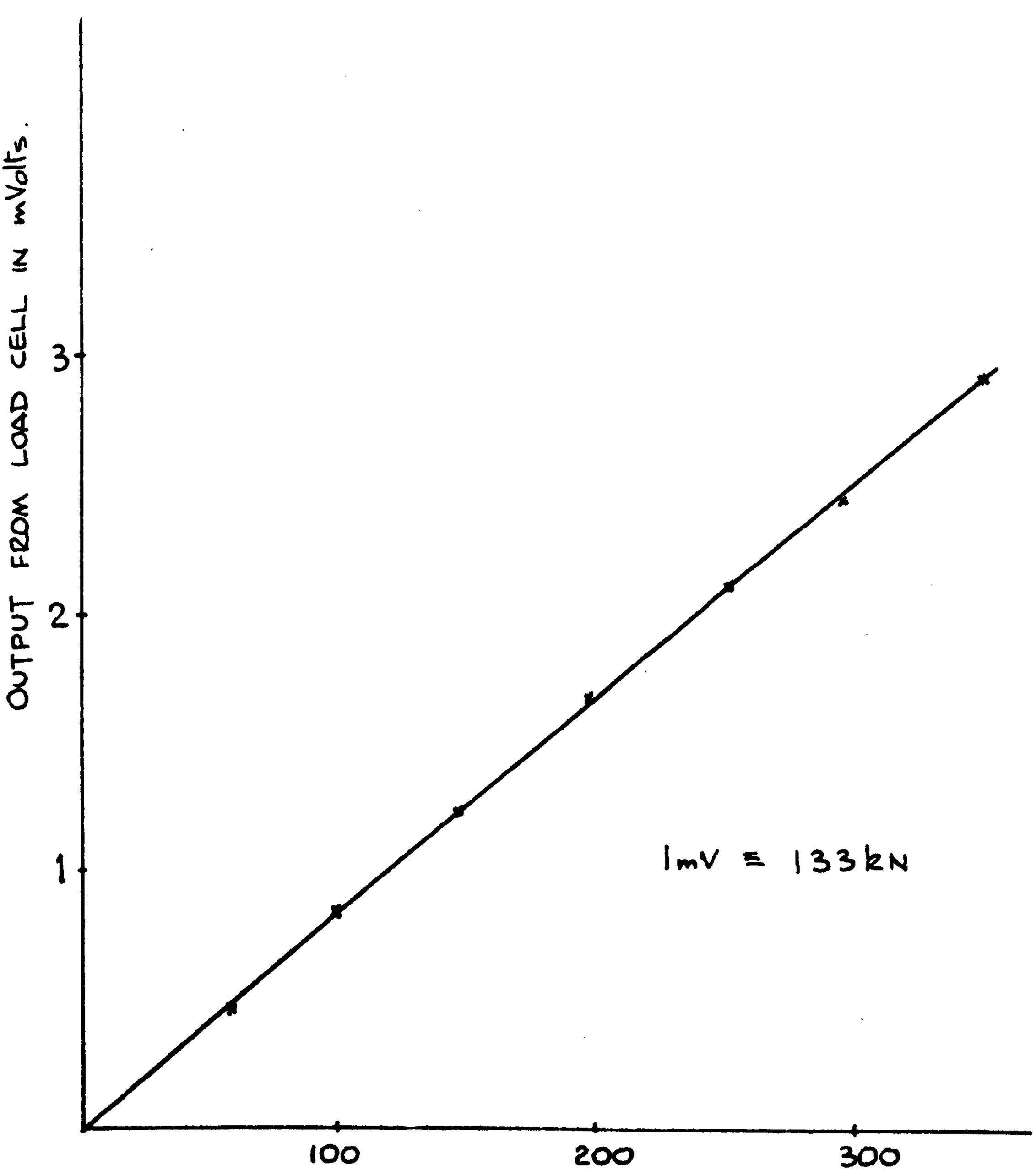

CALIBRATION OF LOAD CELL FIG. 7

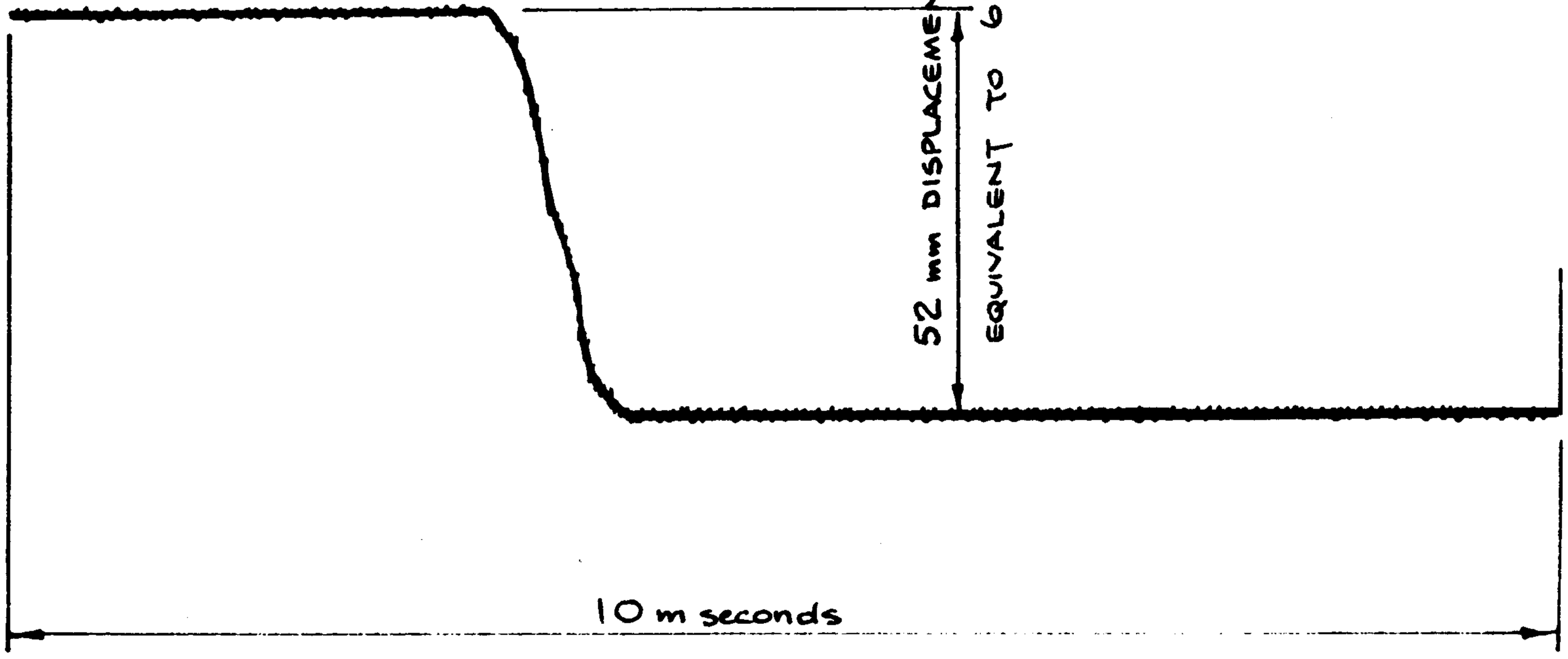

CALIBRATION OF INSTRUMENTATION USED TO MEASURE LOAD.

FIG. 8.

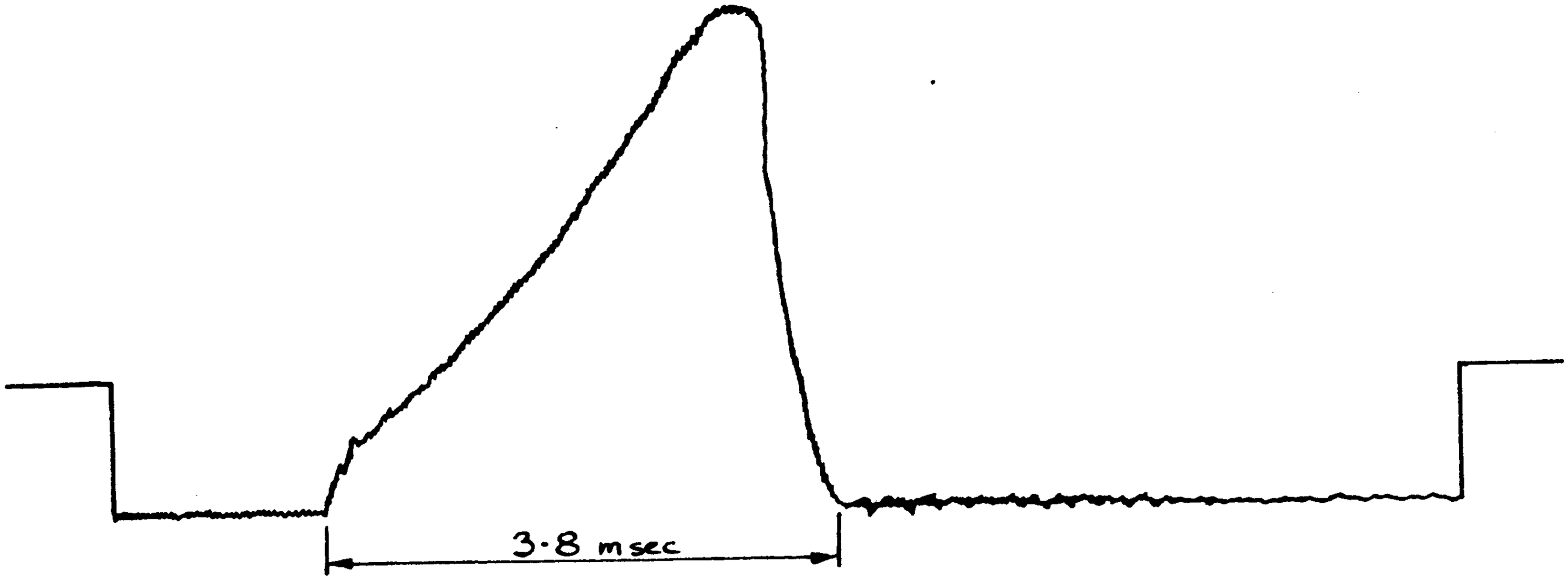

TYPICAL LOAD-TIME TRACE

FIG. 9.

FIG. 10(a)

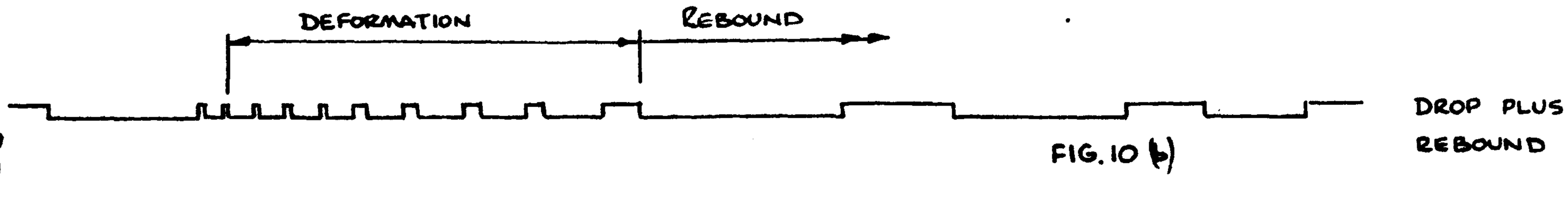

FIG. 10(b)

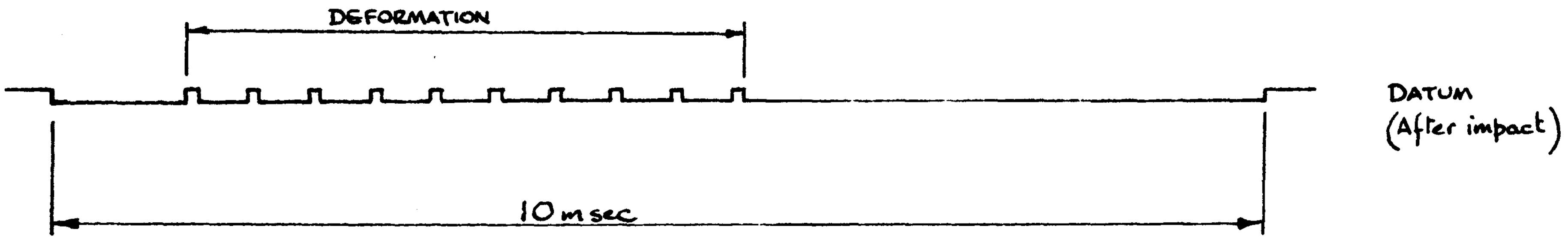

FIG. 10(c)

DISPLACEMENT RECORDINGS.

FIG. 10

$$\sigma = \sigma_1 \left[1 + \left(\frac{\dot{e} + \dot{e}_1}{D} \right)^{\frac{1}{P}} \right]$$

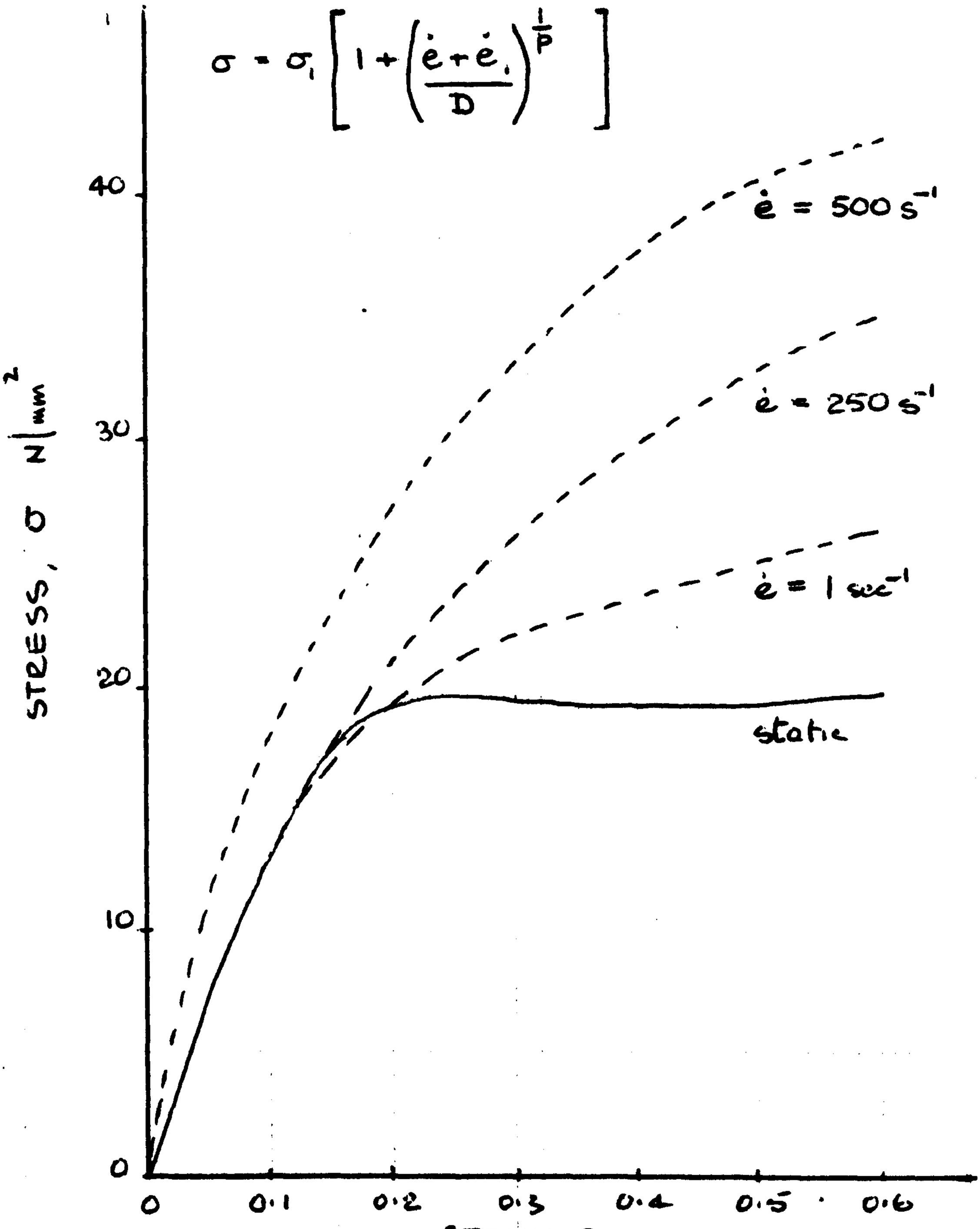

STRESS STRAIN RESULTS FOR DIFFERENT STRAIN RATES

FIG. 11

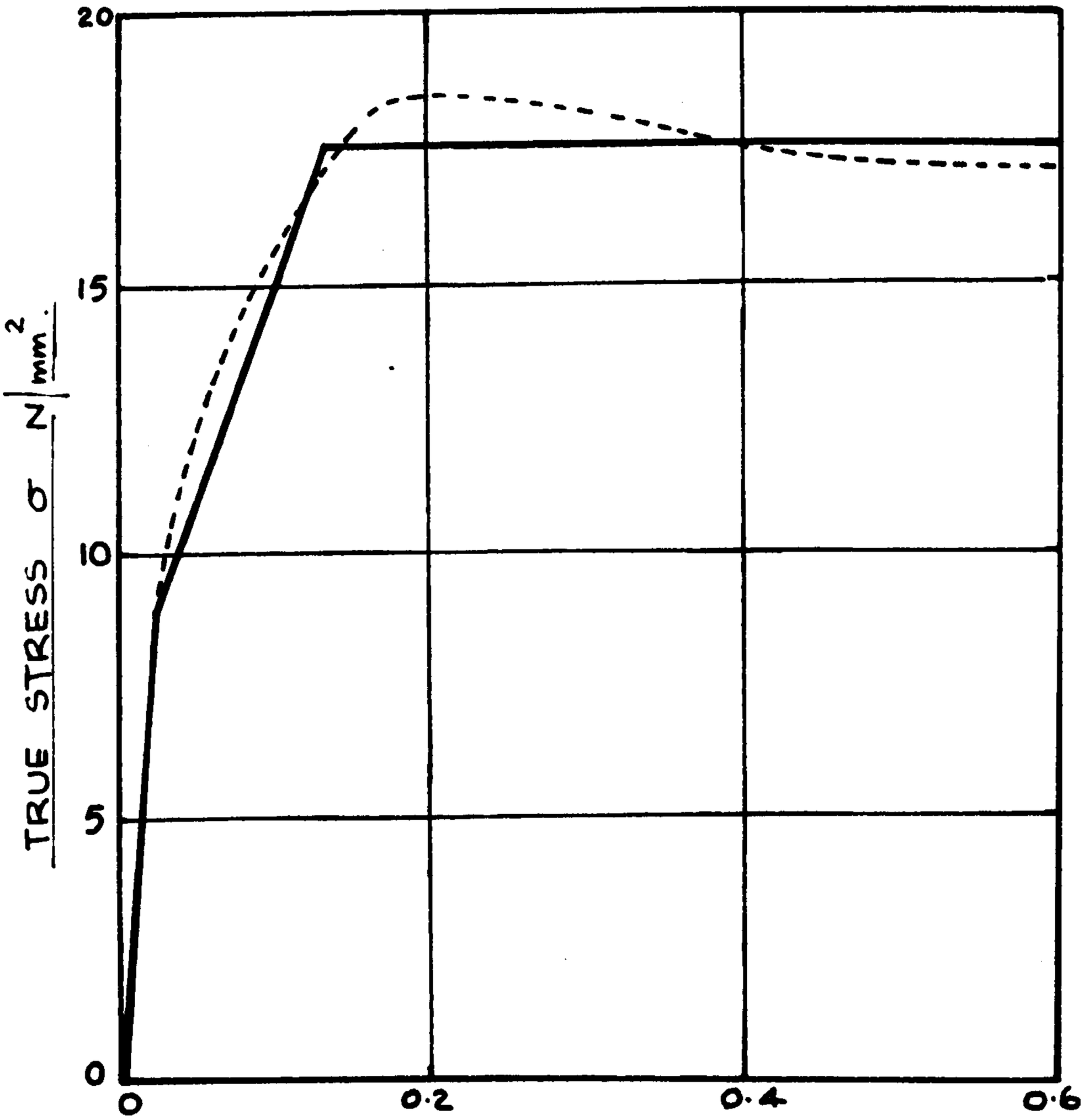

STRESS - STRAIN CHARACTERISTICS FOR LEAD.

FIG. 12.

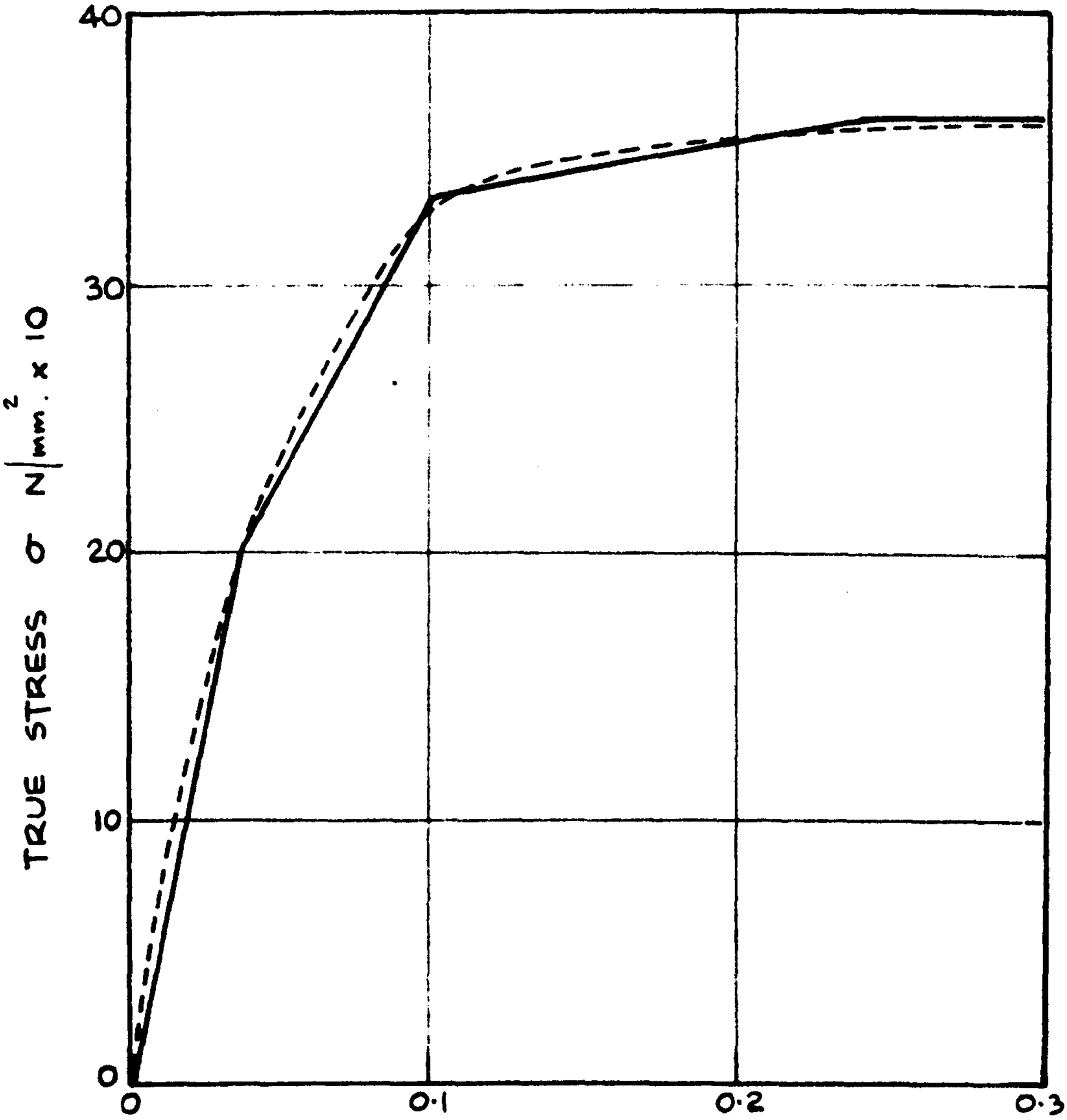

STRESS - STRAIN CHARACTERISTICS FOR ALUMINIUM ALLOY.

FIG. 13

CHAPTER 3

ANALYSIS USING A NUMERICAL TECHNIQUE

3.1 Introduction

In order to study theoretically the deformation mode and hence assess the influence of friction, material inertia, and strain rate sensitivity on the forging load in simple upsetting, a numerical technique has been employed. From this the billet profile, the tup load and velocity can be determined at any stage during the in-process time associated with the simple upsetting of cylindrical billets. The stress and strain time history at any point within the billet can also be determined.

3.2 The Numerical Technique

In this technique a lumped-mass model is used for the actual billet and is based on the following assumptions:

(a) The billet is made up of a number of concentrated connected masses connected to each other by massless links of circular cross section which possess the same strength properties as the material of the billet.

(b) The plane sections remain plane throughout the deformation process.

(c) Uniform axial straining occurs within each individual link.

(d) The frictional stress in the billet-tup interface is proportional to the normal stress in the face of the billet.

(e) The radial expansion for each connecting link is governed by the condition of volume constancy.

(f) There is no resistance to radial expansion of any link from the neighbouring link except for the links in contact with the top and bottom platens in which case interface frictional force resists radial expansion.

The procedure amounts to expressing the dynamic force equilibrium equations for each concentrated mass point in finite-difference form and relating the displacement of each mass point to the strain in the corresponding link after each time increment. The stress in each link, and hence the axial force, is then determined from the material stress-strain characteristics.

SYMBOLS

A annular area in the cross-section model

D material strain-rate constant

E elastic modulus

N axial force

P material strain rate constant

R current billet radius

m mass per unit length

Δs link length in the numerical model

Δt time increment

u,v displacement

x,y co-ordinate axis

ε engineering strain

σ stress

Subscripts

i this refers to the mass point number and the preceeding link

j time position

l refers to the subannulus number

r refers to the annulus number

Superscripts

m modified value

t trial value

$(\dot{\cdot})$ single differentiation with respect to time

$(\ddot{\cdot})$ double differentiation with respect to time

The general equation of motion for an element of the billet, soon after the tup strikes the top face, can be derived by considering the internal forces acting on the element as shown in Fig. 14(a) and is given by

$$\frac{\delta N}{\delta s} - m\ddot{u} = 0 \qquad (1)$$

Fig. 14(b) shows the lumped parameter model for a number of elemental lengths of the billet shown in Fig. 14(a). For convenience each elemental length Δs will be considered to consist of one concentrated mass and a massless link and initially all elemental lengths to be equal. This model replaces the actual billet by a mass-link system. Under the action of the

internal and inertia forces the position of each concentrated mass in the model identifies the position of a corresponding elemental length of the actual billet. The finite-difference equation for the elemental length at the ith location of the model in Fig. 14(b) is given by

$$N_{i+1,j} - N_{i,j} - \Delta s_o m.\ddot{u}_{ij} = 0 \qquad (2)$$

Equation (2) applies to all the elemental lengths along the billet and gives the instantaneous value of the acceleration $\ddot{u}_{i,j+1}$ for any instant of time t_{j+1}.

Using finite difference notation the relation between displacement and time takes the form shown in Fig. 15.

$$\ddot{u}_{ij} = \frac{1}{\delta t}\left[\left(\frac{u_{i,j+1} - u_j}{\delta t}\right) - \left(\frac{u_{ij} - u_{i,j-1}}{\delta t}\right)\right]$$

$$u_{ij+1} = \ddot{u}_{ij}(\delta t)^2 + 2u_{ij} - u_{ij-1} \qquad (3)$$

$$\text{where } \delta t = t_{j+1} - t_j \qquad (4)$$

When equation (2) is combined with equation (3) instantaneous values of $u_{i,j+1}$ for any instant of time t_{j+1} can be determined.

In order to facilitate the calculation of stress which may vary across the cross section of the billet, it is necessary to idealise the actual cross section to an equivalent cross section model which consists of a number of annuli across each of which the stress is

assumed to be uniform. The circular cross section of the billet is assumed to consist of n discrete annuli of material which can carry normal stresses. These annuli are considered to be separated by a material which can not carry any normal stress but has infinite shear rigidity.

With this simplified model the stress in the billet can be defined by the individual normal stresses at the n separate annuli without having to contravene the assumption that plane sections remain plane throughout the deformation process. The cross sectional area of each tubular layer can be calculated by equating the fully plastic pure axial load carrying ability, with that of the actual cross section of the billet. A typical cross section model is shown in Fig. 17.

In order to describe the elastic-plastic stress state in an annulus of the section-model, further idealisation is made and each annulus is assumed to consist of subannuli the number of which is determined by the number of positive sloped sides in the approximated polygonal stress-strain diagram shown in Fig. 18.

Fig. 19 is used in establishing a relationship between subannular area and its parent annular area

Assume that the deformation has reached stage B, ie sublayer $A_{r(\ell-1)}$ is loaded elastically to the condition $\sigma_1\varepsilon_1$ and the remaining subannular areas are

loaded to the condition $\sigma_2\varepsilon_2$.

The stress σ_B is the hypothetical stress that the subannular area A_{rl} would have to be subjected to if it were stressed elastically to a strain value of ε_2. σ_c is similarly related to ε_3 for the subannular area $A_{r(l+1)}$.

Equating forces NOTE: $A_r = A_{r(\ell-1)} + A_{r\ell} + A_{r(\ell+1)}$

$$\sigma_2 A_r = A_{(l-1)r}\sigma_1 + A_{lr}\sigma_B + A_{(l+1)r}\sigma_B \qquad (5)$$

$$= A_{(l-1)r}\sigma_1 + \sigma_B(A_{lr} + A_{(l+1)r})$$

$$= A_{(l-1)r}\sigma_1 + \sigma_B(A_r - A_{(l-1)r})$$

$$= A_{(l-1)r}\sigma_1 + \sigma_B A_r - \sigma_B A_{(l-1)r}$$

$$A_r(\sigma_2 - \sigma_B) = A_{(l-1)r}(\sigma_1 - \sigma_B)$$

$$A_{(l-1)r} = A_r\frac{(\sigma_2 - \sigma_B)}{(\sigma_1 - \sigma_B)}$$

$$= A_r\frac{(\sigma_B - \sigma_2)}{(\sigma_B - \sigma_1)}$$

If the slope of OA = $E_1 = \frac{\sigma_1}{\varepsilon_1}$ = E = Young's modulus

and the slope of AB = $E_2 = \frac{\sigma_2 - \sigma_1}{\varepsilon_2 - \varepsilon_1}$

and the slope of BC = $E_3 = \frac{\sigma_3 - \sigma_2}{\varepsilon_3 - \varepsilon_2}$

then

$$A_{r(1-1)} = A_r\left[\frac{(\varepsilon_2-\varepsilon_1)(E-E_2)}{E(\varepsilon_2-\varepsilon_1)}\right]$$

$$= \frac{A_r}{E}[E - E_2] \quad \text{(6)}$$

Assume deformation has reached Stage C.

Equating forces

$$\sigma_3 A_r = A_{(1-1)r}\sigma_1 + A_{1r}\sigma_B + A_{(1+1)r}\sigma_C \quad \text{(7)}$$

combining equations (5) and (6)

$$\sigma_3 A_r = \sigma_2 A_r - A_{(1+1)r}\sigma_B + A_{(1+1)r}\sigma_C$$

$$A_r(\sigma_3-\sigma_2) = A_{(1+1)r}(\sigma_C-\sigma_B)$$

$$A_{(1+1)r} = A_r \frac{(\sigma_3-\sigma_2)}{(\sigma_C-\sigma_B)}$$

$$= \frac{E_3}{E} \frac{(\varepsilon_3-\varepsilon_2)}{(\varepsilon_3-\varepsilon_2)} A_r$$

$$= \frac{E_3 A_r}{E} \quad \text{(7)}$$

To find A_{1r}

$$A_{1r} = A_r - \frac{A_r}{E}[E_1-E_2] - \frac{A_r E_3}{E}$$

$$= \frac{A_r}{E}[E_2 - E_3] \quad \text{(8)}$$

If the number of subannuli is reduced to two to be compatible with stress strain diagram shown in Fig. (6) then the two subannular areas A_{r1} and $A_{r(1+1)}$ are related to the parent annular area A_r by the

relationships

$$A_{rl} = \frac{A_r}{E_1}[E_l - E_{l+1}] \qquad (9)$$

and

$$A_{r(l+1)} = A_r \frac{E_{l+1}}{E_1} \qquad (10)$$

When the number of positive sloped sides in the approximated polygonal stress-strain diagram exceeds two, the subannular areas, as a fraction of the annular area, for any two adjacent positive sloped sides, can be obtained using equations (9) and (10) where E_l is as defined in Fig. (20).

Knowing the subannular stress $\sigma_{irl,j-1}$ at time t_{j-1} at the lth subannuli of the rth annulus at the ith link and the strain increment $\delta\varepsilon_{ir,j}$ at time t_j at the rth annulus of the ith link, the subannular stress $\sigma_{irl,j}$ at time t_j, at the lth subannuli is determined as follows.

First a trial value $\sigma^t_{irl,j}$ of the subannular stress $\sigma_{irl,j}$ is calculated by assuming an elastic path, thus

$$\sigma^t_{irl,j} = \sigma_{irl,j-1} + E\delta\varepsilon_{ir,j} \qquad (11)$$

Once the trial value is calculated, the correct value can be ascertained by using the following conditions: Let σ_{yl} be the subannular yield stress and be given by $\sigma_{yl} = E_{\varepsilon l}$, where ε_l is the strain defining the lth corner of the polygonal stress strain diagram.

Denoting $\sigma_{irl,j}$ as σ_l for convenience,

$$\left.\begin{aligned} &\text{If } -\sigma_{yl} < \sigma_l^t < \sigma_{yl} \quad \text{then } \sigma_l = \sigma_l^t \\ &\text{If } \sigma_l^t < -\sigma_{yl} \quad \text{then } \sigma_l = -\sigma_{yl} \\ &\text{If } \sigma_l^t > \sigma_{yl} \quad \text{then } \sigma_l = \sigma_{yl} \end{aligned}\right\} \quad (12)$$

This procedure is applied to all subannuli of each annuli for all the links.

The values of the subannular stresses for the links in immediate contact with the tup and the anvil are then modified, to take into account the interface friction, by using the equation,

$$\sigma = \sigma_o[1 + 2\mu(R-r)/h] \quad (13)$$

Following the terminology applied to the numerical model this equation could be written as

$$\sigma^m_{l,j} = \sigma_{lj}[1 + 2\mu(R_i-R_{ir})/h] \quad (14)$$

where μ is the interface friction coefficient, and $\sigma_{l,j}$ is the subannular stress determined by equations (12). After this modification, the axial forces $N_{i,j}$ in each link are then obtained from the equation

$$N_{i,j} = \sum_{r=1}^{n} \sum_{l=1}^{k} \sigma_{irl,j} A_{l,j} \quad (15)$$

where $A_{l,j}$ is the current subannular area.

If the links can be assumed to have the same mass

density as the billet, then further modification to the values of the subannular stresses can be made to take into account the effect of radial inertia of the billet material, by using the equation

$$\sigma = \sigma_o + 3\rho v^2(R^2-r^2)/8h^2 \qquad (16)$$

Equations (13) and (16) are detailed in appendices 1 and 2.

In its existing form, when using the present numerical approach the time increment cannot be chosen arbitrarily. The value of the time increment should be less than the time needed for the elastic stress wave to propagate through the length of the link.

3.2.1 Strain Rate Sensitivity

To take into account strain rate sensitivity the stress strain behaviour of the material, for different strain rates, must be known. Approximated stress strain diagrams are shown in Fig. 18, and referring to equations (3) and (4), namely

$$\delta t = t_{j+1} - t_j \qquad (4)$$

$$u_{ij+1} = \ddot{u}_{ij}(\delta t)^2 + 2u_{ij} - u_{ij-1} \qquad (3)$$

The change in length of the element $\delta(\Delta S)_{i,j+1}$ of the link occurring during the time interval δt is

$$\delta(\Delta S)_{i,j+1} = \Delta S_{i,j+1} - \Delta S_{i,j} \qquad (17)$$

The strain increment and strain rate occurring in the link during the time interval are:

$$\delta\varepsilon_{i,j+1} = \frac{\delta(\Delta S)_{i,j+1}}{\Delta S_{i,o}} \qquad (18)$$

where $\Delta S_{i,o}$ is the original length of the link

and

$$\dot{\varepsilon}_{i,j+1} = \frac{\delta\varepsilon_{i,j+1}}{\delta t} \qquad (19)$$

The total strain in the link can now be determined from:

$$\varepsilon_{i,j+1} = \varepsilon_{i,j} + (\dot{\varepsilon}_{i,j+1})\delta t \qquad (20)$$

$$\varepsilon_{i,j+1} = \varepsilon_{i,j} + \delta\varepsilon_{i,j+1} \qquad (21)$$

since the time interval and, hence, the strain increment are both small.

A computer simulation based on the lumped parameter model can be used and strain rate sensitivity incorporated into the analysis in the form of a stress-strain rate law. For lead the law $\sigma = \sigma_1[1 + (\frac{\dot{e}-\dot{e}_1}{D}\frac{1}{p}]$ was used as detailed in Chapter 2.

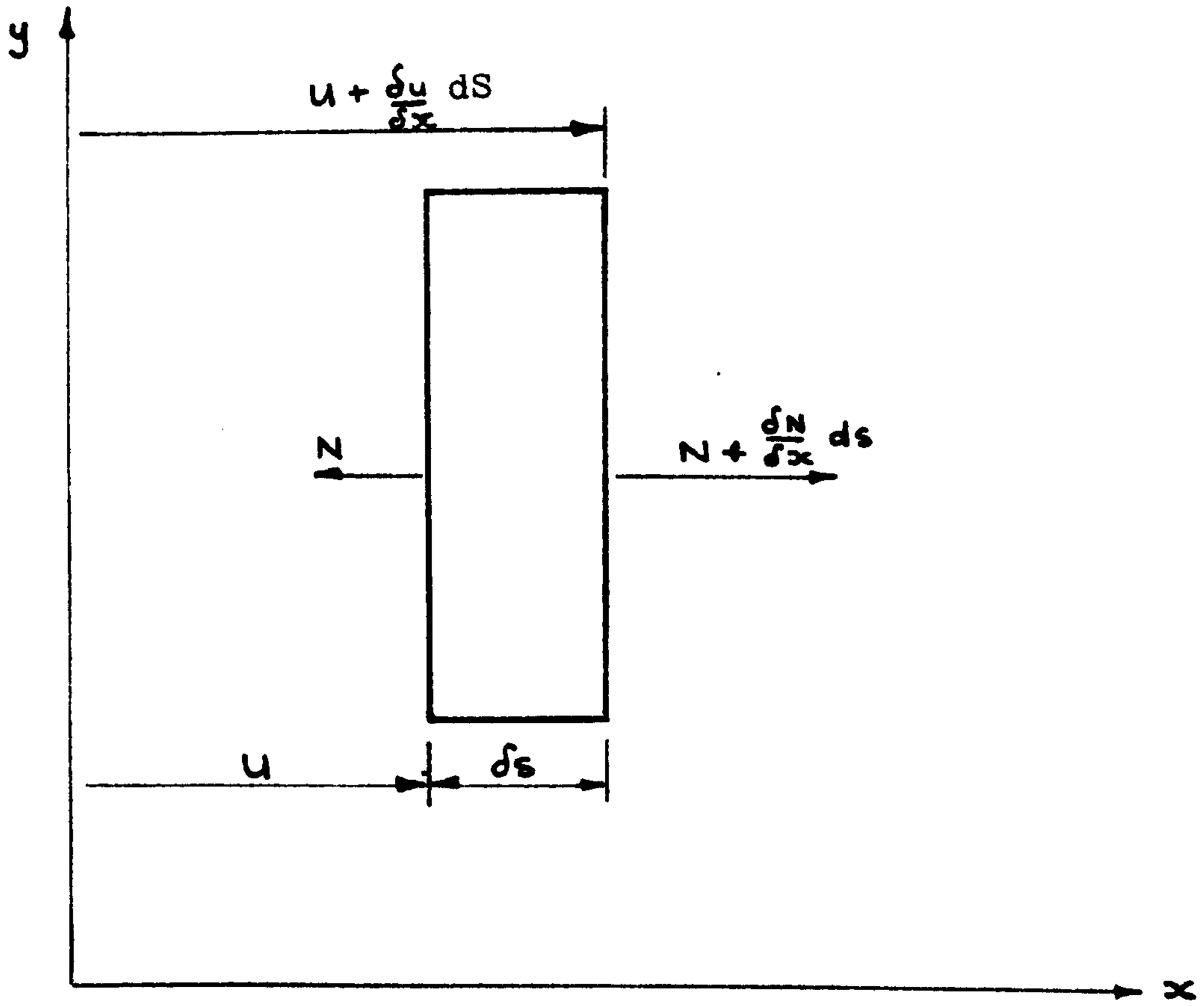

AN ELEMENT OF THE BILLET

FIG. 14a.

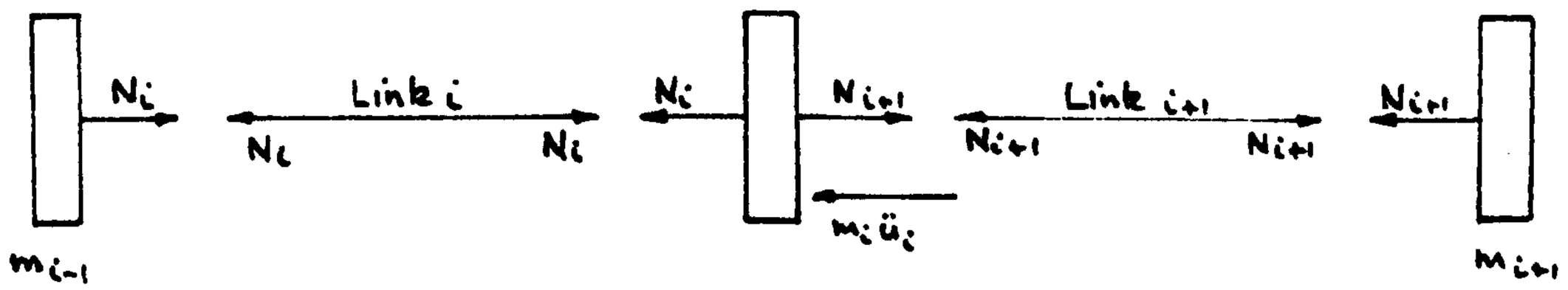

EQUIVALENT FINITE - DIFFERENCE MODEL

FIG. 14b.

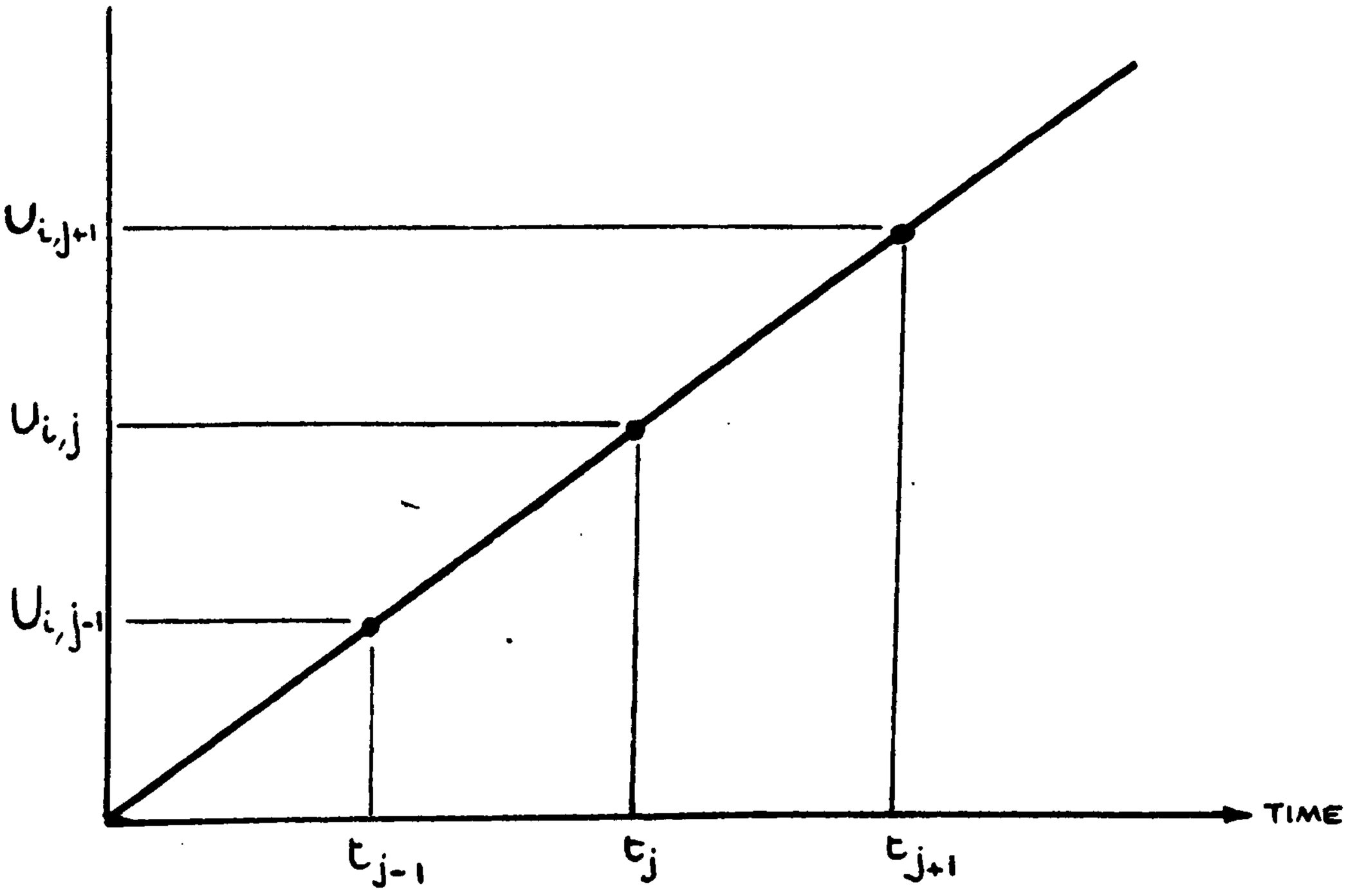

FINITE DIFFERENCE TIME DISPLACEMENT RELATIONSHIP

FIG. 15.

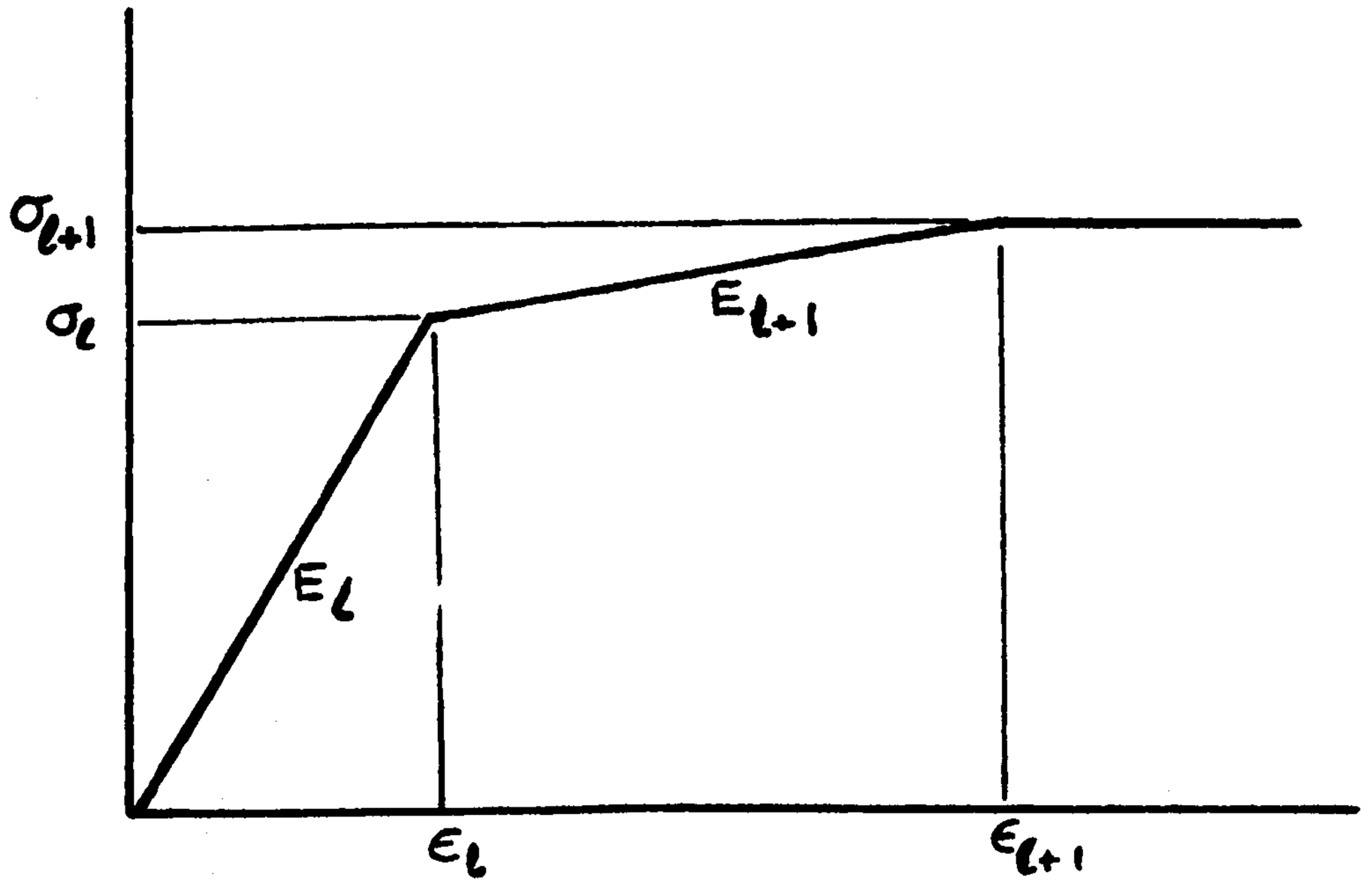

ELASTIC BINARY STRAIN HARDENING STRESS STRAIN PROPERTY

FIG. 16

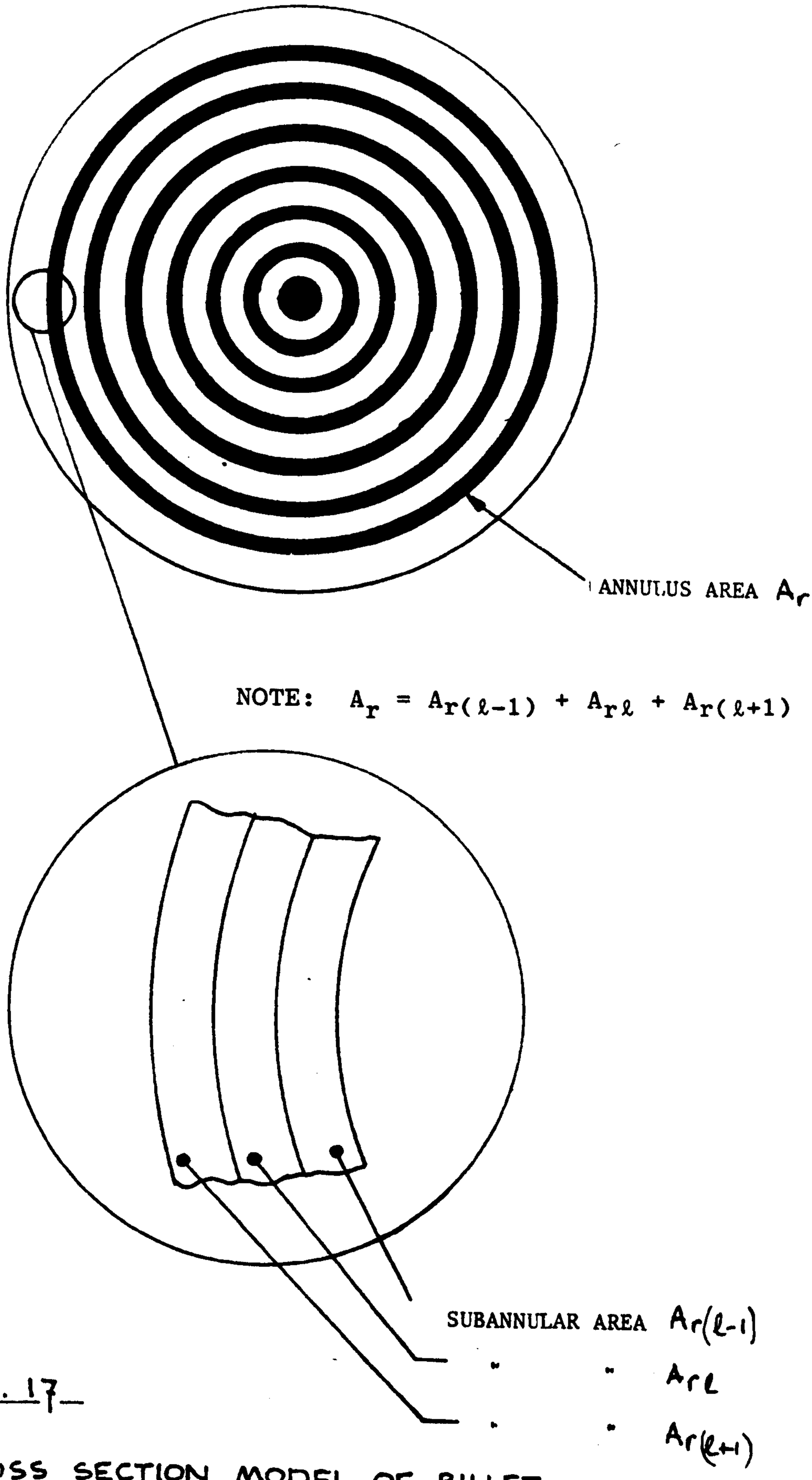

FIG. 17

CROSS SECTION MODEL OF BILLET

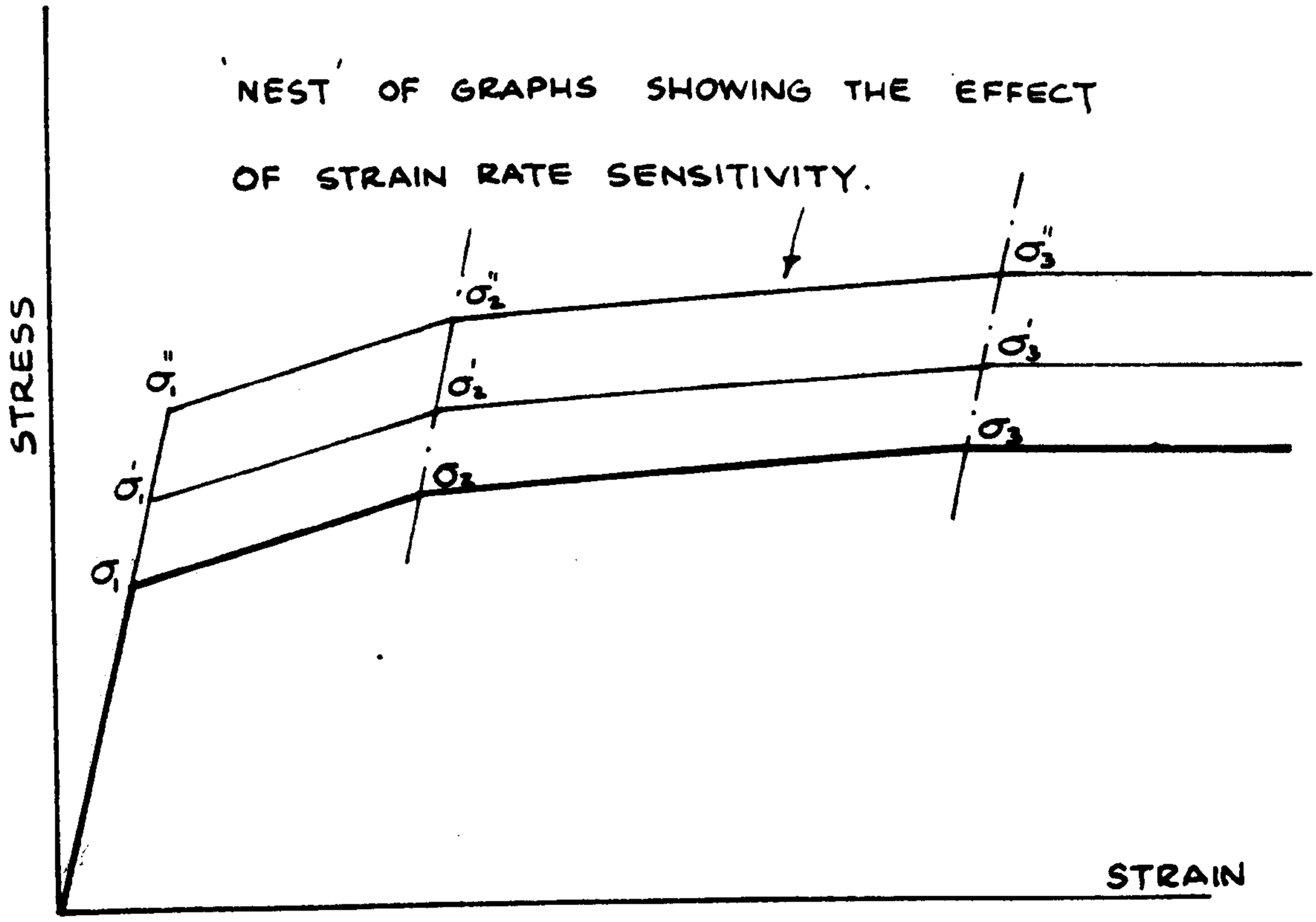

APPROXIMATED POLYGONAL STRESS STRAIN DIAGRAM

FIG. 18

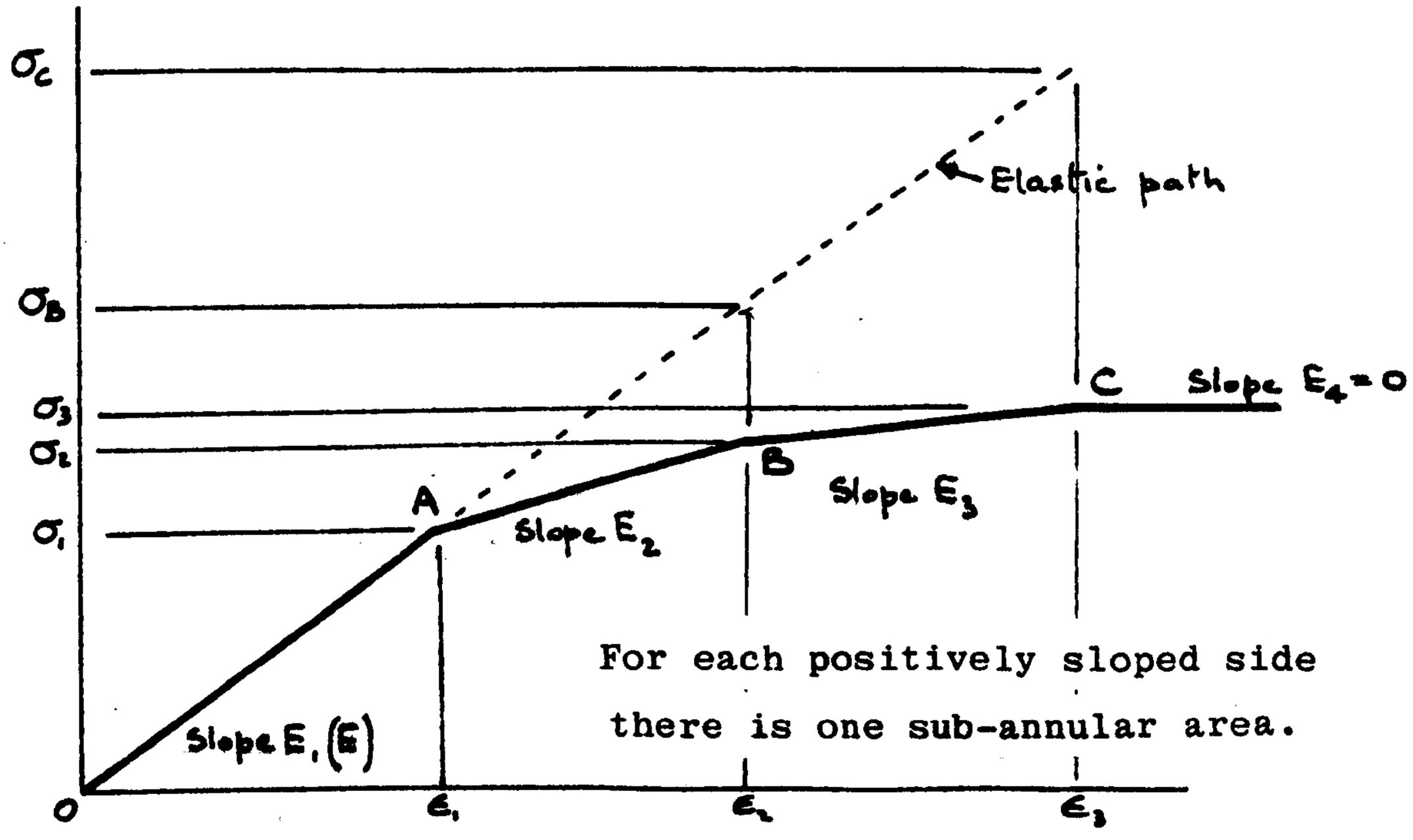

STRESS STRAIN DIAGRAM IDENTIFYING SYMBOLS USED

IN THEORETICAL ANALYSIS

FIG. 19

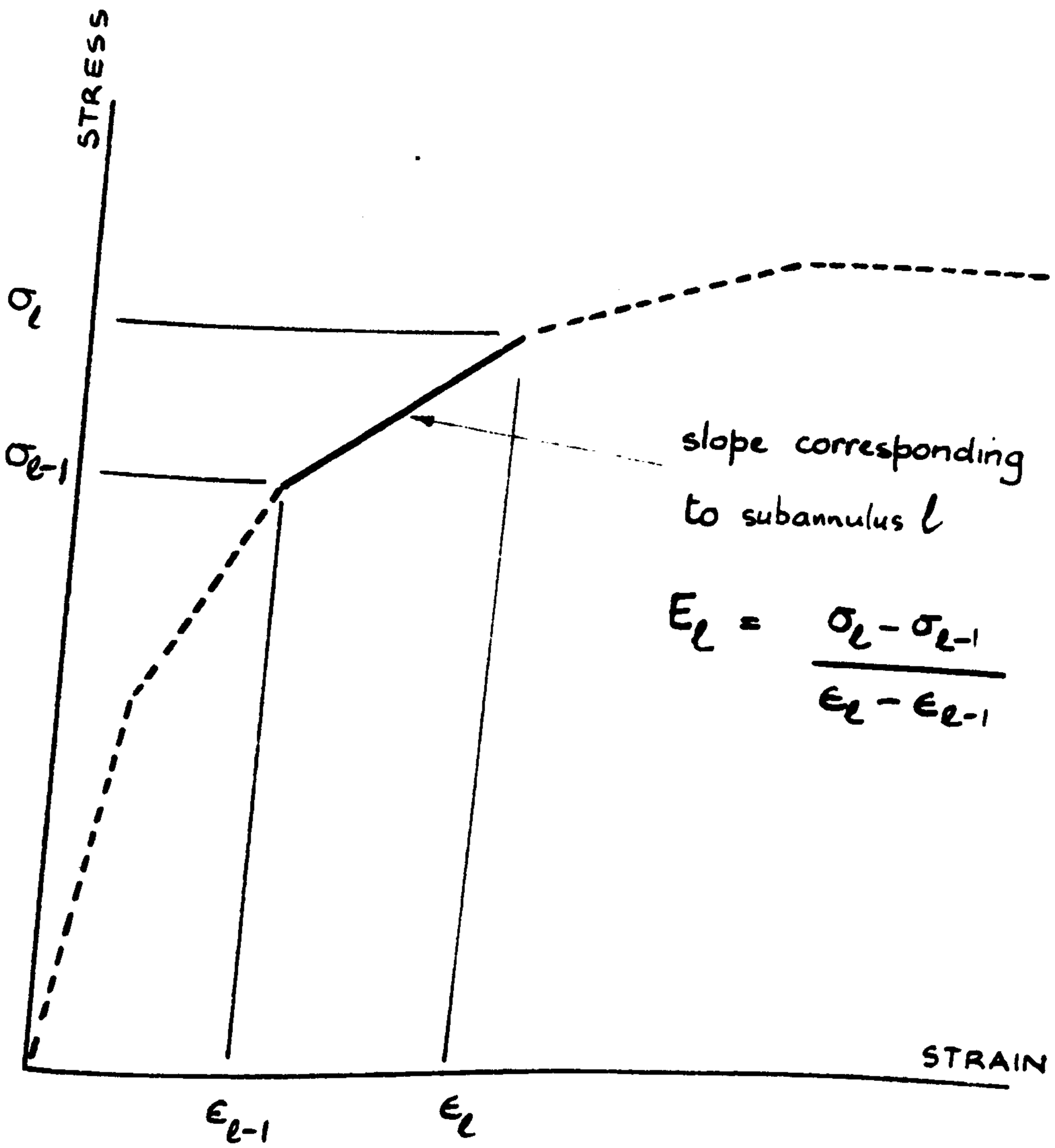

APPROXIMATED POLYGONAL STRESS STRAIN DIAGRAM

FIG. 20

CHAPTER 4

SIMPLE UPSETTING OF CYLINDRICAL BILLETS

4.1 Introduction

Simple upsetting or dynamic compression of cylindrical billets is one of the most commonly used and relatively simple operations used to increase the diameter of the billet. The dimensions of larger sized billets are usually changed by hot upsetting at moderately high speeds and hence the forging load is influenced by interface friction and strain-rate sensitivity of the material. The object of this part of the work is to investigate the effects of friction and strain rate sensitivity on the forging load and final shape of the billet, both experimentally and theoretically.

4.2 Experimental Work

Simple upsetting tests were carried out under the drop hammer and a different degree of deformation was imparted to each billet by releasing the tup from different heights. For each test the following data were obtained:

(a) the forging load

(b) impact velocity

(c) deformation-time history.

The deformation sequence of a number of test specimens were recorded using a Hi-Cam high speed camera.

Using the drop hammer set to give maximum impact, velocity tests were carried out on lead billets

25 mm diameter x 24 mm long and aluminium alloy billets 19 mm diameter x 19 mm long. Two types of friction condition were studied, one, using a paste of graphite in petroleum jelly as lubricant to induce low friction and the other, without any lubricant, to induce dry friction conditions. High speed photographs were used to obtain experimental data giving instantaneous billet profiles and tup-displacement-time curves. Elastic strain hardening and stress-strain characteristics of the billet material were obtained from quasi-static tests. The dynamic stress-strain properties were established from drop hammer tests (described in Chapter 2).

The load time variation was obtained from the tracings recorded on the oscilloscope. A typical photograph of such a trace for an aluminium alloy billet is shown in Fig. 21.

4.3 Theoretical Predictions

In order to predict the results theoretically, the numerical technique described in the previous Chapter was employed. In predicting the results it was assumed that a constant frictional coefficient $\mu = 0.06$ existed for both lead and aluminium billets. This value of μ was thought to be a reasonable estimate of what graphite in jelly would induce. For dry test conditions the value of $\mu = 0.577$ was incorporated in the analysis for

lead billets [51] while for aluminium billets $\mu = 0.18$ was used [59].

The actual loading configuration and its equivalent numerical model, applied to both the lead and aluminium billets, is shown in Fig. 22. The quasi-statically obtained stress strain characteristics and their polygonal approximations, as required by the numerical technique, for lead and aluminium alloy used for these tests are shown in Fig. 12 and Fig. 13 respectively.

4.4 Results and Discussions

The instantaneous profiles of a lead billet at various instants of time after the onset of the process were obtained from the high speed photographs and are shown in Fig.23(a). This test was carried out under lubricated conditions. The billet deformed in such a manner that the profile shape remained right cylindrical throughout the deformation process. The theoretically predicted instantaneous profiles for the same billet are shown in Fig.23(b) which shows profile shapes having either upwards or downwards directed slightly tapered sides. Slight barrelling also becomes apparent in the profiles corresponding to higher reductions in billet height. This slight discrepancy is thought to have arisen due to instability in the technique used. Experimentally it was not possible to identify such behaviour.

The instantaneous profiles shown in Fig. 24(a) for a lead billet deformed under dry lubrication conditions are seen to compare reasonably well with those in Fig. 24(b), which were predicted using the numerical technique. The die load determined experimentally was plotted in Figs. 25 and 26 against reduction in billet height measured from the high speed photographs for lead and aluminium alloy billets respectively, both tests being carried out under lubricated conditions.

The theoretically predicted curves are also included in the respective figures for comparison. It can be seen that for the lead billet both theoretical curves predict lower die loads. For 14.4mm reduction in height the curve excluding the strain rate term predicts a load which is 38% of the actual load, whereas the curve including the strain rate term predicts a load which is 60% of the actual load. The effect of strain rate is clearly shown by these two theoretical curves. During the initial stages of deformation the theoretical curve matches closely with the experimental curve when strain rate sensitivity is incorporated in the analysis. For greater deformation

the frictional effect becomes predominant. The discrepancy between the theory and experiment for larger deformation may thus be attributed to frictional effect. Although the effect of friction has been

incorporated in the analysis, in reality the coefficient of friction may change from what was assumed originally, generally becoming much higher and approaching that of sticking friction in hot forging.

Since aluminium alloy is not a strain rate sensitive material, only a single theoretical load curve is shown. The load predicted is comparable with that obtained experimentally, being slightly higher during the initial part of the deformation and slightly lower thereafter.

In order to compare the effect of friction the die load/deformation curves obtained experimentally for the aluminium alloy billets under lubricated and dry conditions are plotted in Fig. 27. The corresponding predicted curves are also shown in this figure. It is seen that a maximum increase in die load of less than 10% occurs for reductions of billet height of up to 3 mm (16%). The increase in die load due to friction as predicted using the numerical technique is much less than that obtained experimentally.

The increase in friction, when the billet is deformed under dry test conditions, results in increased barrelling of the billet. Fig. 28 shows the increase in radii at the middle and top section of the aluminium alloy billet. The extent of barrelling can be readily appreciated from this figure. The theoretically predicted results suggest slightly less barrelling of

the billet.

Tup displacement-time curves were obtained using high-speed photographs which upon graphical differentiation enabled a velocity time curve to be used to calculate the kinetic energy of the tup still unused at any time instant during the deformation process. Figs. 29 and 30 show the variation in percentage kinetic energy absorbed with deformation for lead and aluminium billets respectively both deformed under lubricated test conditions. The theoretical curve for the lead billet shows that much less energy is required where more than 55% reduction in height is obtained. This is again an underestimation of the actual energy requirement due to the exclusion of the strain-rate sensitivity. On the other hand, it is evident from Fig. 30, which shows similar kinetic energy vs. deformation curves for the aluminium alloy billet, that there is close agreement between the experimental results of predictions obtained theoretically, despite the exclusion of the strain rate sensitivity.

The deformation vs. time curves for lead and aluminium alloy billets deformed under lubricated test conditions are shown in Fig. 31 and 32 respectively. The experimental and theoretical correlation is very good for lead billets when the theoretical curve which takes into account strain rate is used. The theoretical curve which does not take strain rate into account gave good

results for up to 55% deformation.

For aluminium alloy billets, close agreement exists during the whole of the deformation process.

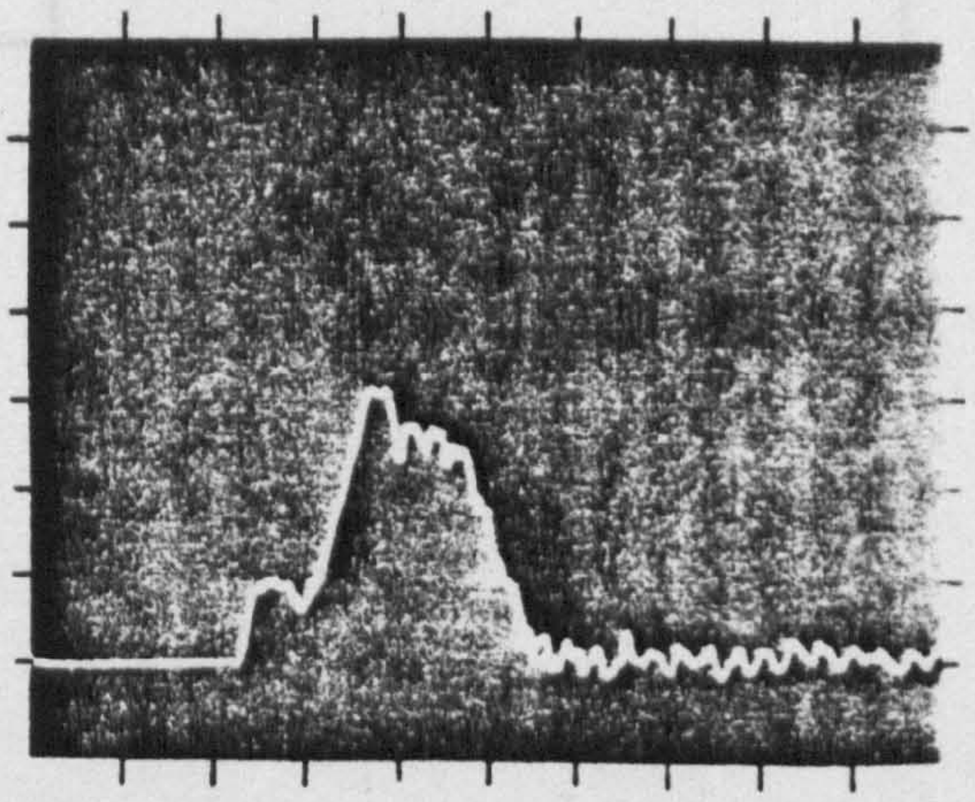

TYPICAL LOAD-TIME TRACE FOR ALUMINIUM BILLET.

FIG. 21.

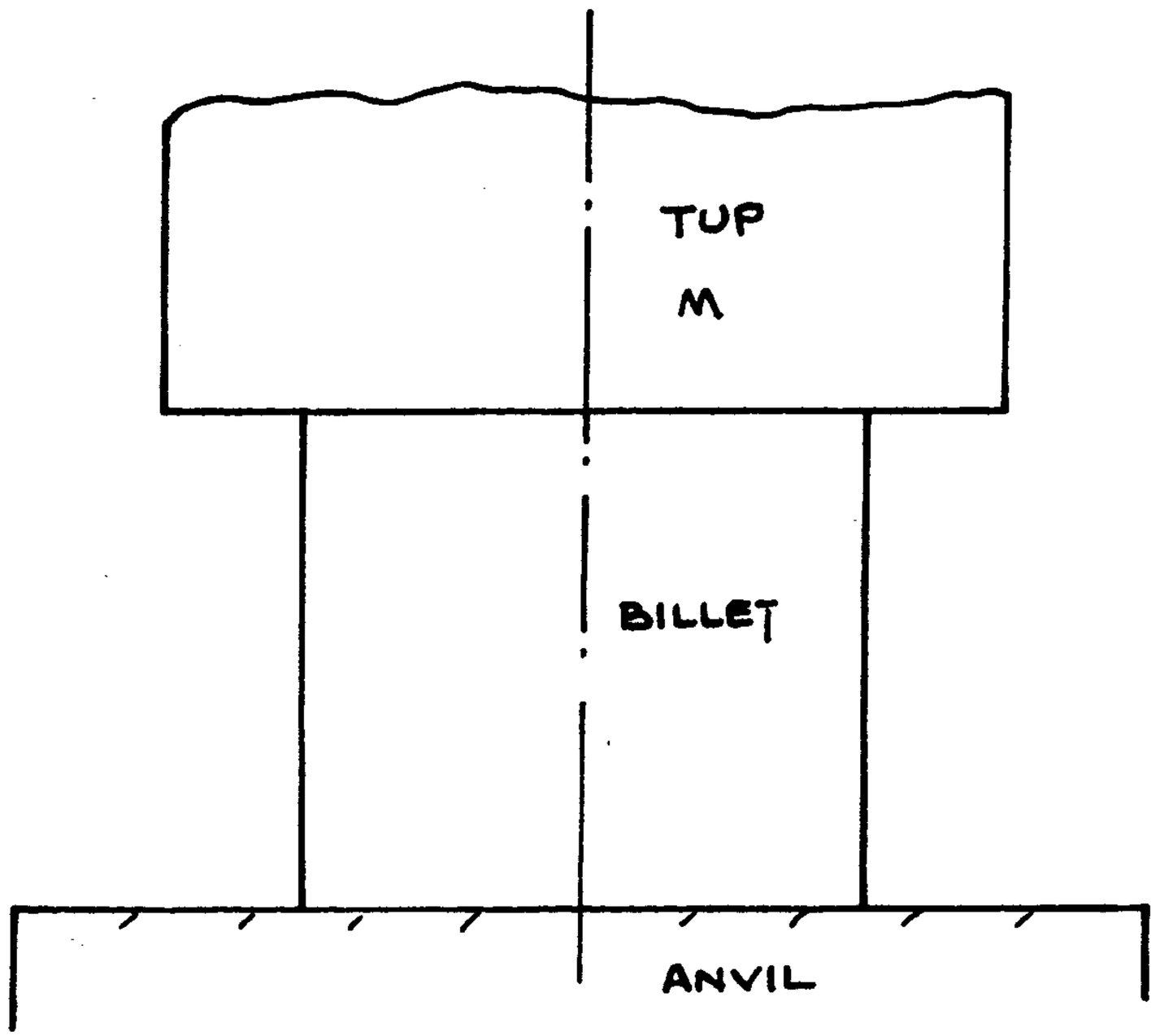

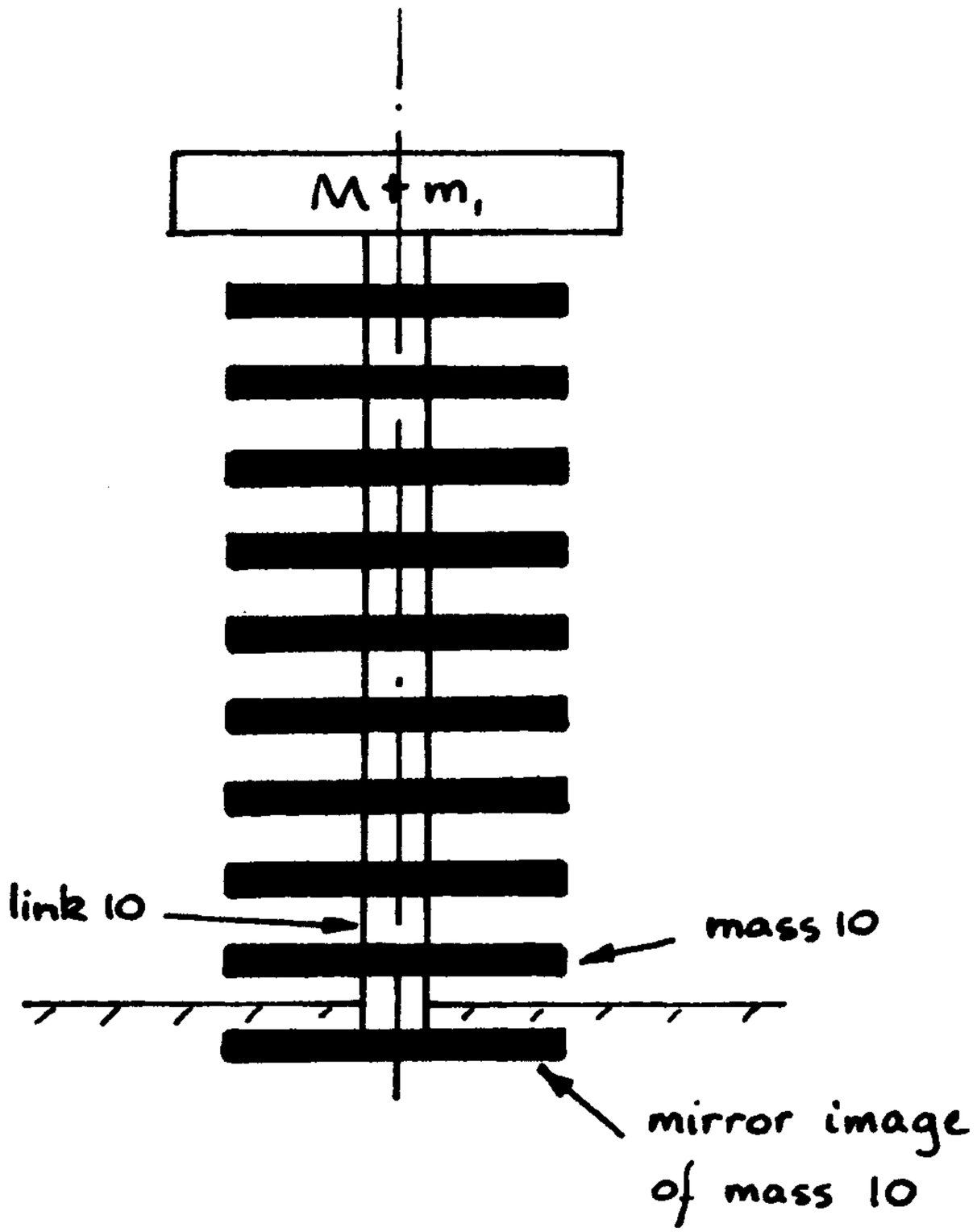

ACTUAL LOAD CONFIGURATION AND THE CORRESPONDING NUMERICAL MODEL

FIG. 22

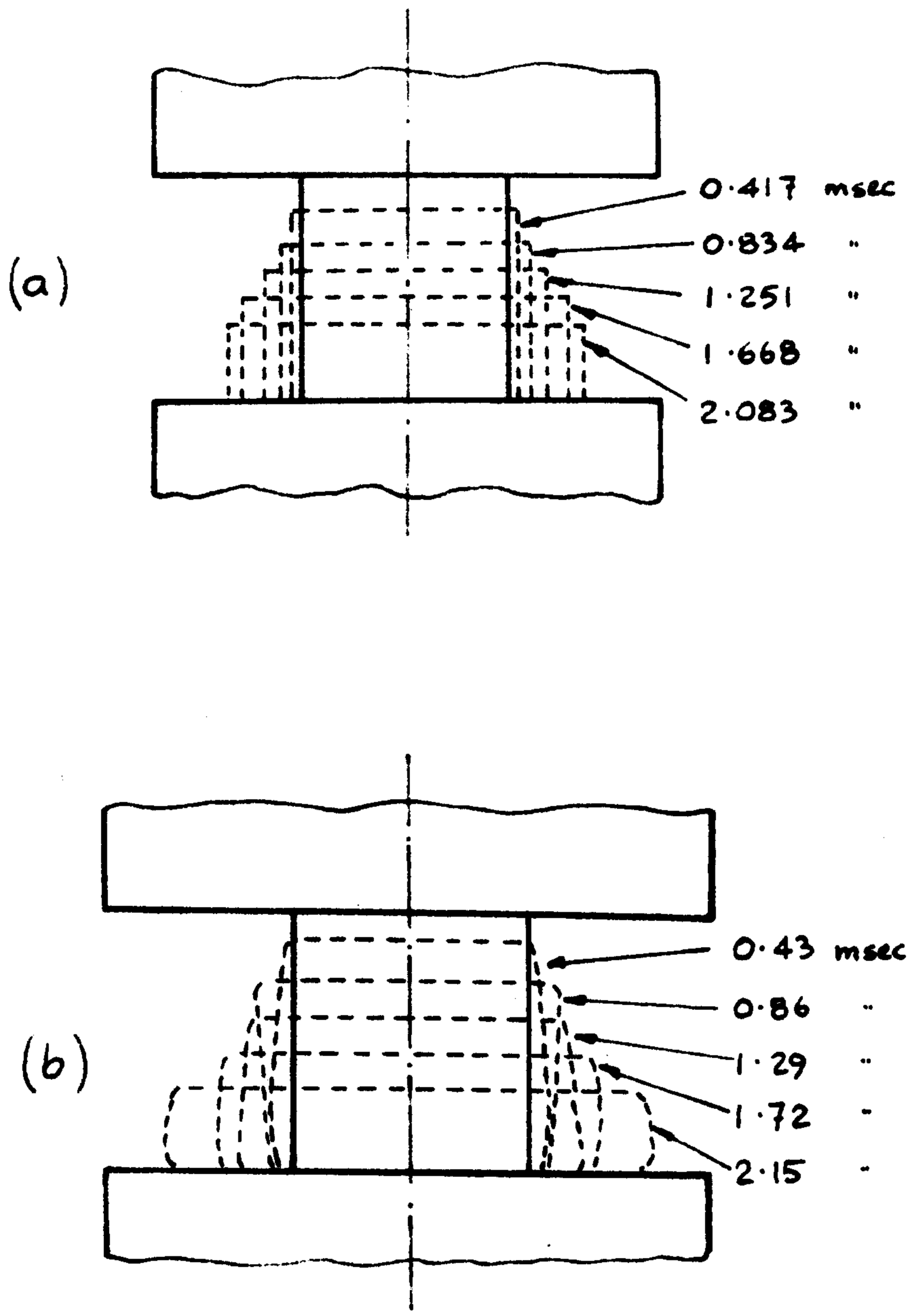

FIG. 23(a) SHOWING THE INSTANTANEOUS PROFILES OF A LEAD BILLET DEFORMED UNDER LUBRICATED TEST CONDITION AND

(b) CORRESPONDING INSTANTANEOUS PROFILES PREDICTED THEORETICALLY.

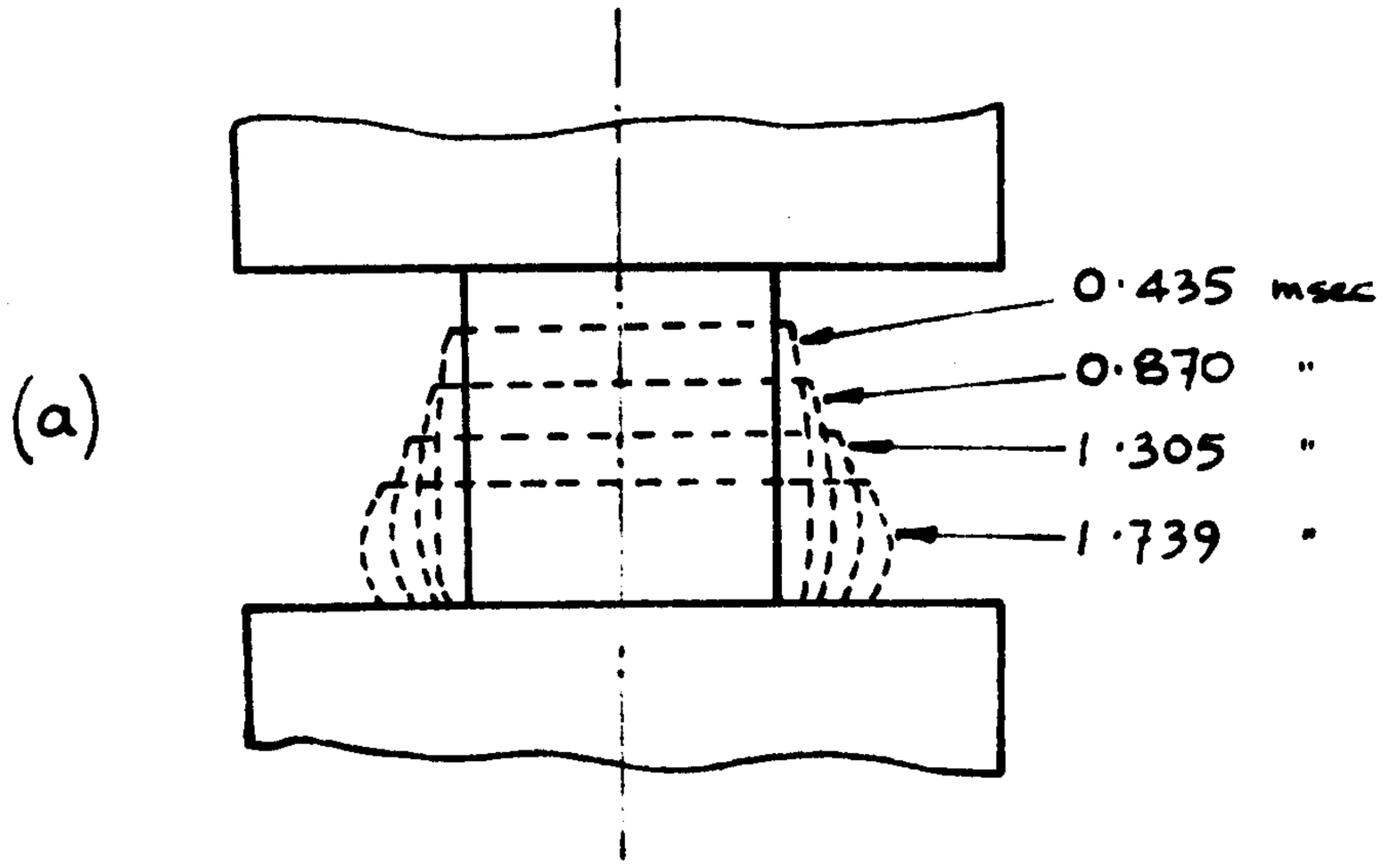

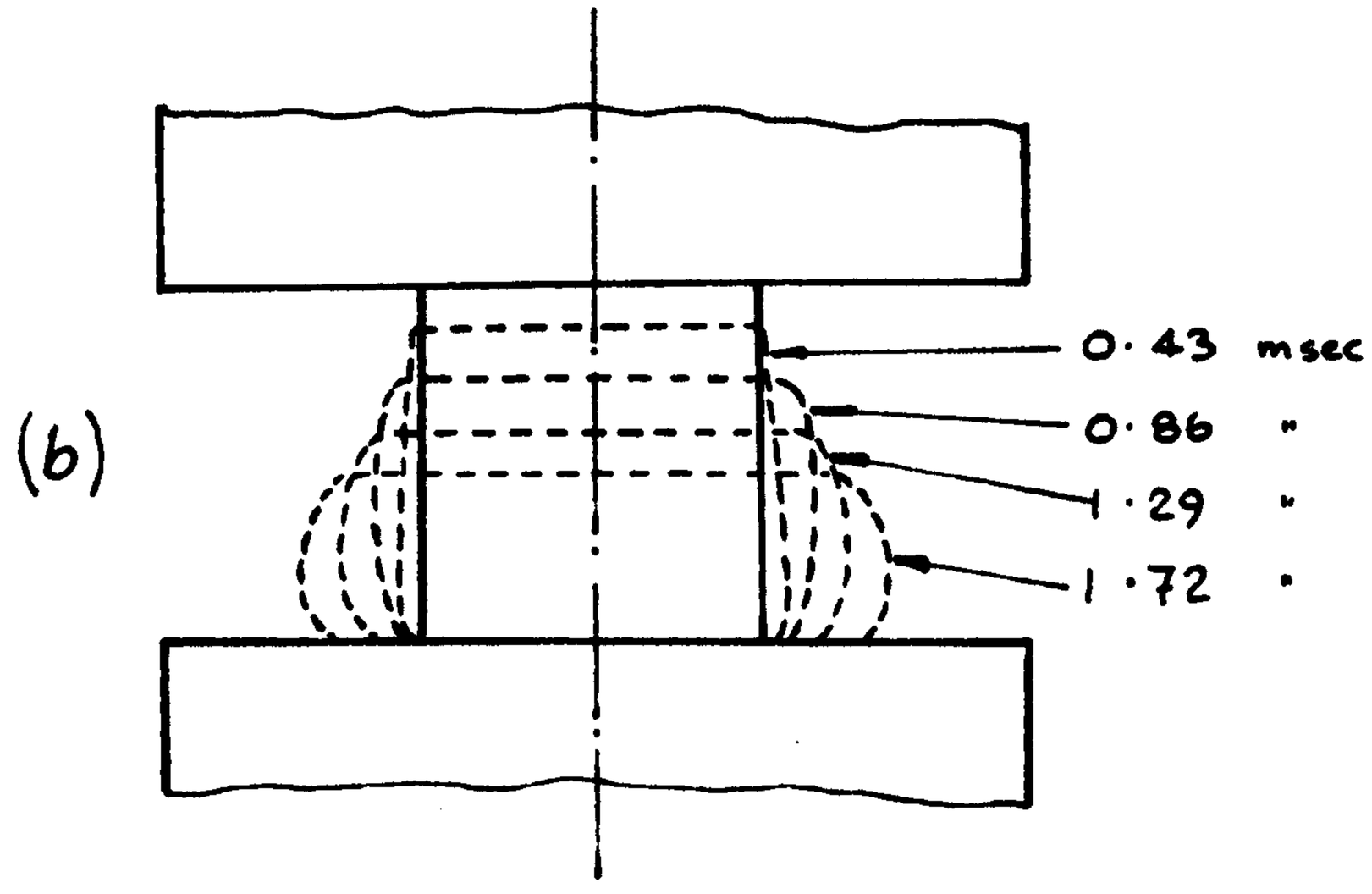

FIG.24(a) SHOWING THE INSTANTANEOUS PROFILES OF A LEAD BILLET DEFORMED UNDER DRY TEST CONDITIONS, AND

(b) CORRESPONDING INSTANTANEOUS PROFILES PREDICTED THEORETICALLY

THEORETICAL CURVES

CURVE 'A' WITHOUT STRAIN RATE

CURVE 'B' WITH STRAIN RATE

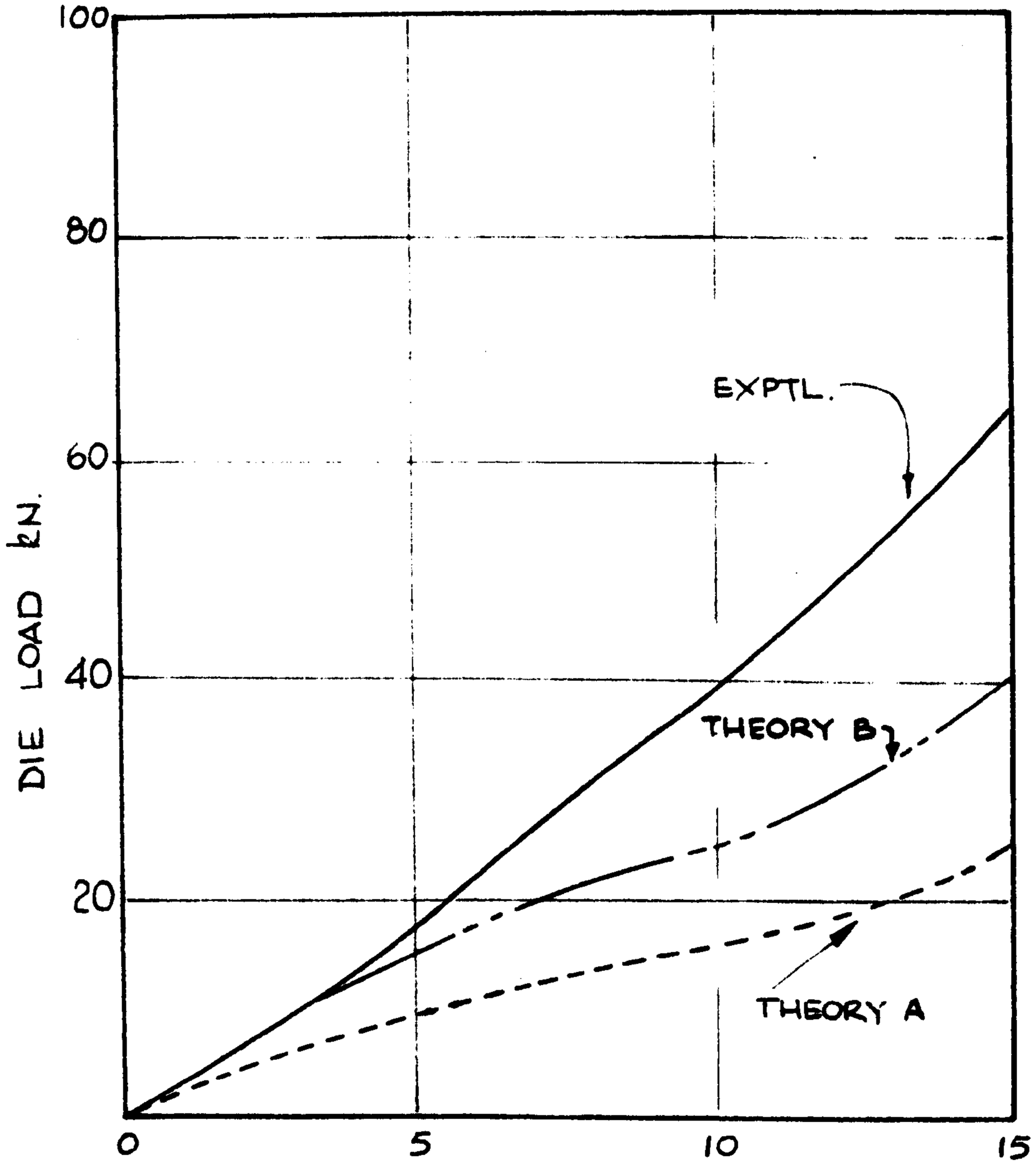

UPSETTING OF LEAD CYLINDER (LUBRICATED)

FIG. 25.

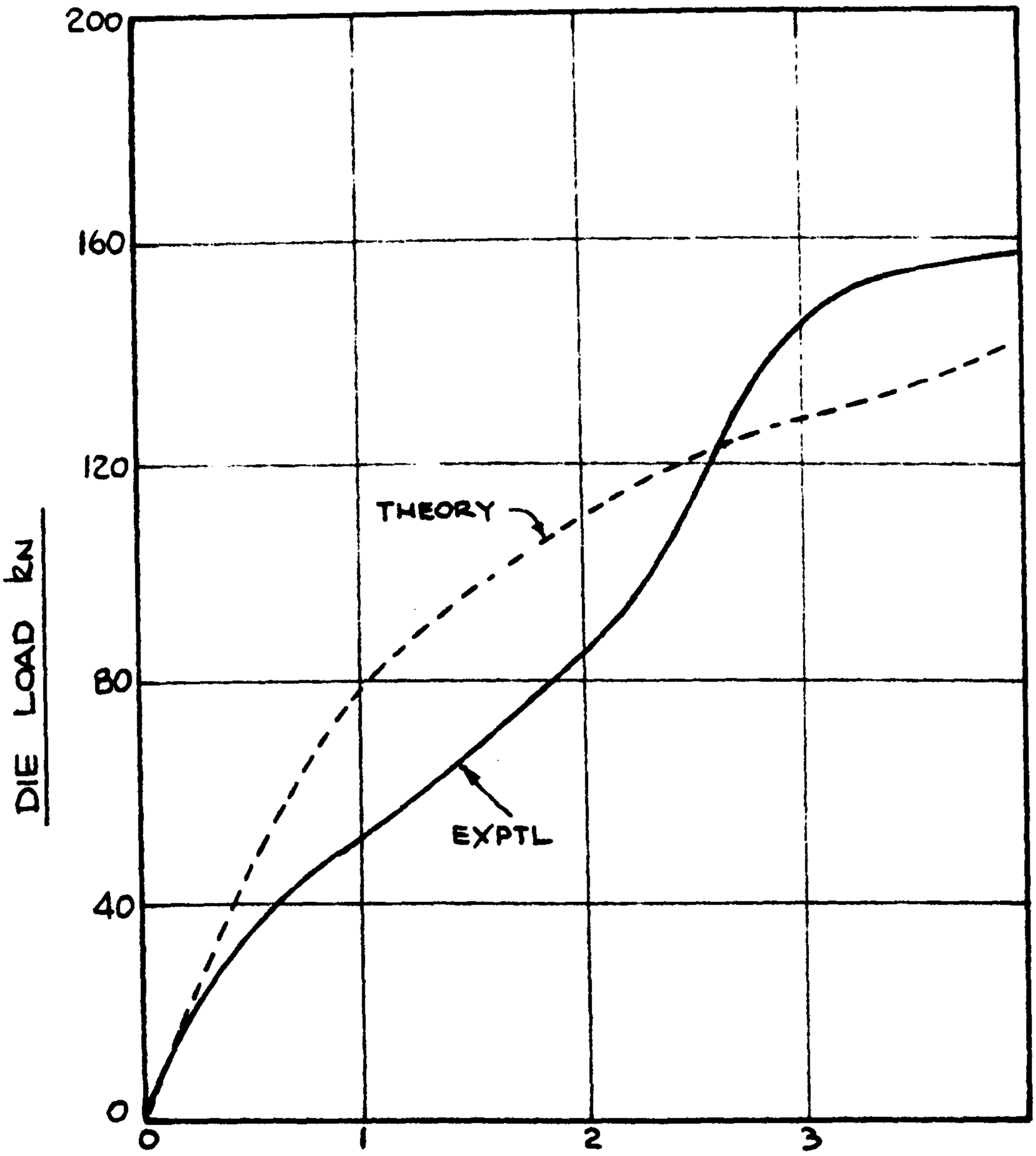

UPSETTING OF ALUMINIUM ALLOY CYLINDER (LUBRICATED)

FIG. 26.

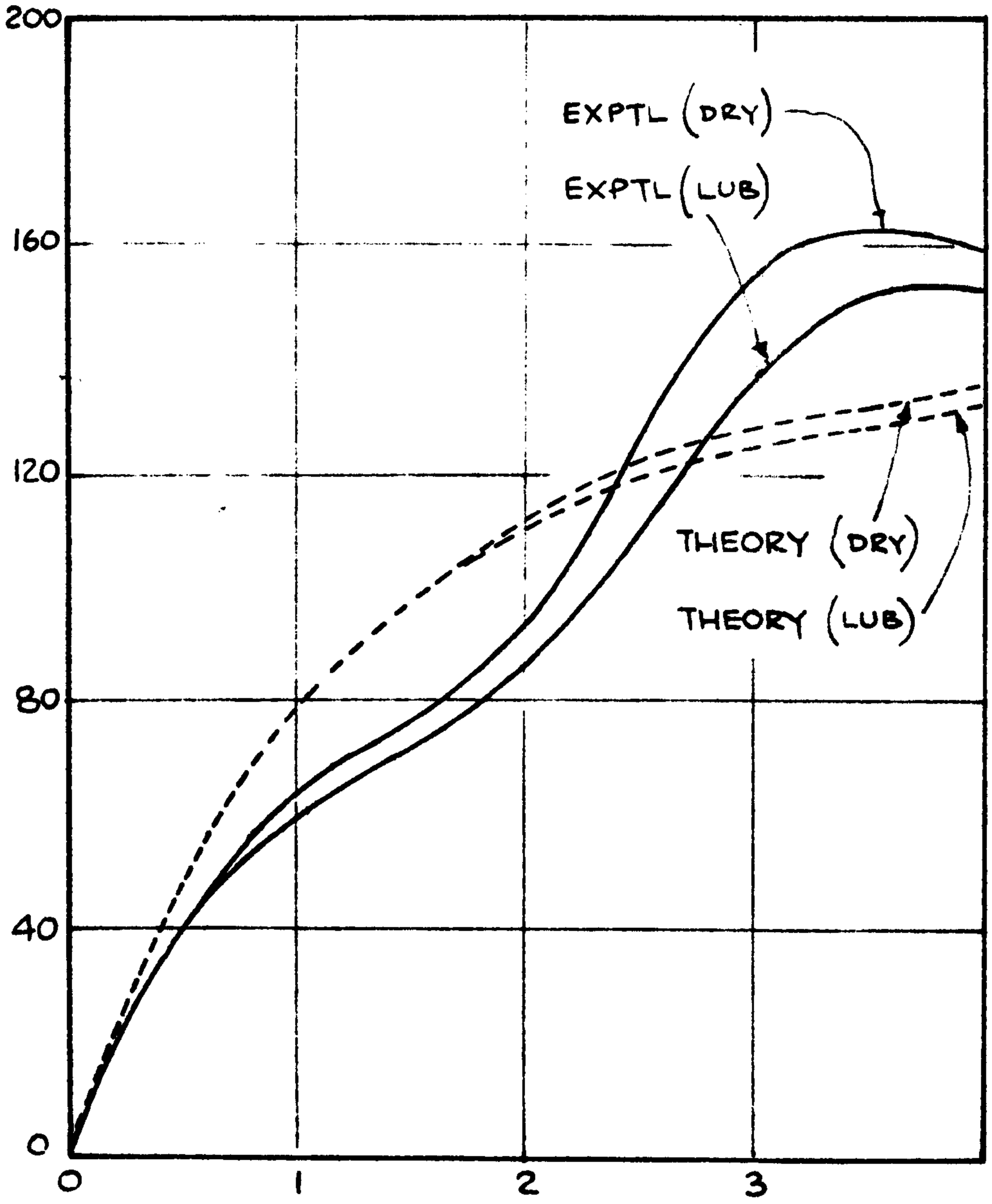

UPSETTING OF ALUMINIUM ALLOY CYLINDER DEFORMED UNDER LUBRICATED AND DRY TEST CONDITIONS.

FIG. 27.

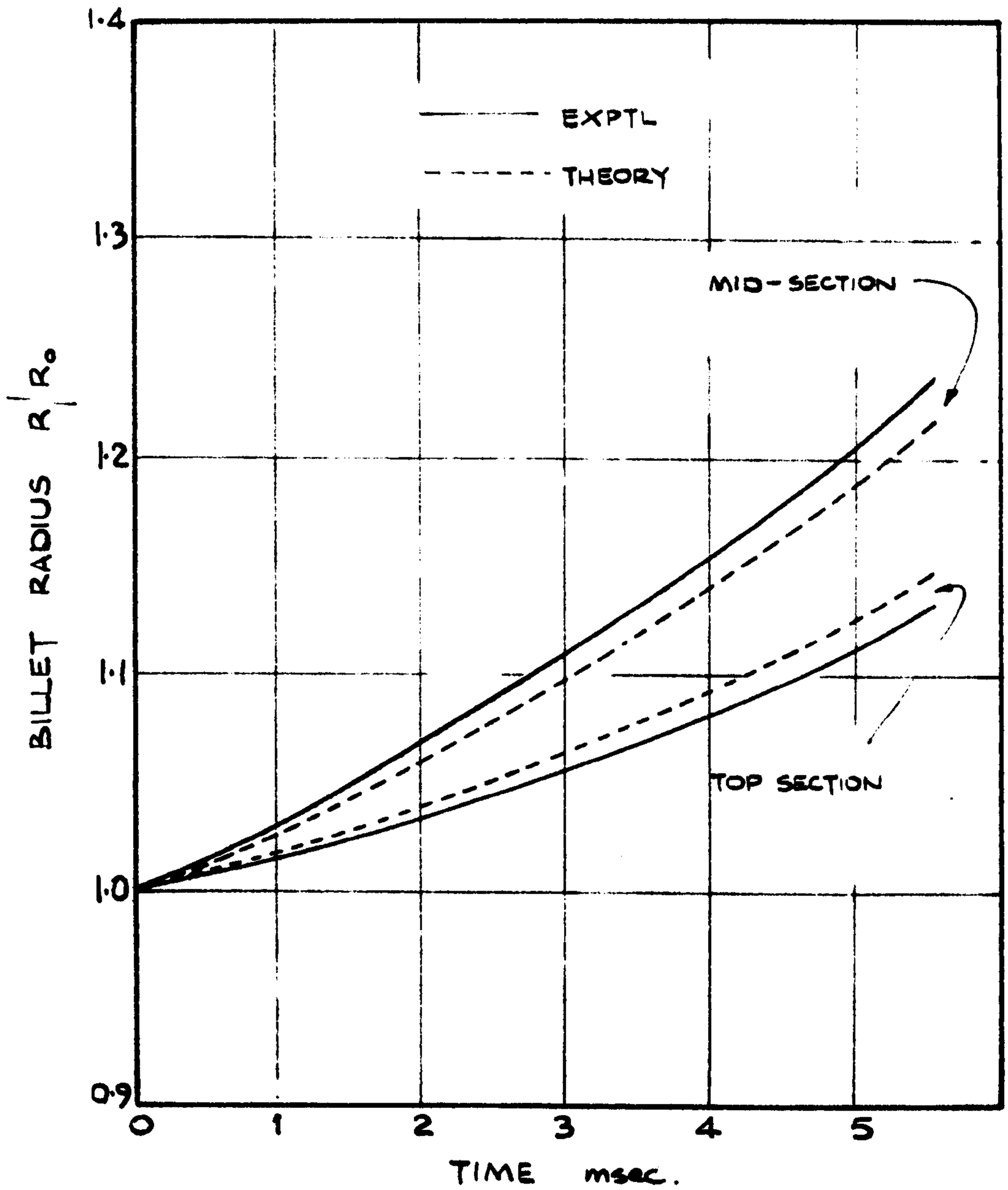

UPSETTING OF ALUMINIUM ALLOY CYLINDER UNDER DRY TEST CONDITIONS.

FIG. 28.

THEORETICAL CURVES

CURVE 'A' WITHOUT STRAIN RATE

CURVE 'B' WITH STRAIN RATE.

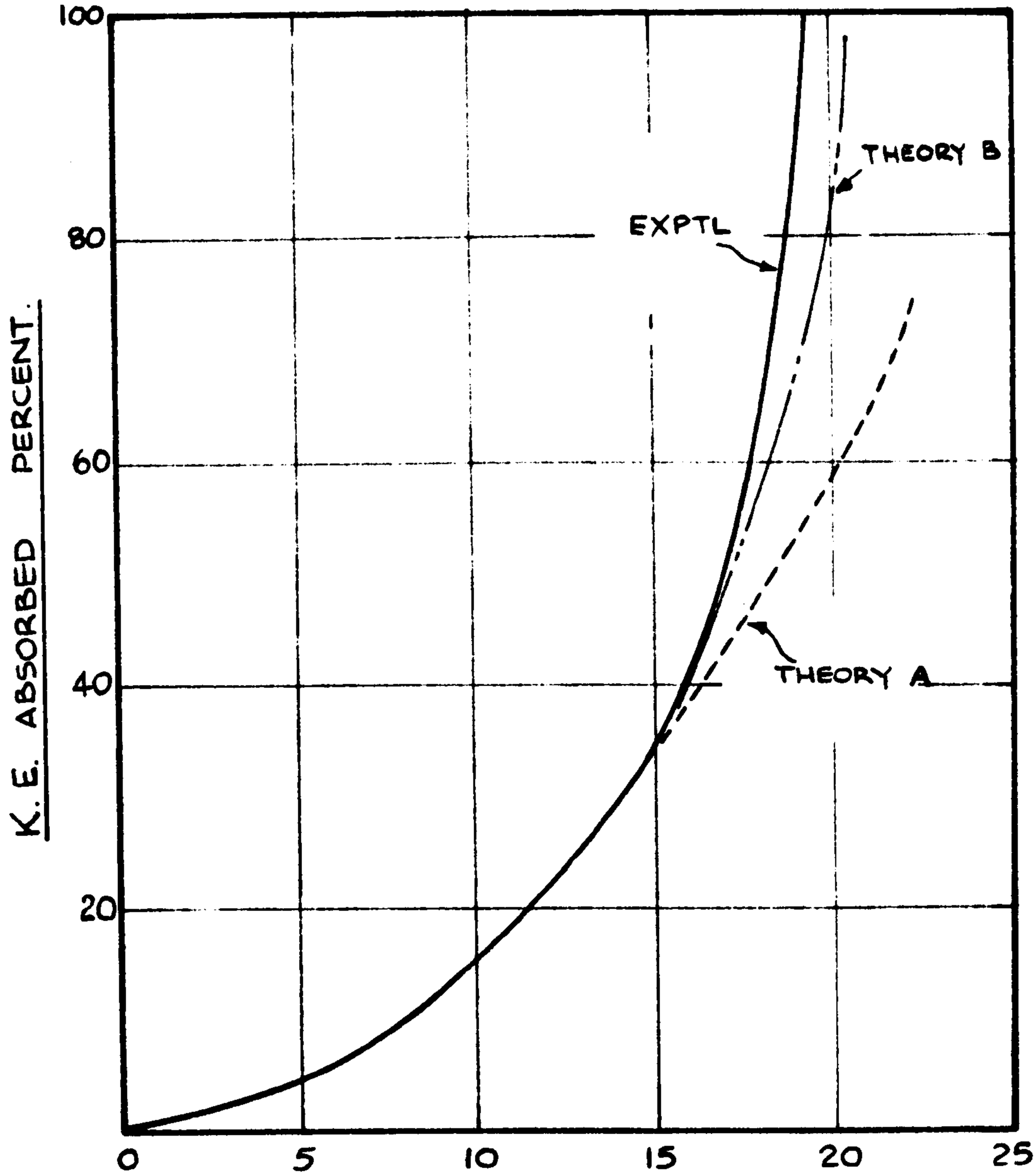

PERCENTAGE KINETIC ENERGY ABSORBED Vs. DEFORMATION CURVES FOR LEAD BILLETS DEFORMED UNDER LUBRICATED TEST CONDITIONS.

FIG. 29

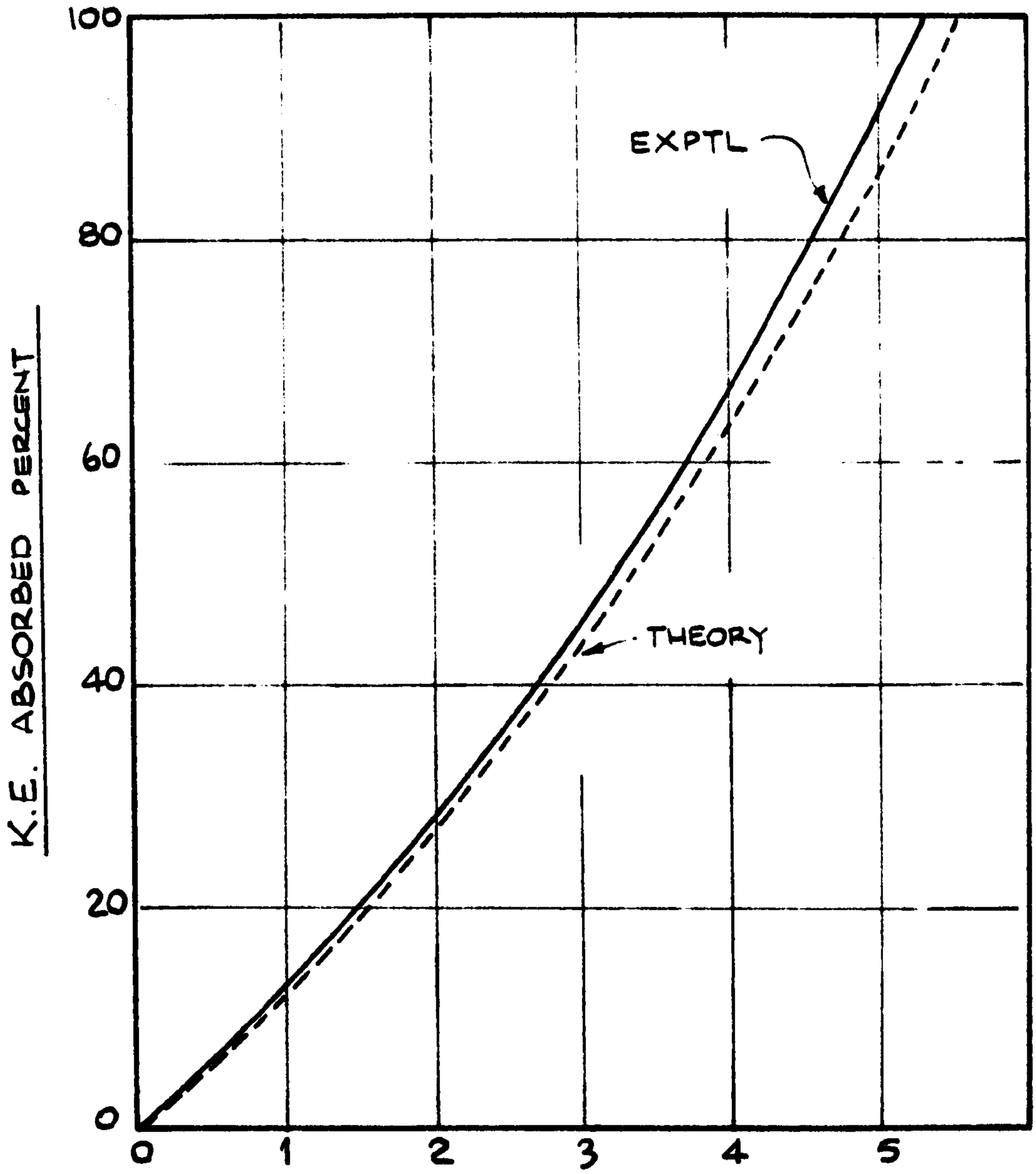

UPSETTING OF ALUMINIUM ALLOY CYLINDER UNDER LUBRICATED TEST CONDITIONS.

FIG. 30

THEORETICAL CURVES

CURVE 'A' WITHOUT STRAIN RATE.
CURVE 'B' WITH STRAIN RATE.

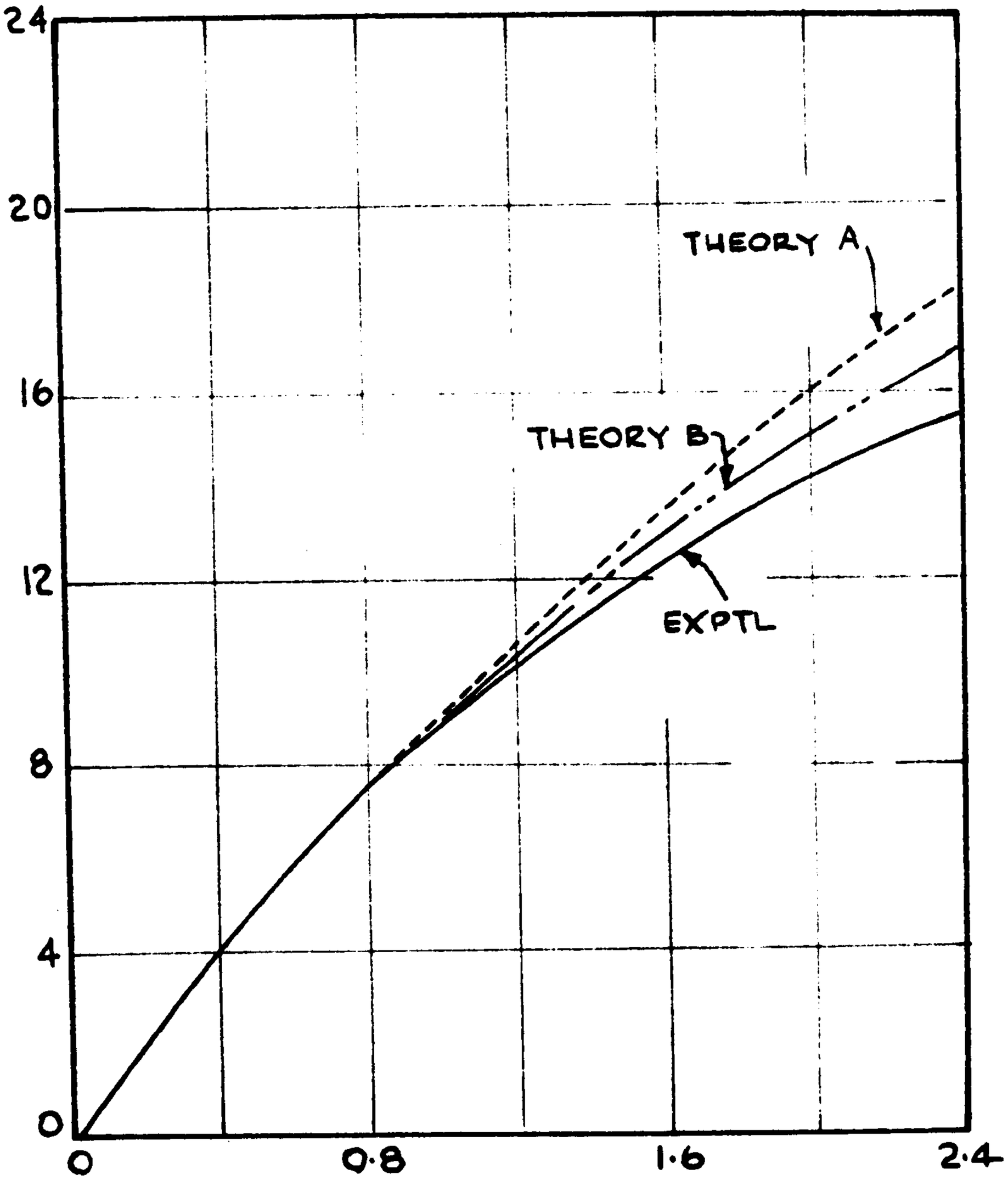

UPSETTING OF LEAD CYLINDER
(LUBRICATED)

FIG. 31

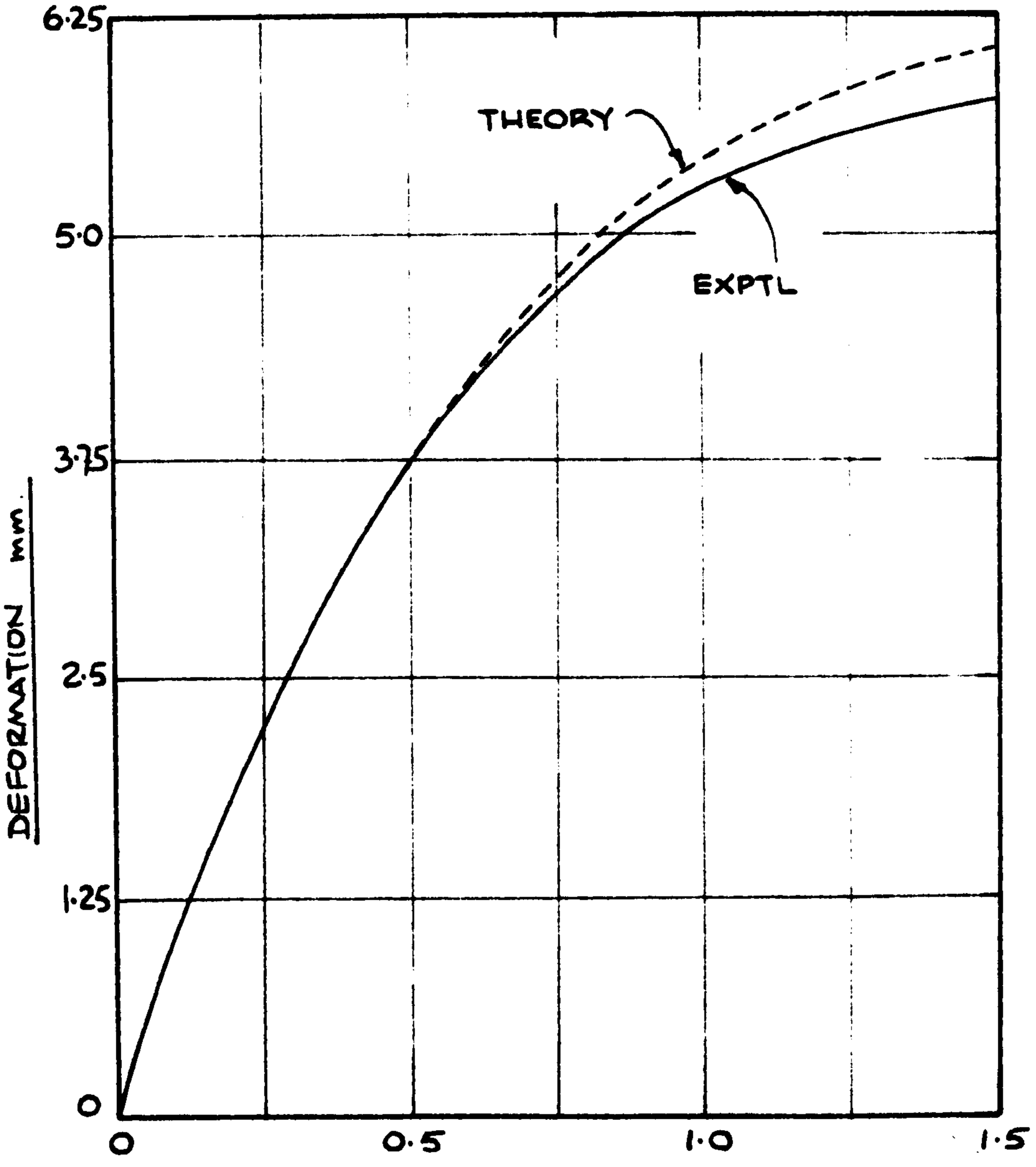

UPSETTING OF ALUMINIUM ALLOY CYLINDER (LUBRICATED)

FIG. 32

CHAPTER 5

CLOSED DIE FORGING

5.1 Introduction

Apart from upsetting tests on cylindrical billets closed die forming tests were also carried out using lead billets of 24 mm diameter and 46 mm in height. These were formed into axisymmetric shapes. Unlike simple upsetting it was not possible to photograph the deformation mode of the billet. The load time history was recorded and the impact velocity was measured. Tests were carried out under both dry and lubricated conditions.

5.2 Experimental Work

Experiments were conducted using the drop hammer. The tup was dropped from its highest position so that the velocity at impact reached its maximum value of 9 m/s. The actual loading configuration of the billet is shown in Fig. 33(a). Billet details are shown in Fig. 34.

Experimental results were obtained in terms of the load deformation history, final shape of the billet, kinetic energy and friction effects.

5.3 Theoretical Prediction

The numerical technique detailed in Chapter 3 was applied to predict theoretically the deformation mode for each loading situation. The finite-difference equivalent model of the actual loading situation is shown in Fig. 33(b). The stress strain properties shown in Fig. 11 were incorporated in the analysis.

The effects of material inertia and interface friction at the die-billet constraint were also taken into account. The die load, instantaneous billet profiles, die pressure and strain rate within the billet, for both the lubricated and dry friction condition, were predicted theoretically and compared with experimental results where appropriate. In the analysis, the friction factor for the dry friction condition was taken as unity whilst for the lubricated condition it was taken as zero along the die-billet interfaces. For shearing friction within the billet at the die-billet constraint the friction factor was again taken as unity to simulate sticking friction. Fig. 35 shows theoretically predicted instantaneous profiles at various times during the deformation process for a billet forged under lubricated condition. The instantaneous profiles for a billet forged under dry friction conditions are shown in Fig. 36. It was not possible to record the experimental instantaneous profiles due to the nature of the forming process. Therefore only the corresponding experimentally obtained final profiles are shown in these figures. It is clearly evident that forging under dry friction conditions gives rise to considerable barrelling of the billet during the development process. This causes the billet material to get into the flash land relatively earlier than under lubricated forging conditions.

5.4 Results and Discussions

In Fig. 37 the variation in forging loads with tup displacement measured experimentally are compared with those predicted theoretically for forging under lubricated and dry friction conditions. The effect of strain rate and material inertia on the forging load was found to be significant when the experimentally established dynamic stress strain properties shown in Fig.11 were incorporated in the analysis. The agreement between the theoretical and forging load under both frictional conditions show close agreement. Fig. 37 also shows the quasi-static forging load under dry friction conditions. This static load is seen to be considerably lower than both the experimental and theoretically predicted dynamic forging loads. This discrepancy may be explained by the apparent strain hardening of the lead, used for these experiments, under dynamic loading conditions. The instantaneous profiles in Fig. 35 and 36 showed barrelling of the billet in a qualitative manner. In Fig. 38 this is shown in a quantitative manner in terms of the variation in the billet radius at mid-section and at the die-billet constraints. It is clearly evident from this figure that forging under dry friction conditions causes the billet radius at mid-span to increase at a relatively faster rate with deformation than under lubricated forging conditions. This may result in appreciable loss of material as flash.

The theoretically predicted variation in strain rate at mid-section and at the section along the die-billet constraint is shown in Fig. 39 for lubricated and dry friction conditions. This figure shows that during most of the deformation process the maximum strain rate within the billet remains above about 200/sec for an impact velocity of 9 m/s and hence makes appreciable difference in the forging load even during the later stages of deformation.

Comparing the theoretically estimated die pressures with those obtained experimentally as shown in Fig.40. shows close agreement under both forging conditions. It is evident, however, that in the case of dry friction, the theoretically predicted die pressure is slightly greater than that obtained experimentally whilst this trend is reversed when a lubricant is used. The main reason for this behaviour could be the fact that for dry friction conditions the friction factor, taken as unity, was too high and that the use of graphite in petroleum jelly as a lubricant did not result in a friction factor of zero.

Feasibility tests were carried out on shapes involving the use of split dies, Fig. 41. Photographs showing the different shapes produced are shown in Fig. 42. These shapes have not been investigated analytically but could serve as a basis for further work.

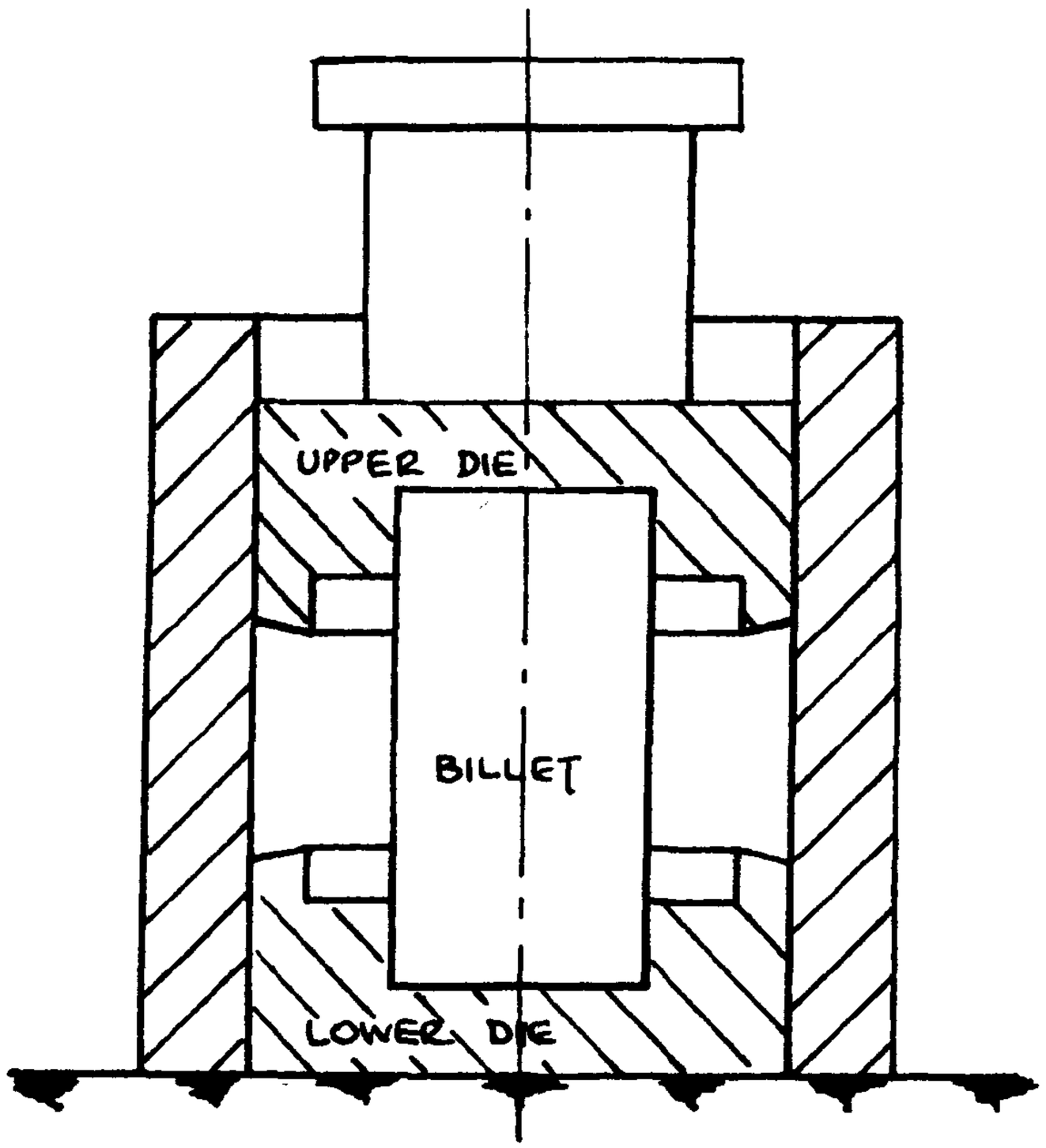

(a)

ACTUAL LOADING CONFIGURATION OF THE BILLET

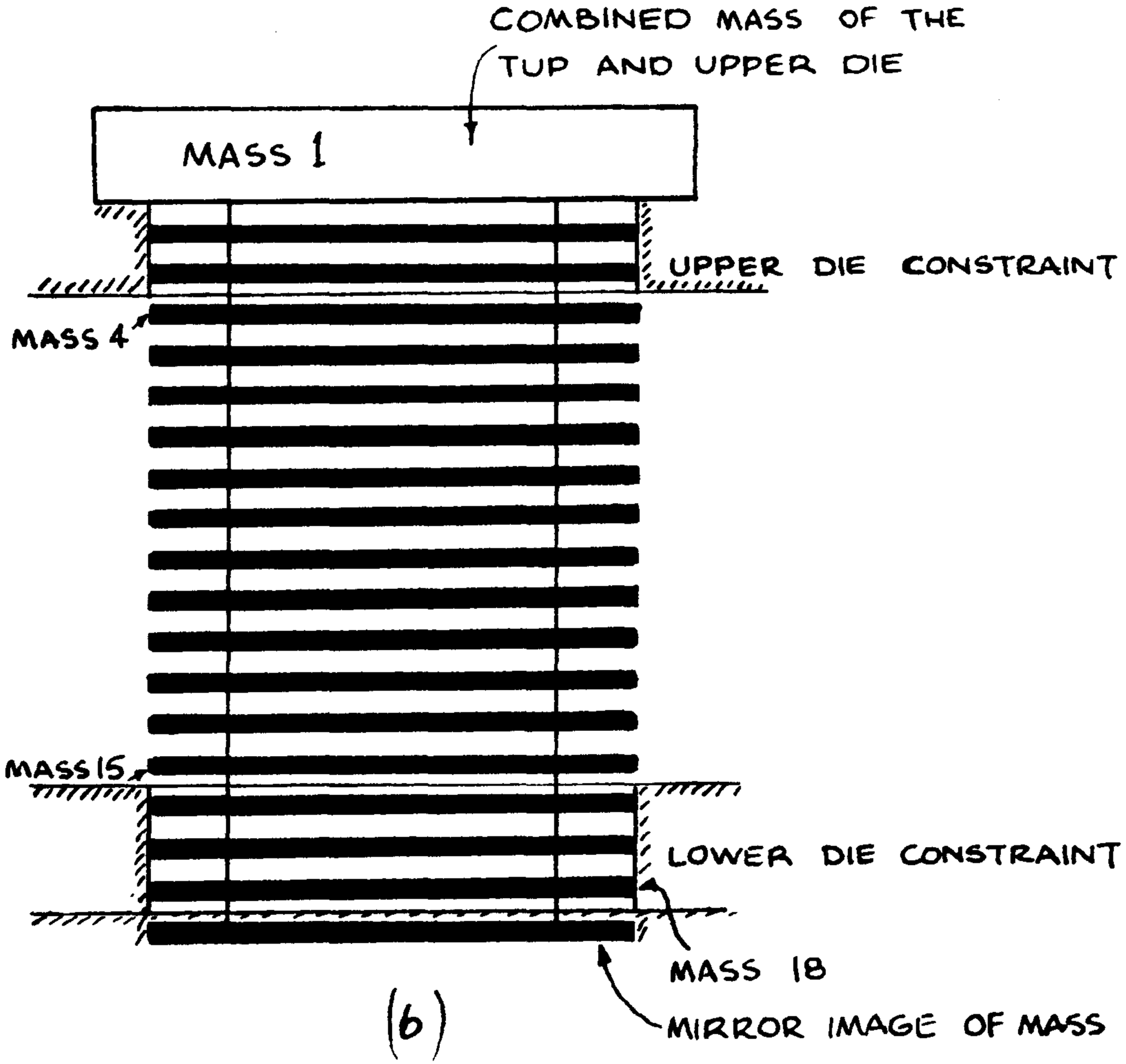

(b)

EQUIVALENT NUMERICAL MODEL

FIG. 33.

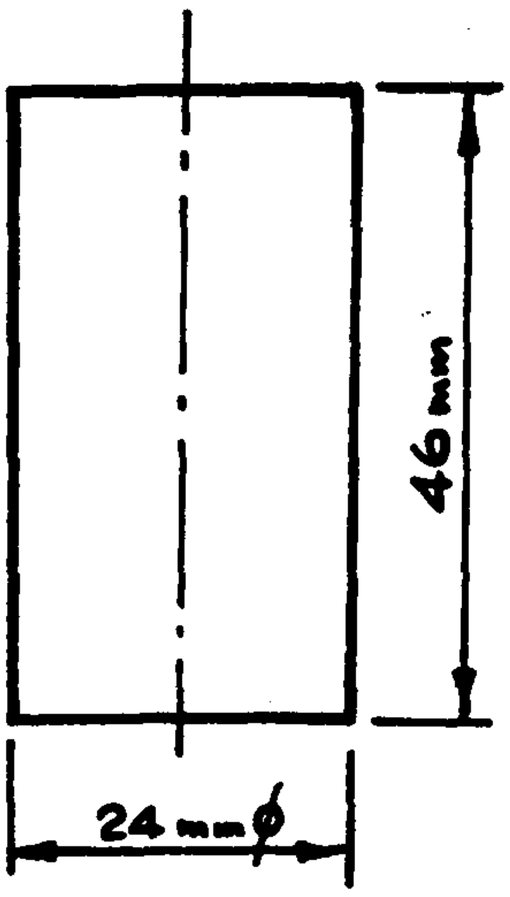

CYLINDRICAL LEAD BILLET

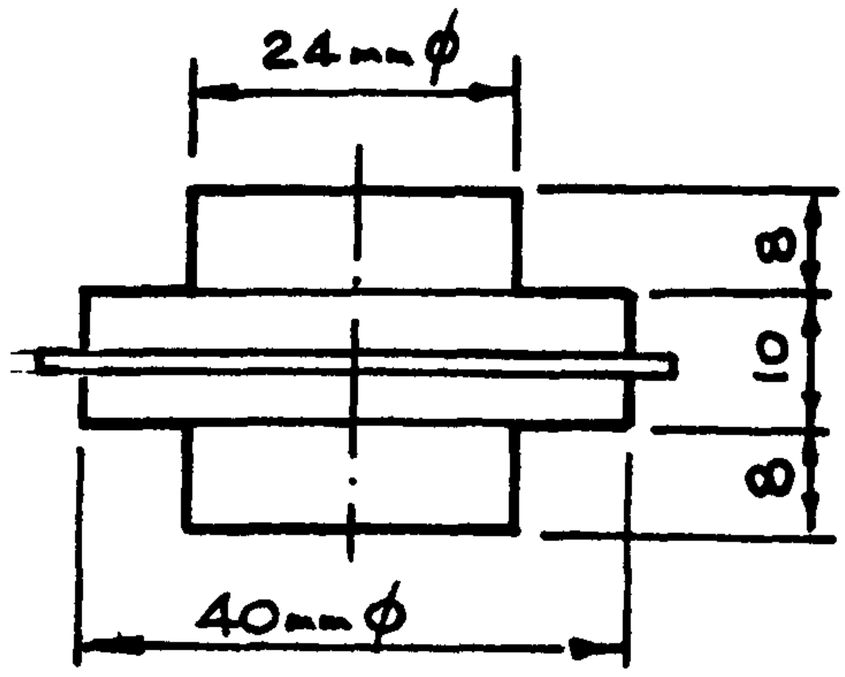

FINAL DEFORMED SHAPE

FIG. 34.

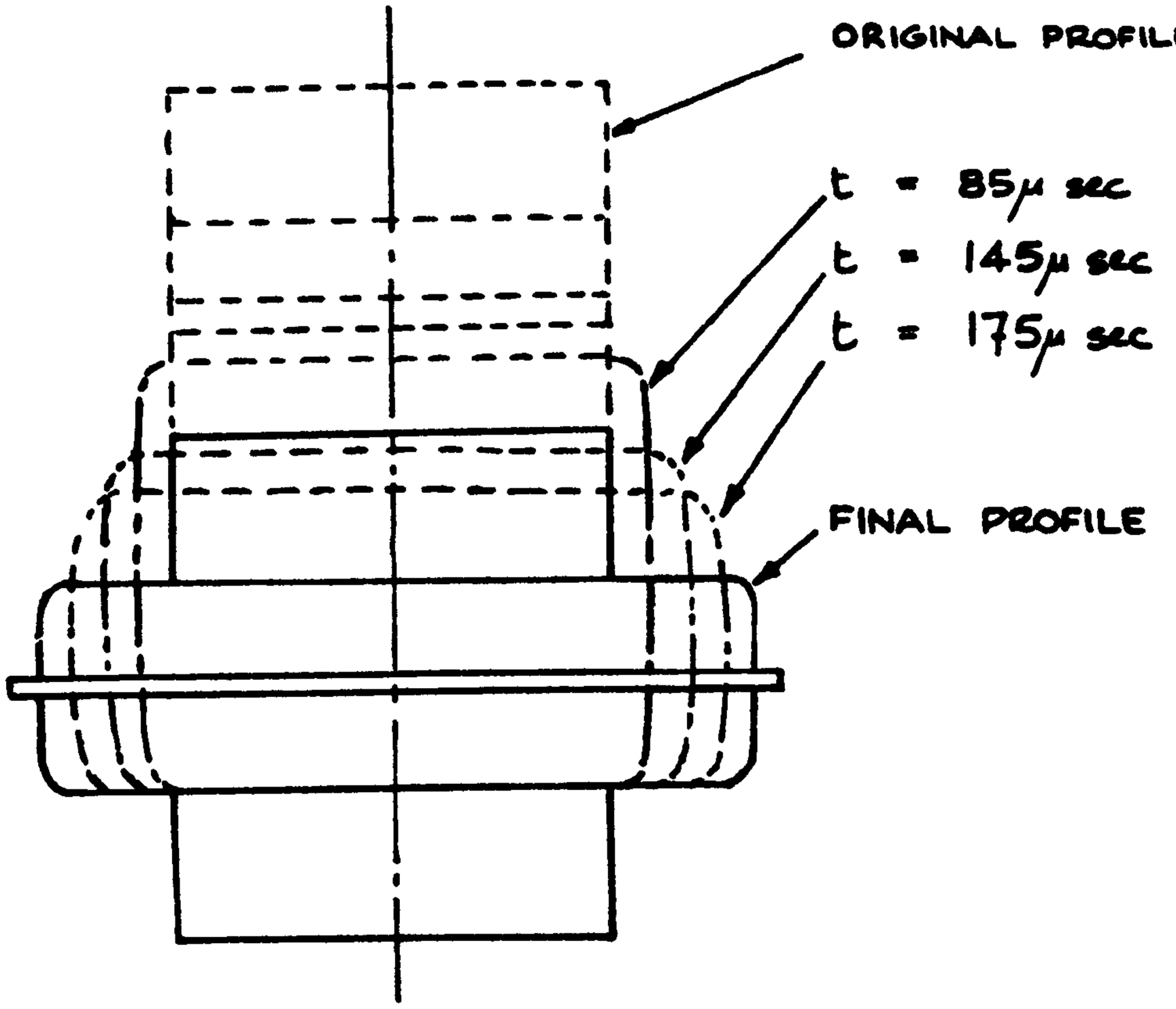

THEORETICALLY PREDICTED INSTANTANEOUS PROFILES UNDER LUBRICATED CONDITIONS.

FIG. 35

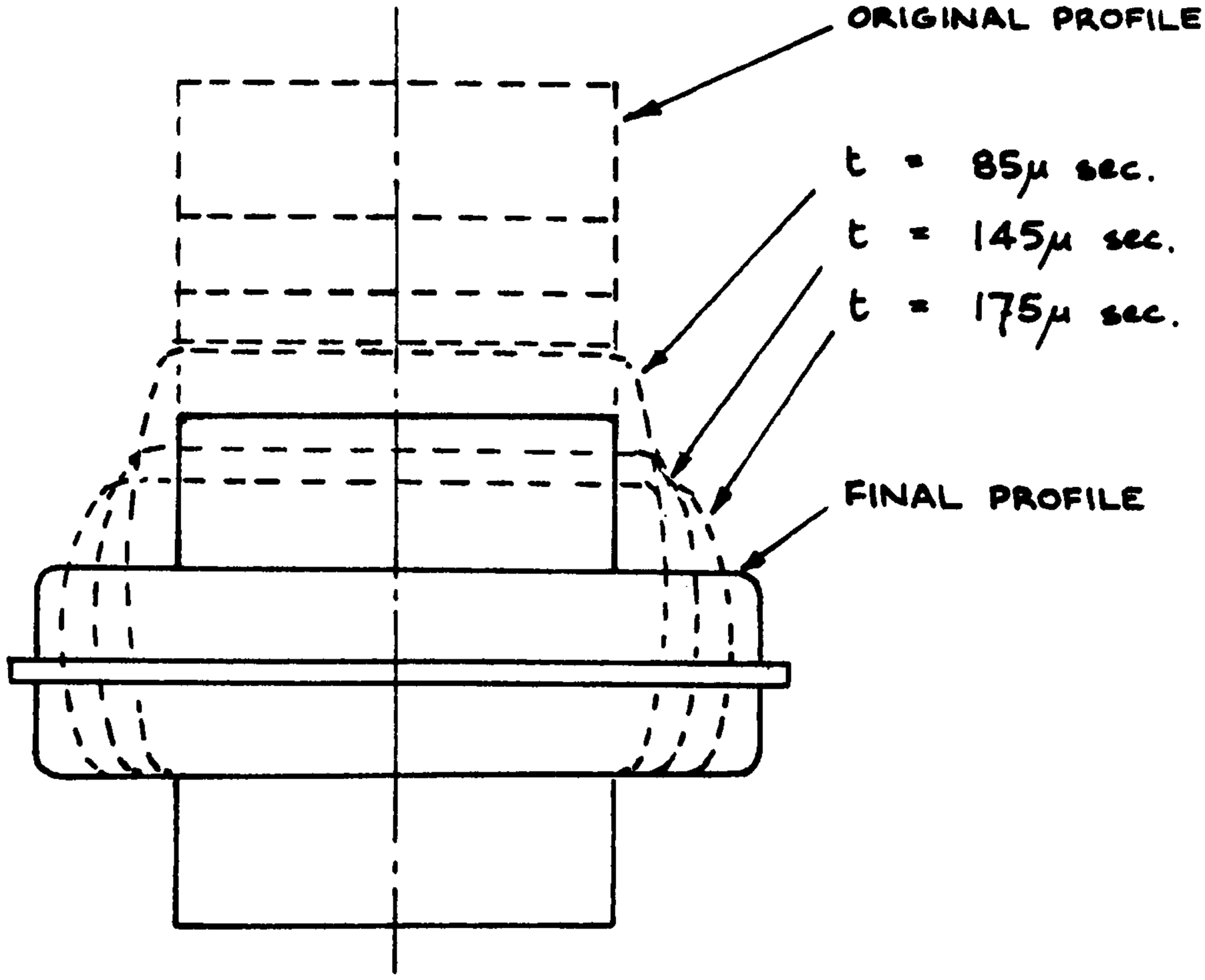

THEORETICALLY PREDICTED INSTANTANEOUS PROFILES UNDER DRY FRICTION CONDITIONS

FIG. 36

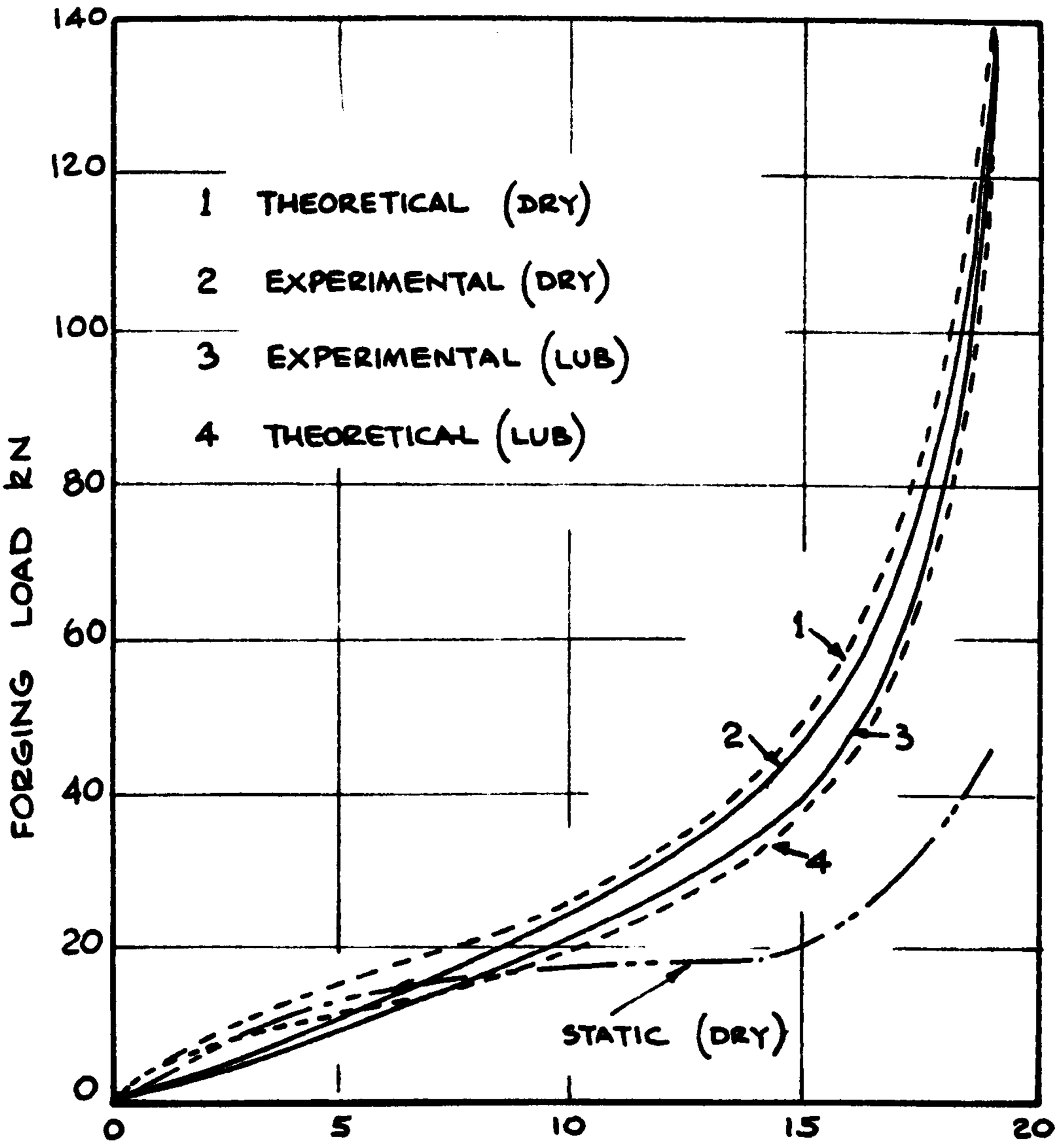

COMPARISON OF THEORETICAL AND EXPERIMENTAL FORGING LOAD Vs TUP-DISPLACEMENT CURVES.

FIG. 37

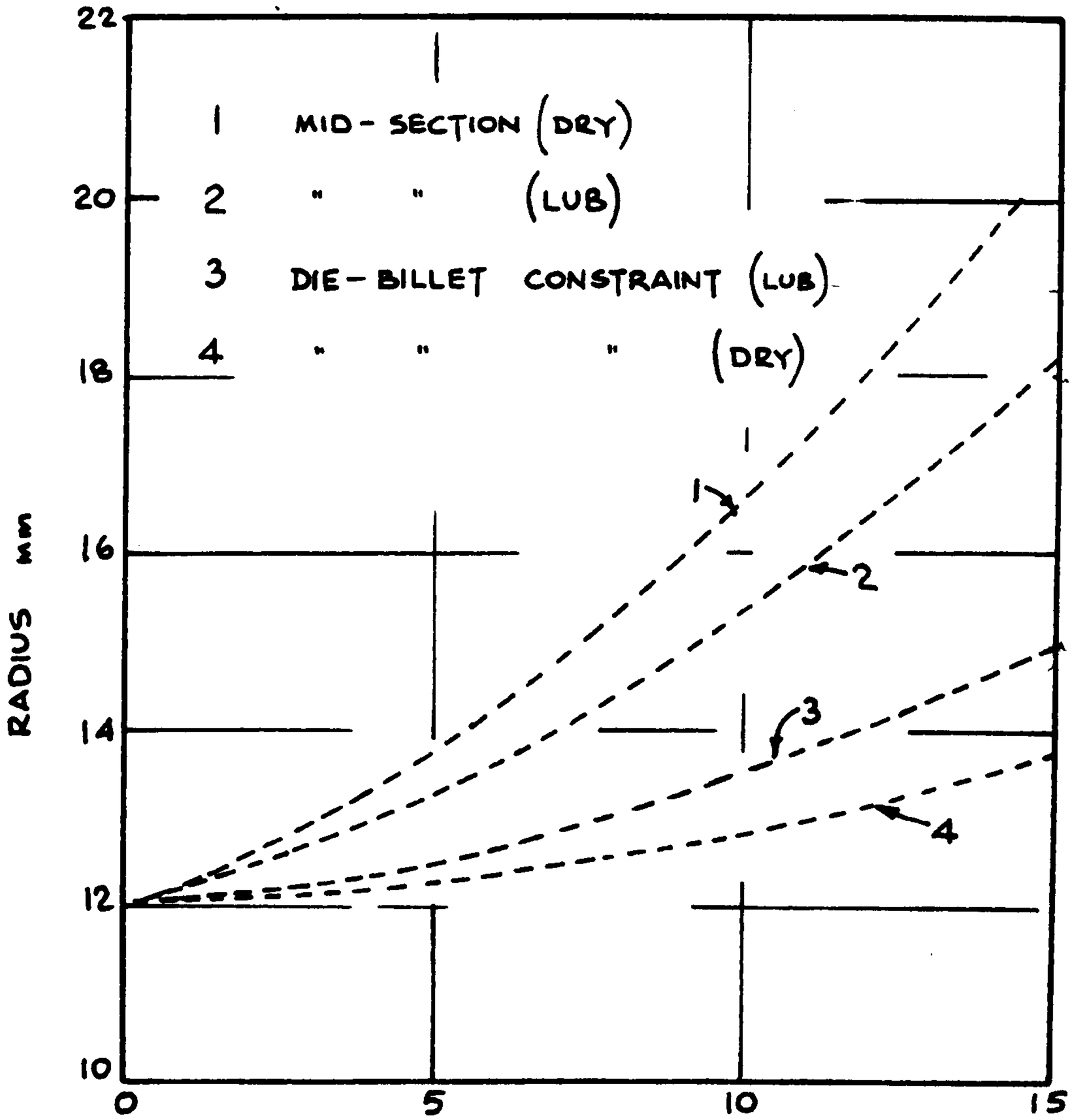

VARIATION IN BILLET RADIUS WITH TUP DISPLACEMENT AT MID-SECTION AND DIE-BILLET CONSTRAINT.

FIG. 38

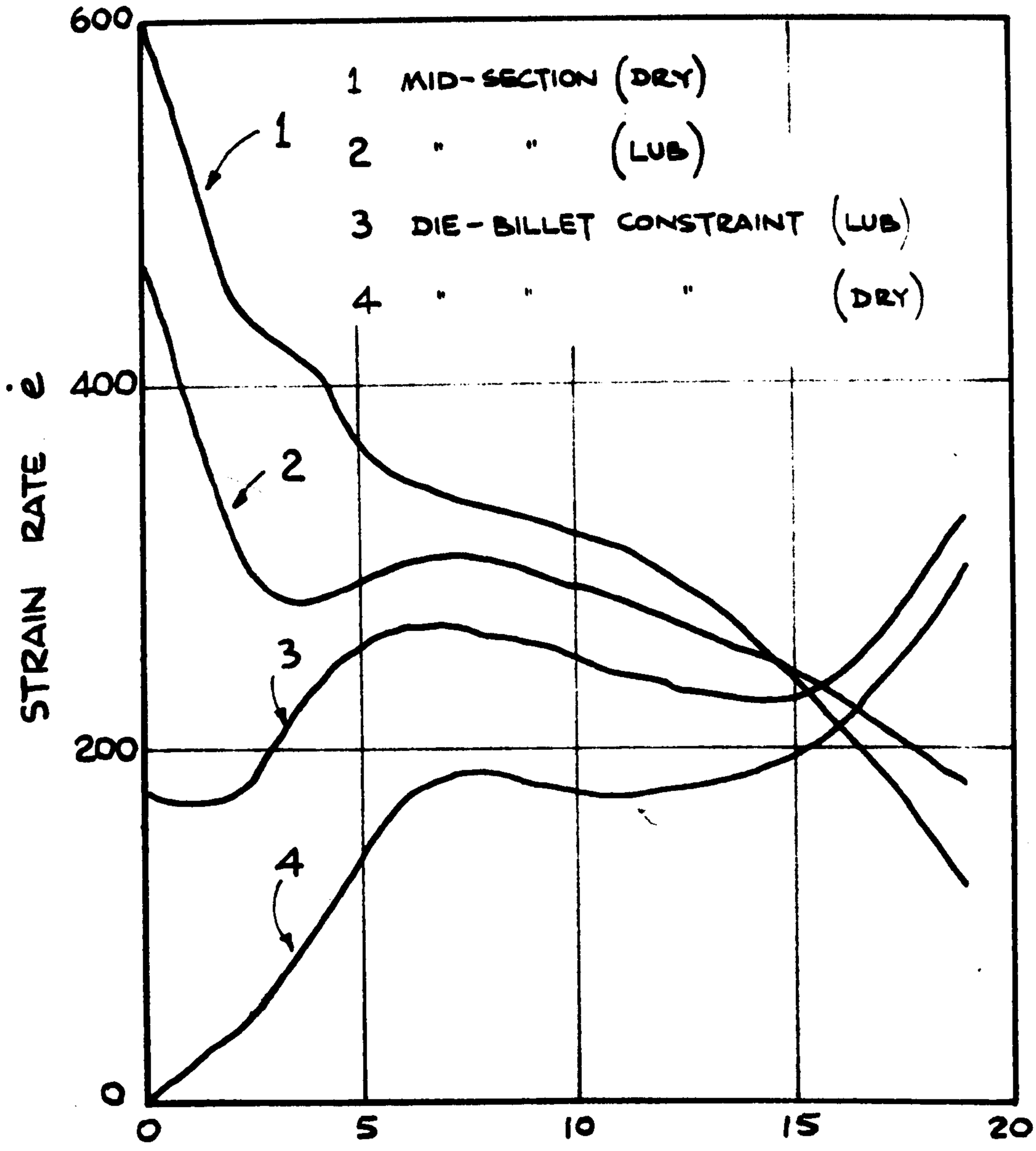

VARIATION IN STRAIN RATE WITH TUP DISPLACEMENT AT MID-SECTION AND DIE BILLET CONSTRAINT.

FIG. 39

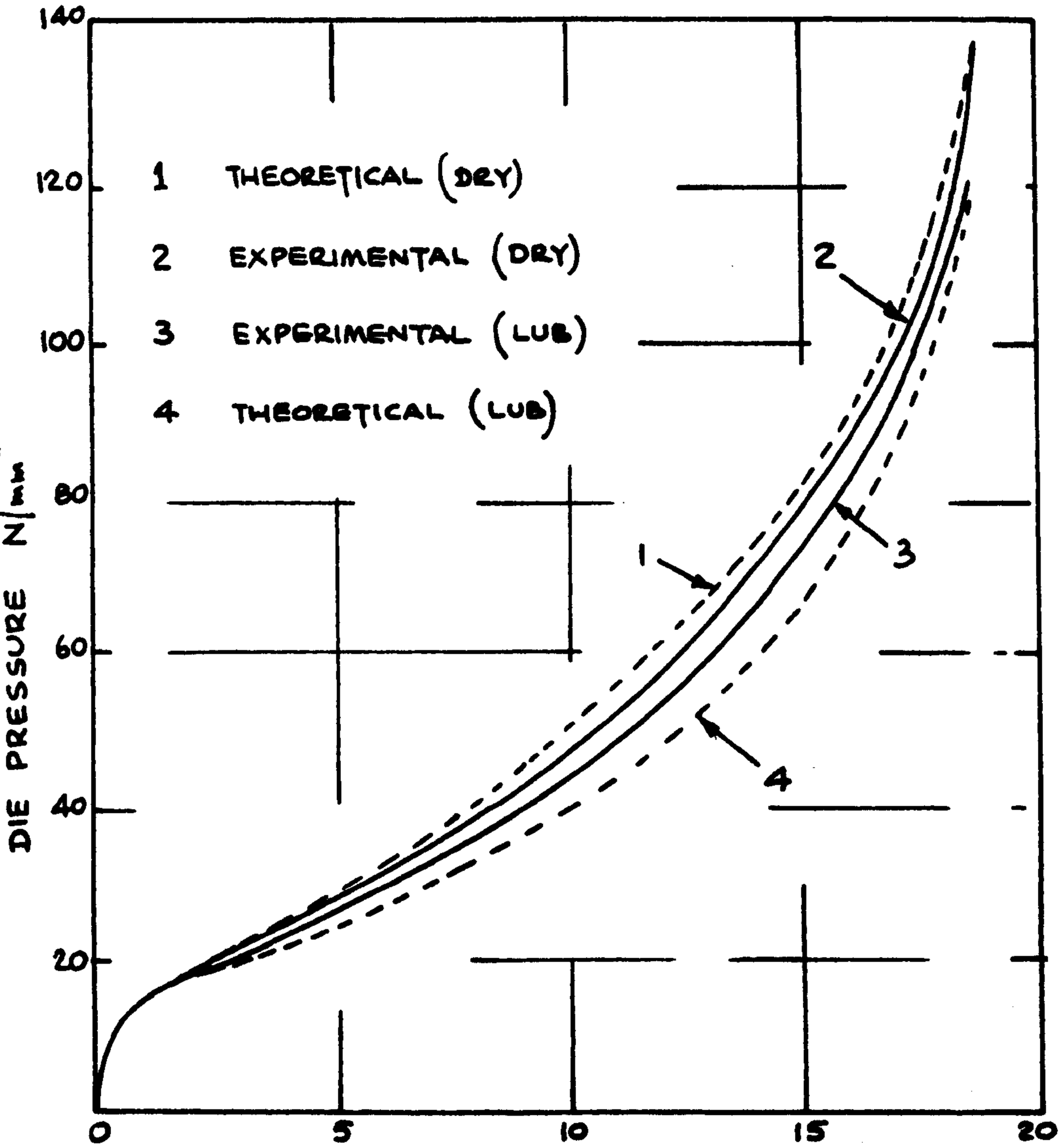

SHOWING DIE PRESSURE Vs TUP DISPLACEMENT CURVES PREDICTED THEORETICALLY AND OBTAINED EXPERIMENTALLY.

FIG. 40.

SPLIT DIES. FIG. 41

CLOSED DIE FORGINGS. FIG. 42.

CHAPTER 6

EXTRUSION FORGING

6.1 Introduction

In chapter 3 the mathematical model used was formulated to take into account forging conditions where the flow of metal during deformation was entirely radial. A more complex material flow situation is where flow is partly radial and partly axial ie. extrusion forging. In this chapter extrusion forging is analysed by assuming that the energy absorbed during deformation is used to deform the material plastically, while being strained axially, and at the same time shear energy is required as the boss is being formed.

A relevant analysis has been presented earlier in reference [61] in which the equations for predicting various parameters during extrusion forging were formulated based on an assumed velocity field. In this analysis attempts were taken to take into account the influence of billet and tool geometry speed and frictional conditions. However, the analysis, which appears to be very complex was derived on the basis of the assumption that the billet deformed in a purely cylindrical manner throughout the deformation period. Furthermore the frictional effect on the total height of the deformed specimen was found to be exaggerated and the correspondence between the theoretical and experimental shapes of the billet for deformations up to about 70% have never been demonstrated. This aspect of the product shape during the earlier stages

of deformation which shows significant deviation from the assumption of purely cylindrical deformation, should be taken into account in formulating an analysis.

In this work such an analysis has been attempted, initially under frictionless condition, which predicts the shape during the first 70% of the deformation which shows severe tapering of the flange during the deformation especially when the boss to billet ratio is more than 40%. Very good agreement between the theoretically predicted and experimentally observed flange shapes was predicted over a large range of boss to billet diameter ratios. This is thought to be the main contribution of this work towards the study of extrusion forging. Subsequently an attempt has been made to incorporate the effect of friction in the analysis in an approximate and simple manner, and has been outlined in Section 6.2.4.

In the analysis outlined in the following sections the deformation is shown to be in two stages. In the first stage deformation of the top surface begins when the applied load is just sufficient to cause local yielding of the billet. This yielding causes the top surface to spread radially while the lower portion of the billet retains its original radial dimension. However the lower portion of the billet begins to expand radially when the applied load is large enough to cause yielding in that area. This

marks the beginning of the second stage. At the end of the first stage the overall depth at which plastic yielding occurs is shown to be equal to half the boss diameter.

From the commencement of the second stage any increase in load causes deformation such that axial compression becomes directly related to a simultaneous increase in the billet diameter.

Equations have been derived which enabled the tup load, total energy absorbed, boss and flange heights and profile of the deformed billet to be calculated.

6.2 Analysis under Frictionless Conditions

SYMBOLS

D	billet diameter at depth h
H	depth *
k	shear yield stress = ($\frac{\tau}{2}$ for Tresca Yield Criterion)
K	constant
Y	yield stress
h	axial depth *
w	plastic work done per unit volume
D_B	billet diameter
D_C	boss diameter
P_H	load at depth H
P_O	load required to initiate formation of boss
W_S	shear work done
W_P	plastic work done
W_T	total work done
H_1	depth of shear zone
H_2	depth of flange taper
H_0	depth of plastic yield zone
L_0	original length of billet
h_0	depth of flange taper
h_1	flange dimension *
h_2	depth of flange with constant diameter
x_1	axial displacement
H'	depth *
D'_B	bottom diameter of flange
P'_H	load *
ε	true strain

* defined in text

6.2.1 First Stage

In formulating the equations it is assumed that the material of the billet is rigid perfectly plastic with a yield stress Y. Referring to Fig. 43 D_B is the diameter of the billet, D_C is the diameter of the die cavity and L_o is the height of the undeformed billet. Let P_o be the load which is just sufficient to initiate plastic deformation to the ring area of the billet. Thus:

$$P_o = \frac{\pi}{4}Y(D_B^2 - D_C^2) \qquad (1)$$

Let P be the applied load which is greater than P_o and which is sufficient just to cause plastic yielding to the ring area at a location H_o. At any other intermediate location the compressive load available to deform the ring area is given by:

$$P_H = P_o + \pi D_C kH \qquad (2)$$

where H is the distance as shown in Fig. 43 and k is the shear yield stress of the material which may be taken as equal to Y/2. Substituting for k in equation (2) we have

$$P_H = P_o + \frac{\pi}{2}D_C YH \qquad (3)$$

when $H = H_o$ (denoting the top contact surface), P_H is simply given by the applied force P. Thus

$$P = P_o + \frac{\pi}{2}D_C YH_o \qquad (4)$$

which upon substitution for P_o becomes

$$P = \frac{\pi}{4}Y(D_B^2 - D_C^2) + \frac{\pi}{2}D_C Y H_o \qquad (5)$$

when P reaches a value P_1 which is sufficient to cause plastic yielding of the billet as a whole, then

$$P = P_1 = \frac{\pi}{4}D_B^2 Y \qquad (6)$$

substituting for P in equation (5) we get

$$\frac{\pi}{4}D_B^2 Y = \frac{\pi}{4}(D_B^2 - D_C^2)Y + \frac{\pi}{2}D_C Y H_o$$

which upon rearrangement and simplification gives the depth, H_o, of the plastically yielded zone before the billet starts to deform, thus:

$$H_o = D_C/2 \qquad (7)$$

Hence during the first stage of deformation, the plastic zone will extend to a depth equal to half the diameter of the boss.

Assuming that the billet deforms under the action of P in the manner shown in Fig (43), let an element at a location H before deformation correspond to an element at a location h of the deformed billet. P_H will thus be the load just sufficient to deform plastically the new element of outer diameter D. Thus:

$$P_H = \frac{\pi}{4}Y(D^2 - D_C^2) \qquad (8)$$

Substituting for P_H in equation (3) and noting that $P_o = \frac{\pi}{4}Y(D_B^2 - D_C^2)$ and $k = \frac{Y}{2}$ we get,

$$\frac{\pi}{4}Y(D^2 - D_C^2) = \frac{\pi}{4}Y(D_B^2 - D_C^2) + \frac{\pi}{2}YD_CH$$

which upon simplification and rearrangement becomes:

$$H = (D^2 - D_B^2)/2D_C \qquad (9)$$

Equation (9) gives the relationship between the diameter of the deformed shape and the parameter H which locates the position of the element of the undeformed billet. During this first stage of deformation the total work done may be expressed in terms of the plastic work and shear work done in the billet.

The plastic work per unit volume may be given by:

$$w = \int_0^{\varepsilon} \sigma d\varepsilon \qquad (10)$$

since for a rigid plastic material

$$\sigma = Y \text{ (constant)}$$

hence, $w = Y\varepsilon$, which for the small element of original thickness 'dH' becomes:

$$w = Y\ln(\frac{dH}{dh}) \qquad (11)$$

Plastic work done on the element is thus given by

$$w_d = dVY\ln(\frac{dH}{dh})$$

where dV is the volume of the element.

Thus

$$w_d = \frac{\pi}{4}(D^2 - D_C^2)dhY\ln(\frac{dH}{dh}) \quad \text{(12)}$$

Total work done on the outer sleeve

$$p = \frac{\pi}{4}Y\int_o^{h_o}(D^2 - D_C^2)\ln(\frac{dH}{dh})dh \quad \text{(13)}$$

From volume constancy of the element

$$dH(D_B^2 - D_C^2) = dh(D^2 - D_C^2)$$

$$\text{or } \frac{dH}{dh} = \frac{D^2 - D_C^2}{D_B^2 - D_C^2} \quad \text{(14)}$$

and

$$dh = dH(\frac{D_B^2 - D_C^2}{D^2 - D_C^2}) \quad \text{(15)}$$

so that combining equations (13), (14) and (15)

$$W_p = \frac{\pi}{4}Y\int_o^{H_o}(D^2 - D_C^2)\ln(\frac{D^2 - D_C^2}{D_B^2 - D_C^2})x(\frac{D_B^2 - D_C^2}{D^2 - D_C^2})dH$$

or

$$W_p = \frac{\pi}{4}\int_o^{H_o}(D_B^2 - D_C^2)\ln(\frac{D^2 - D_C^2}{D_B^2 - D_C^2})dH \quad \text{(16)}$$

From equation (9)

$$H = (D^2 - D_B^2)/2D_C \quad \text{(17)}$$

$$\text{or } \frac{dH}{dD} = \frac{2D}{2D_C}$$

and

$$dH = \frac{D}{D_C}dD \quad \text{(18)}$$

Combining equations (18) and (16)

$$W_p = \frac{\pi}{4}Y\int_{D_B}^{D_1}(D_B^2 - D_C^2)\ln(\frac{D^2 - D_C^2}{D_B^2 - D_C^2})\frac{D}{D_C}dD$$

or

$$W_p = \frac{\pi}{4}Y\left(\frac{D_B^2 - D_C^2}{D_C}\right)\left[\int_{D_B}^{D_1} \ln(D^2 - D_C^2)DdD - \int_{D_B}^{D_1} \ln(D_B^2 - D_C^2)DdD\right] \text{———} (19)$$

Now the integral:

$$\int_{D_B}^{D_1} \ln(D_B^2 - D_C^2)D.dD = \ln(D_B^2 - D_C^2)\left(\frac{D_1^2 - D_B^2}{2}\right)$$

——— (20)

and the integral

$$\int_{D_B}^{D_1} \ln(D^2 - D_C^2)DdD \text{———————————} (21)$$

may be carried out as follows:

let $\ln(D^2 - D_C^2) = Z$

$$\therefore \quad D^2 - D_C^2 = e^Z$$

$$\text{or} \quad \frac{dZ}{dD} = \frac{2D}{D^2 - D_C^2}$$

$$\text{hence } DdD = \left(\frac{D^2 - D_C^2}{2}\right)dZ = \frac{e^Z}{2}\,dZ$$

Back substitution into equation (21) and integrating we have:

$$\tfrac{1}{2}\int_{D_B}^{D_1} Ze^Z dZ = \frac{e^Z}{2}(Z - 1)$$

hence

$$\int_{D_B}^{D_1} \ln(D^2 - D_C^2)DdD = \tfrac{1}{2}\left[(D^2 - D_C)\{\ln(D^2 - D_C^2) - 1\}\right]_{D_B}^{D_1}$$

$$= \tfrac{1}{2}\left[(D^2 - D_C^2)\{\ln(D_1^2 - D_C^2) - 1\}\right] - \tfrac{1}{2}\left[(D_B^2 - D_C^2)\{\ln(D_B^2 - D_C^2) - 1\}\right] \text{——(22)}$$

combining equations (19), (20) and (22)

$$W_p = \frac{\pi}{4}Y\left(\frac{D_B^2 - D_C^2}{2D_C}\right)[(D_1^2 - D_C^2)\{\ln(D_1^2 - D_C^2) - 1\} -$$

$$(D_B^2 - D_C^2)\{\ln(D_B^2 - D_C^2) - 1\} - (D_1^2 - D_B^2)$$

$$\ln(D_B^2 - D_C^2)]$$

which after simplification and rearrangement becomes

$$W_p = [(D_1^2 - D_C^2)\{\ln(D_1^2 - D_C^2) - 1 - \ln(D_B^2 - D_C^2)\} +$$

$$(D_B^2 - D_C^2)]\frac{\pi}{4}Y\left(\frac{D_B^2 - D_C^2}{2D_C}\right) \qquad (23)$$

The shear work done along the interface of the outer sleeve and inner core material gives:

$$W_S = \frac{\pi}{2}D_C\frac{Y}{2}(H_o - x_o)x_o \qquad (24)$$

Total work done

$$W_T = W_P + W_S$$

The total work done by the **tup** load = average tup load x displacement

$$\left(\frac{P_o + P_1}{2}\right)x_o = W_P + W_S \qquad (23b)$$

When the tup load reaches P_1

$$P_1 = \frac{\pi}{4}(D_1^2 - D_C^2)Y = \frac{\pi}{4}D_B^2 Y$$

which gives the diameter of the billet at the tup interface. Thus,

$$D_1 = \sqrt{D_B^2 + D_C^2}$$

To determine the shape of the billet profile at the end of the first stage of deformation we have, from equation (15)

$$dh = dH\frac{(D_B^2 - D_C^2)}{(D^2 - D_C^2)} \qquad (24)$$

let $(D^2 - D_C^2) = Z$

then $DdD = \frac{dZ}{2}$ (25)

from equation (18)

$$DdD = D_C dH \qquad (26)$$

combining equations (24), (23) and (26)

$$dh = \frac{DdD}{D_C}\left(\frac{D_B^2 - D_C^2}{Z}\right)$$

$$dh = \left(\frac{D_B^2 - D_C^2}{2D_C}\right)\frac{dZ}{Z}$$

$$dh = K\frac{dZ}{Z} \qquad (27)$$

where $K = \left(\frac{D_B^2 - D_C^2}{2D_C}\right)$

integrating equation (27)

$$h + C = K\ln(D^2 - D_C^2)$$

when $h = 0$, $C = K\ln(D_B^2 - D_C^2)$

hence $h = K\ln(D^2 - D_C^2) - K\ln(D_B^2 - D_C^2)$ (28)

6.2.2 Second Stage

During this stage, any increase in load will cause deformation such that the outer sleeve will be compressed axially with a simultaneous increase in the billet diameter.

Let the load P be greater than P_1 such that

$$P = \frac{\pi}{4}(D_B')^2 Y \qquad (29)$$

where D_B' is the expanded billet diameter at the lower end. Equation (5) is equally applicable to this new situation. Thus

$$P_H' = \frac{\pi}{4}Y(D_B'^2 - D_C^2) + \frac{\pi}{2}D_C Y H' \qquad (30)$$

where H' locates an element of the deformed sleeve as shown in Fig. 44.

In this case, at $H' = H_1$, $P_{H'} = P$

so that $P = \frac{\pi}{4}Y(D_B'^2 - D_C^2) + \frac{\pi}{2}D_C Y H_1$ (31)

By combining equations (29) and (31) it can be seen that

$$H_1 = \frac{D_C}{2} \qquad (32)$$

Thus the shear zone is extended axially by an amount H_1 and the lower part of the billet, of height $(L_1 - H_1)$, will deform in a pure compression mode.

For an axial compression of x_1 the shear zone changes from H_1 to H_2. Thus the axial strain

$$\varepsilon = \ln\left(\frac{L_1}{L_1 - x_1}\right) = \ln\left(\frac{H_1}{H_2}\right) \qquad \text{(32a)}$$

$$\text{or} \quad H_2 = \frac{H_1}{L_1}(L_1 - x_1) = \left(H_1 - H_1\frac{x_1}{L_1}\right) \qquad \text{(33)}$$

The mean shear zone is thus given by:

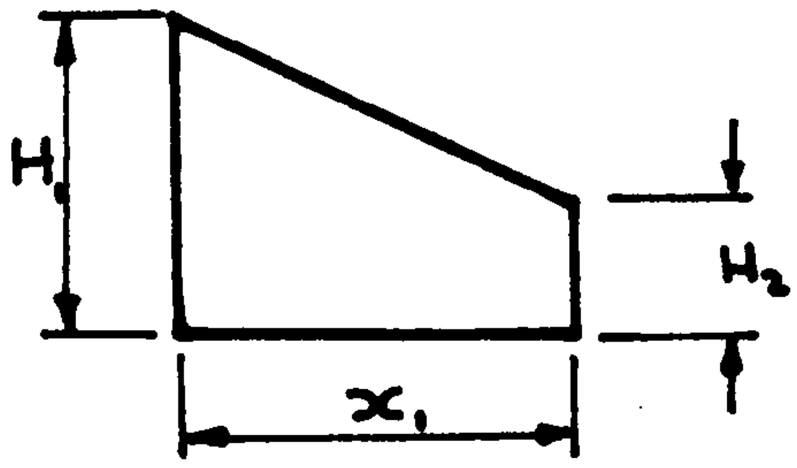

$$\frac{H_1 + H_2}{2} = \tfrac{1}{2}\left(H_1 + H_1 - \frac{H_1 x_1}{L_1}\right)$$

$$= \left(H_1 - \frac{H_1 x_1}{2L_1}\right)$$

The height of the section of the billet under pure compression may be obtained as follows:

$$\varepsilon = \ln\left(\frac{L_1}{L_1 - x_1}\right) = \ln\left(\frac{h_1}{h_2}\right)$$

$$\text{or} \quad h_2 = \frac{h_1}{L_1}(L_1 - x_1) \qquad \text{(34)}$$

<u>Total work done in the second stage</u>

Plastic work done on the sleeve may be expressed as:

$$W_{ps} = \frac{\pi}{4}(D_B^2 - D_C^2)Y\ln\left(\frac{h_1}{h_2}\right)(H_1 + x_o) \qquad \text{(35)}$$

and the shear work done between the sleeve and the inner core can be expressed as

$$W_S = \frac{\pi D_C Y}{2} x_1\left(H_1 - \frac{H_1 x_1}{2L_1}\right) \qquad \text{(36)}$$

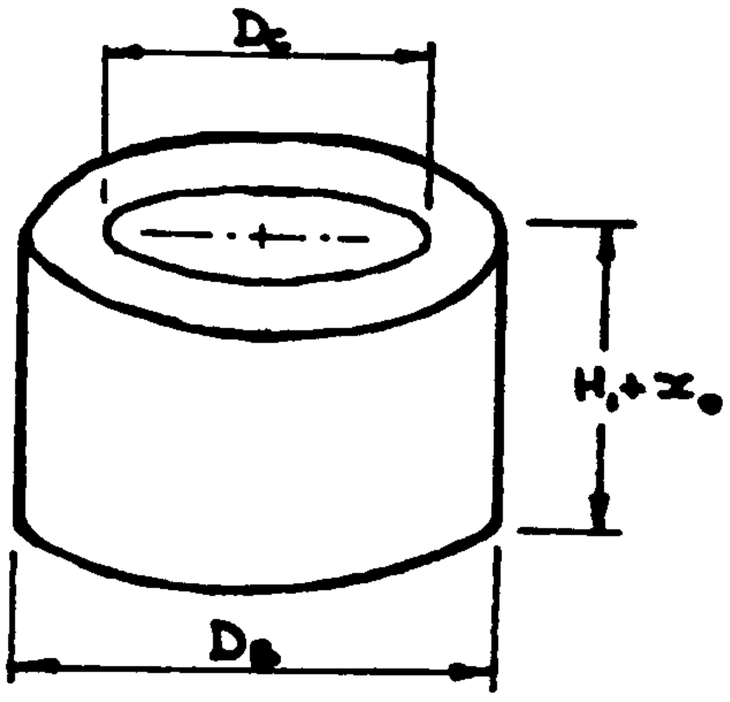

SLEEVE

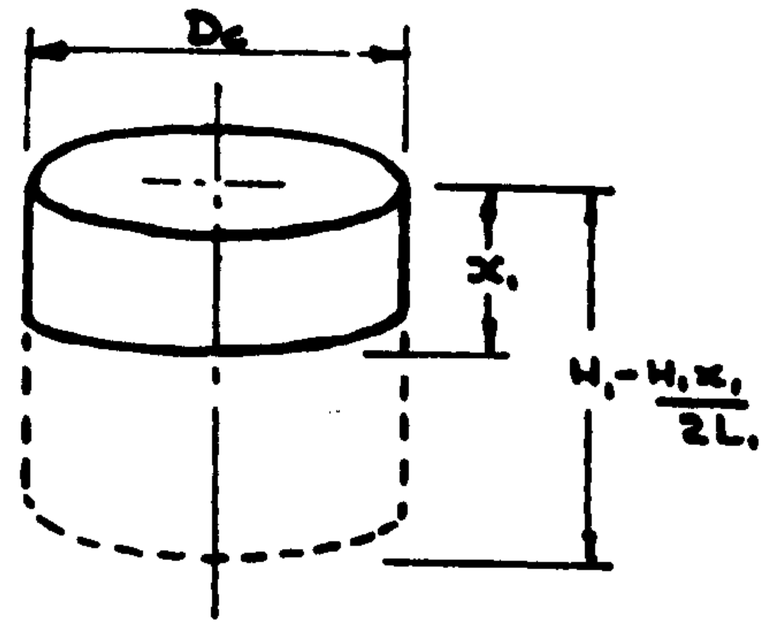

INNER CORE

The shear work done at the junction of the boss and the lower part of the flange which is deforming in a pure compression mode

$$W_{s_1} = \frac{\pi D^2 Y_Q}{8} (D_C' - D_C)$$

where D_C' is the virtual increase in D_C due to an incremental compression x_1.

Also the plastic work done on the lower part of the billet is given by

$$W_P = (L_o - x_o - H_1)\frac{\pi}{4}D_B^2 Y \ln(\frac{h_1}{h_2}) \quad \text{——————} \quad (37)$$

Total work done in the second stage is thus obtained by the sum total of all the works expressed by equations (35), (36) and (37). Thus,

$$W_t = \frac{\pi}{4}(D_B^2 - D_C^2)Y\ln(\frac{h_1}{h_2}) \times (H_1 + x_o) + \frac{\pi D_C Y}{2}$$

$$x_1(H_1 - \frac{H_1 x_1}{2L_1}) + (L_o - x_o - H_1)\frac{\pi}{4}D_B^2 Y \ln(\frac{h_1}{h_2})$$

$$+ \frac{\pi D^2 Y_Q}{8} (D_C' - D_C) \quad \text{———} \quad (37a)$$

The tup load at the end of a small axial compression, x_1, can be calculated by equating the total plastic work done to the work done by the external load. Thus,

$$(\frac{P_1 + P_2}{2})x_1 = W_t$$

$$\text{hence } P_2 = \frac{2W_t}{x_1} - P_1 \quad \text{——————————} \quad (38)$$

From Fig. 44 the boss height is given by

$$h_b = x_o + [x_1 - h_1 + h_2] \quad \text{——————————} \quad (39)$$

and the flange height is given by:

$$h_f = H_2 + h_2 \quad \text{——————————————————} \quad (40)$$

where H_2 and h_2 are given by equations (33) and (34) respectively.

The radial strain at the top of the sleeve may be expressed as

$$\varepsilon_r = \ln[\frac{(D_2 - D_C)}{(D_1 - D_C)}]$$

which is equal to half the axial strain ε given by equation (32a) hence,

$$D_2 - D_C = (D_1 - D_C) \exp(\frac{\varepsilon}{2})$$

so that

$$D_2 = D_C + (D_1 - D_C) \exp(\frac{\varepsilon}{2}) \quad \text{——————————} \quad (41)$$

Equation (41) thus enables calculation of the diameter at the top of the flange.

Similarly, the radial strain at the bottom of the sleeve may be expressed as

$$\varepsilon_1 = \ln[\frac{(D_B' - D_C)}{(D_B - D_C)}] = \frac{\varepsilon}{2}$$

which gives

$$D_B' = D_C + (D_B - D_C) \exp(\frac{\varepsilon}{2}) \quad \text{——————————} \quad (42)$$

Equation (42) thus gives the diameter at the bottom

of the flange.

These equations were used to obtain theoretical values for later comparison with those obtained experimentally. The results tabulated on pages A3.1 to A3.6were calculated using a computer program given in Appendix 4. The foregoing equations were used in the following sequence in evaluating the theoretical results.

a) Equations (1) and (6) were used to calculate the values of P_o and P_1, the forces needed to initiate stages one and two respectively.

b) Equation (7) was used to obtain H_o, the amount of plastic deformation at the end of the first stage.

c) Equation (23) was used to calculate W_p, the plastic work done at the end of the first stage.

d) Equation (23a) was used to calculate W_s the amount of shear work done at the end of the first stage.

e) Equations (23), (23a) and (23b) together with equations (1)and (6) were used to find $\dot{x}_o$, the boss height at the end of stage 1.

f) Equation (37a) was used to calculate W_t, the total work done during the second stage, for known values of x_1.

g) Equation (38) was used to calculate P_2, the maximum forging load for compression up to $(x_o + x_1)$.

h) Equations (39) and (40) were used to calculate h_b and h_f, the boss and flange heights at this stage.

Finally, equations (41) and (42) were used to calculate D_2 and D_B' the top and bottom flange diameters respectively. The procedure is repeated taking incremental values of x_1, each time the final values of the previous stage is taken as the starting value for the next stage. During this stage the energy requirement for deformation under the second and third modes are continuously compared until the extent of deformation is reached after which less energy is required to deform the billet in the third mode. The deformation there after carries on until the end of compression.

6.2.3 Third Stage

At some point during the deformation according to the mode prescribed in the second stage the billet will require less energy to deform in a mode in which only the outer sleeve is compressed and the central core remains rigid. The energy required is given by the sum of the energy to compress the outer sleeve and the shear energy at the sleeve-core interface.

Thus, the plastic energy in the sleeve is given by:

$$W_{psi} = \frac{\pi}{4} Y L_o (D_B^2 - D_C^2) \ln\left(\frac{L_1}{L_1 - x_1}\right) \quad \text{——————} \quad (43)$$

and the shear energy is given by:

$$W_{si} = \frac{\pi D C}{2} Y x_1 (L_1 - \frac{x_1}{2}) \quad \text{——————————} \quad (44)$$

6.2.4 Effect of Friction

The effect of friction at the die-billet interface on the load and deformation modes in extrusion forging may be accounted for in the above analysis in an approximate but simple manner outlined below.

Assuming that the frictional shear stress can be expressed in terms of mk where m is the friction factor and k is the shear yield stress given by $k = Y/2$ according to the Tresca yield criterion. Equations (1) and (6) become:

$$P_o = \frac{\pi}{4} Y (D_B^2 - D_C^2)(1 + \frac{mD_B}{6L_o}) \quad \text{——————————} \quad (45)$$

and

$$P_1 = \frac{\pi}{4} Y D_B^2 (1 + \frac{mD_B}{6L_o}) \quad \text{——————————} \quad (46)$$

respectively. In the above equations it is assumed that the mean forging pressure at the top and bottom interfaces are modified by the friction term $(1 + \frac{mD_B}{6L_o})$ for $\frac{D_B}{L_o}$ ratios of about unity.

The depth H_o, of the initial plastic zone given by equation (7) becomes

$$H_o = \frac{D_C}{2} + \frac{m}{12L_o}(\frac{D_B}{D_C}) \quad \text{——————————} \quad (47)$$

In calculating the boss height, x_o, at the end of the first stage of deformation, equation (23b) needs

to be modified by the addition of frictional work done at the top die interface. No frictional work is done at the bottom interface during this stage. The frictional force at the top interface at the start of deformation is given by:

$$F_1 = 2\pi mK\int_{R_C}^{R_B} Rdr$$

which after integrating and expressing in terms of the diameters and noting that $k = Y/2$, becomes

$$F_1 = \frac{\pi mY}{8} (D_B^2 - D_C^2)$$

similarly, the friction force at the end of the first stage is given by

$$F_2 = \frac{\pi mY}{8} (D_1^2 - D_C^2)$$

where D_1 is the top interface diameter and Y is assumed to remain constant during this stage.

The frictional work done during this stage may then approximately be expressed as

$$W_{f1} = \text{average frictional force x displacement}$$

or

$$W_{f1} = \frac{F_1 + F_2}{2} \times (D_1 - D_B)$$

which after substitution for F_1 and F_2 becomes:

$$W_{f1} = \frac{\pi mY}{16} (D_1^2 + D_B^2 - 2D_C^2)(D_1 - D_B)$$

equation (23b) thus becomes

$$\left(\frac{P_o + P_1}{2}\right) x_o = W_p + W_s + W_{f1} \quad \text{——————} \quad (48)$$

At the end of the first stage the lower end of the billet also starts to deform plastically and the second stage of deformation commences. For any increment, x_1, in compression the diameter D_1 at the top interface becomes D_2 and that at the bottom interface becomes D_B'.

The frictional force at the top interface at the start of the second stage is given by:

$$F_{2t} = \frac{\pi m Y}{8} (D_1^2 - D_C^2)$$

and that at the end of deformation is given by:

$$F_{3t} = \frac{\pi m Y}{8} (D_2^2 - D_C^2)$$

The frictional work done at the top interface during this stage is thus obtained in the same manner as before. Hence,

$$W_{ft} = \frac{\pi m Y}{16} (D_2 - D_1)(D_2^2 + D_1^2 - 2D_C^2) \quad \text{———}(49)$$

similarly, the frictional work done at the bottom interface is given by:

$$W_{fb} = \frac{\pi m Y}{16} (D_B' - D_B)(D_B'^2 + D_B^2) \quad \text{——————}(50)$$

Total frictional work done during this incremental compression, x_1, is thus,

$$W_{f2} = W_{ft} + W_{fb} \quad \text{——————————————} \quad (51)$$

The forging load P_2 is then given by equation (38) as:

$$P_2 = \frac{2}{x_1}(W_t + W_{f2}) - P_1$$

or the mean forging load P_m is given by:

$$P_{m2} = (W_t + W_{f2})/x_1 \quad \text{——————————} \quad (52)$$

The deformation mode changes at some stage during the second mode of deformation. In this changed mode the central core remains rigid and the outer sleeve deforms plastically. The forging load in this mode becomes less than that required for the previous mode. The plastic work done during this third stage is given by:

$$W_{3p} = \frac{\pi}{4}(D_B^2 - D_C^2)Y \; L_o \ln(\frac{L_1}{L_1 - x_1}) \quad \text{————} \quad (53)$$

where L_1 and x_1 are the current billet height and incremental compression respectively.

The shear work done between the inner rigid core and outer sleeve is given by:

$$W_{3s} = \frac{\pi}{2}D_C \; Y \; x_1(L_1 - \frac{x_1}{2}) \quad \text{——————————} \quad (54)$$

The frictional work at the top and bottom interfaces are given by equations (49) and (50) respectively.

The mean forging load during any incremental compression, x_1, is given by:

$$P_m = (W_{3P} + W_{3S} + W_{ft} + W_{fb.})/x_1 \quad \text{————————} \quad (55)$$

In the absence of friction, the deformation continues in this manner. However, due to the presence of friction, at some stage of deformation, which is dependent on the friction factor, m, the billet starts to deform in pure extrusion mode. This only happens when the frictional constraint is so high that the force required to extrude the billet becomes less than that to cause radial expansion. In reference [63] it has been suggested that the extrusion pressure for axisymmetric extrusion of lead may be expressed as

$$P = Y(0.8 + 1.5\ln\frac{A_1}{A_2}) \qquad (56)$$

The extrusion force is thus given by

$$P_e = A_1 p \qquad (57)$$

where A_1 is the current area at the bottom end of the billet.

If at any point during the deformation the mean forging load P_m given by equation (55) becomes greater than P_e, the extrusion force, then the billet will start to deform in pure extrusion mode. In this mode, no further radial expansion of the billet will take place and axial compression will cause the boss height to increase obeying the rule of volume constancy. Hence the increase in the boss height for any incremental compression, x_1, is given by

$$\Delta L = \frac{x_1}{D_C^2}\left(D_2^2 - D_C^2\right) + x_1$$

or

$$\Delta L = x_1 \frac{D_2^2}{D_C^2} \qquad (58)$$

6.3 Experimental Work

Cylindrical lead billets of 24 mm diameter and 24 mm height were forged dynamically under the drop hammer and quasi-statically using a compression testing machine. Quasi-static tests were also carried out on copper and aluminium billets of 24 mm diameter and 24 mm height. The tool and die arrangement is shown in Fig. 45. Fig. 46 shows the use of a positioning ring to centralise the billet over the die cavity. Two types of friction conditions were investigated, one, using acetone to dry the contacting surfaces and the other, using a mixture of graphite in petroleum jelly to induce low friction. Three different die cavities of diameters 18, 12 and 9 mm were used to obtain different billet to cavity diameter ratios. For double ended extrusion tests die cavities of 18 mm diameter only were used. The instrumentation used is as described in Chapter 2. From the compression test results shown in Fig. 12, it was found reasonable to assume that for comparison with quasi-static tests, the lead billets behaved as a rigid-perfectly plastic material with a constant yield stress of 17 N/mm^2. Under dynamic test conditions, of course, strain rate sensitivity and material inertia effects would render this value inapplicable as far as forging load is concerned.

6.4 Results and Discussions

The extrusion forging tests produced specimens with

a distinct profile irrespective of the material used and of the method of deformation. The profile produced lent itself to ready measurement using micrometers and vernier calipers. Quasi-static and dynamic tests were carried out, with and without lubrication, for different billet to boss diameter ratios. These results were compared with those calculated theoretically by applying the appropriate equations in the analysis.

6.4.1 Single Ended Extrusion Forging

Fig. 47 and 48 shows a series of predicted profiles of billets when dies of 18 mm and 9 mm diameter cavities are used. The predicted profiles show close similarity with those observed experimentally. Where the boss diameter is small the deformed billet will exhibit a small shoulder which quickly tapers back to the original diameter. A die with a large cavity diameter causes the deformed billet to expand radially producing a large shoulder and a considerable taper. Figs. 49 and 50 show a number of photographs which depict the deformation mode of lead billets. The shapes of the lead specimens at different stages of deformation having a boss diameter of 18 mm can be seen in the photograph in Fig. 49. The shapes of lead specimens having different billet to boss diameter ratios can be seen in the photograph shown in Fig. 50. The

first photograph clearly demonstrates the tapering nature of the profile of the flange. The second photograph shows how this tapering effect is influenced by the diameter of the boss.

The difference between the top and bottom flange diameters gives a clear indication of the extent of the flange taper. Fig. 51 shows experimental and theoretically predicted variations in the top and bottom diameters of the flange with the axial compression under static lubricated condition. Both the experimental and theoretical results show significant difference between the top and bottom diameters. A similar trend is demonstrated in Fig. 52 in which the experimental results were obtained under dynamic forging conditions. Figs. 53 and 54 demonstrate the tapering effect of the flange profile when the boss diameter was 12 mm and the billet was forged under quasi-static and dynamic conditions respectively. The tapering effect is visibly less than that seen in Figs. 51 and 52.

Figs. 55 and 56 show this tapering effect of the flange in terms of the ratio of the top and bottom diameters for boss diameters of 12 mm and 18 mm respectively. Fig. 57 shows the same diameter ratio in a comprehensive manner for three different boss diameters. It is evident that when the boss diameter is 9 mm negligible tapering

occurs over the entire range of axial compression.

The effect of friction on the flange diameters is demonstrated experimentally when Figs.58, 59 and 60 are compared with Figs. 51, 52 and 53 respectively. The most revealing effect of friction is shown in Fig. 61 where the variation in the upper diameter with the axial compression, for a boss diameter of 18 mm, is clearly affected by the absence of lubrication. Without lubrication the upper diameter will be less and this will be reflected in the billet profile. Fig. 62 shows the effect of friction on the lower flange diameter, with a boss diameter of 18 mm. Here the effect of friction is minimal, possibly due to the small amount of radial material flow involved. Figs. 63 and 64 show the effect of friction on the top and bottom diameters respectively for a boss diameter of 12 mm. Here friction can be seen to marginally influence the upper diameter size but its effect on the lower diameter is again very small. Photographs showing the effect of friction on the upper flange diameters are shown in Fig. 65 the sharp ended profiles (a) should be compared with (b) where the profiles are rounded due to the absence of lubrication.

Although the profile of the billet is affected by friction it does not appear to be affected significantly by the rate of deformation. This can be

seen if reference is made to Figs. 66 and 67 which compares the flange diameters for both static and dynamic tests. These show that for a boss diameter of 18 mm equal amounts of deformation should result in similar profiles under both quasi-static and dynamic forging. The height of the boss obtainable for different billet lengths and different boss diameters as predicted theoretically are shown in Figs. 68, 69 and 70 for billet lengths of 18, 22 and 30 mm respectively. Results are shown for boss diameters of 9, 12, 16 and 20 mm. It is evident that for a given amount of axial compression and for a given boss diameter the boss height is greater for the smaller billet length. For a billet 24 mm diameter and 24 mm long the boss height for boss diameters of 9 and 18 mm is shown in Fig. 71 in which experimentally observed results obtained from dynamic and static tests carried out under lubricated conditions are also plotted for comparison. It is evident that for larger compressions, the boss heights obtainable are predicted to be more than those observed experimentally. For total axial compression of up to 55 per cent the agreement between the theory and experiment is very close.

Theoretical curves showing the variation in flange thickness for billets of different lengths and boss diameters are shown in Figs. 72, 73 and 74 for boss diameters of 9, 16 and 22 mm respectively. The

billet diameter being 24 mm for all cases. Billet lengths of 18, 24 and 30 mm were considered in these figures. For a given displacement the flange thickness is directly related to the billet length and is independent of the boss diameter. As illustrated in these figures, for an axial compression of 12 mm the flange thickness is about 6 mm for a billet of length 18 mm, irrespective of the boss diameter.

One of the most informative parameters in extrusion forging is the ratio of the boss to flange height obtainable for different boss diameters. This parameter for boss diameters of 18 mm and 20 mm is shown in Figs. 75 and 76 respectively for billet diameter of 24 mm and billet lengths of 18, 20, 24 and 30 mm. These theoretical curves show that for a given displacement the shorter the billet and the larger the boss diameter - the greater the height ratio. Fig. 77 shows the variation in boss to flange height ratio with axial compression for billet diameters of 24 mm and length of 24 mm and boss diameters of 9, 12 and 18 mm as predicted theoretically. Theoretical and experimental results for boss diameters of 9 mm and 18 mm diameter are compared in Fig. 78 for a billet diameter of 24 mm and length 24 mm. It is evident that a more reliable prediction for the height ratio is made for the larger boss diameter. For smaller boss diameters

considerable discrepancy arises between the theoretical and experimental results. In Fig. 78(a) theoretical and experimental results show the variation in percentage total billet height with percentage deformation for boss sizes of 18, 12 and 9 mm, billet lengths of 24 mm were used and tests were undertaken under lubricated quasistatic and dynamic conditions. The transition from the second to the third deformation stage can be inferred from this figure. If allowance is made for 'scatter' there is a very reasonable correlation between the theoretical and experimental results for all three boss sizes, for both quasi-static and dynamic tests. Fig. 79 shows the theoretical relation between the height ratio and the diameter ratio for the forging loads of 14 kN and 13 kN applicable to a billet of diameter 24 mm and length 24 mm and constant flow stress of 17 N/mm^2. For a given billet size and material the load required to initiate axial displacement P_o will depend on the boss diameter. The variation of P_o with boss diameter for a lead billet of diameter 24 mm and length 24 mm is shown in Fig. 80.

The variation in forging load with axial compression for different boss diameters and billet lengths have been calculated for billet diameters of 24 mm. These results are shown in Figs. 81 to 86 for boss diameters ranging from 9 to 20 mm. For boss to

billet diameter ratios of up to 0.5 the forging load is generally greater for smaller lengths of the billet. This trend, however, reverses as the ratio becomes as high as 0.8 (see Fig. 86) and the axial compression is not more than about 60 per cent. The forging load for a billet of length 24 mm and diameter 24 mm but with boss diameters of 9, 12 and 18 mm are shown in Fig. 87. In Figs. 88(a) and 88(b) theoretically calculated forging loads for a 24 mm long and 24 mm diameter billet having a boss diameter of 18 mm and 12 mm are compared with those obtained experimentally from static and dynamic forging tests. It is evident that the load recorded from the quasi-static forging tests, for both 18 mm and 12 mm boss diameters, agrees reasonably well in terms of the magnitude with that predicted theoretically. To predict the load under dynamic conditions the flow stress is modified and incorporated in the theory used for the quasi-static forging condition to take into account the effect of strain rate. For the boss diameter of 18 mm there is an overestimation of the forging load required when the billet is deformed dynamically, whereas for the boss diameter of 12 mm there is an underestimation. In both these cases it is evident that the modified flow stress used to predict forging load gives agreement between theory and experiment similar to the static tests.

As the inertia effect has not been included in the analysis some error in load prediction must be expected. The effect of friction as observed experimentally on the forging load for boss diameters of 12 mm and 18 mm diameter is shown in Figs. 89 and 90 respectively. It is evident that friction adversely affects the forging load for a given displacement and that the larger the boss diameter the greater the influence of friction on the forging load. The forging load calculations were also carried out for mild steel at hot working temperatures for providing a basis of comparison with the forging loads predicted for lead used in this study. Theoretical curves showing the variation in forging load with axial compression for different boss diameters and billet lengths for steel at forging temperatures of 800, 1000 and 1200°C are shown in Figs. 91-96. These results help estimation of the load requirement if extrusion forging was to be carried out with steel at hot working temperatures and show that the temperature of the billet is of paramount importance when calculating forging loads.

The total energy requirement predicted theoretically and measured from quasi-static lubricated tests via load displacement traces, are shown in Figs. 97-99 for boss diameters of 9, 12 and 18 mm respectively with a billet diameter of 24 mm. These values are again

shown in Figs. 100, 101 and 102 and are compared with dynamic forging test results where the amount of energy used was calculated from the tup mass and its total displacement. Again it is clearly evident that close agreement is demonstrated between statically measured and theoretically predicted results. Dynamically forged results show much greater energy requirement for the same amount of axial deformation.

The total energy curves, based on the theoretical (dynamic) load results shown in Figs. 88(a) and 88(b), are shown in Figs. 101 and 102. In each case there is an underestimation of the total energy required. This could be due to the fact that not all energy given up by the tup is actually used to deform the billet. Energy losses occur by way of elastic deformation of dies and the load cell housing, together with losses due to impact noise. A further improvement in predicting the dynamic forging energy requirement could be obtained if allowance for material inertia could be incorporated in the analysis.

6.4.2 Tests on Materials other than Lead

To check if the profile of the deformed billet is material dependent quasi-static lubricated extrusion forging tests were carried out on copper and it was found that the copper billets deform in just about the same manner as the lead billets did. Fig. 103

shows a photograph of copper billets at different stages of deformation with boss diameters of 18 mm. These profiles are similar to those observed for lead billets and shown in the photograph in Fig. 49. It is evident from these tests that when different billet materials are used similar profiles can be expected from the same set of dies.

6.4.3 Double-Ended Extrusion Forging

To confirm that the analysis developed in this study could be applied to cylindrical billets in which forging was combined with extrusion at both ends, static lubricated tests on lead billets 24 mm diameter, 24 mm long with boss diameters of 18 mm were carried out. Figs. 104, 105 and 106 show how Displacement is related to Energy, Flange diameter ratio and the Top and Bottom flange diameters respectively. In each case a close relation between theoretical and experimental results was found and it is thus evident that the double ended extrusion forgings could be analysed in the same way as the single ended ones.

A further check on material dependency was made with billets made from copper and aluminium. Fig. 107 shows photographs of copper billets at various stages of deformation in double ended extrusion forging modes for boss diameters of 18 mm. Fig. 108 shows a photograph of aluminium copper and lead

billets partially deformed in double-ended extrusion forging mode. The deformation modes appear to be independent of the billet material.

Dynamic forging also gives rise to increase in forging load due to material inertia. Any influence in the forging load observed in this study for tests under the drop hammer is thus due to the combined effects of strain rate sensitivity and inertia.

Some unexpected results associated with these tests is shown in the photograph in Fig. 109 which shows a lead billet flanked by two aluminium billets. In each case the flange profile is uneven. This is thought to be due to the use of recast metal having a large grain size. This phenomenon did not occur when 'bar' material was used.

6.4.4 Discussion on the effect of friction

Figs. 110 and 111 show the effect of friction (m = 1) and (m = 0.5) on the variation in percentage total height with percentage displacement for boss sizes of 12, 15, 18 and 21 for lead billets 24 mm diameter and 24 mm high. The onset of the third and fourth stages can be seen clearly, but in practice the abrupt changes shown would be more gradual. It is clearly evident that the larger the boss size the lower the percentage displacement needed to initiate flow in the third mode. This would appear to be

in good agreement with earlier works[62,61] although it is not possible to make a direct comparison because of the difference in the size of die and test piece used. The experimental results show close agreement with the theory when deformation takes place in the second and third modes for boss diameters of 12 and 18 mm.

Fig. 112 shows the effect of three different friction factors in predicting the percentage total height with percentage displacement for a boss size of 12 mm. Again the onset of the third and fourth stages can be clearly seen and it is evident that the larger the friction factor the earlier the fourth mode of deformation is likely to occur. This is in agreement with earlier works[62,61]. It is evident from the results in Fig. 112 that the friction has insignificant effect on the total height of the deformed billet until the fourth mode of deformation commences. The agreement between the theory and experiment is very close. Fig. 113 shows the effect of friction on the forging load with percentage displacement for a die size of 12 mm. Theoretically the higher the friction factor, m, the greater the forging load required. The experimental curve shown in the figure indicates that the predicted load is an overestimation when forging was carried out under lubricated condition. It is to be noted,

however, that experimentally the difference in forging loads under lubricated and dry conditions was found to be very small for deformation of up to about 50 per cent (See Fig. 89).

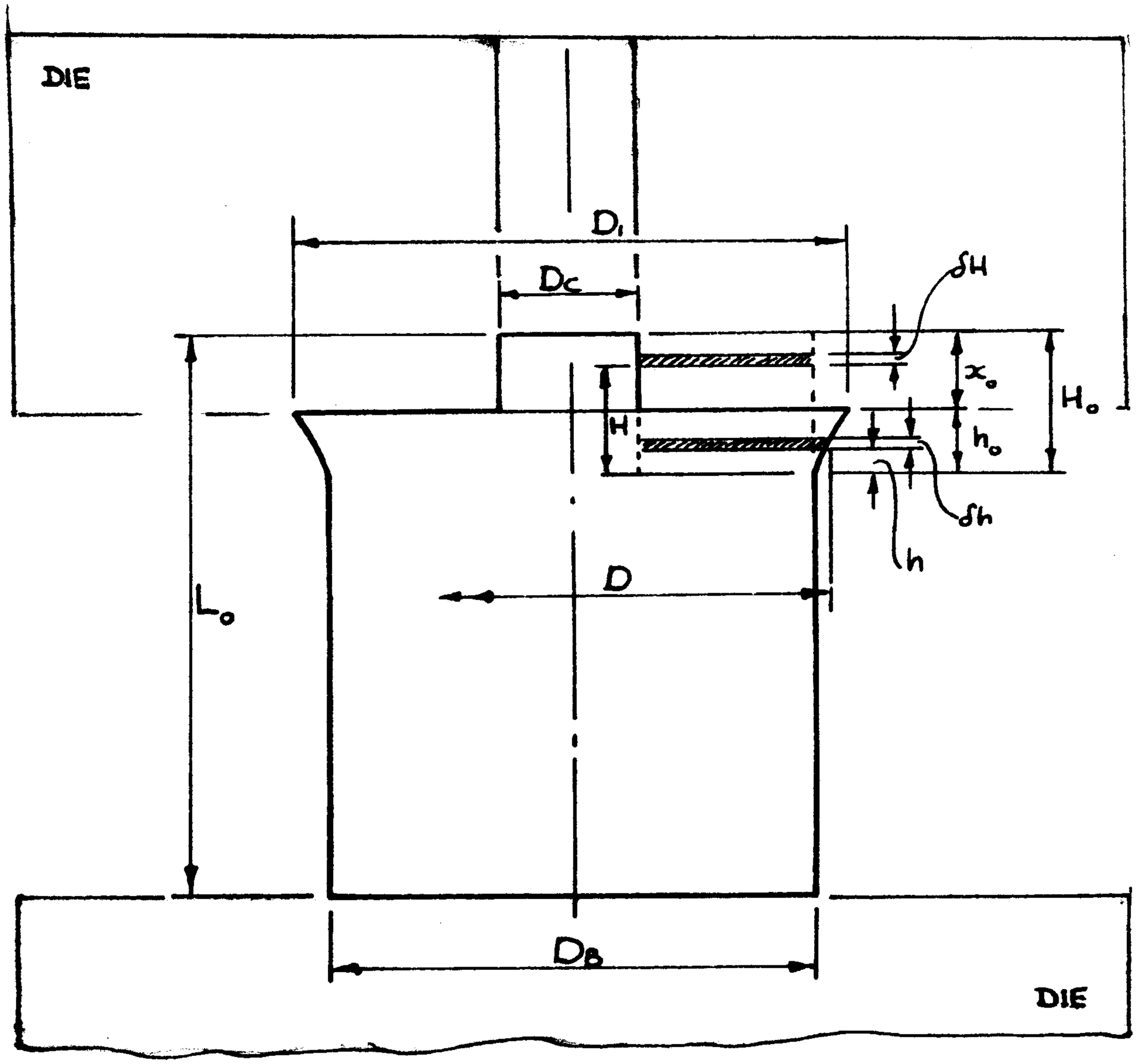

FIRST STAGE OF DEFORMATION

FIG. 43

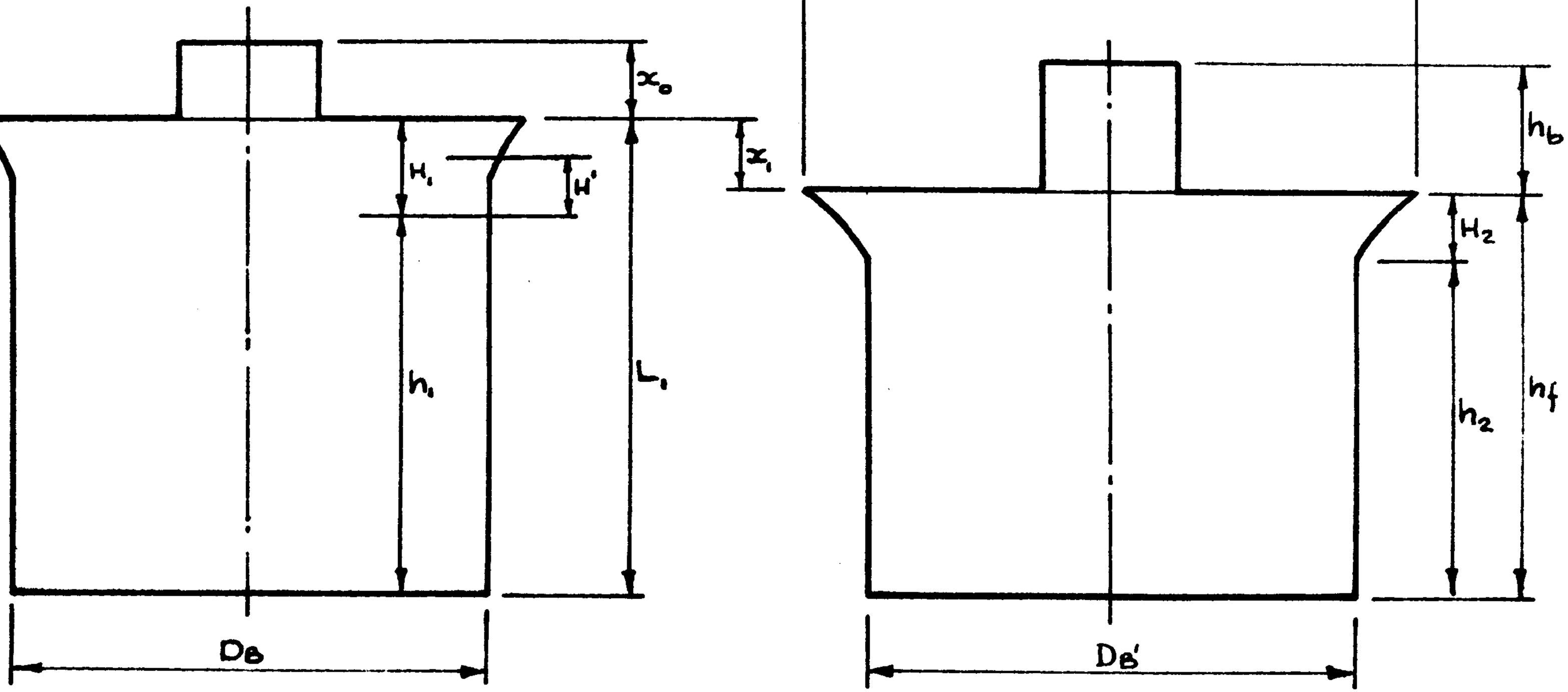

SECOND STAGE OF DEFORMATION

FIG. 44.

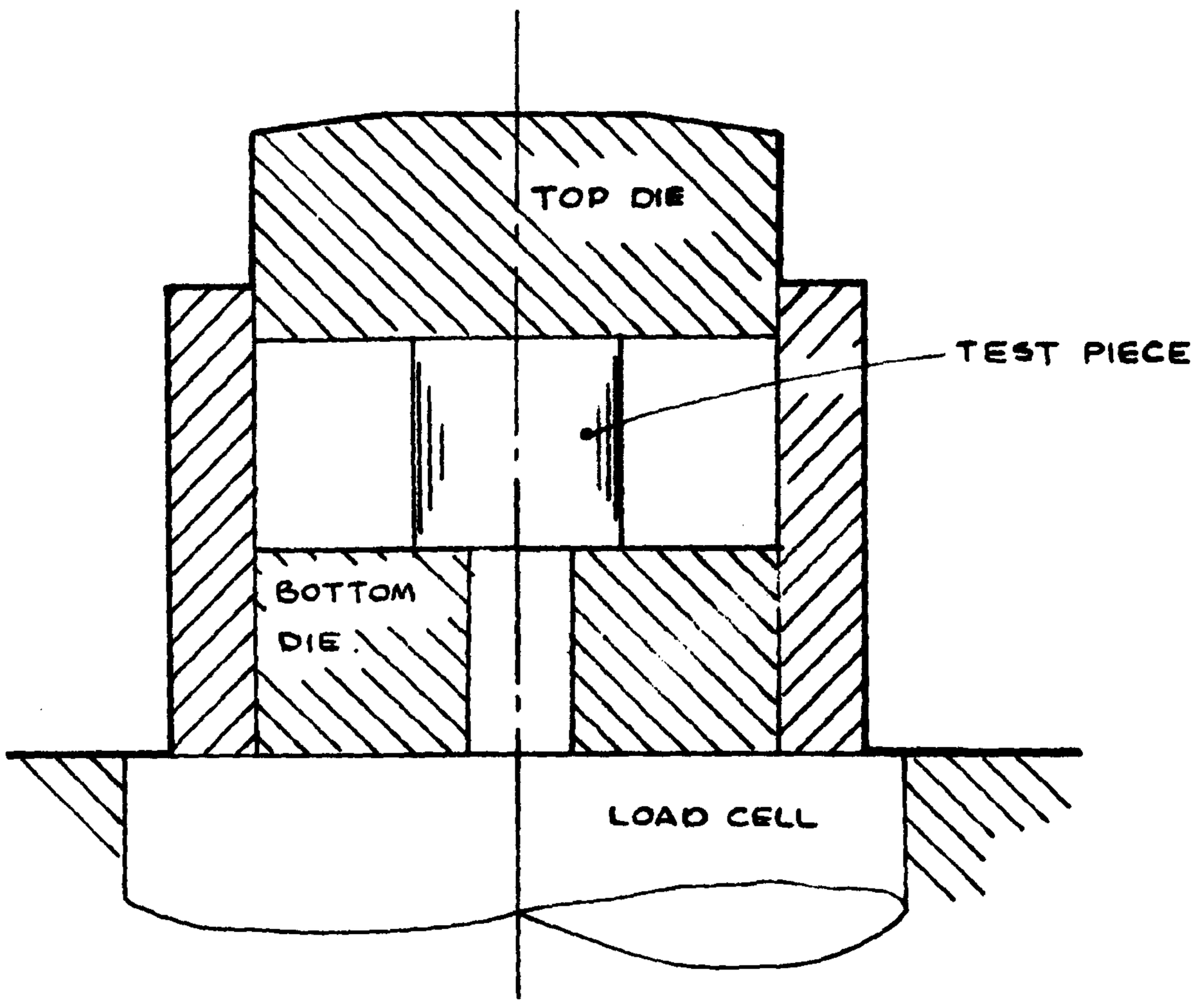

DIE - BILLET CONFIGURATION

FIG. 45.

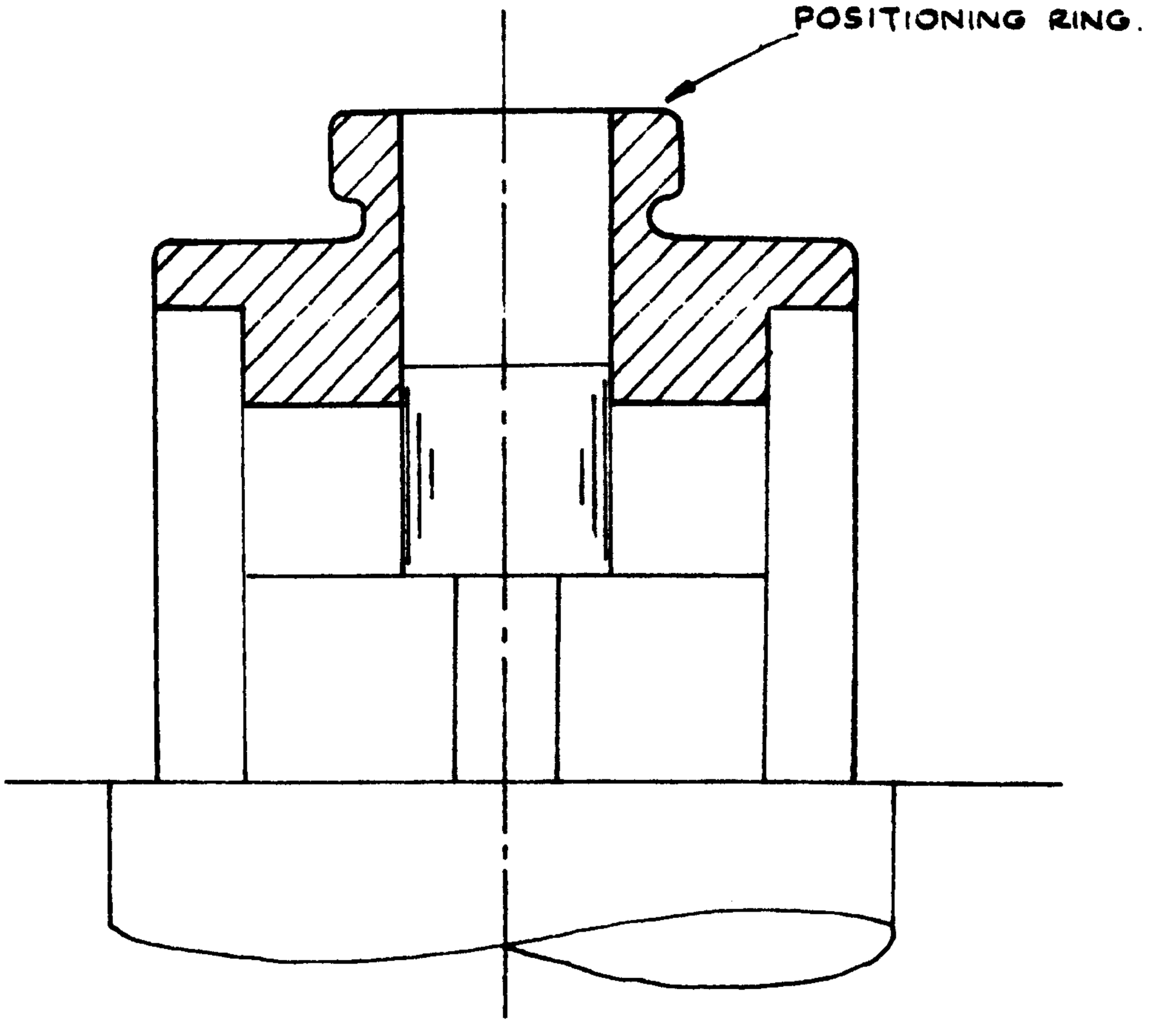

USE OF POSITIONING RING TO CENTRALISE TEST PIECE

FIG. 46

THEORETICAL PROFILES

D_c = 18mm

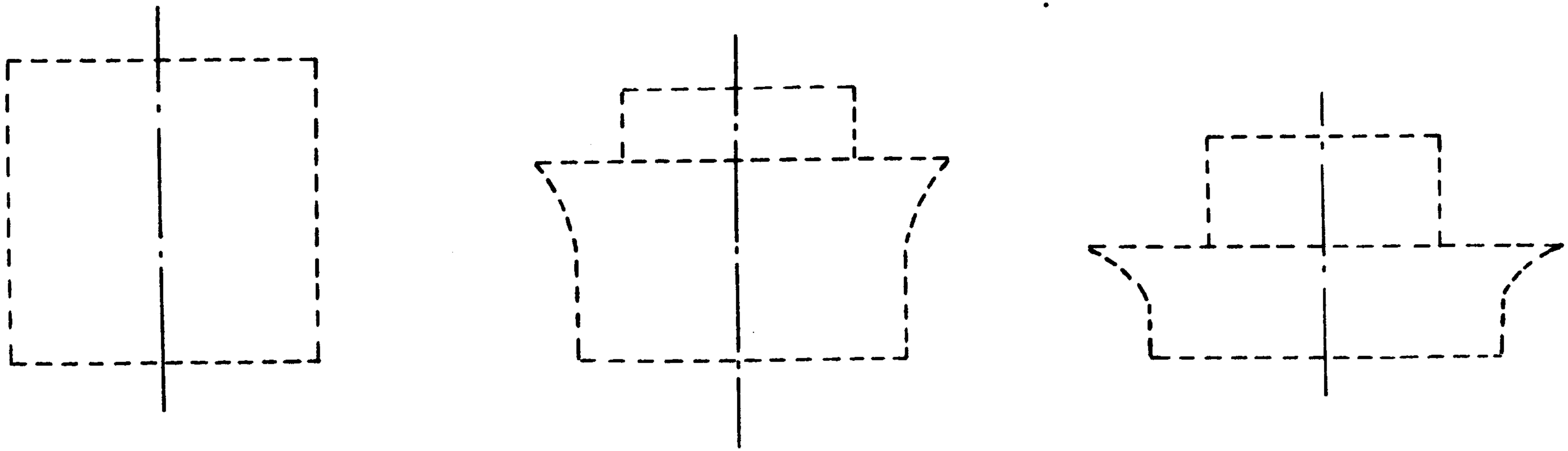

FIG. 47

THEORETICAL PROFILES

$2c = 9mm$

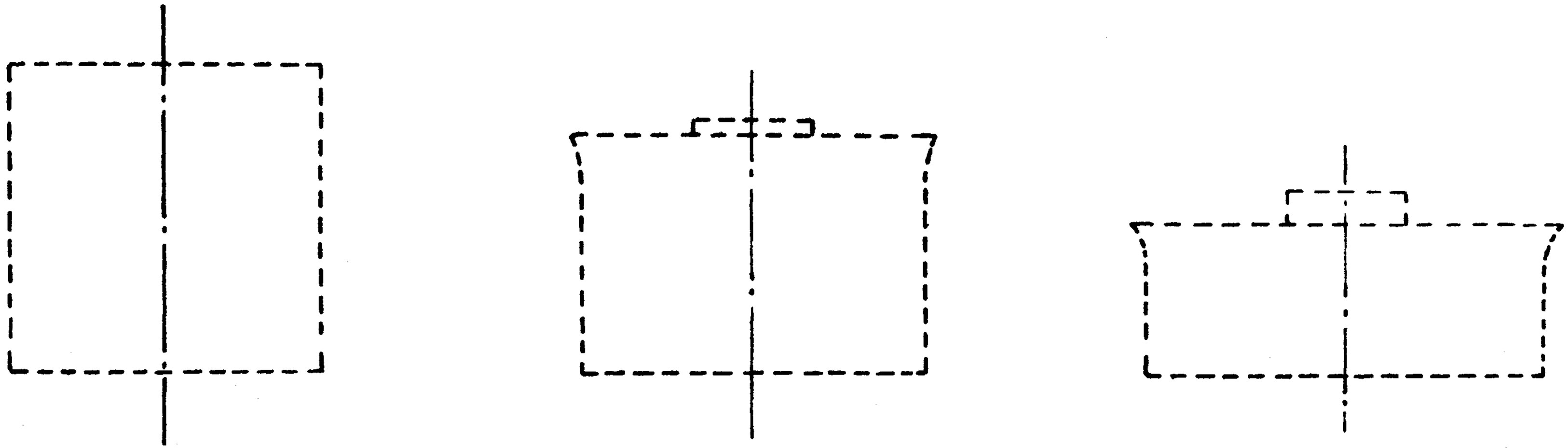

FIG. 48.

DEFORMATION MODE OF LEAD BILLETS.

FIG. 49.

EXTRUSION FORGINGS. THREE DIFFERENT SIZES.

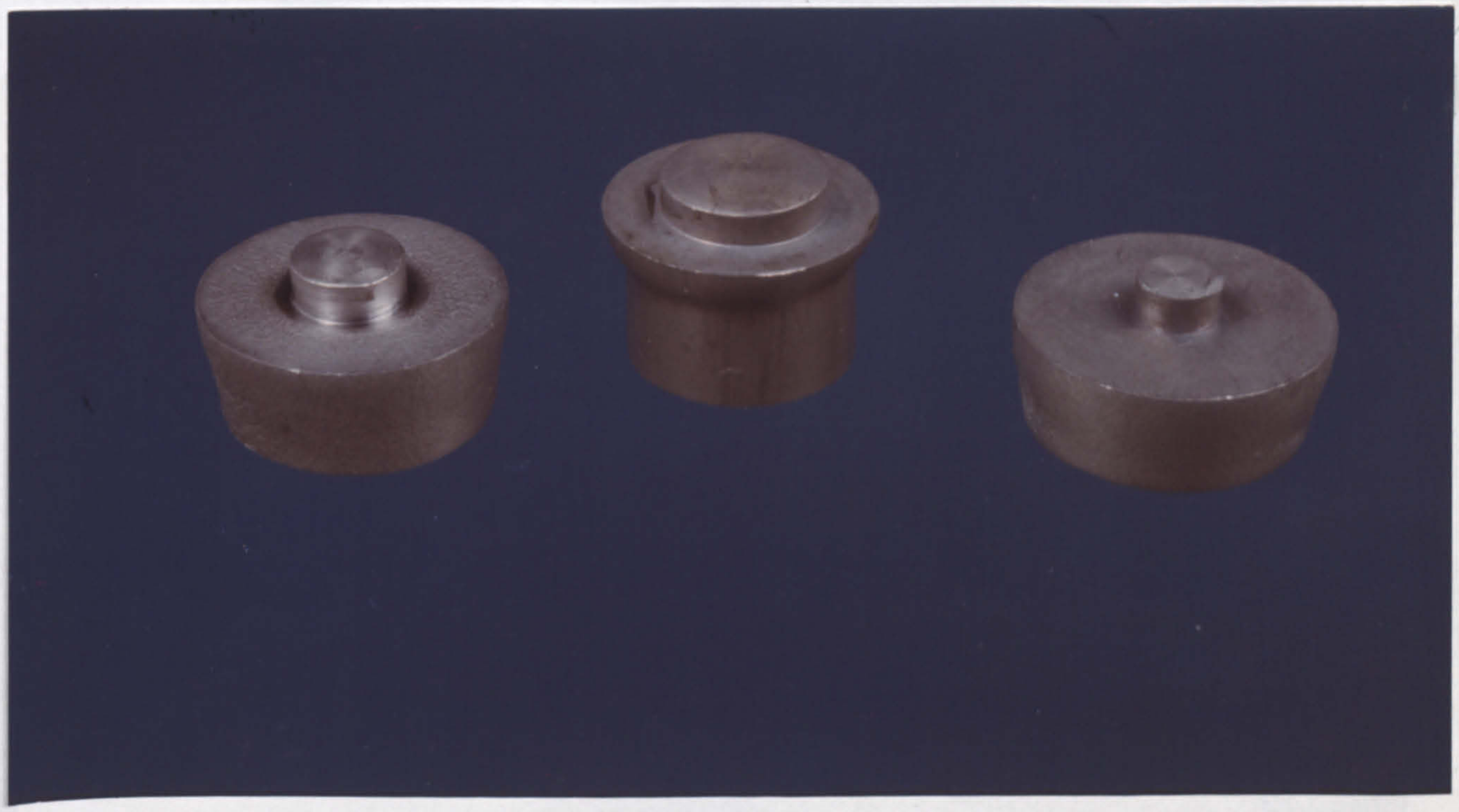

FIG. 50

THEORETICAL | EXPERIMENTAL CURVES

BOSS DIA. = 18 mm Y = 17 N/mm²

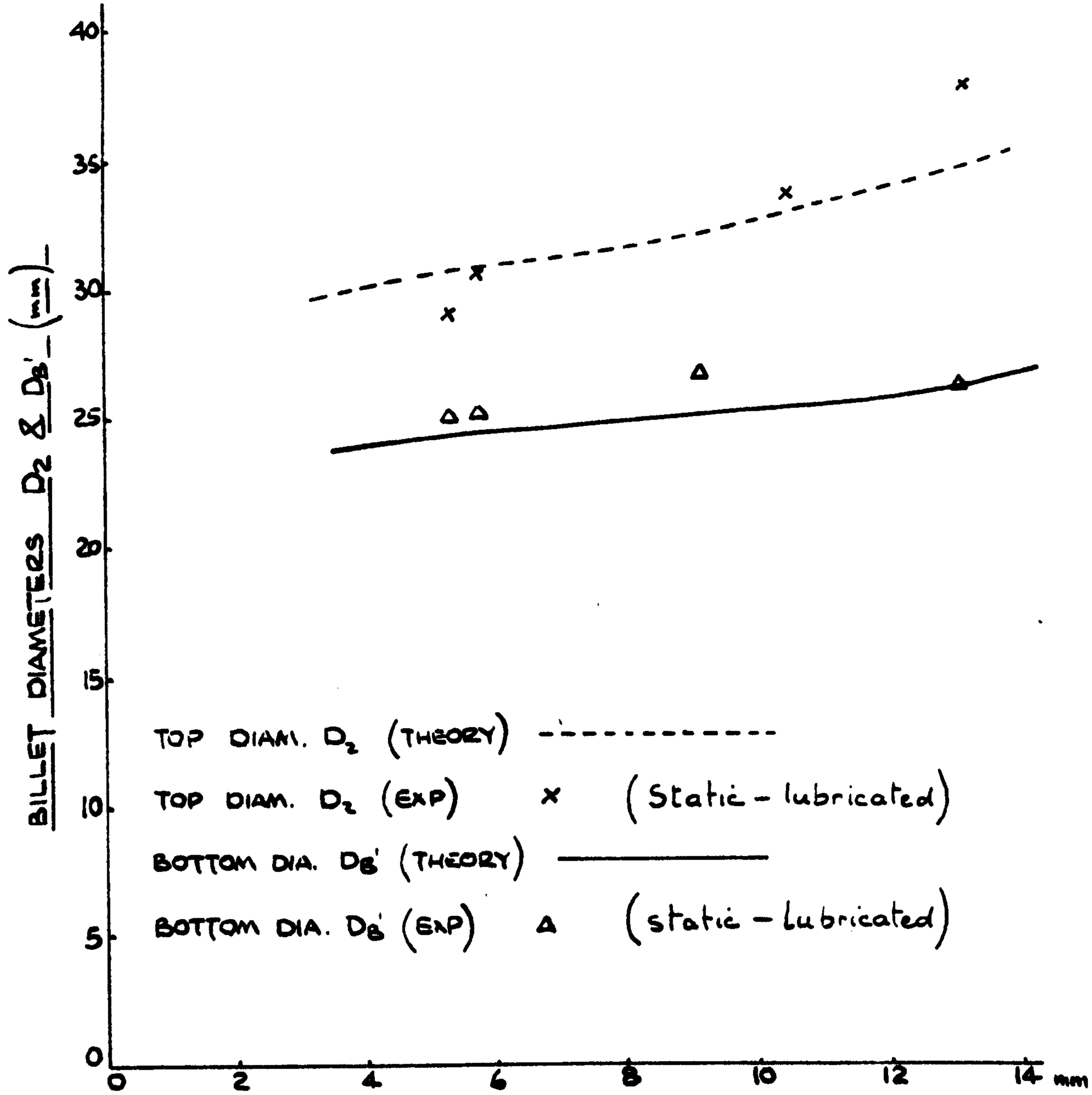

TOTAL DISPLACEMENT $x_0 + x_1$

FLANGE DIAMETERS v. TOTAL DISPLACEMENT.

FIG. 51.

THEORETICAL / EXPERIMENTAL CURVES

BOSS DIA. = 18mm Y = 17 N/mm²

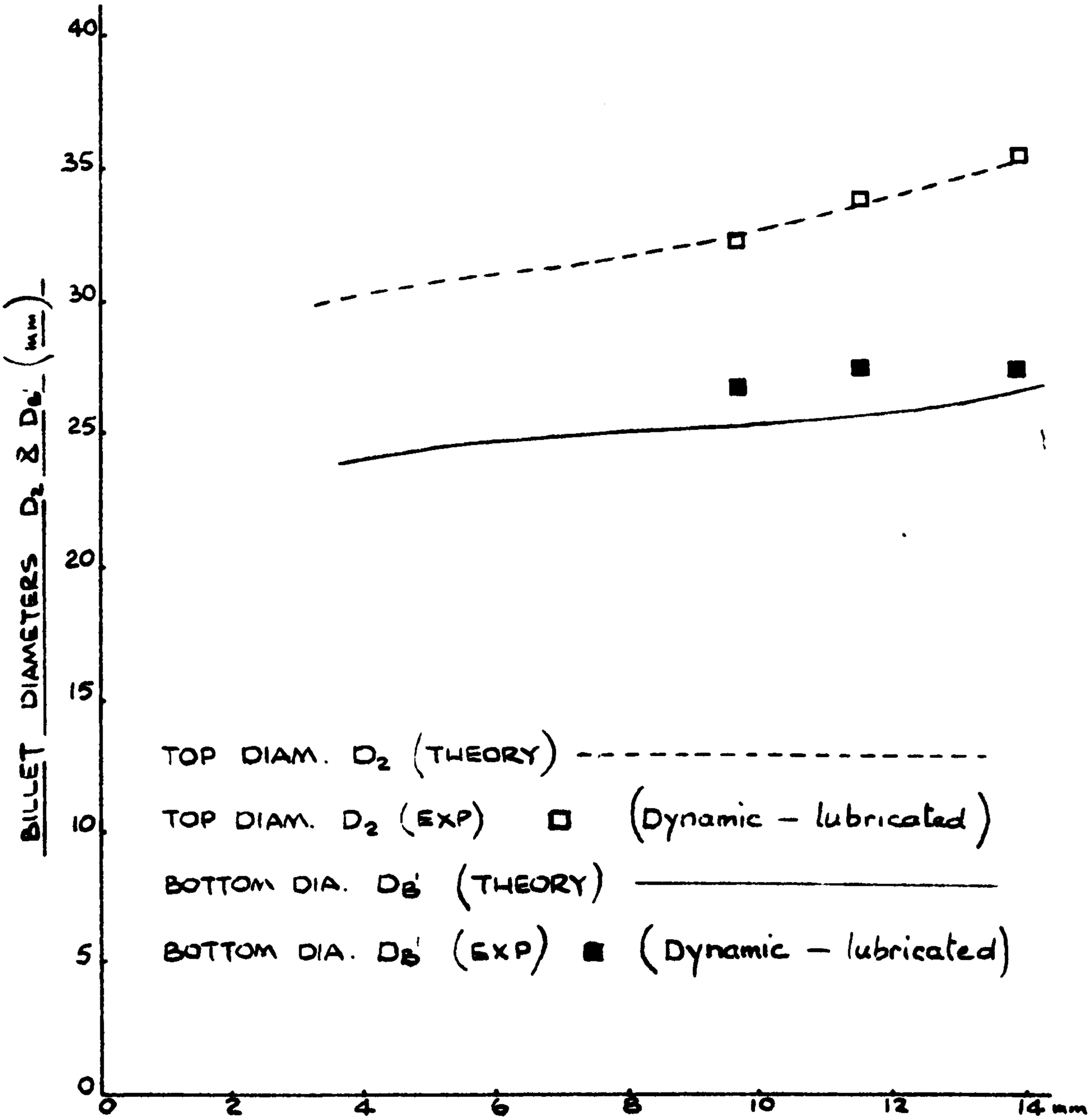

TOTAL DISPLACEMENT $x_0 + x_1$

FLANGE DIAMETERS v. TOTAL DISPLACEMENT

FIG. 52.

THEORETICAL / EXPERIMENTAL CURVES

BOSS DIA. = 12mm

$Y = 17 \; N/mm^2$

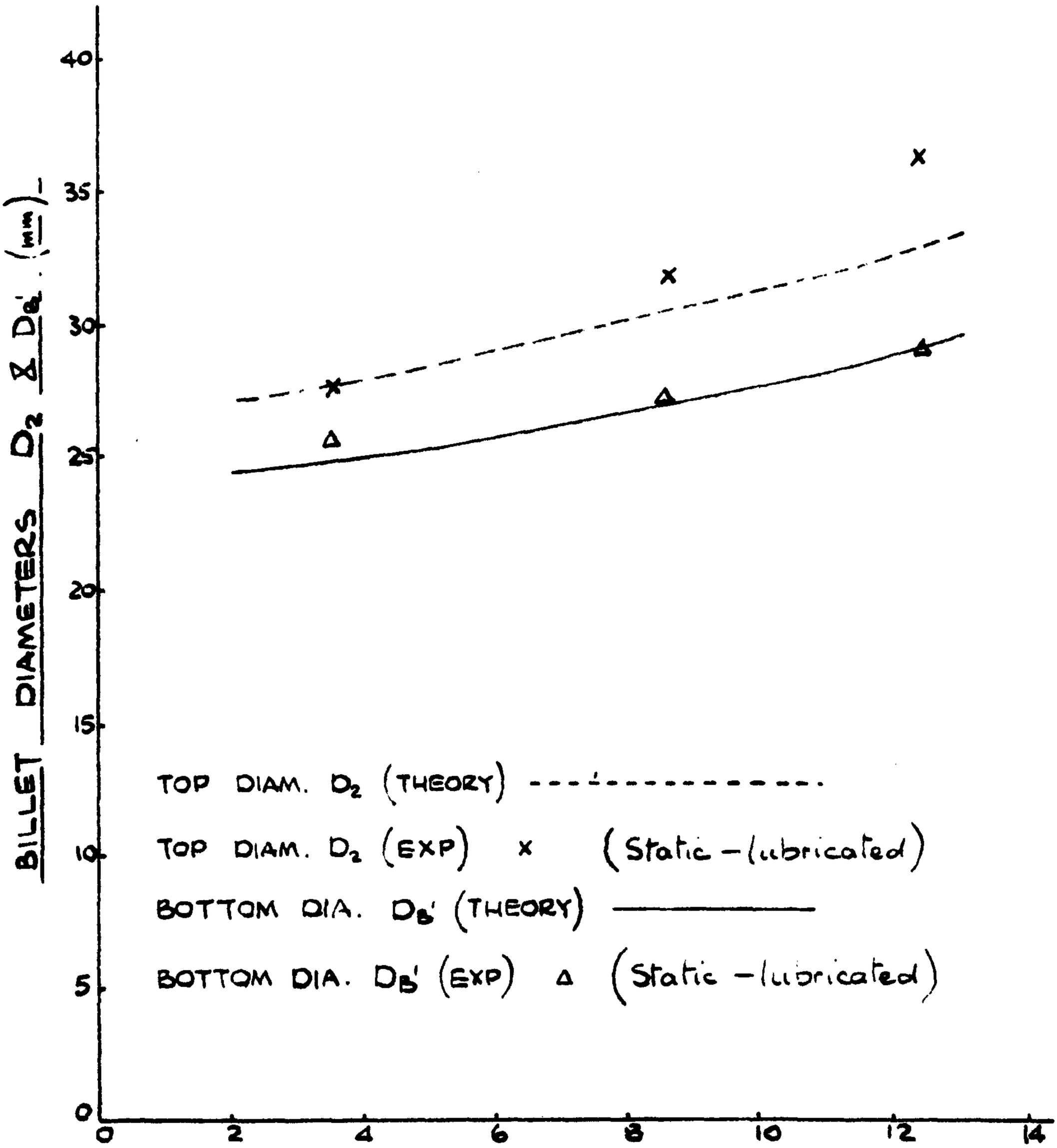

FLANGE DIAMETERS v. TOTAL DISPLACEMENT

FIG. 53.

THEORETICAL / EXPERIMENTAL CURVES

BOSS DIA = 12mm Y = 17 N/mm².

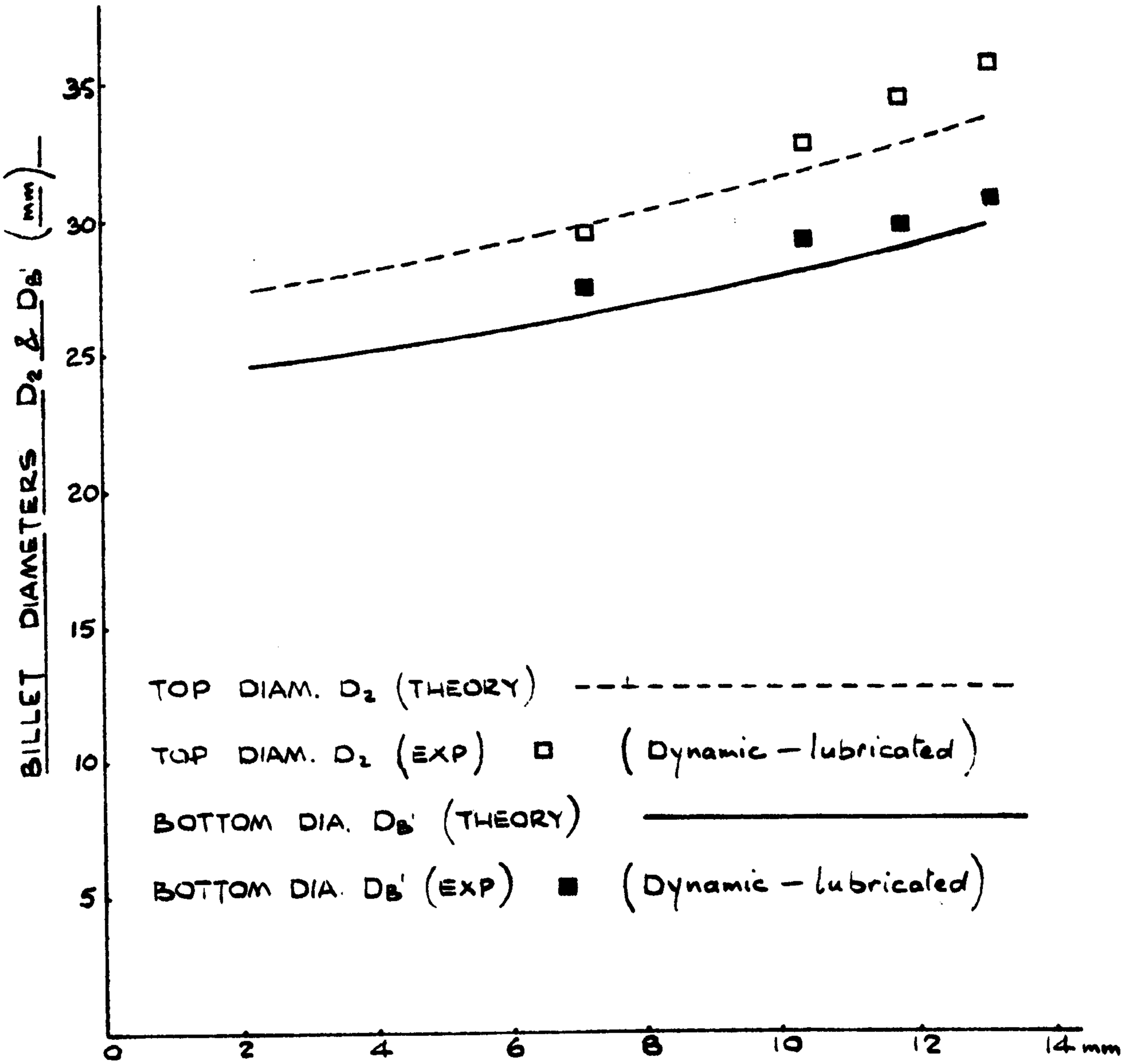

FLANGE DIAMETERS v. TOTAL DISPLACEMENT.

FIG. 54.

THEORETICAL / EXPERIMENTAL CURVES

BOSS DIA = 12mm

Y = 17 N/mm².

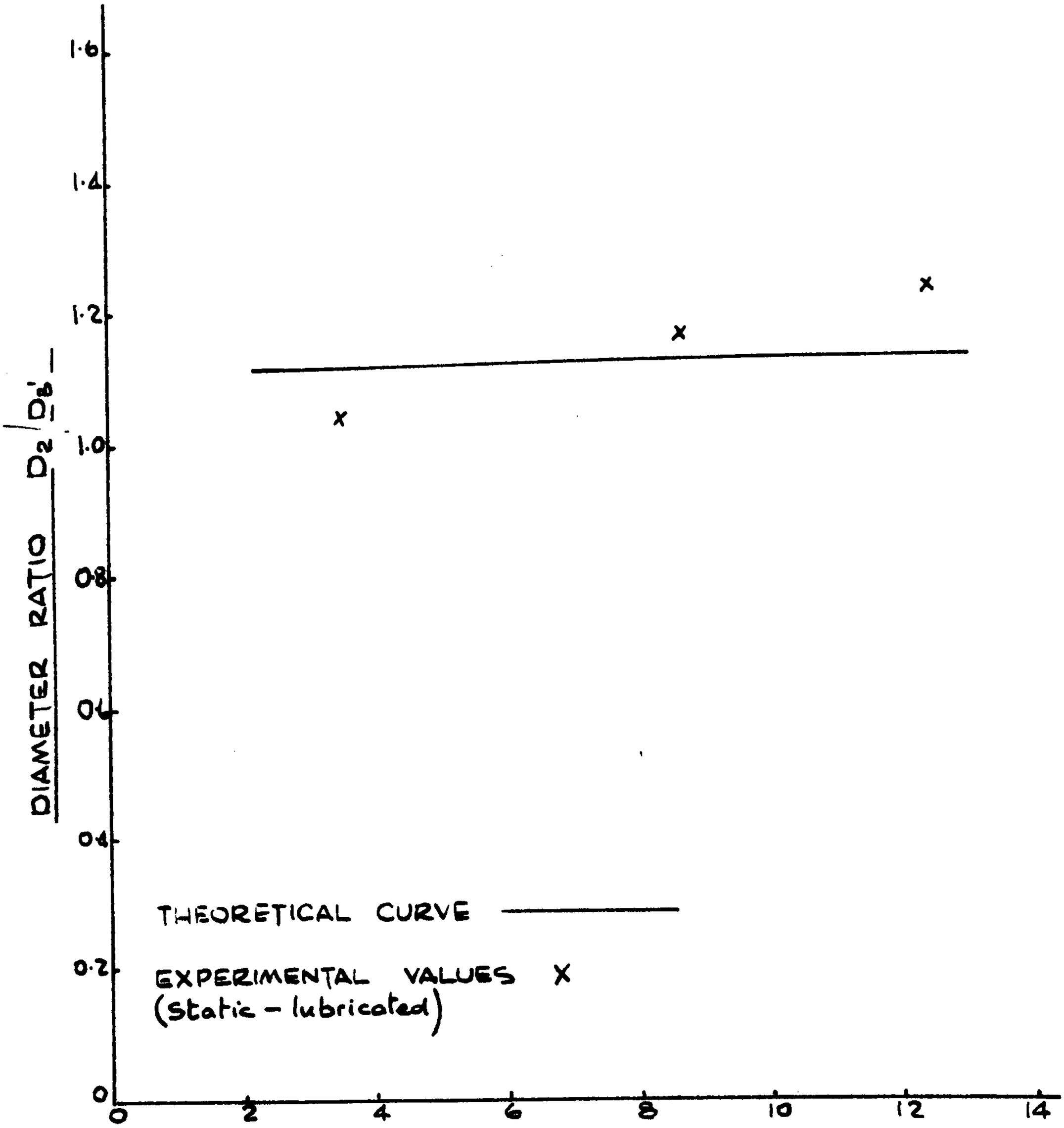

DIAMETER RATIO v. TOTAL DISPLACEMENT

FIG. 55.

THEORETICAL / EXPERIMENTAL CURVES

BOSS DIA = 18 mm Y = 17 N/mm²

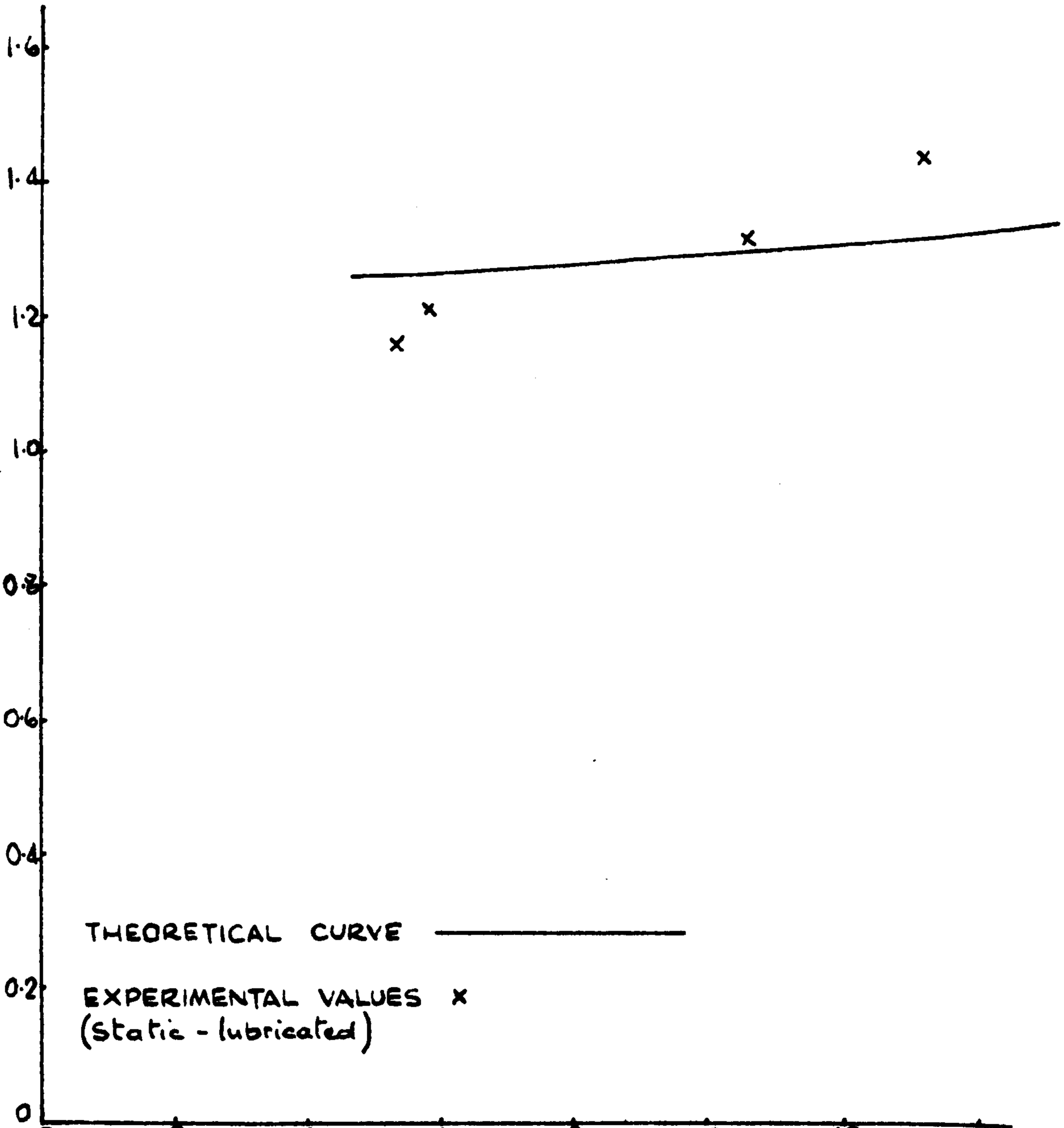

DIAMETER RATIO v. TOTAL DISPLACEMENT.

FIG. 56.

THEORETICAL / EXPERIMENTAL CURVES

$Y = 17\ N/mm^2$

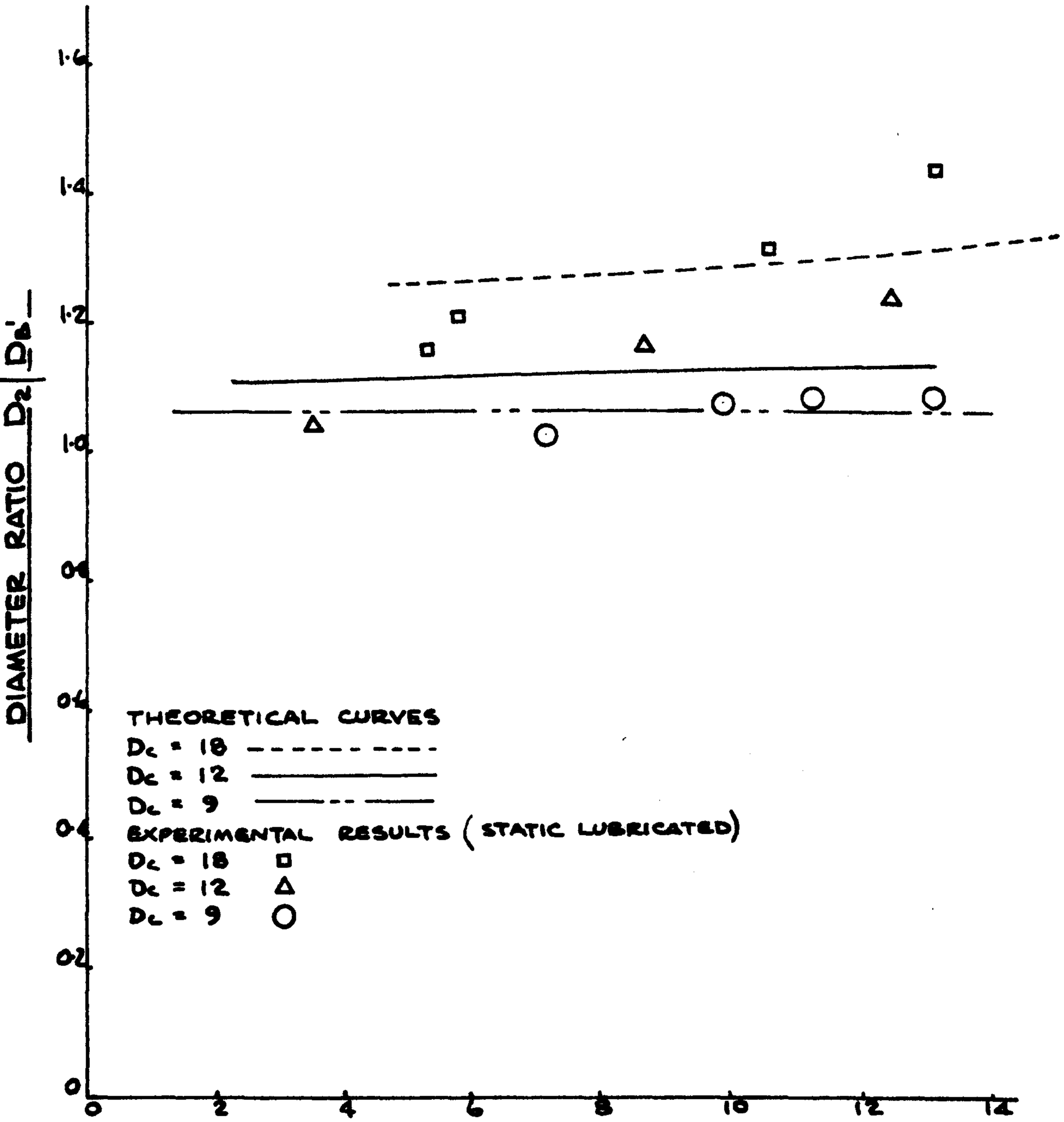

DIAMETER RATIO v. TOTAL DISPLACEMENT

FIG. 57.

THEORETICAL / EXPERIMENTAL CURVES

BOSS D.A = 18mm

Y = 17 N/mm²

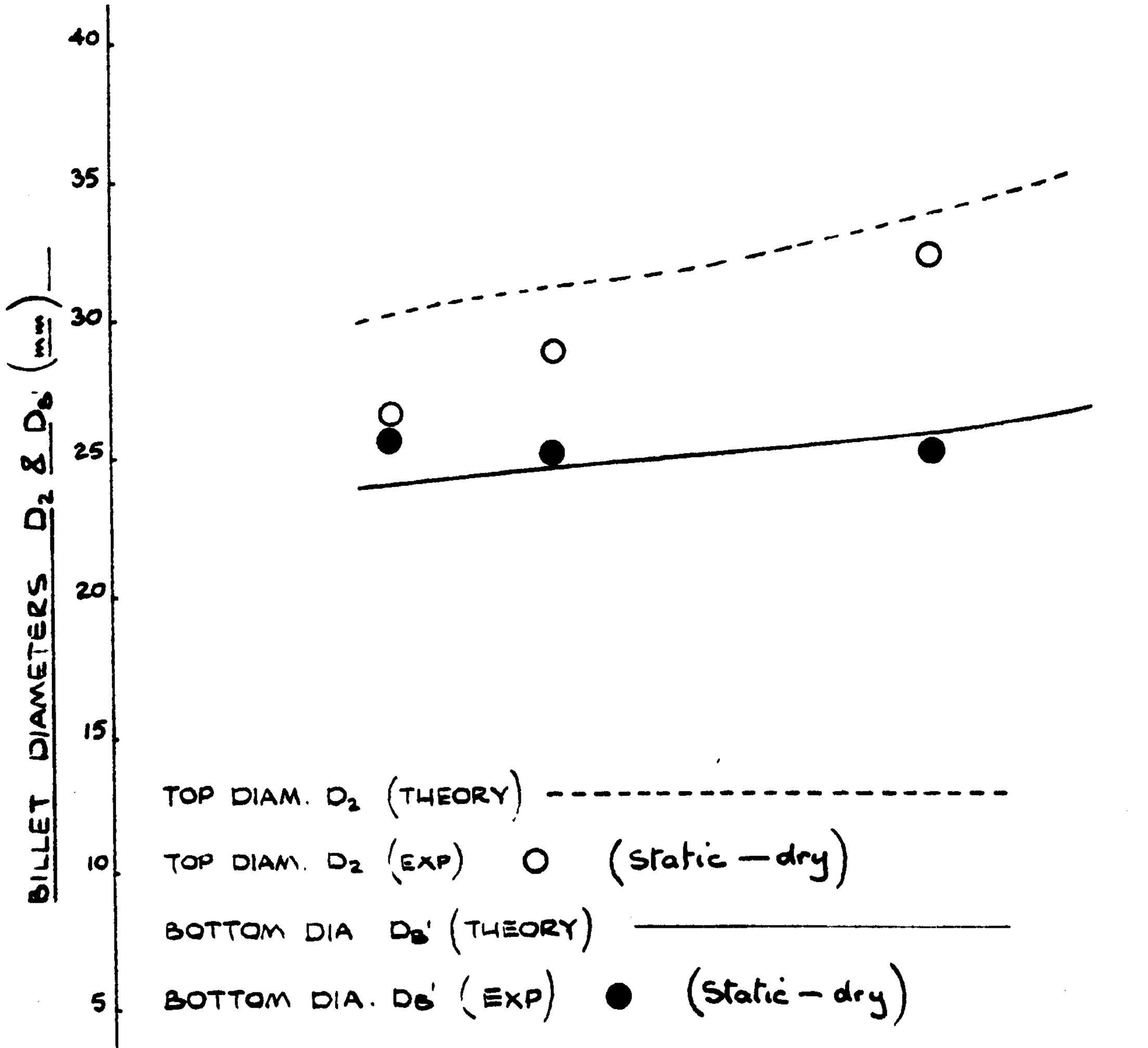

FLANGE DIAMETERS v. TOTAL DISPLACEMENT.

FIG. 58.

THEORETICAL EXPERIMENTAL CURVES

BOSS DIA. = 18mm Y = 17 N/mm²

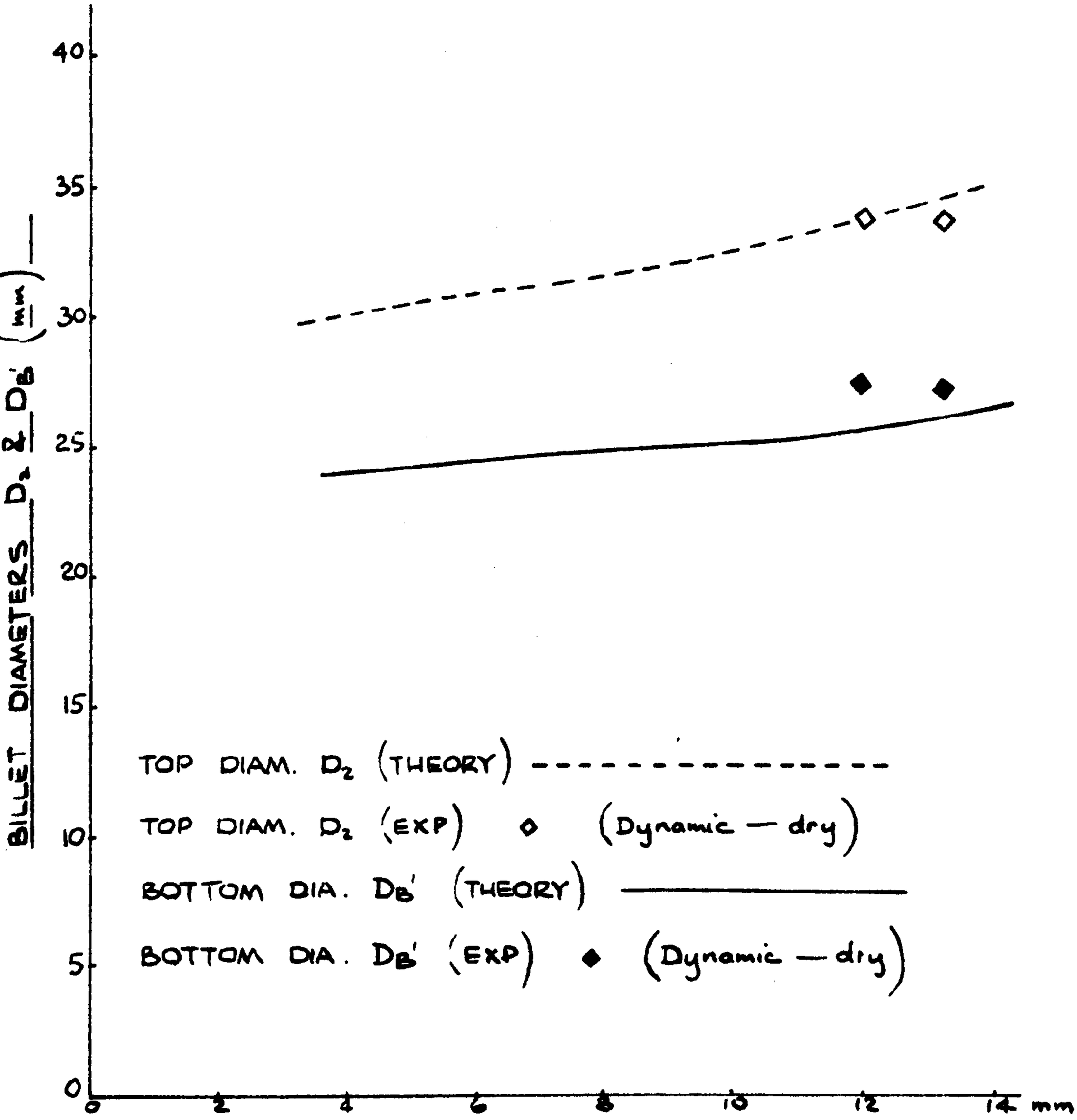

TOTAL DISPLACEMENT $x_0 \pm x_1$

FLANGE DIAMETERS v. TOTAL DISPLACEMENT

FIG. 59.

THEORETICAL / EXPERIMENTAL CURVES

BOSS DIA = 12 mm

Y = 17 N/mm².

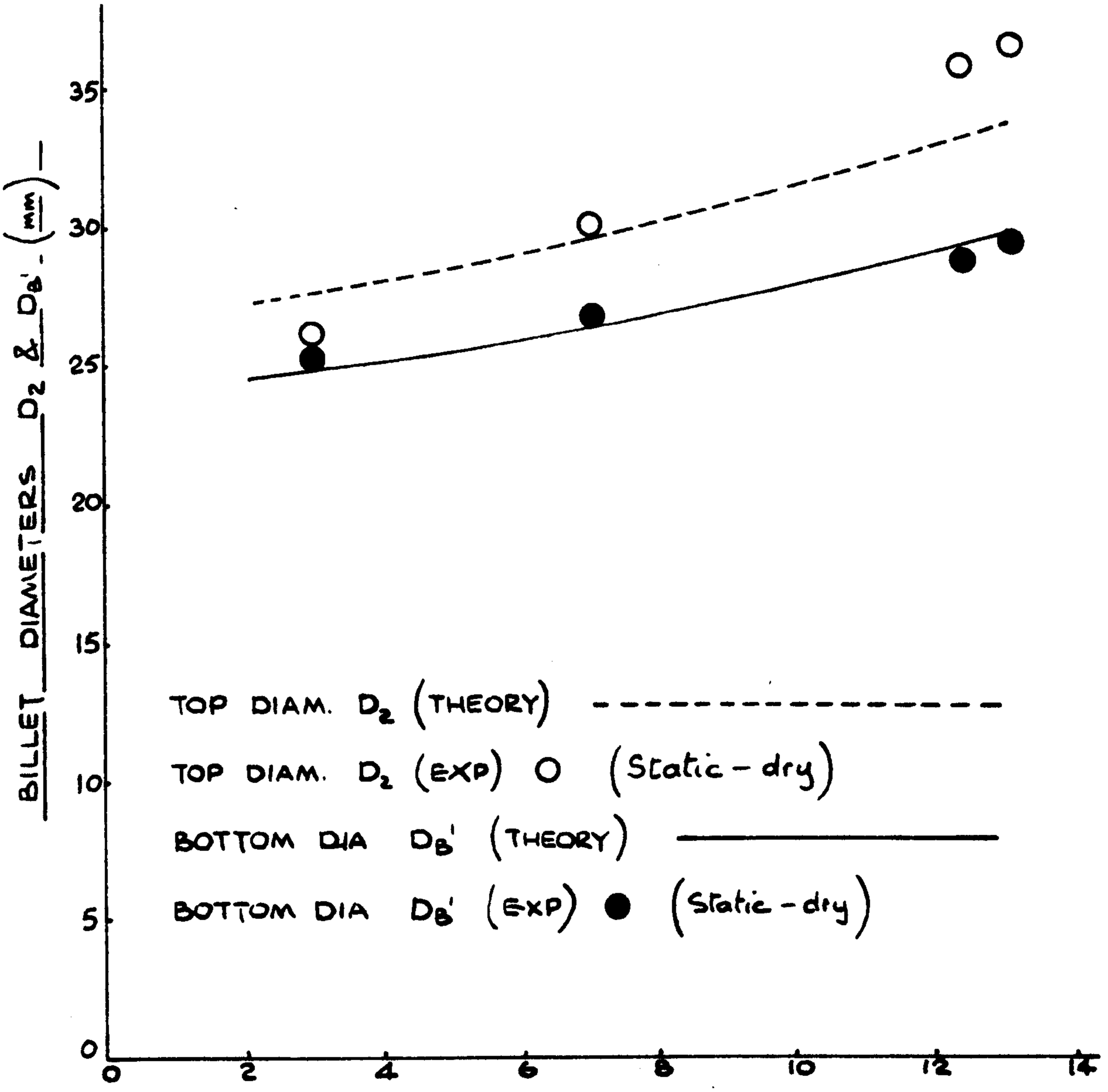

FLANGE DIAMETERS v. TOTAL DISPLACEMENT.

FIG. 60.

EXPERIMENTAL RESULTS

BOSS DIA = 18mm

Y = 17 N/mm²

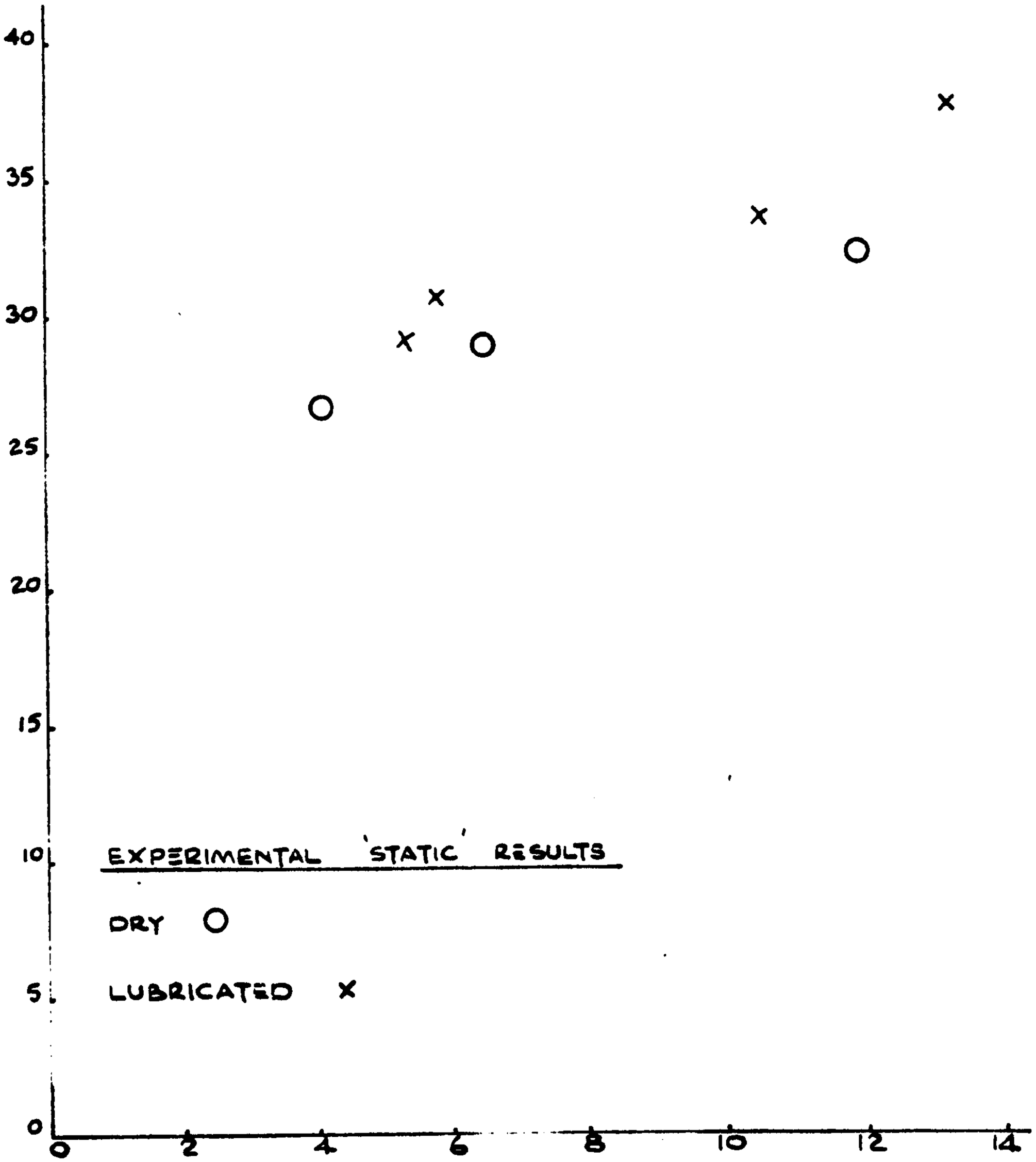

TOP DIAMETER OF FLANGE v. TOTAL DISPLACEMENT.

FIG. 61.

EXPERIMENTAL RESULTS

BOSS D.A = 18mm

Y = 13 N mm⁻²

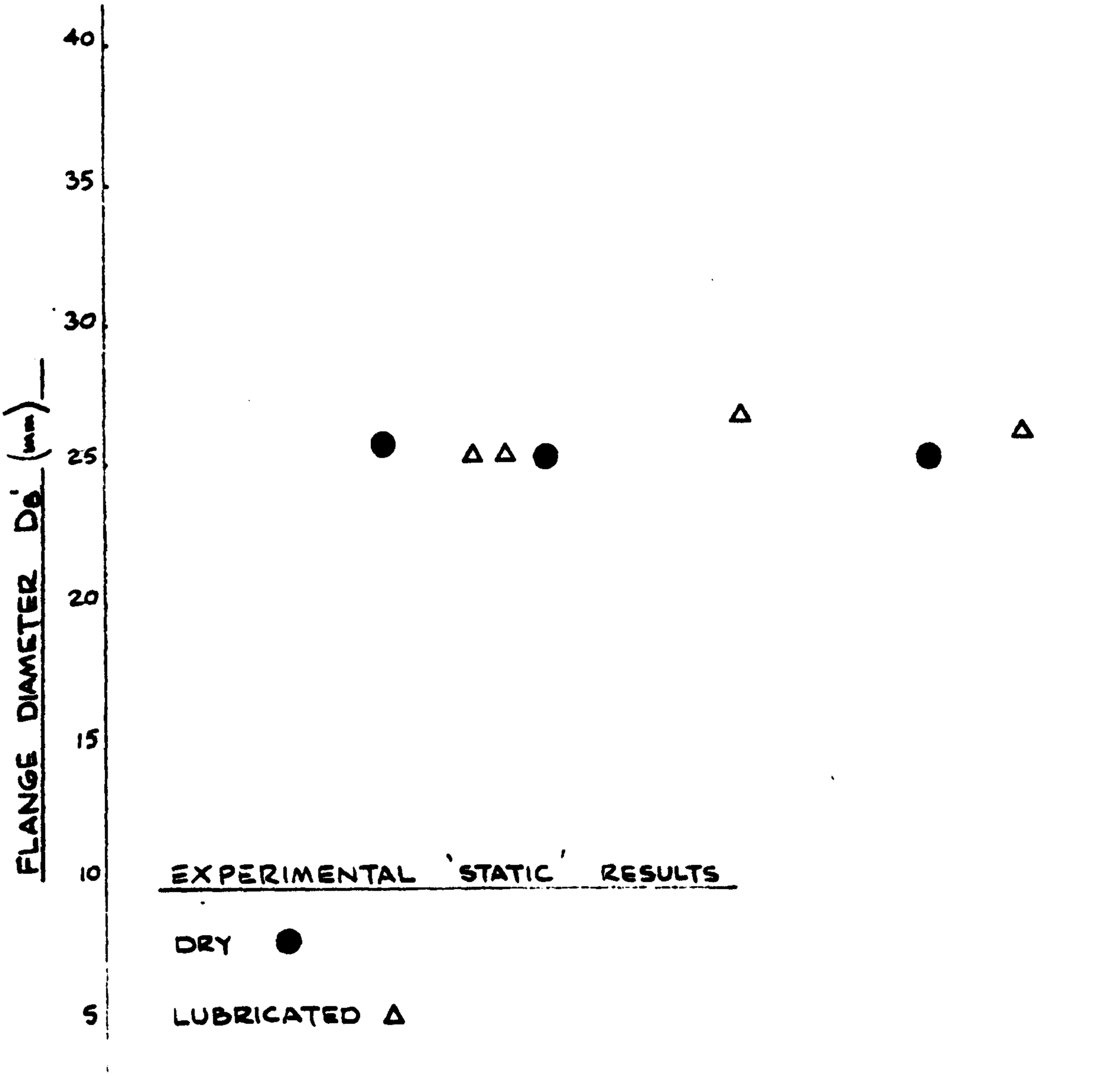

BOTTOM DIAMETER OF FLANGE v. TOTAL DISPLACEMENT

FIG. 62.

EXPERIMENTAL RESULTS

BOSS DIA = 12 mm

Y = 17 N/mm²

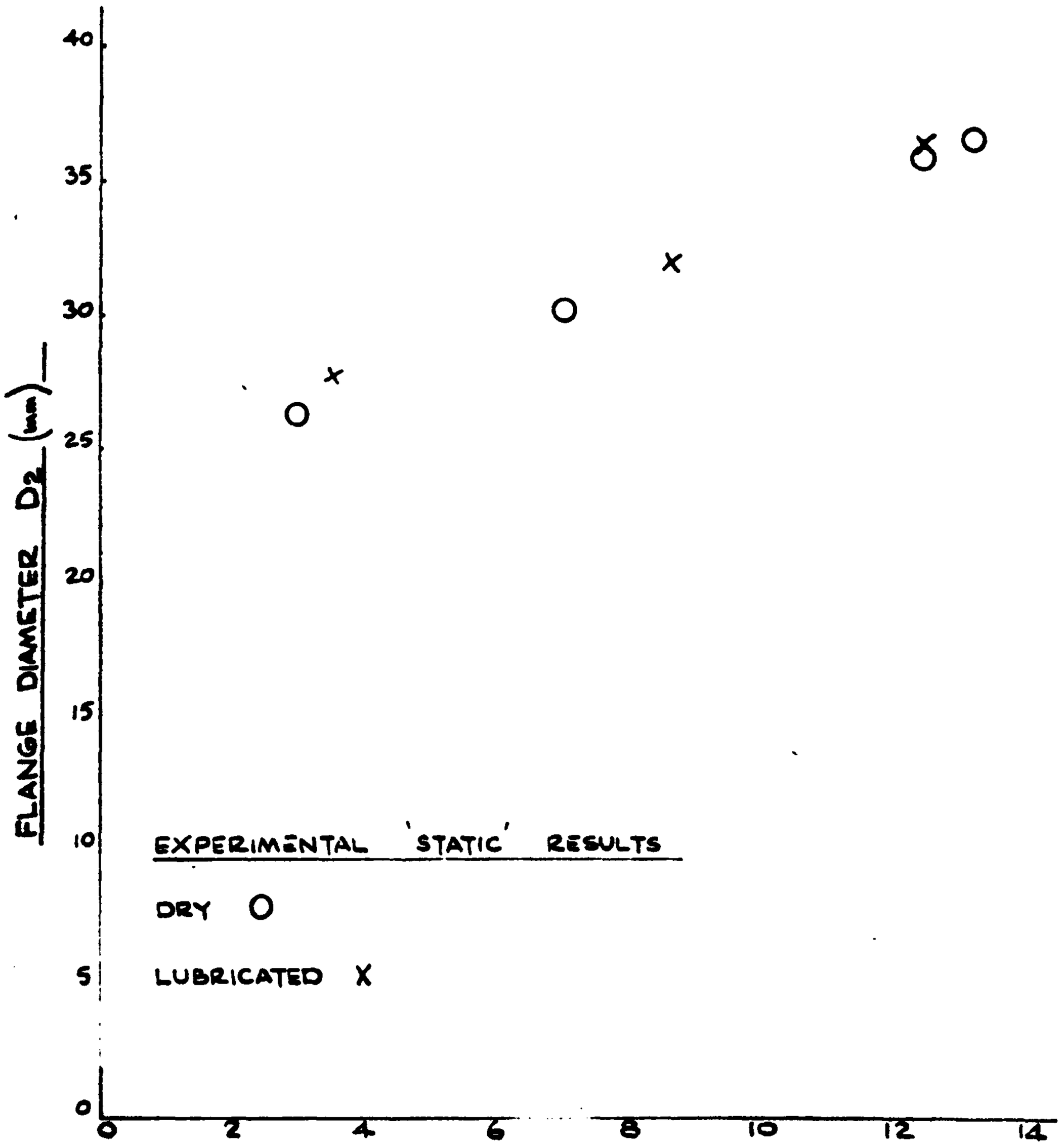

TOP DIAMETER OF FLANGE v. TOTAL DISPLACEMENT.

FIG. 63.

EXPERIMENTAL RESULTS

BOSS D.A = 12 mm

Y = 17 N/mm²

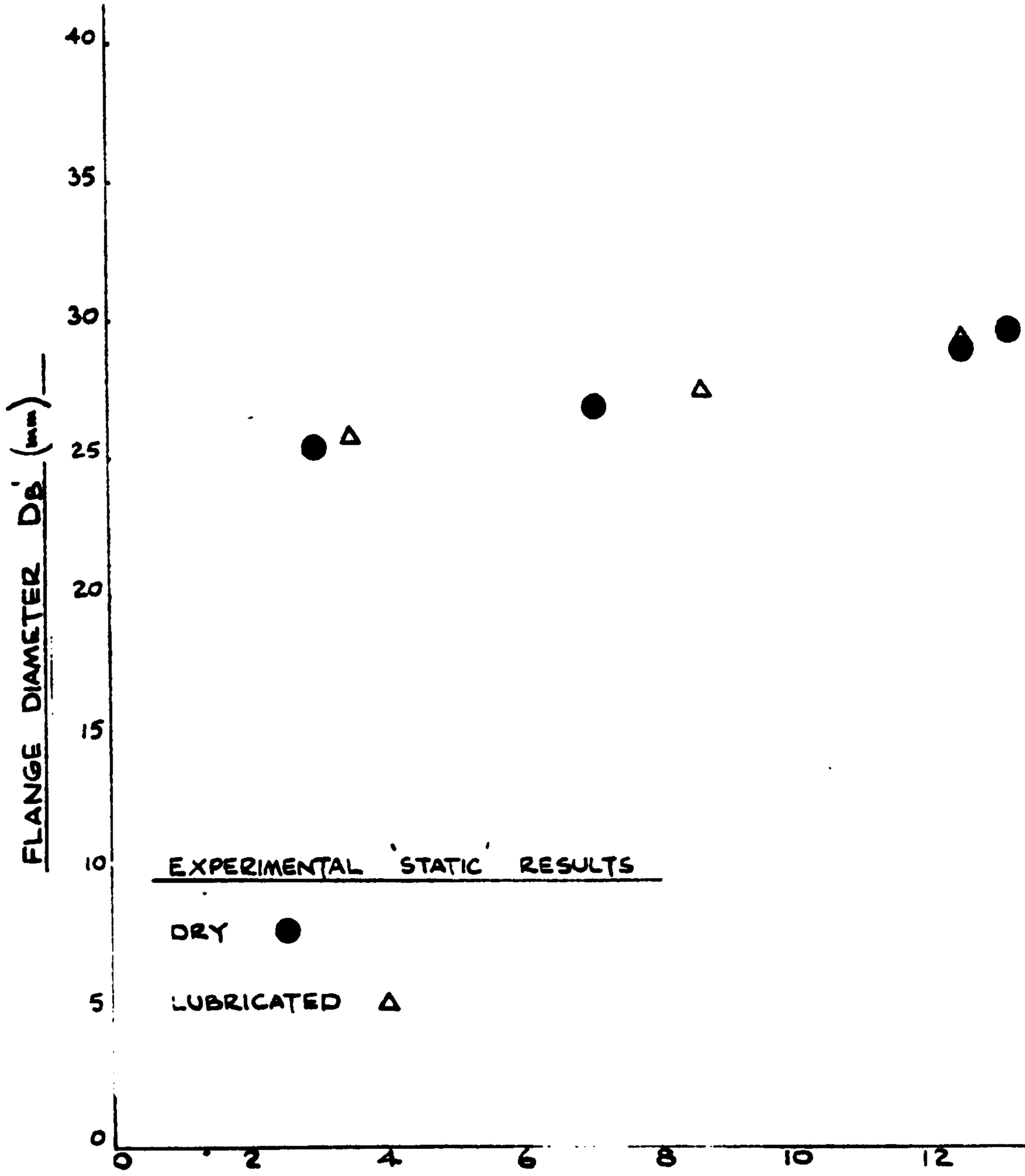

BOTTOM DIAMETER OF FLANGE v. TOTAL DISPLACEMENT.

FIG. 64.

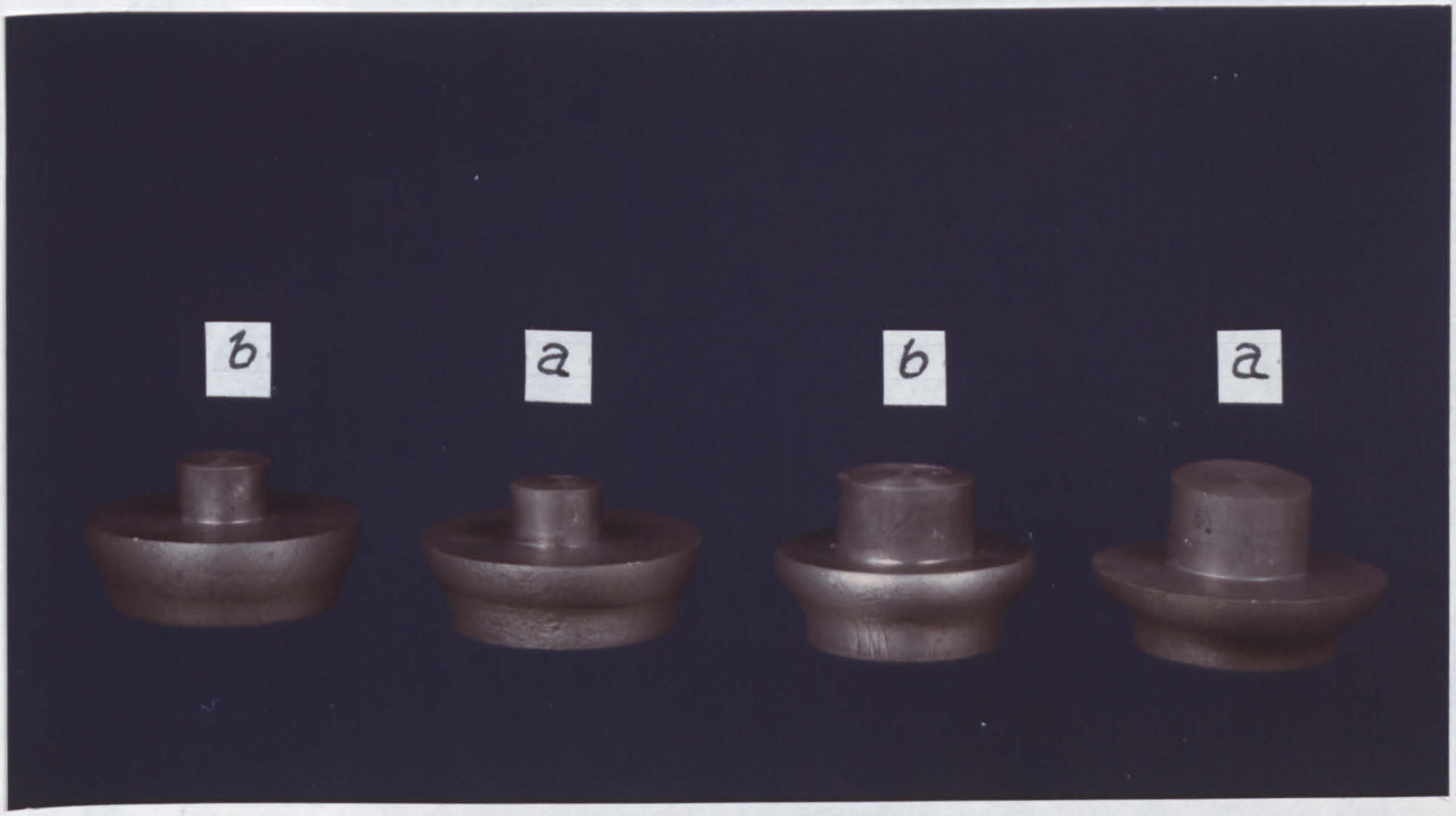

EFFECT OF FRICTION ON BILLET PROFILE

FIG. 65

FIG. 66.

EXPERIMENTAL RESULTS

BOSS DIA = 18mm Y = 17 N/mm²

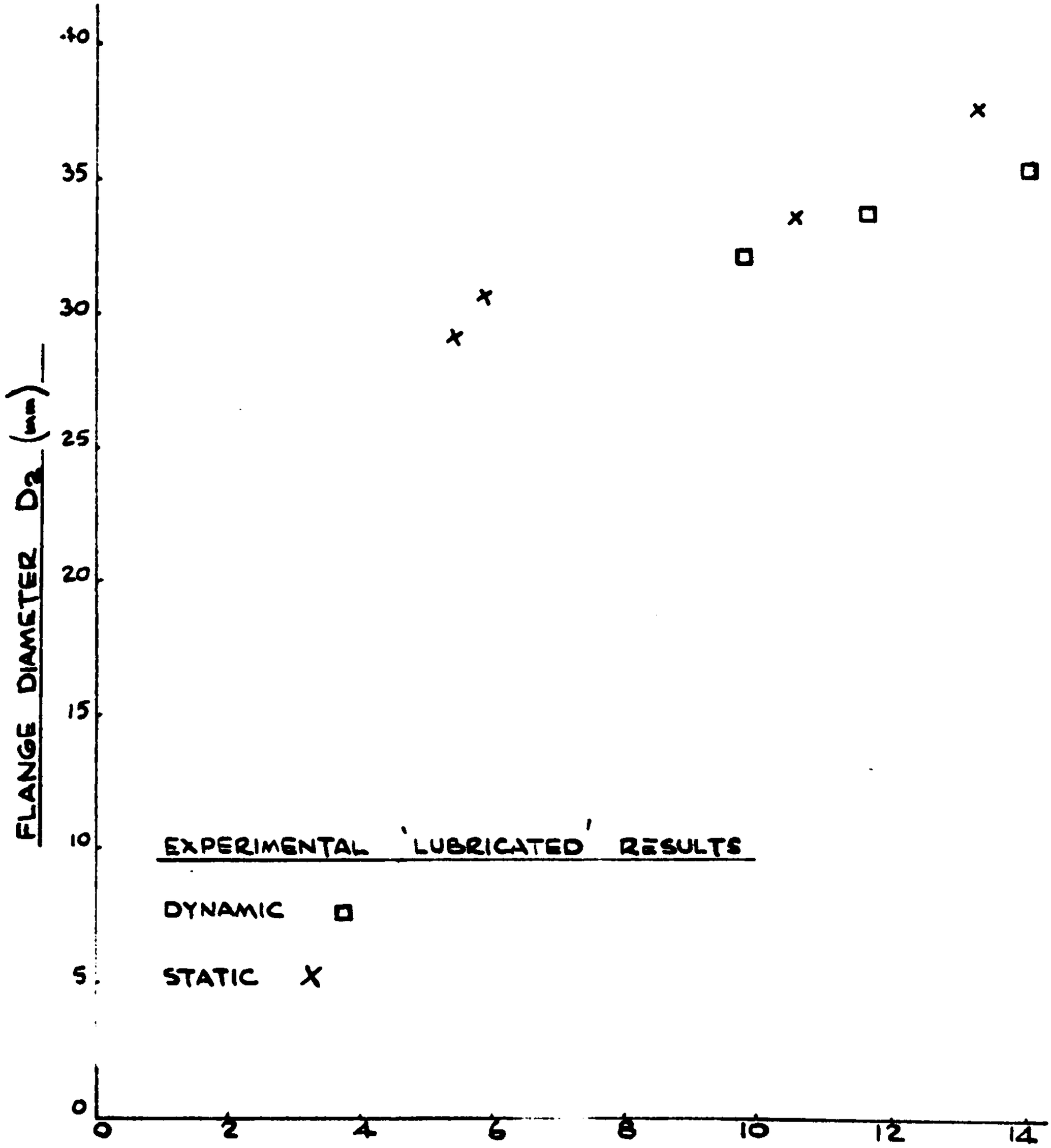

TOP DIAMETER OF FLANGE v. TOTAL DISPLACEMENT.

FIG. 66.

EXPERIMENTAL RESULTS

BOSS DIA = 18mm

Y = 17 N/mm²

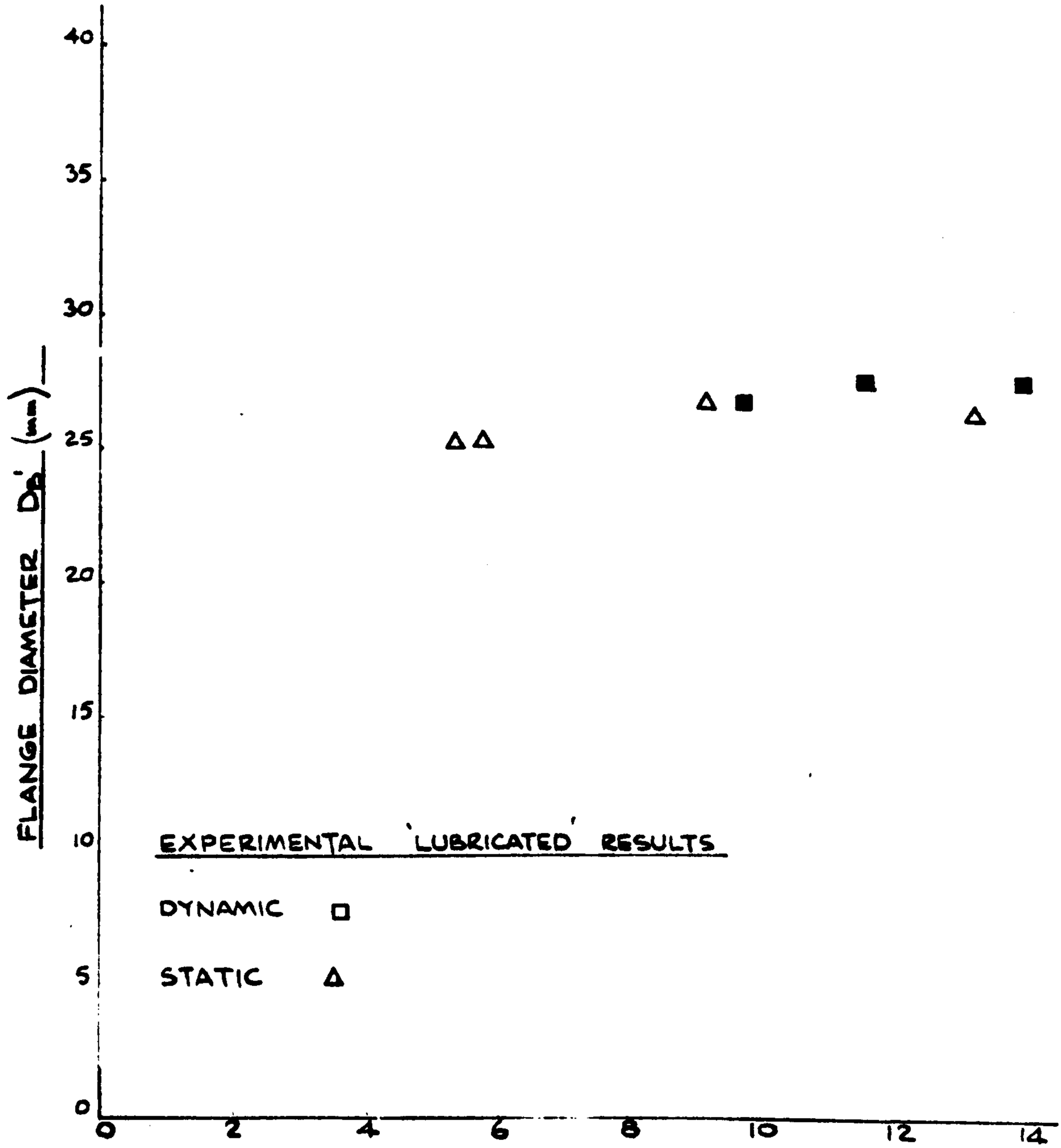

TOP DIAMETER OF FLANGE v. TOTAL DISPLACEMENT.

FIG. 67.

THEORETICAL CURVES

$L_0 = 18$ $\qquad$ $Y = 17\ N/mm^2$

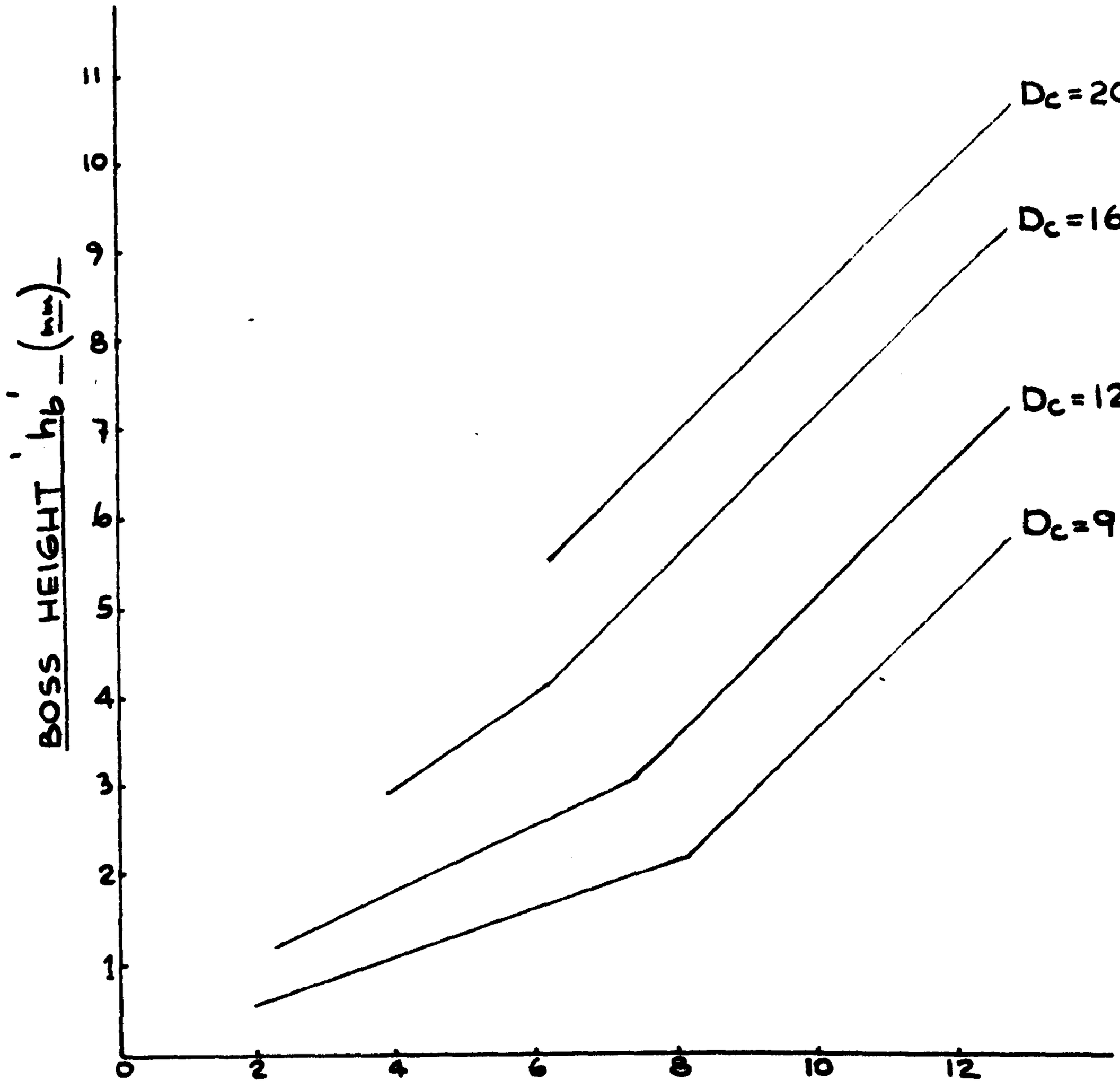

BOSS HEIGHT v. TOTAL DISPLACEMENT

FIG. 68.

THEORETICAL CURVES

$L_o = 22\,mm.$ $Y = 17\ N/mm^2$

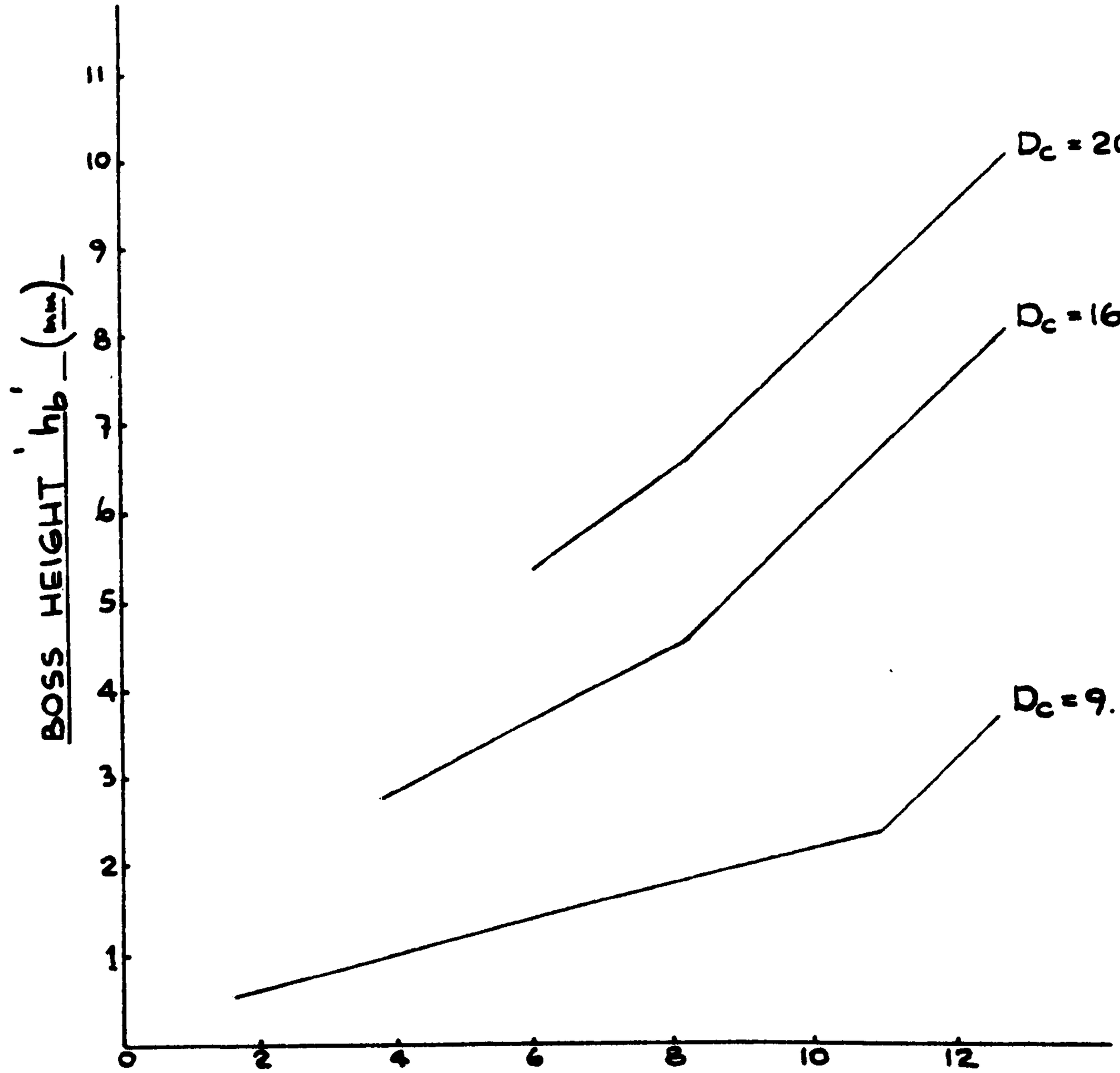

TOTAL DISPLACEMENT $x_0 + x_1$ (mm).

BOSS HEIGHT v. TOTAL DISPLACEMENT.

FIG. 69.

THEORETICAL CURVES

$L_o = 30\,mm.$ $Y = 17\,N/mm^2$

BOSS HEIGHT v. TOTAL DISPLACEMENT

FIG 70.

THEORETICAL / EXPERIMENTAL CURVES

$Y = 17\ N/mm^2$ $L_o = 24\ mm$

THEORETICAL VALUES ——————

EXPERIMENTAL RESULTS STATIC LUBRICATED

$D_c = 18$ —— ··■—————·—————

$D_c = 9$ - - - -▲- - - - - - - - - - -

EXPERIMENTAL RESULTS DYNAMIC LUBRICATED

$D_c = 18$ ——□··——————·—————

$D_c = 9$ - - - -△- - - - - - - - - - -

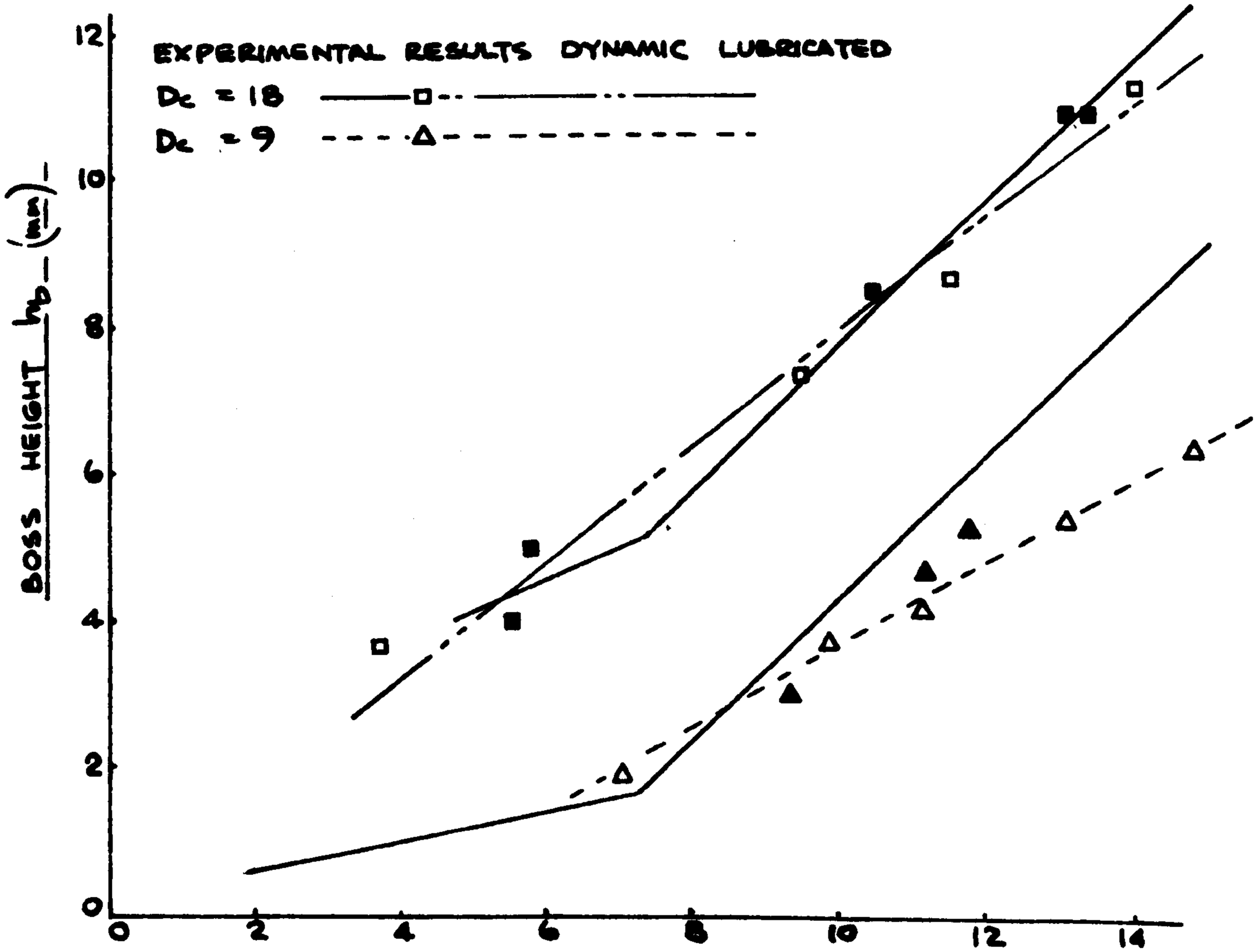

BOSS HEIGHT v. TOTAL DISPLACEMENT

FIG. 71.

THEORETICAL CURVES

BOSS DIA = 9 mm $Y = 17\ N/mm^2$.

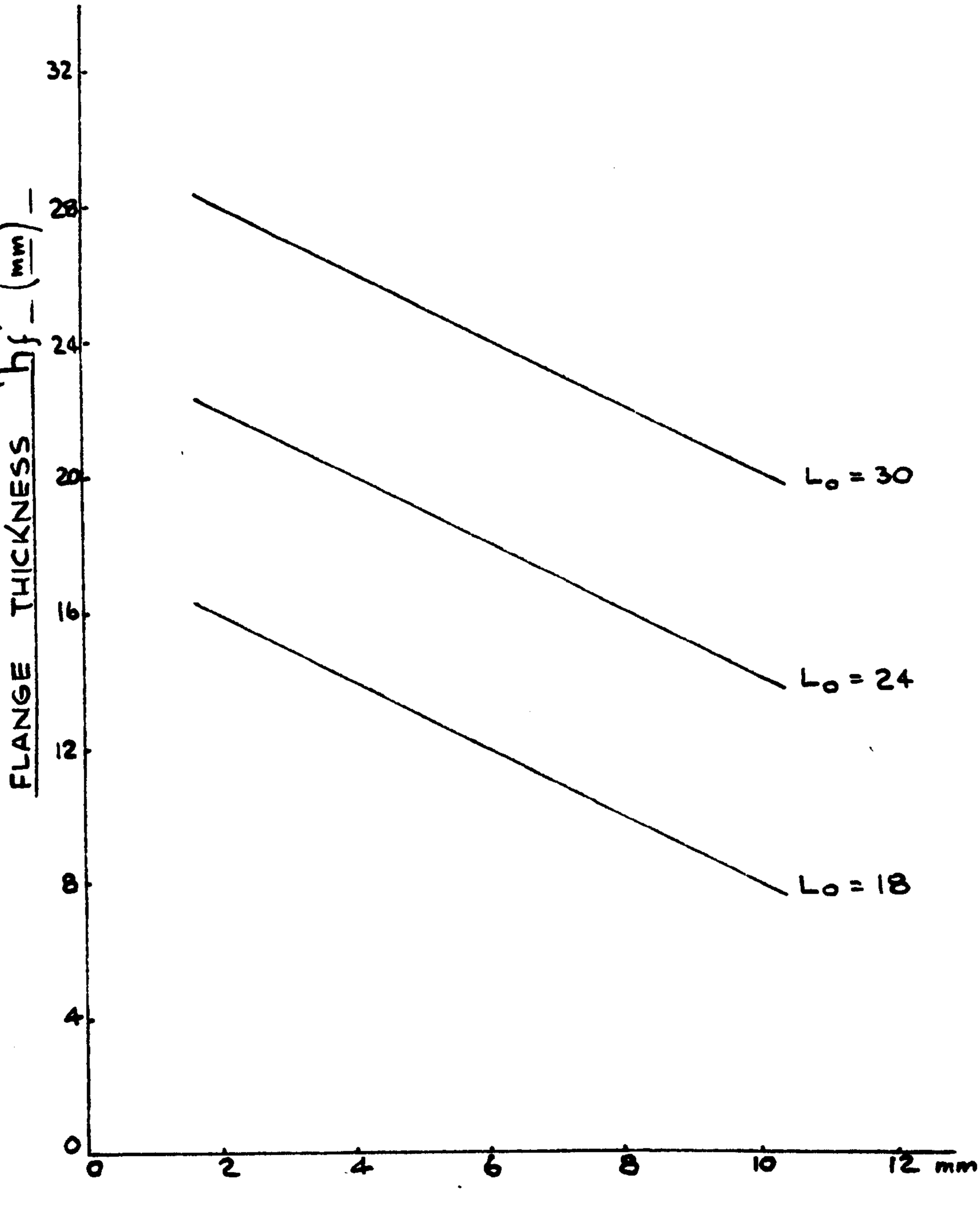

FLANGE THICKNESS v. TOTAL DISPLACEMENT

FIG. 72.

THEORETICAL CURVES

BOSS DIA = 16 mm Y = 17 N/mm²

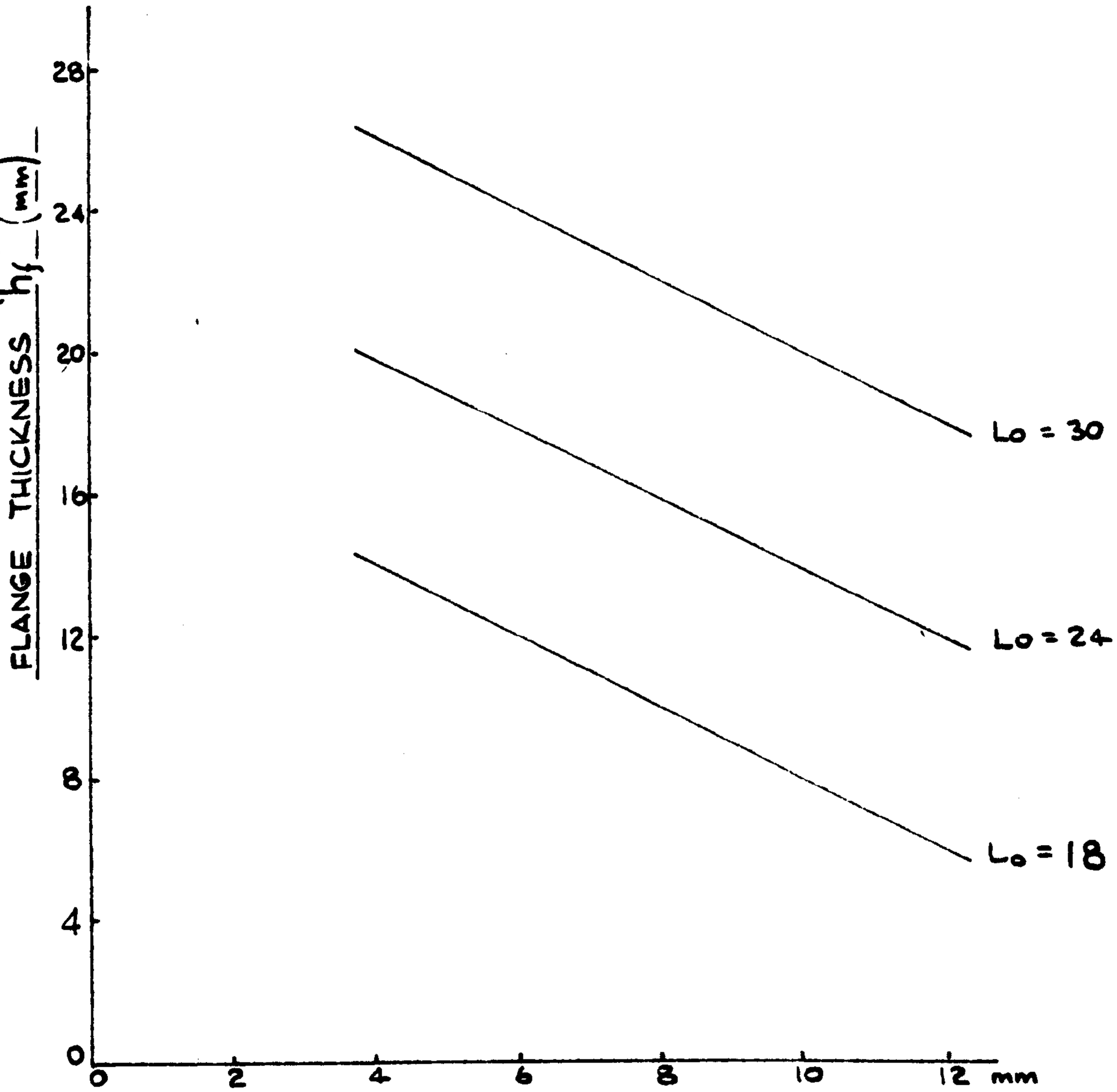

FLANGE THICKNESS v. TOTAL DISPLACEMENT.

FIG. 73.

THEORETICAL CURVES

BOSS DIA = 20 mm Y = 17 N/mm²

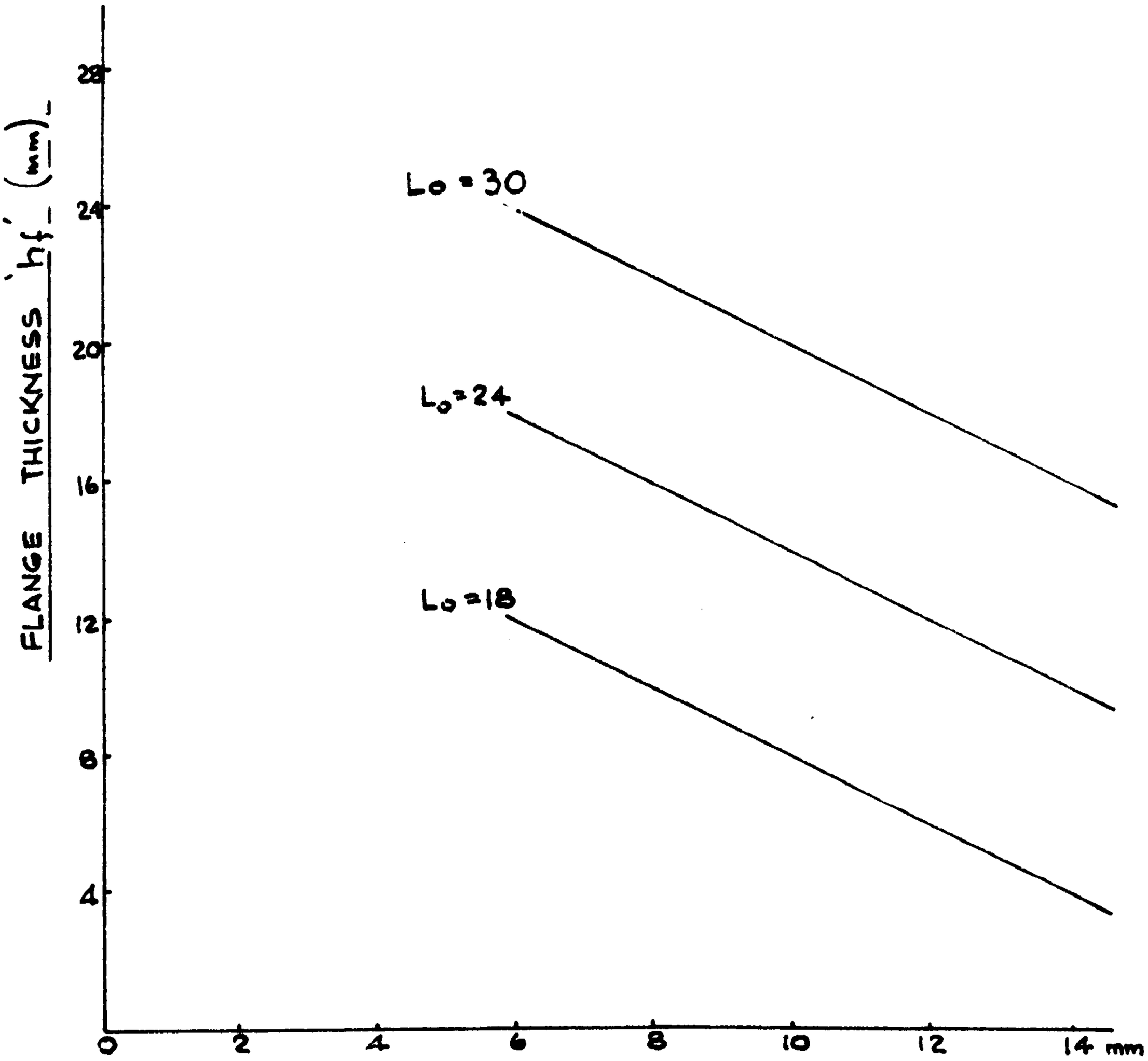

TOTAL DISPLACEMENT $x_o + x_1$

FLANGE THICKNESS v. TOTAL DISPLACEMENT

FIG. 74.

THEORETICAL CURVES

BOSS DIA = 18 mm Y = 17 N/mm²

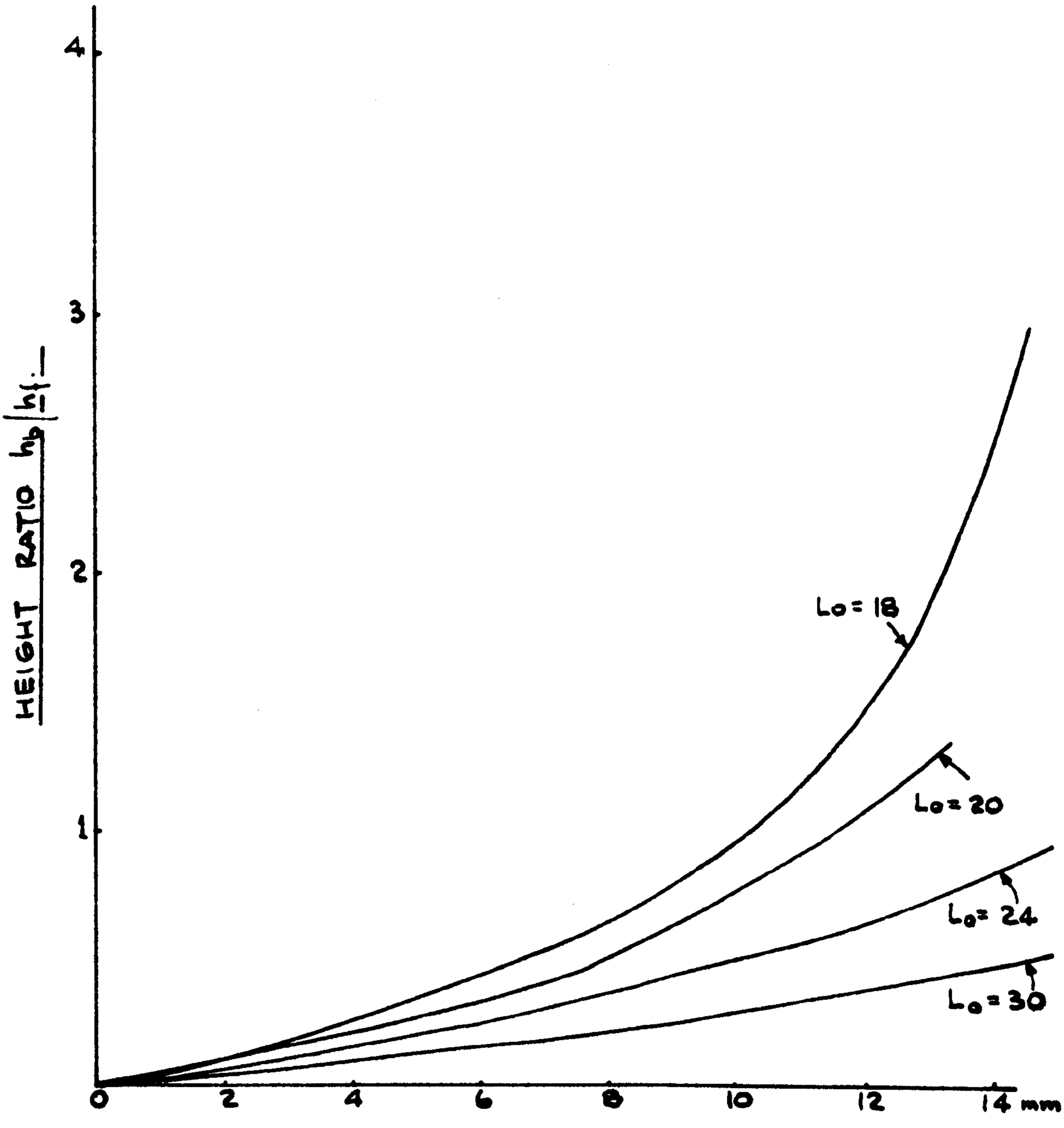

TOTAL DISPLACEMENT $x_0 + x_1$

HEIGHT RATIO v. TOTAL DISPLACEMENT

FIG. 75.

THEORETICAL CURVES

BOSS DIA. = 20 mm Y = 17 N/mm²

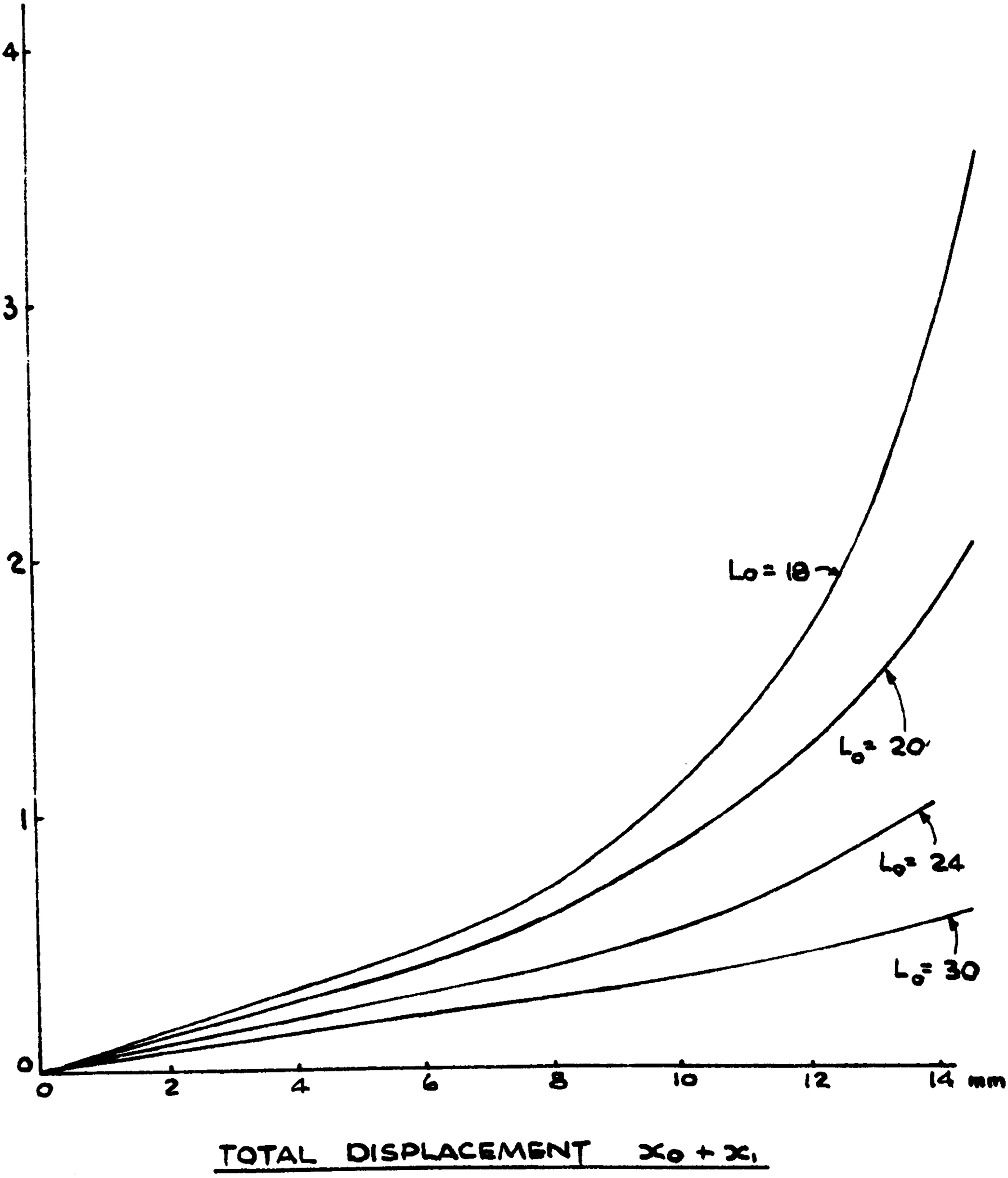

TOTAL DISPLACEMENT $x_0 + x_1$

HEIGHT RATIO v. TOTAL DISPLACEMENT

FIG. 76.

THEORETICAL RESULTS

$L_o = 24$ mm. $Y = 17$ N/mm^2.

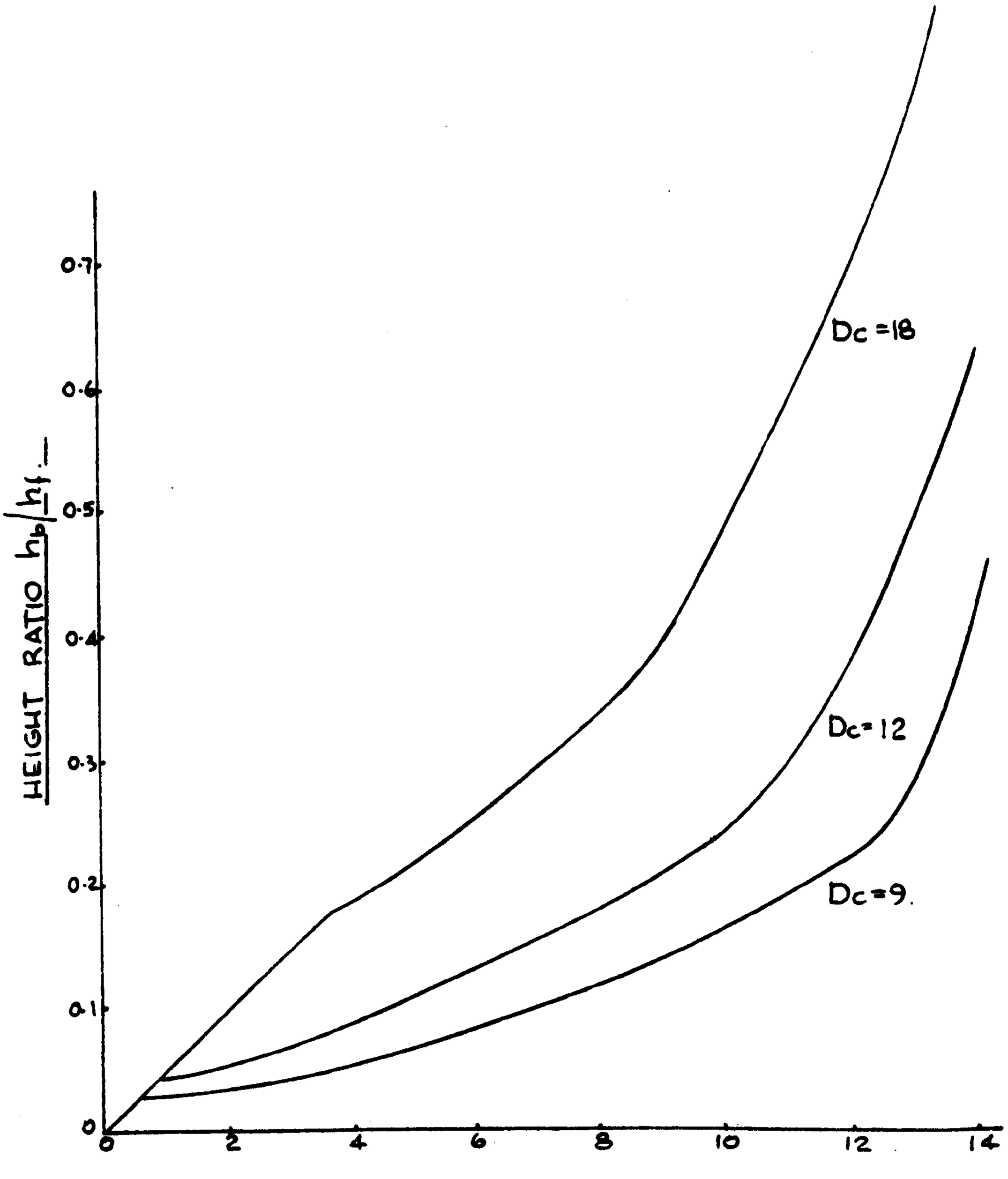

HEIGHT RATIO v. TOTAL DISPLACEMENT.

FIG. 77.

THEORETICAL / EXPERIMENTAL RESULTS

$L_o = 24\,mm.$ $Y = 17\ N/mm^2.$

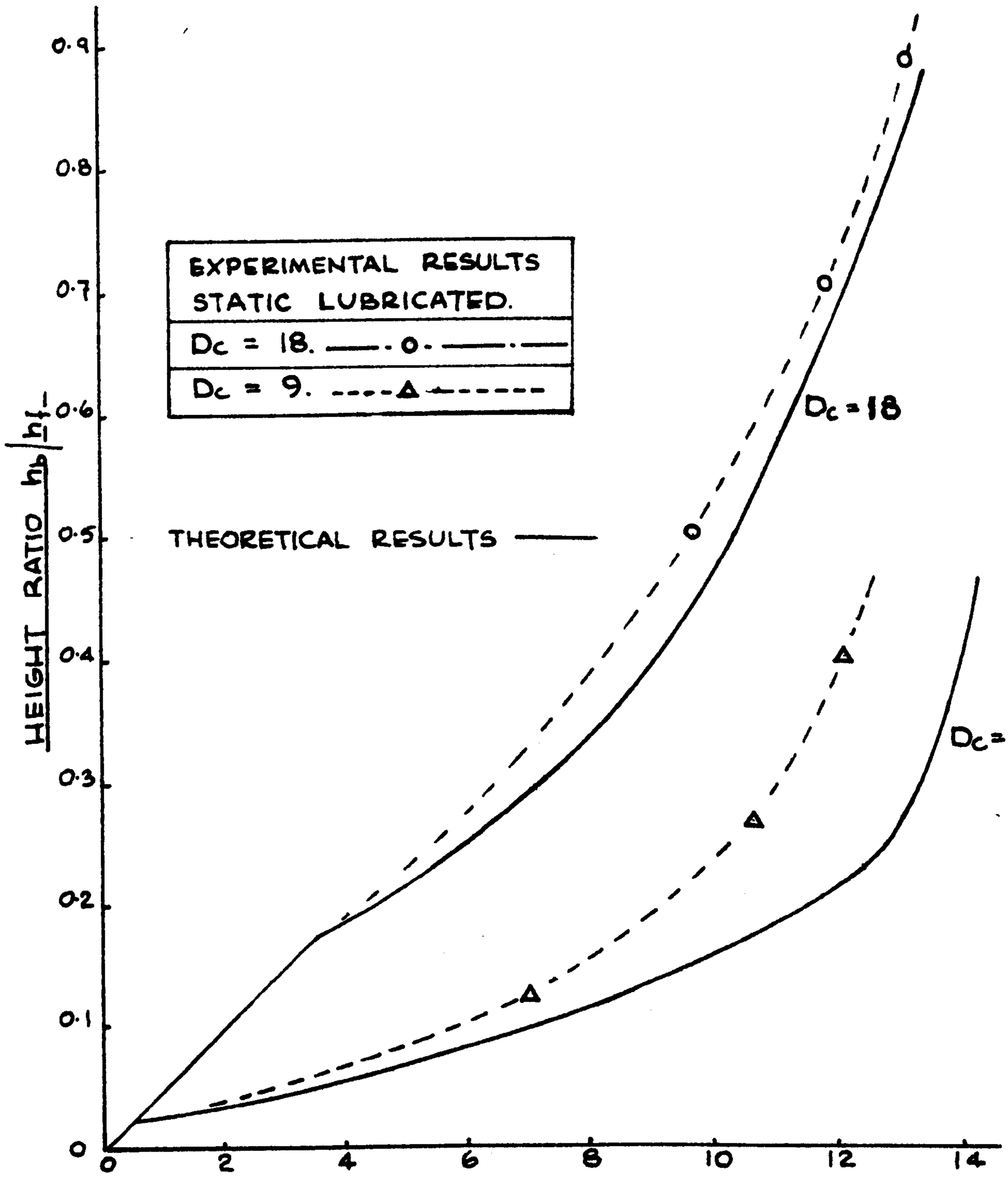

HEIGHT RATIO v. TOTAL DISPLACEMENT

FIG. 78.

THEORETICAL AND EXPERIMENTAL RESULTS

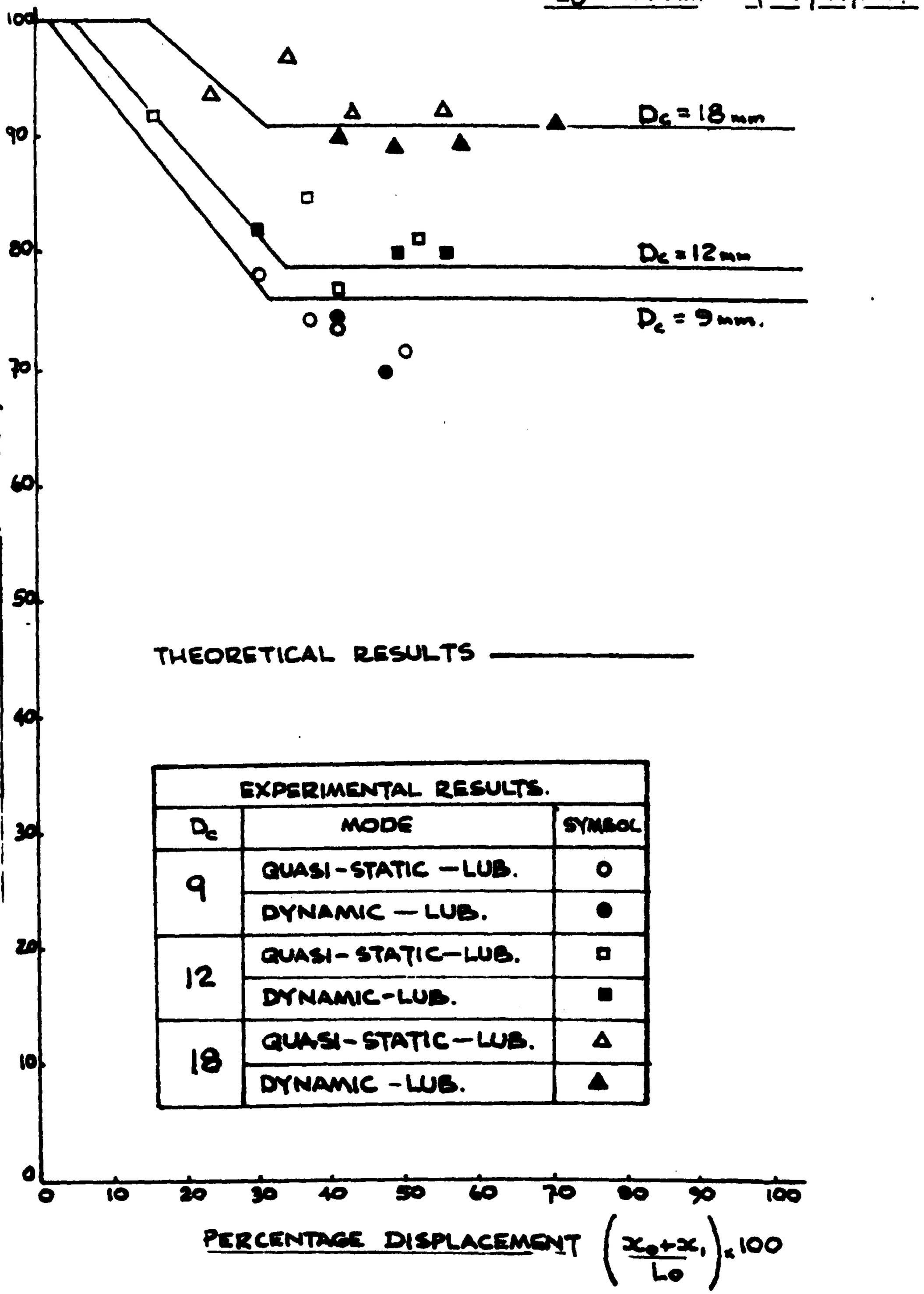

RATIO OF TOTAL BILLET HEIGHT TO TOTAL DISPLACEMENT.

FIG. 78 (a)-

$L_o = 24\,mm$ $Y = 17\ N/mm^2$

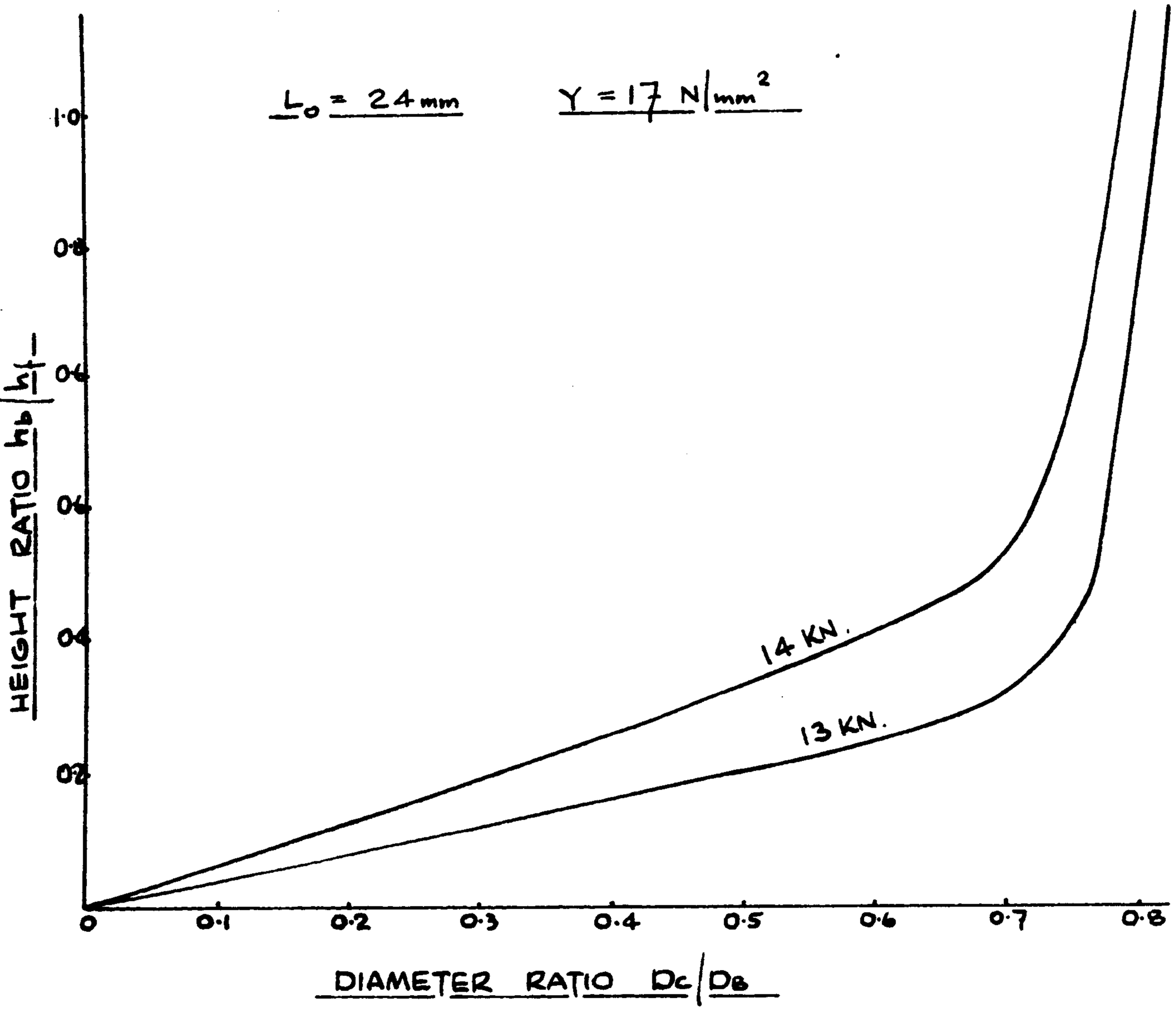

FIG. 79. HEIGHT RATIO v. DIAMETER RATIO.

THEORETICAL CURVE.

BILLET DIA. = 24mm. $Y = 17\ N/mm^2$.

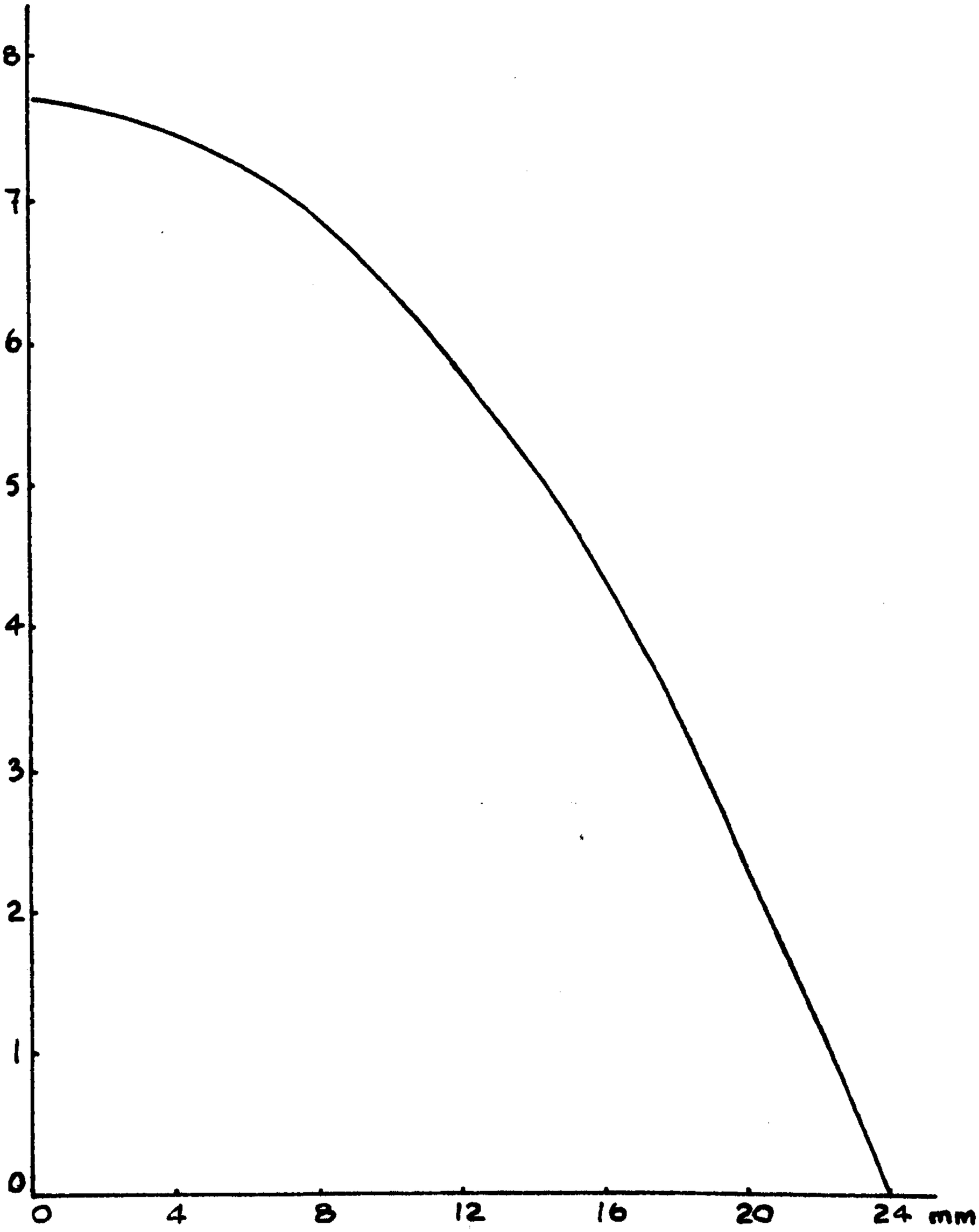

FORCE REQUIRED TO INITIATE DEFORMATION v. BOSS DIAMETER.

FIG.80.

THEORETICAL CURVES

BOSS DIA. = 9 mm $Y = 17\ N/mm^2$.

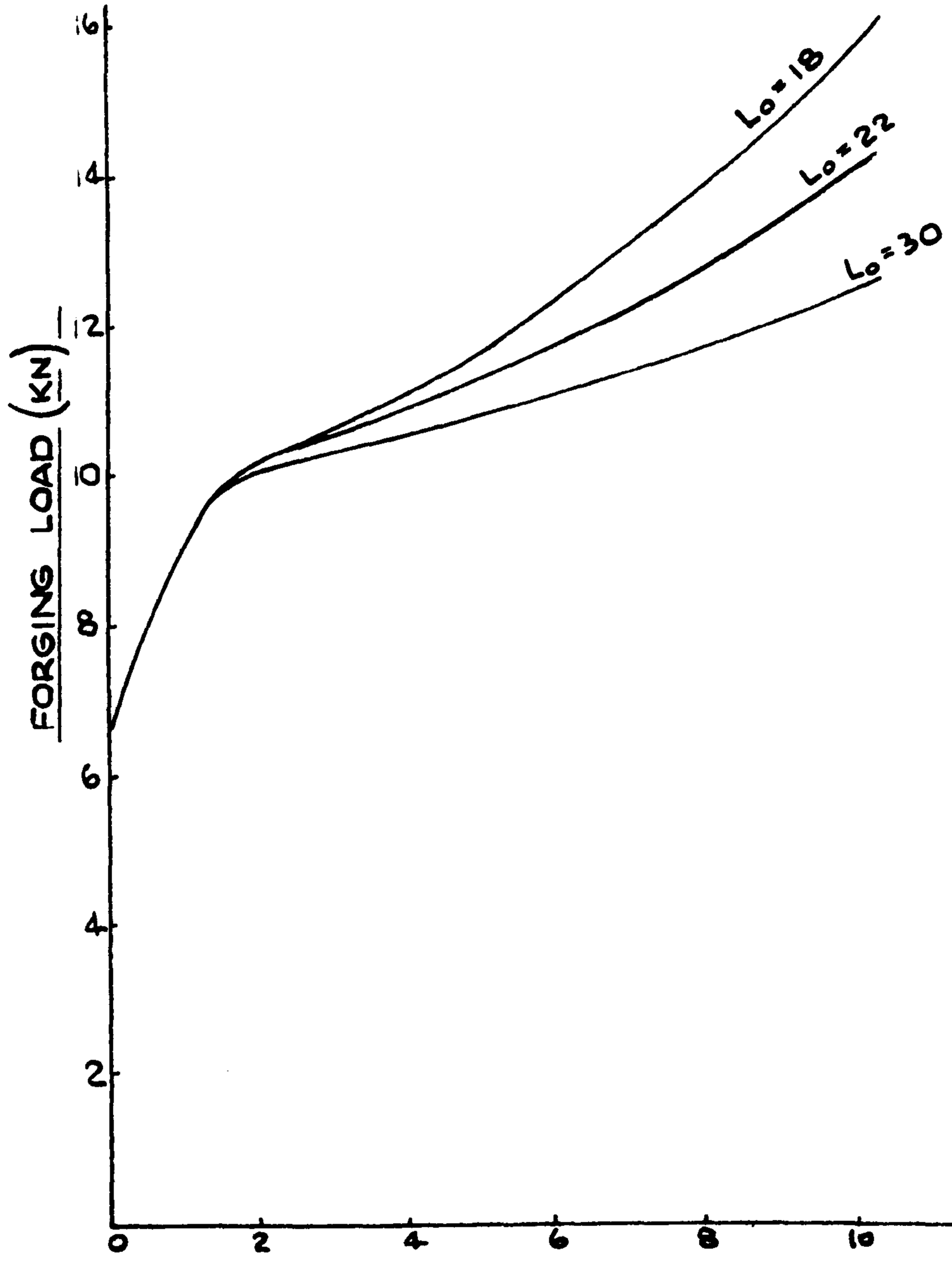

TOTAL DISPLACEMENT $x_o + x_1$

FORGING LOAD v. TOTAL DISPLACEMENT

FIG. 81

THEORETICAL CURVES

BOSS DIA = 12 mm Y = 17 N/mm²

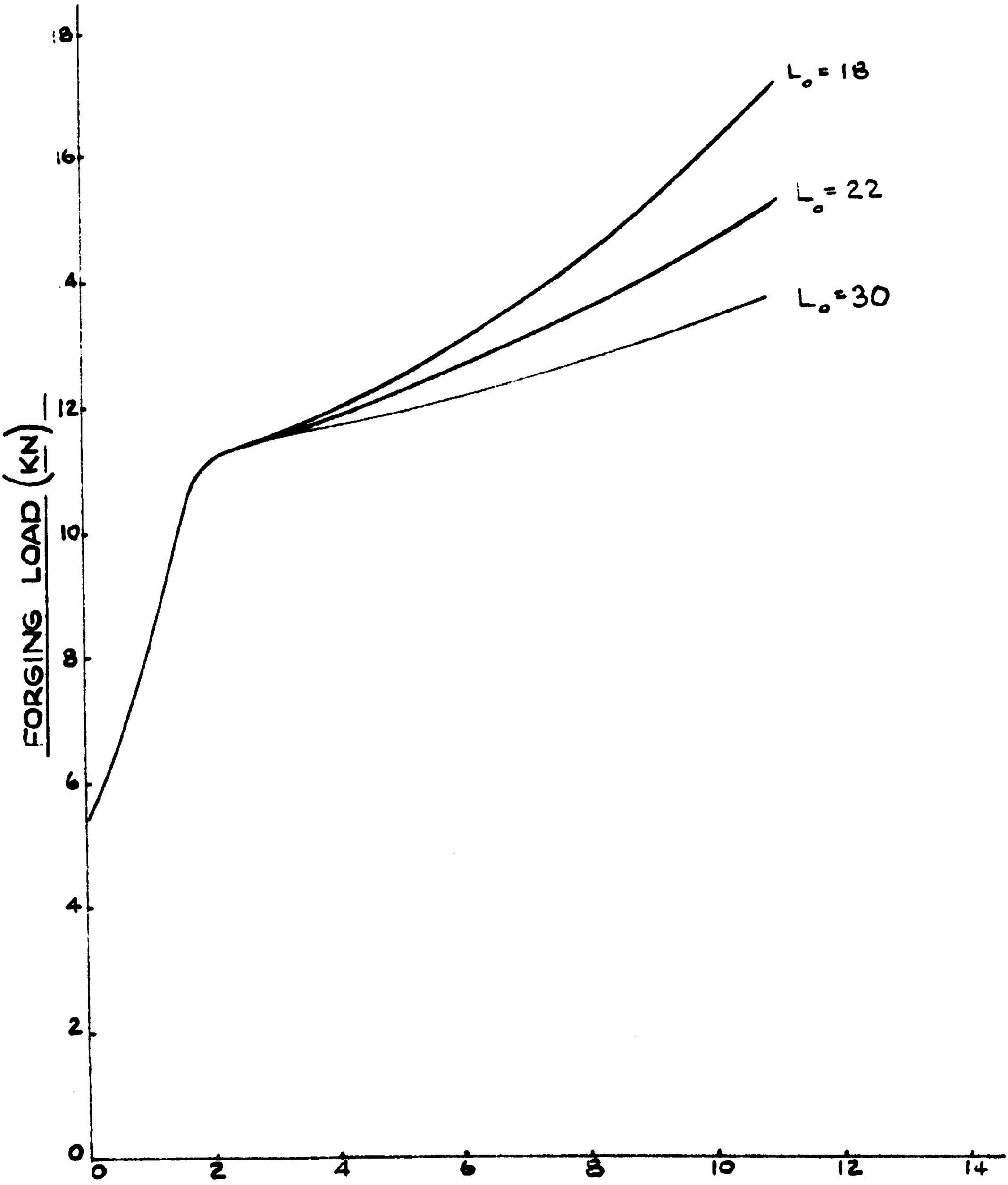

FORGING LOAD v. TOTAL DISPLACEMENT

FIG. 82

THEORETICAL CURVES

BOSS DIA = 14mm Y = 17 N/mm²

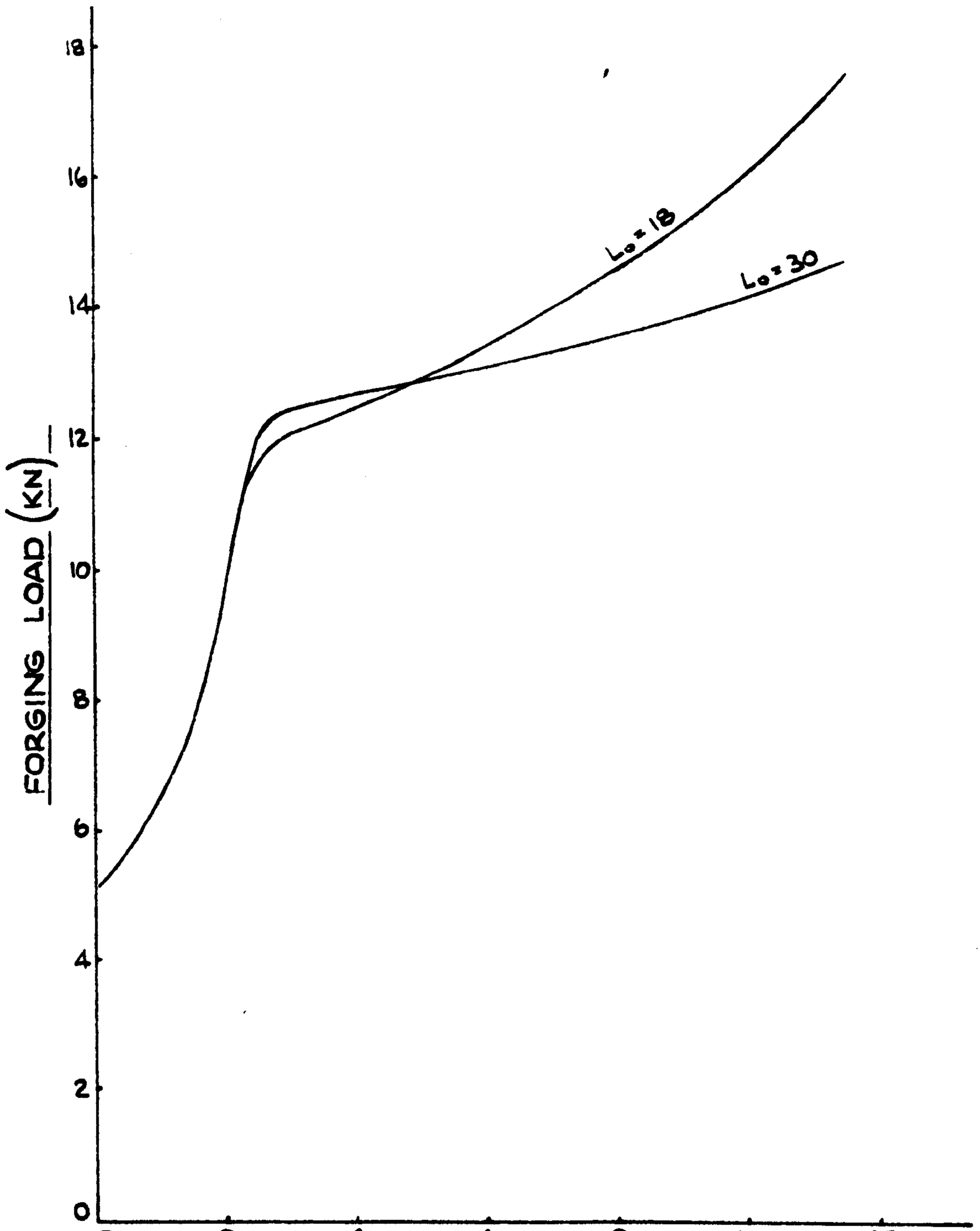

FORGING LOAD v. TOTAL DISPLACEMENT

FIG. 83

THEORETICAL CURVES

BOSS DIA. 16mm $Y = 17\ N/mm^2$.

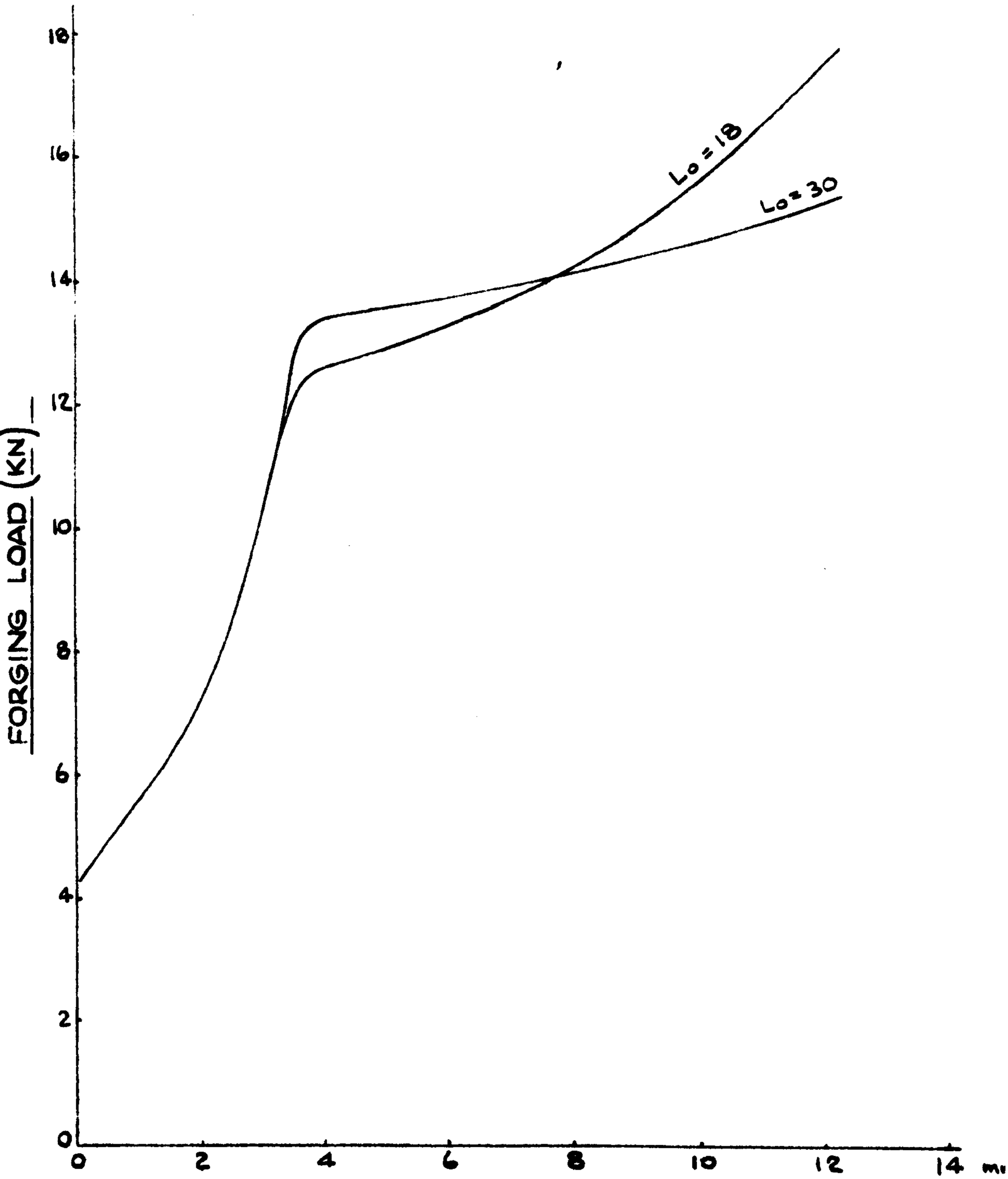

TOTAL DISPLACEMENT $x_0 \pm x_1$

FORGING LOAD v. TOTAL DISPLACEMENT

FIG. 84

THEORETICAL CURVES

BOSS DIA = 18mm Y = 17 N/mm²

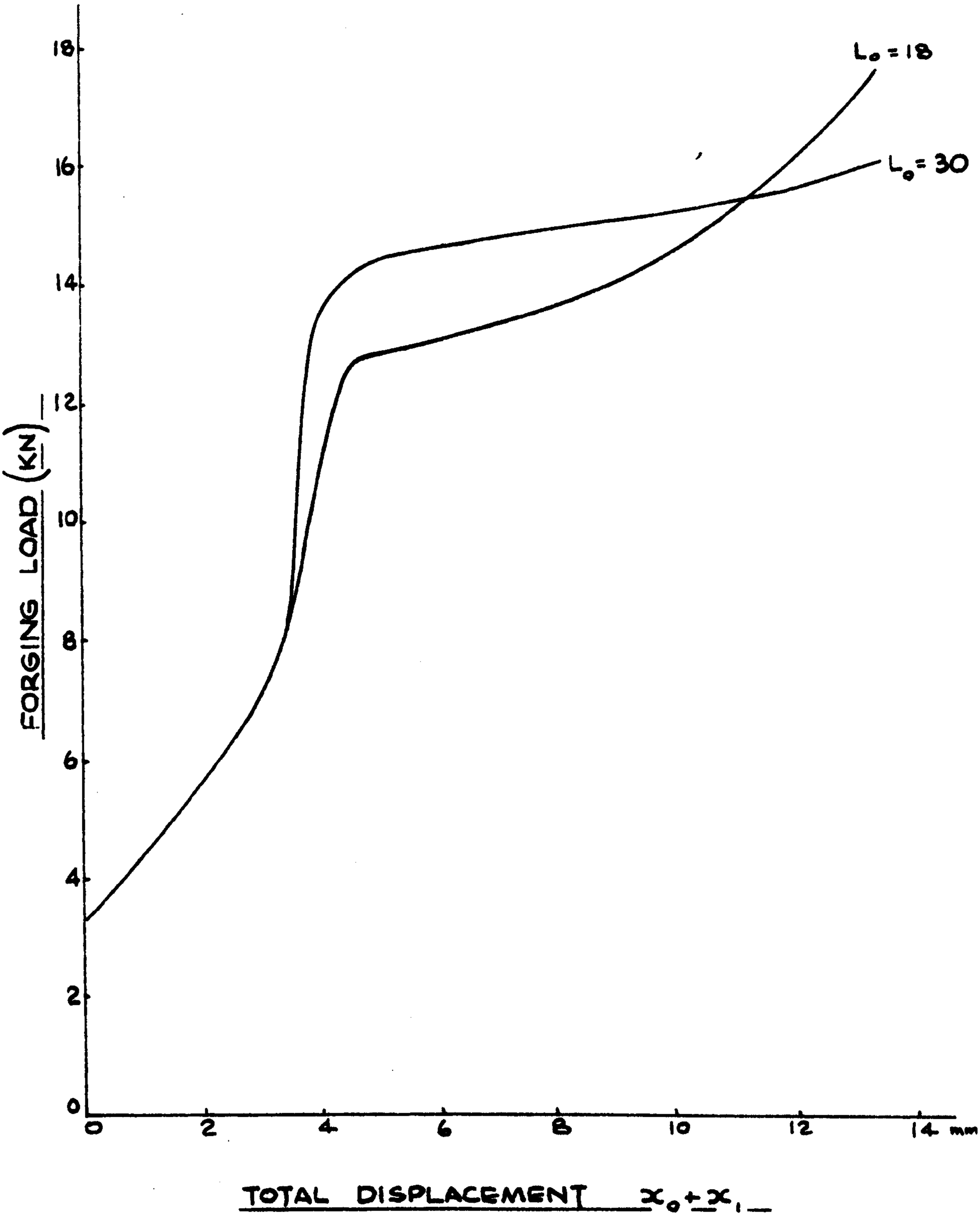

TOTAL DISPLACEMENT $x_0 + x_1$

FORGING LOAD v. TOTAL DISPLACEMENT

FIG. 85

THEORETICAL CURVES

BOSS DIA = 20mm Y = 17 N/mm²

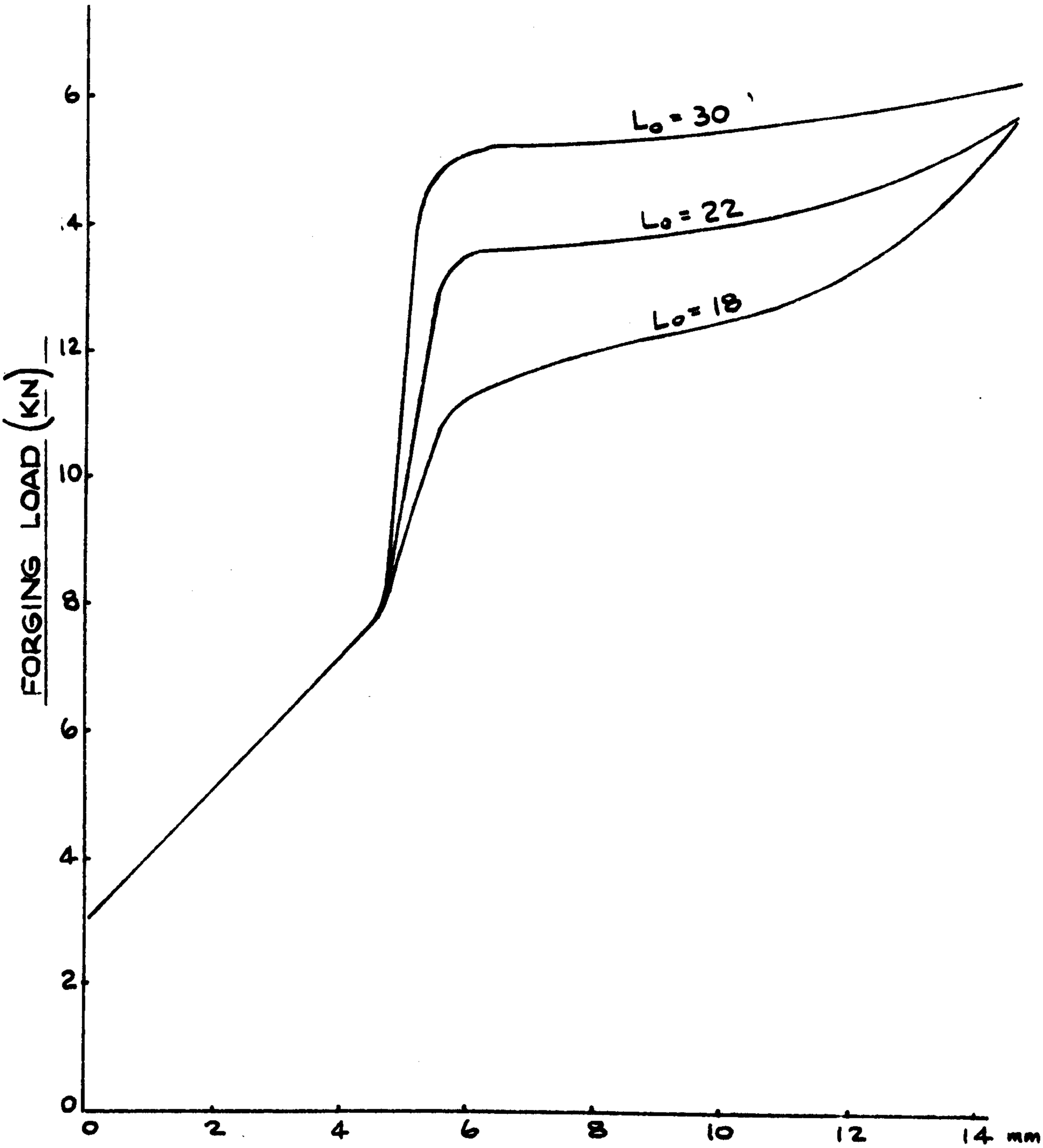

TOTAL DISPLACEMENT $x_o + x_1$

FORGING LOAD v. TOTAL DISPLACEMENT

FIG. 86

THEORETICAL CURVES

$Y = 17\ N/mm^2$ $L_o = 24mm.$

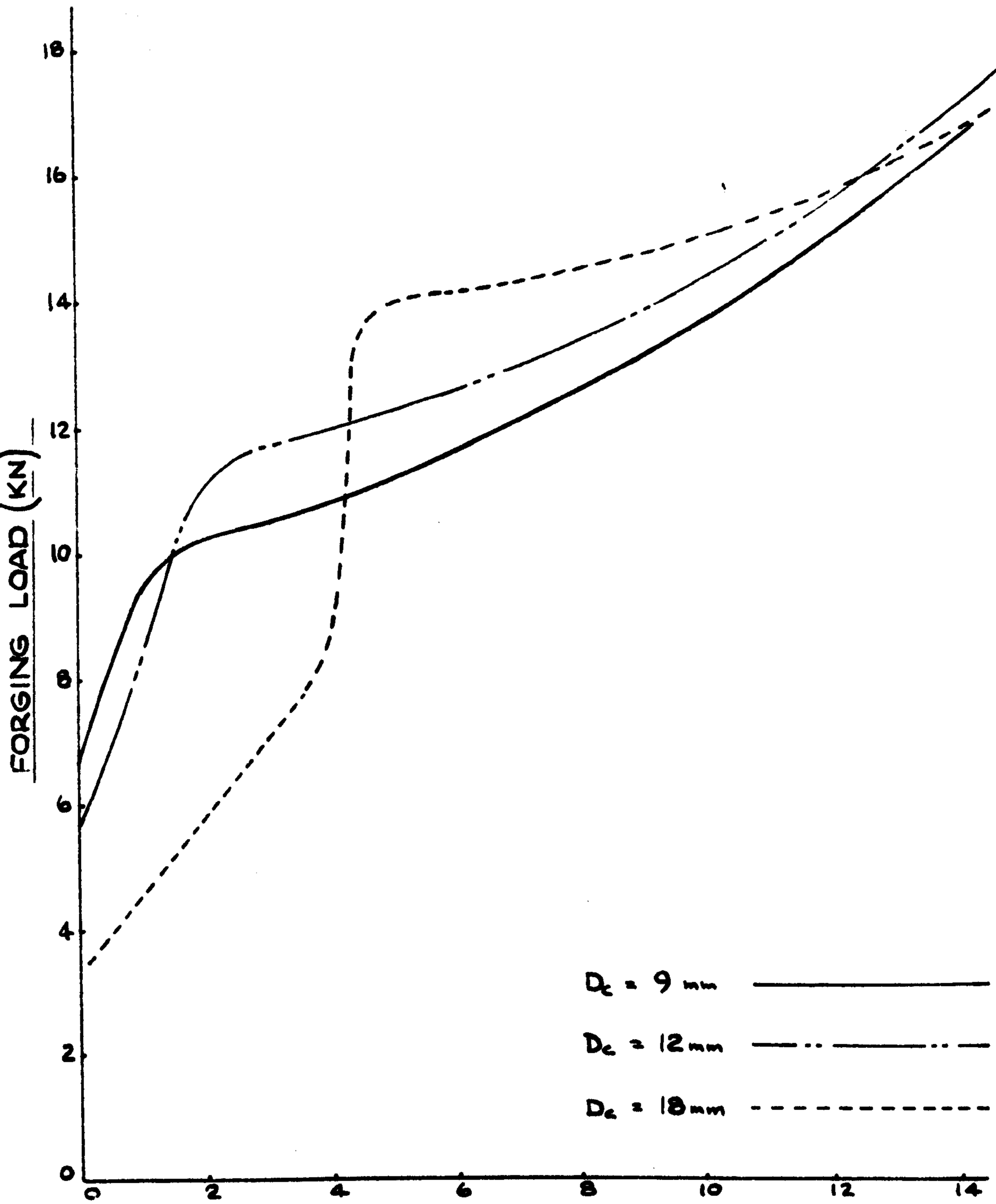

FORGING LOAD v. TOTAL DISPLACEMENT

FIG. 87

THEORETICAL | EXPERIMENTAL RESULTS.

$D_c = 18\,mm.$ $L_o = 24\,mm.$ $Y = 17\ N/mm^2.$

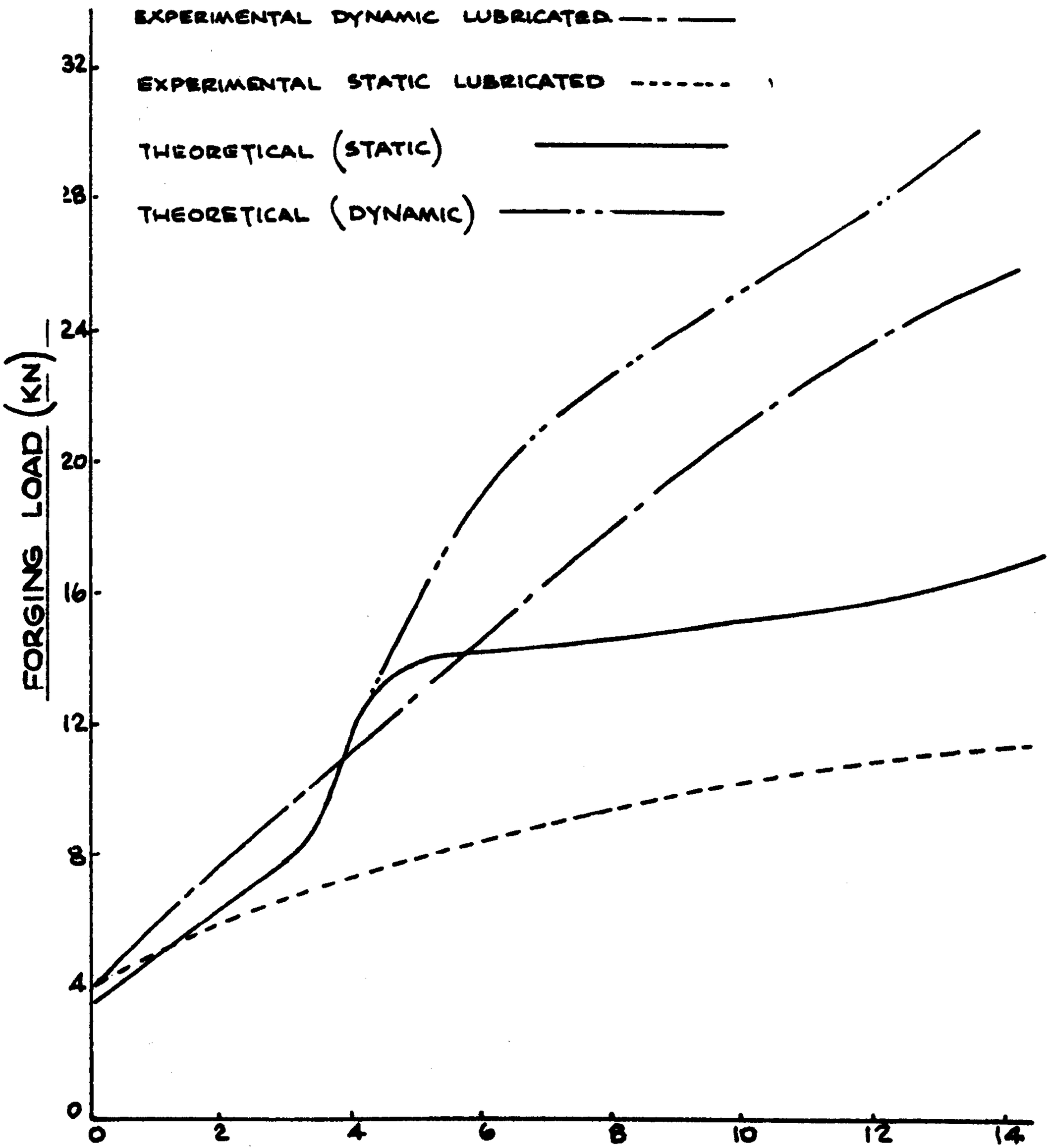

FORGING LOAD v. TOTAL DISPLACEMENT

FIG. 88(a)

THEORETICAL | EXPERIMENTAL RESULTS

$D_c = 12\,mm$ $L_0 = 24\,mm$ $Y = 17\ N/mm^2$

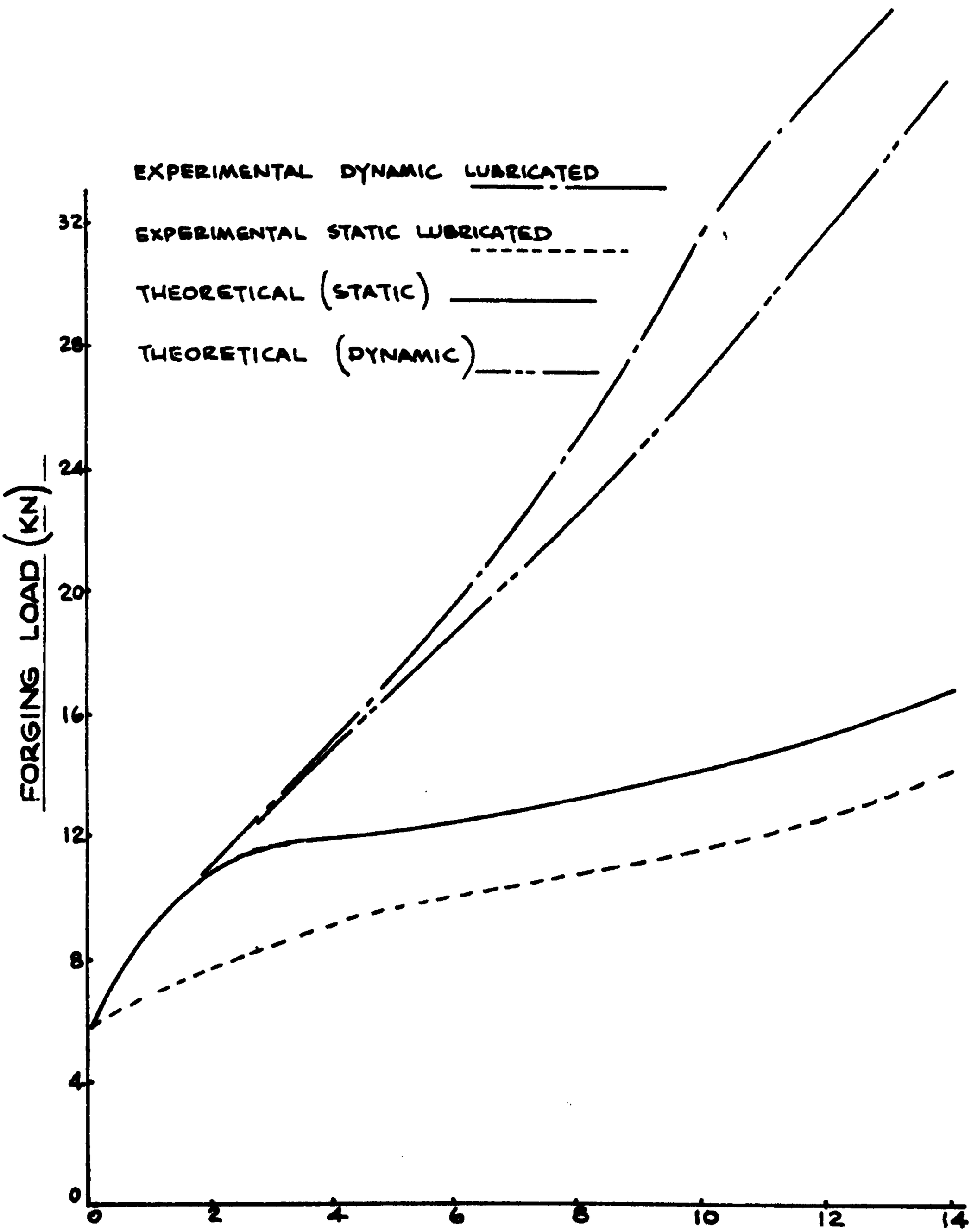

FORGING LOAD v. TOTAL DISPLACEMENT

FIG. 88(b)

EXPERIMENTAL RESULTS

$D_c = 12$ mm $\qquad$ $Y = 17$ N/mm^2

STATIC LUBRICATED - Δ - - - - - - - -

STATIC DRY ——— □ -- ——— -·- ———

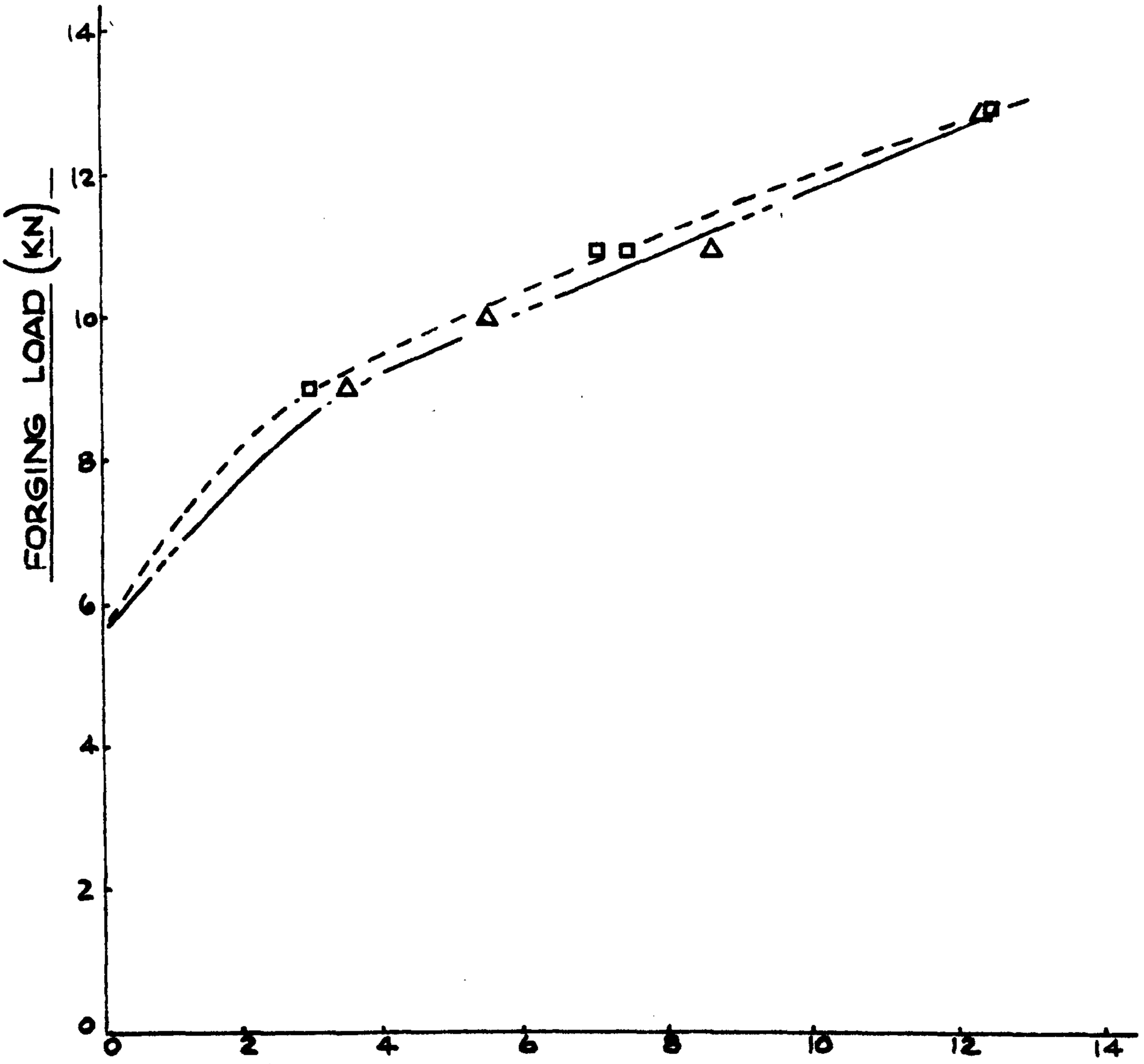

FORGING LOAD v. TOTAL DISPLACEMENT

FIG. 89

EXPERIMENTAL RESULTS

D_c = 18 mm

Y = 17 N/mm²

STATIC LUBRICATED - Δ - - - - - - - -

STATIC DRY —— □ - - —— - - ——

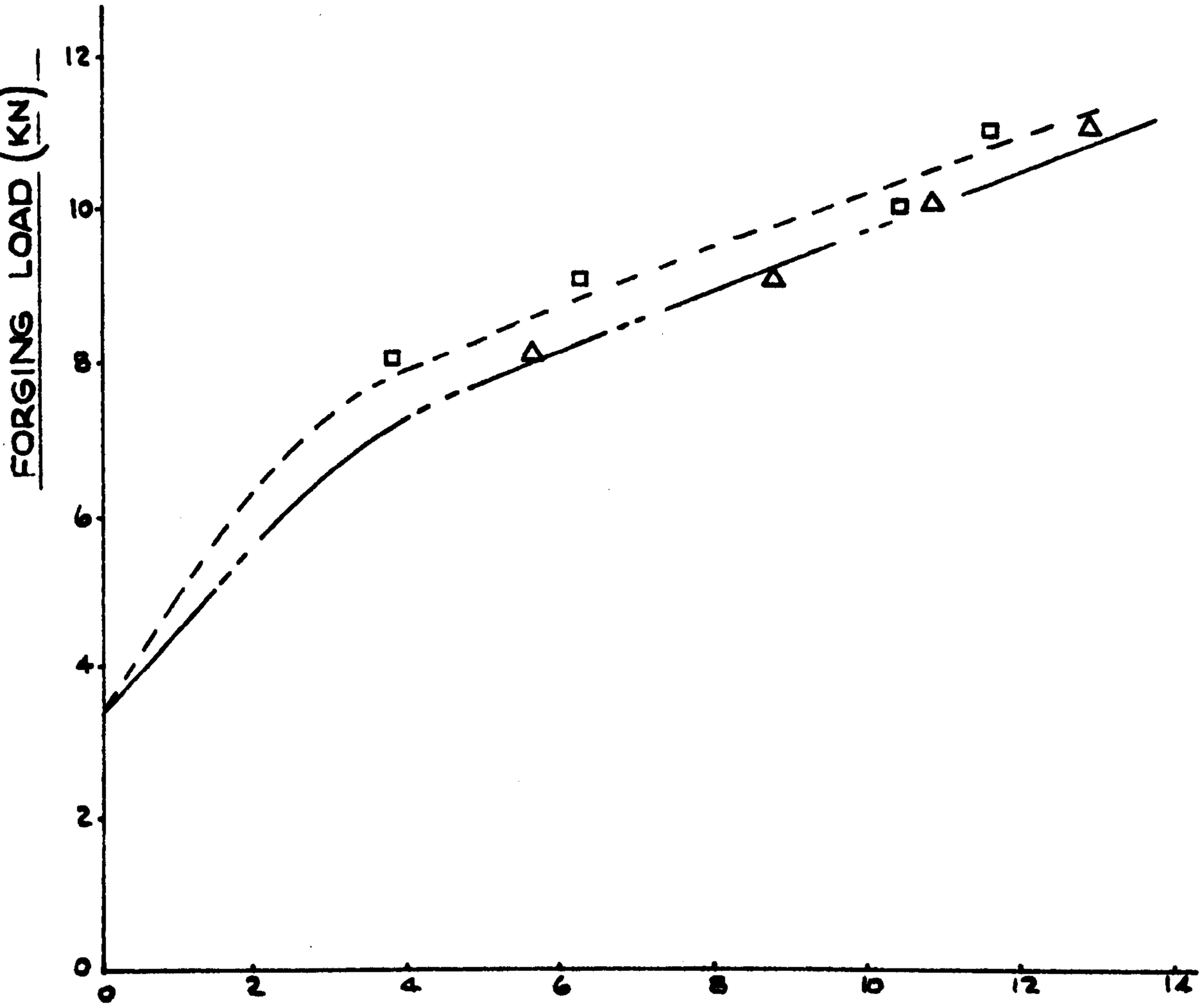

FORGING LOAD v. TOTAL DISPLACEMENT

FIG. 90

THEORETICAL CURVES

BOSS DIA = 9mm L_o = 24 mm

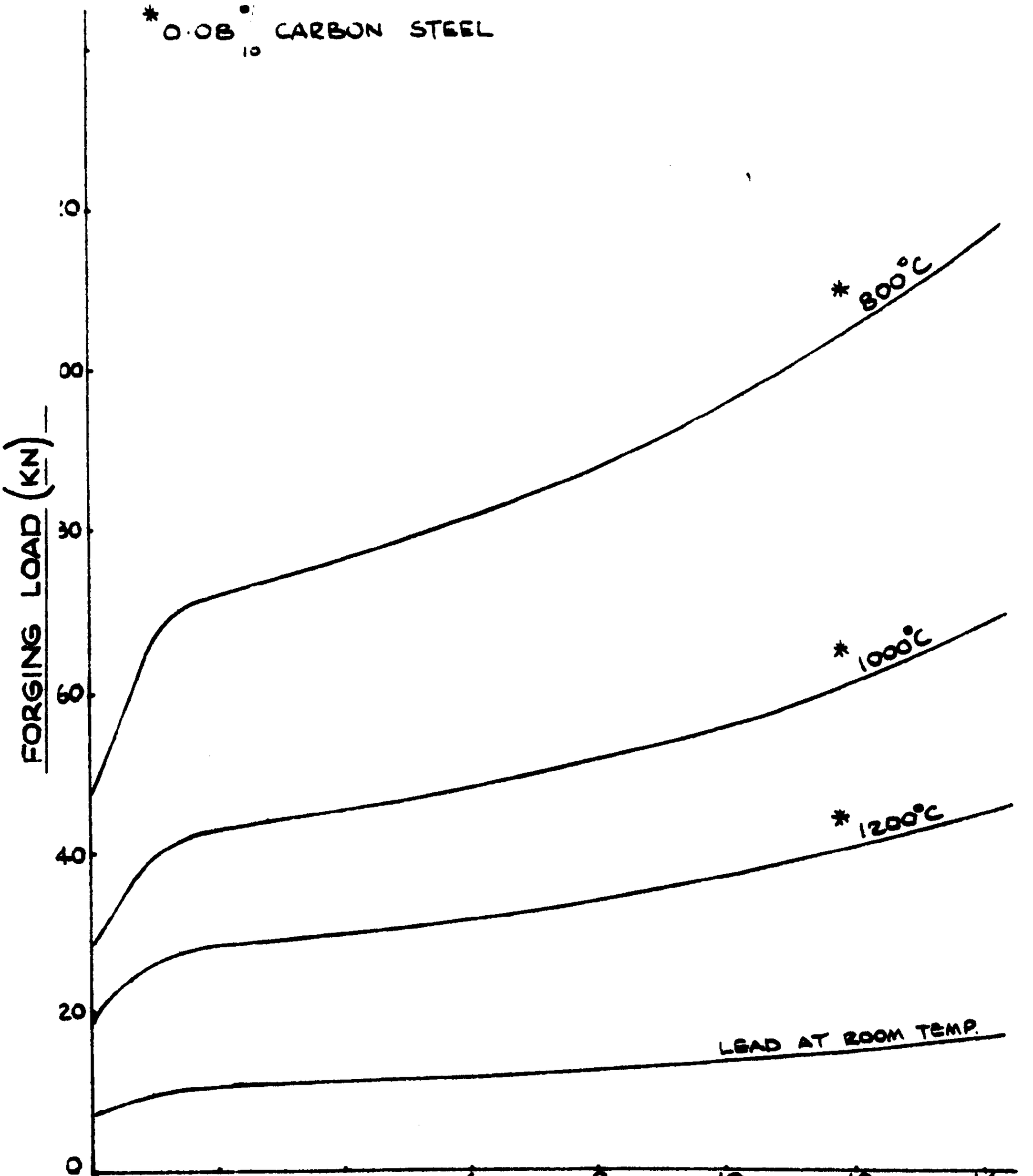

FORGING LOAD v. TOTAL DISPLACEMENT

FIG. 91

THEORETICAL CURVES

BOSS DIA = 12mm **L_0 = 24 mm**

* 0·08% CARBON STEEL

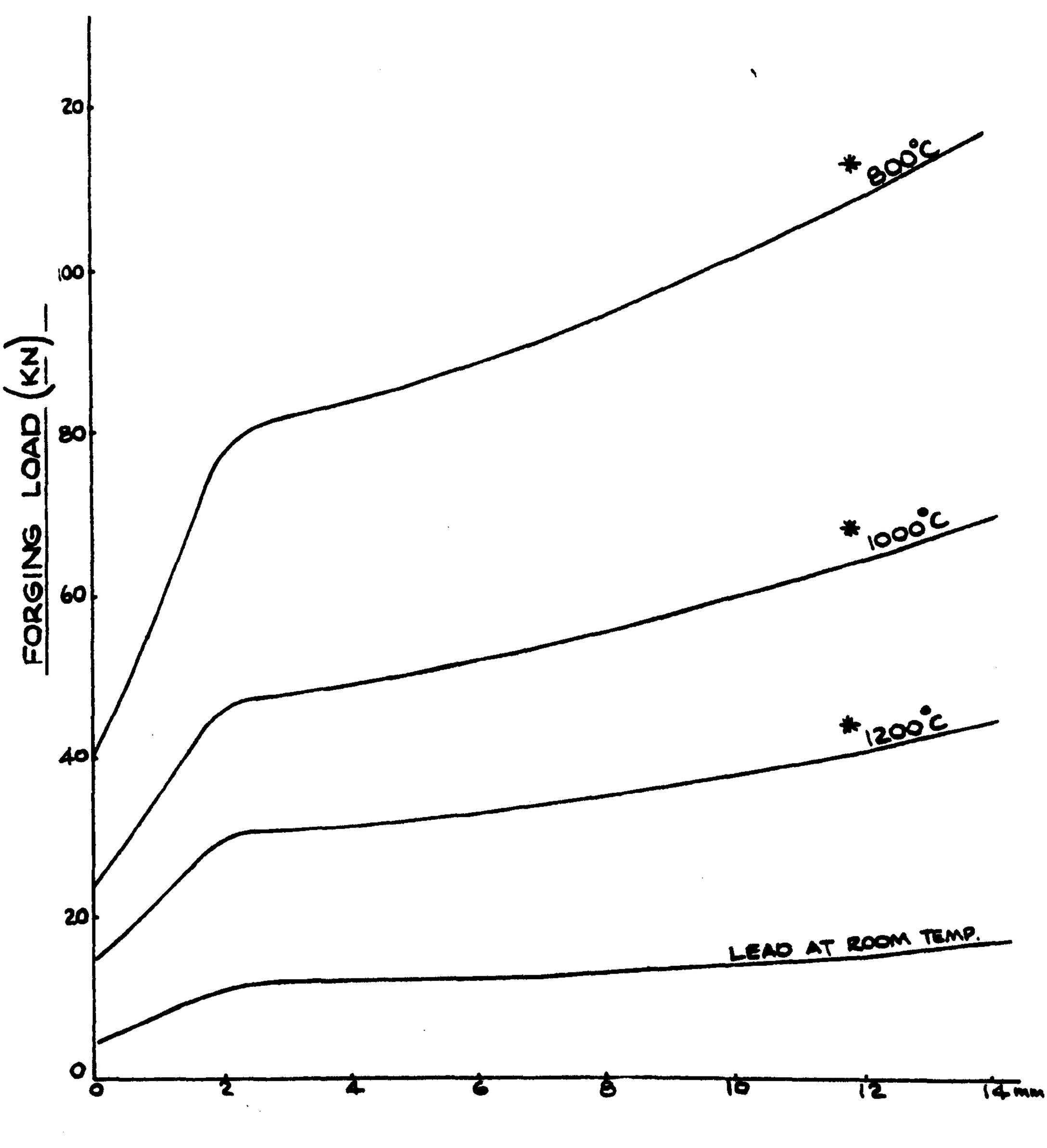

TOTAL DISPLACEMENT $x_0 + x_1$

FORGING LOAD v. TOTAL DISPLACEMENT

FIG. 92

THEORETICAL CURVES

BOSS DIA. = 14 mm

L_o = 24 mm

* 0·08% CARBON STEEL

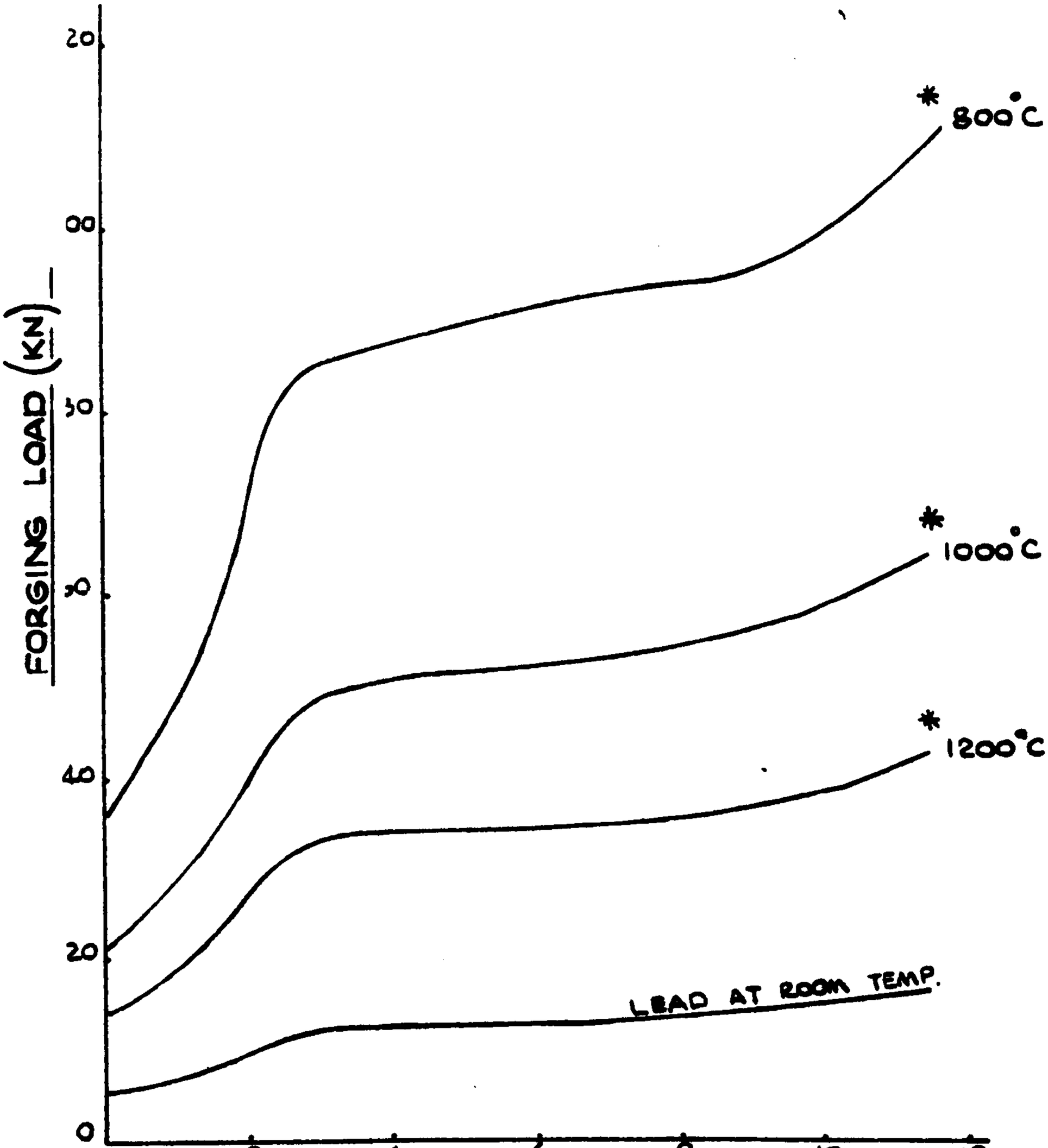

TOTAL DISPLACEMENT $x_o + x_1$

FORGING LOAD v. TOTAL DISPLACEMENT

FIG. 93

THEORETICAL CURVES

BOSS DIA = 16mm

L_o = 24mm

* 0·08% CARBON STEEL

TOTAL DISPLACEMENT $x_o + x_1$

FORGING LOAD v. TOTAL DISPLACEMENT

FIG. 94

THEORETICAL CURVES

BOSS DIA = 18 mm **L_o = 24 mm**

* 0·08 % CARBON STEEL

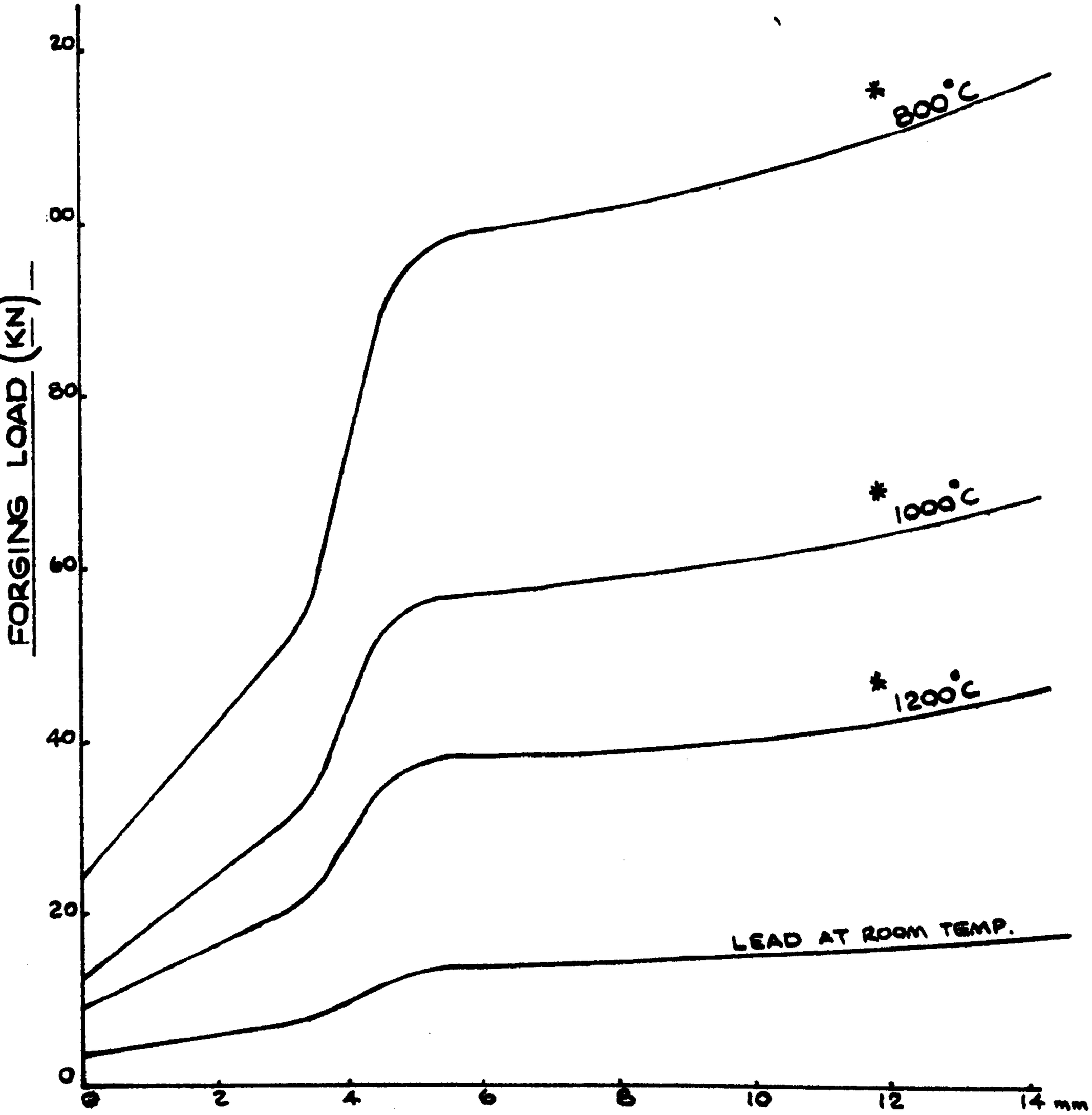

TOTAL DISPLACEMENT $x_o + x_1$

FORGING LOAD v. TOTAL DISPLACEMENT

FIG. 95

THEORETICAL CURVES

BOSS DIA = 20mm L_0 = 24 mm.

*0·08 % CARBON STEEL

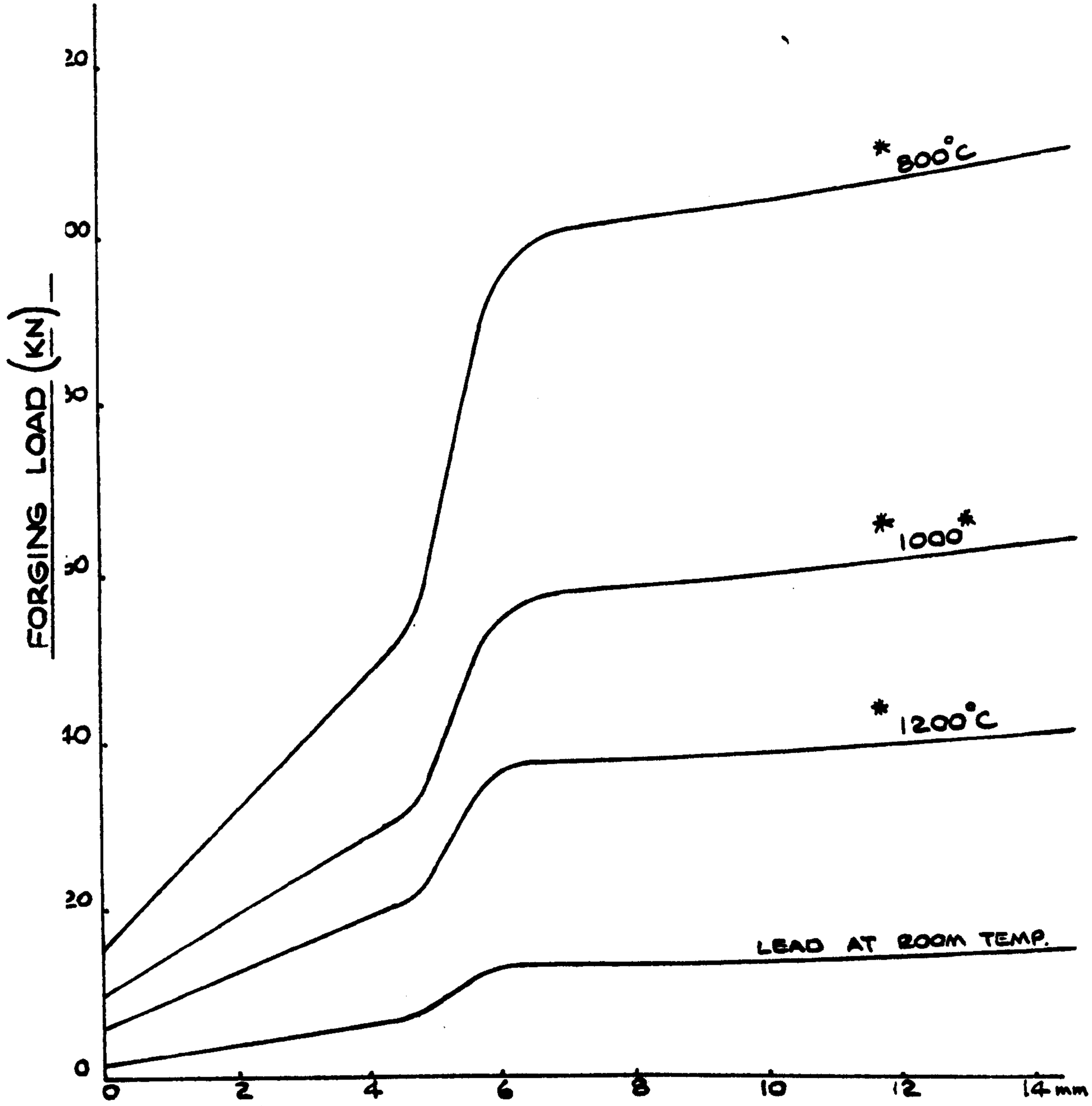

TOTAL DISPLACEMENT $x_0 + x_1$

FORGING LOAD v. TOTAL DISPLACEMENT

FIG. 96

THEORETICAL / EXPERIMENTAL CURVES

BOSS DIA = 9mm Y = 17 N/mm²

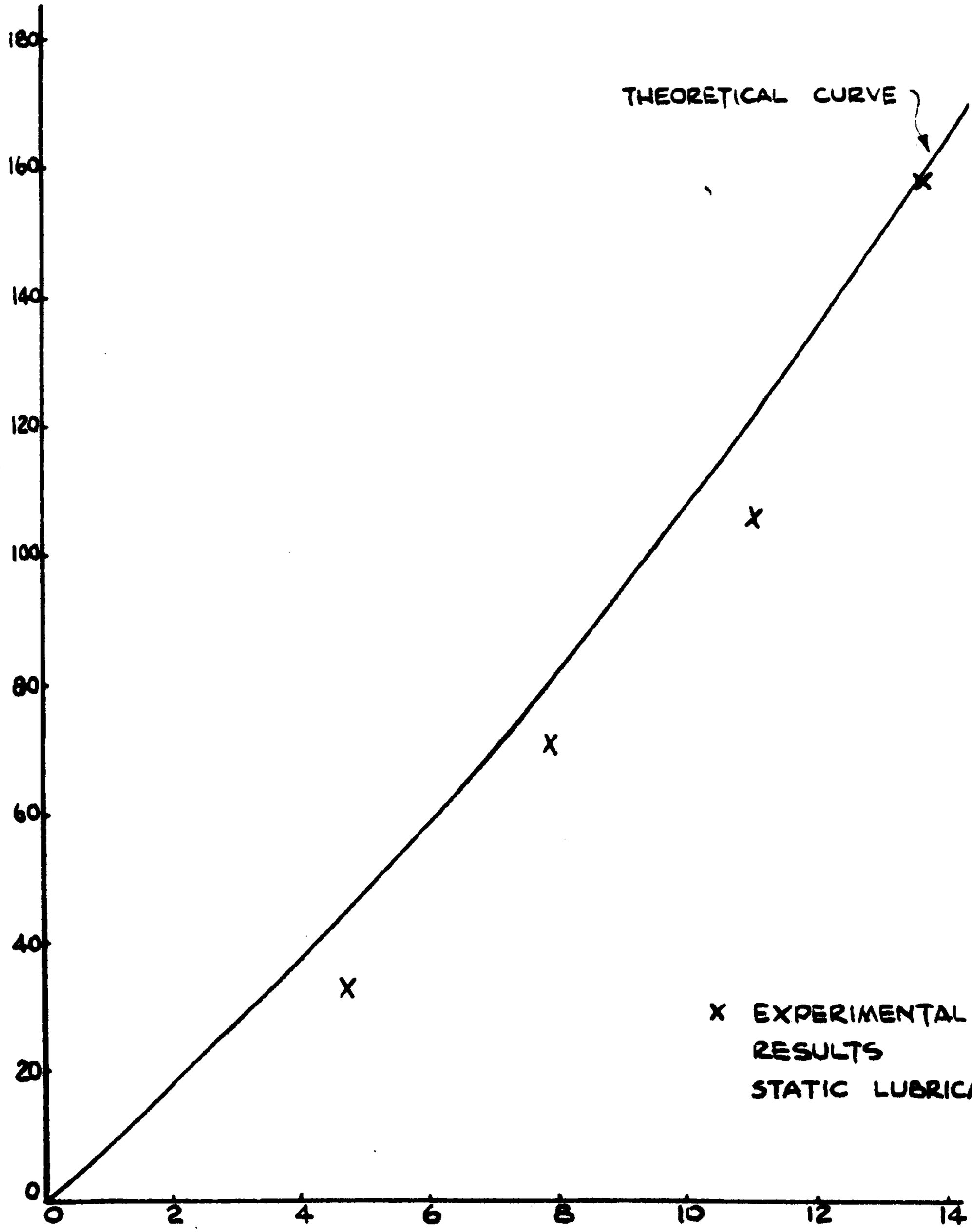

TOTAL ENERGY ABSORBED v. TOTAL DISPLACEMENT.

FIG. 97.

THEORETICAL / EXPERIMENTAL CURVES

BOSS DIA. = 12 mm $Y = 17\ N/mm^2$.

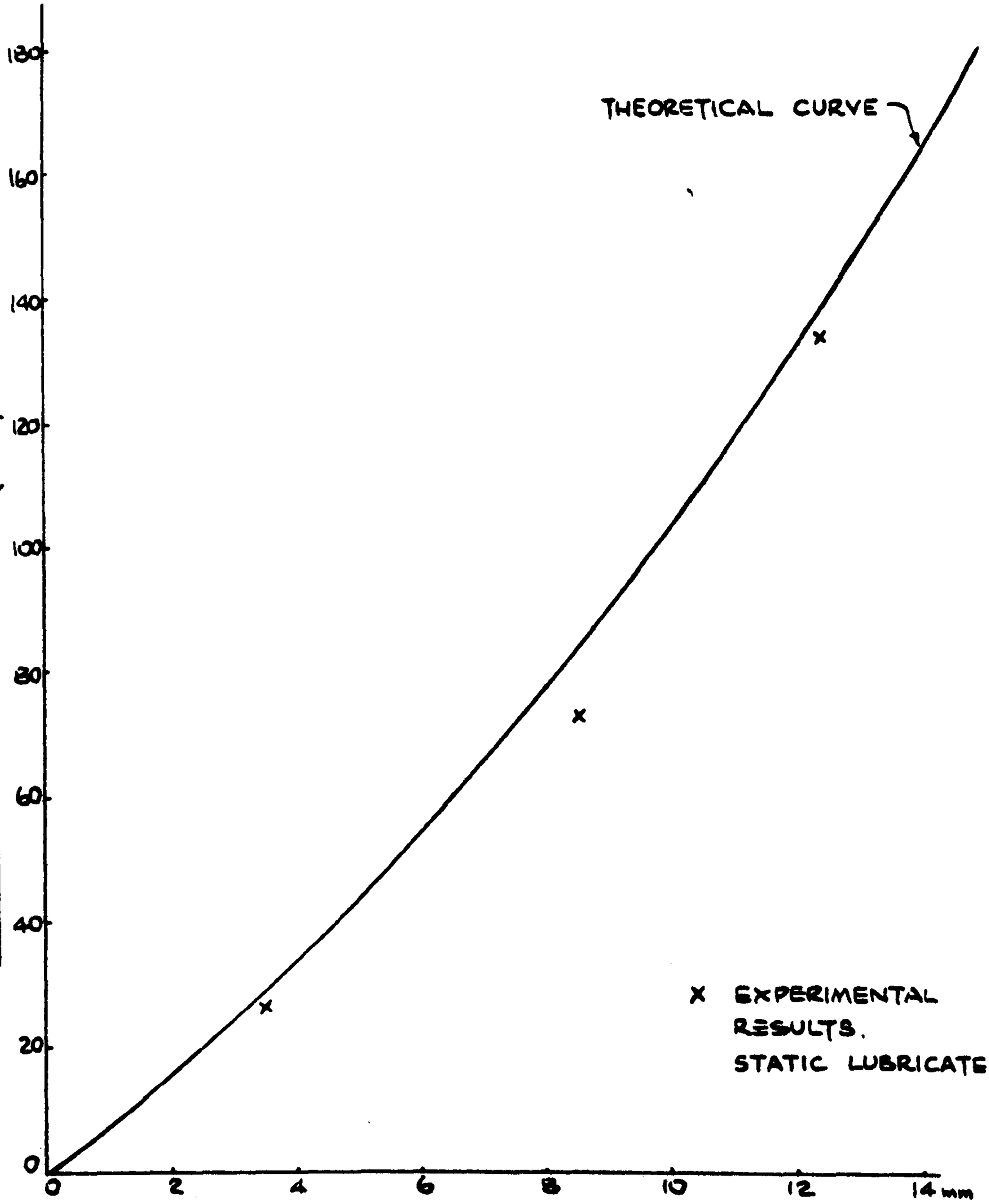

TOTAL ENERGY ABSORBED v. TOTAL DISPLACEMENT.

FIG. 98.

THEORETICAL / EXPERIMENTAL CURVES

BOSS DIA = 18mm $Y = 17\ N/mm^2$.

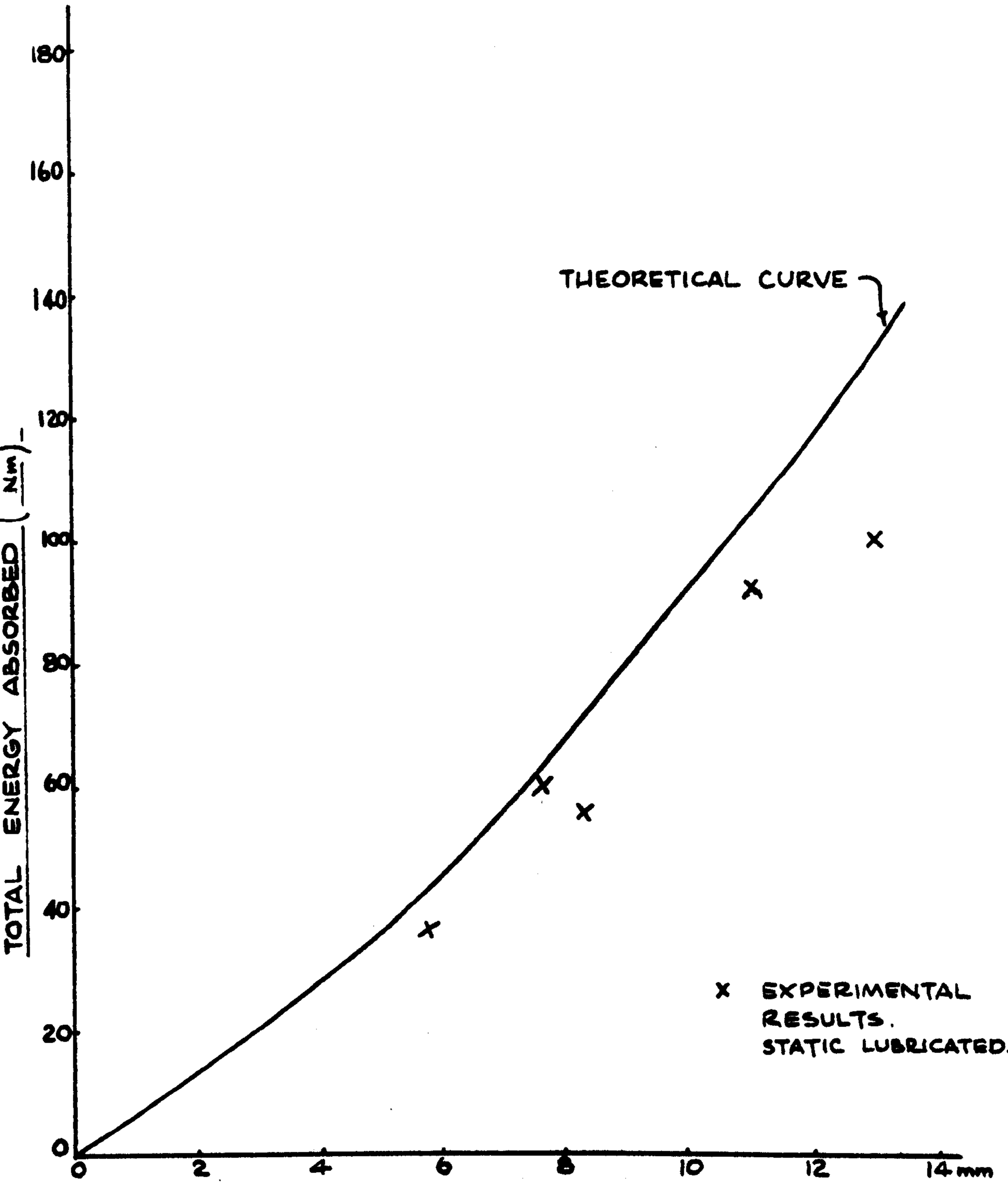

TOTAL DISPLACEMENT $x_0 + x_1$.

TOTAL ENERGY ABSORBED v. TOTAL DISPLACEMENT.

FIG.99

THEORETICAL / EXPERIMENTAL CURVES

BOSS DIA = 9mm Y = 17 N/mm²

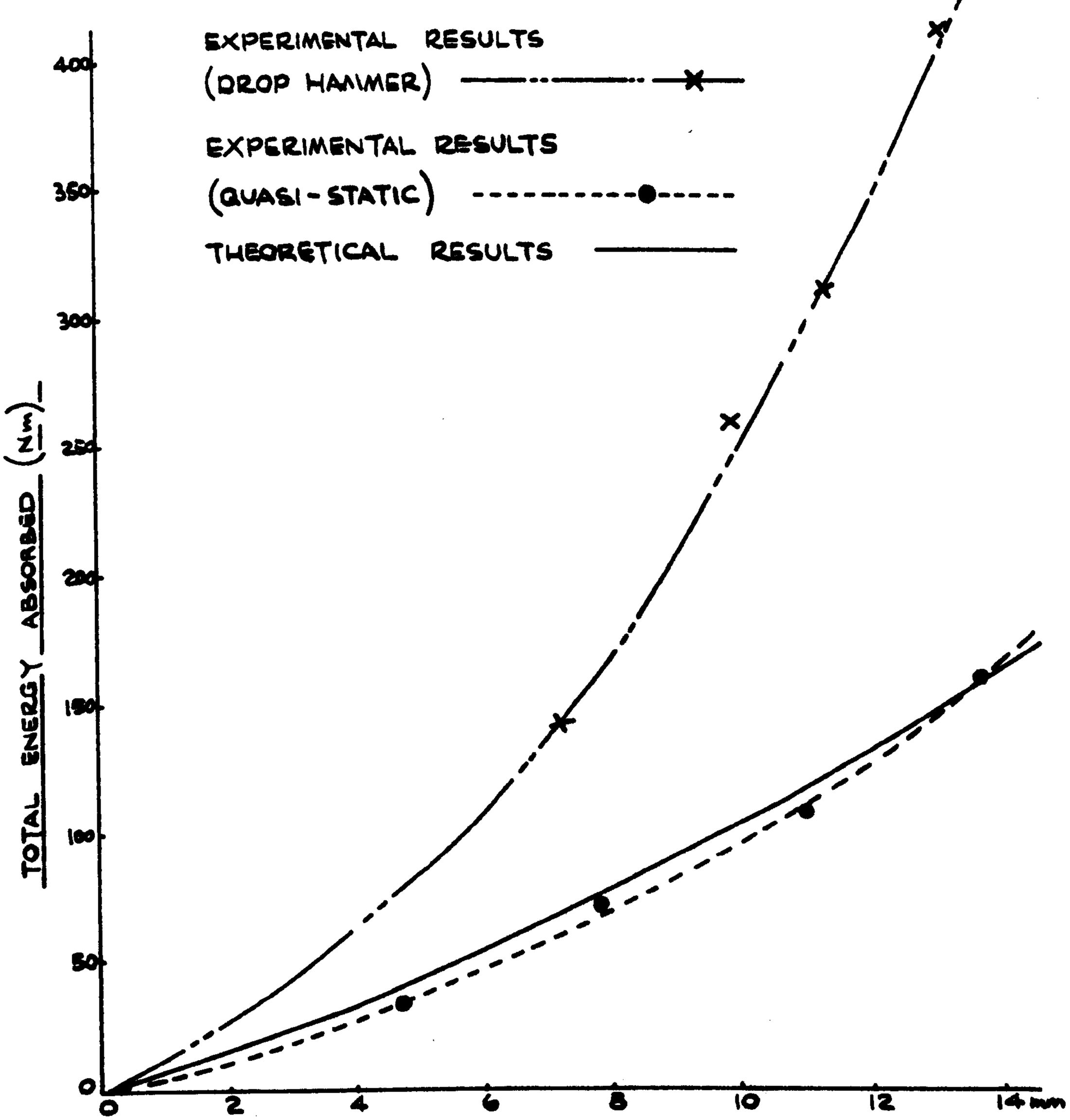

TOTAL DISPLACEMENT $x_0 + x_1$

TOTAL ENERGY ABSORBED v. TOTAL DISPLACEMENT.

FIG. 100

THEORETICAL / EXPERIMENTAL CURVES

BOSS DIA. = 12 mm $Y = 17\ N/mm^2$

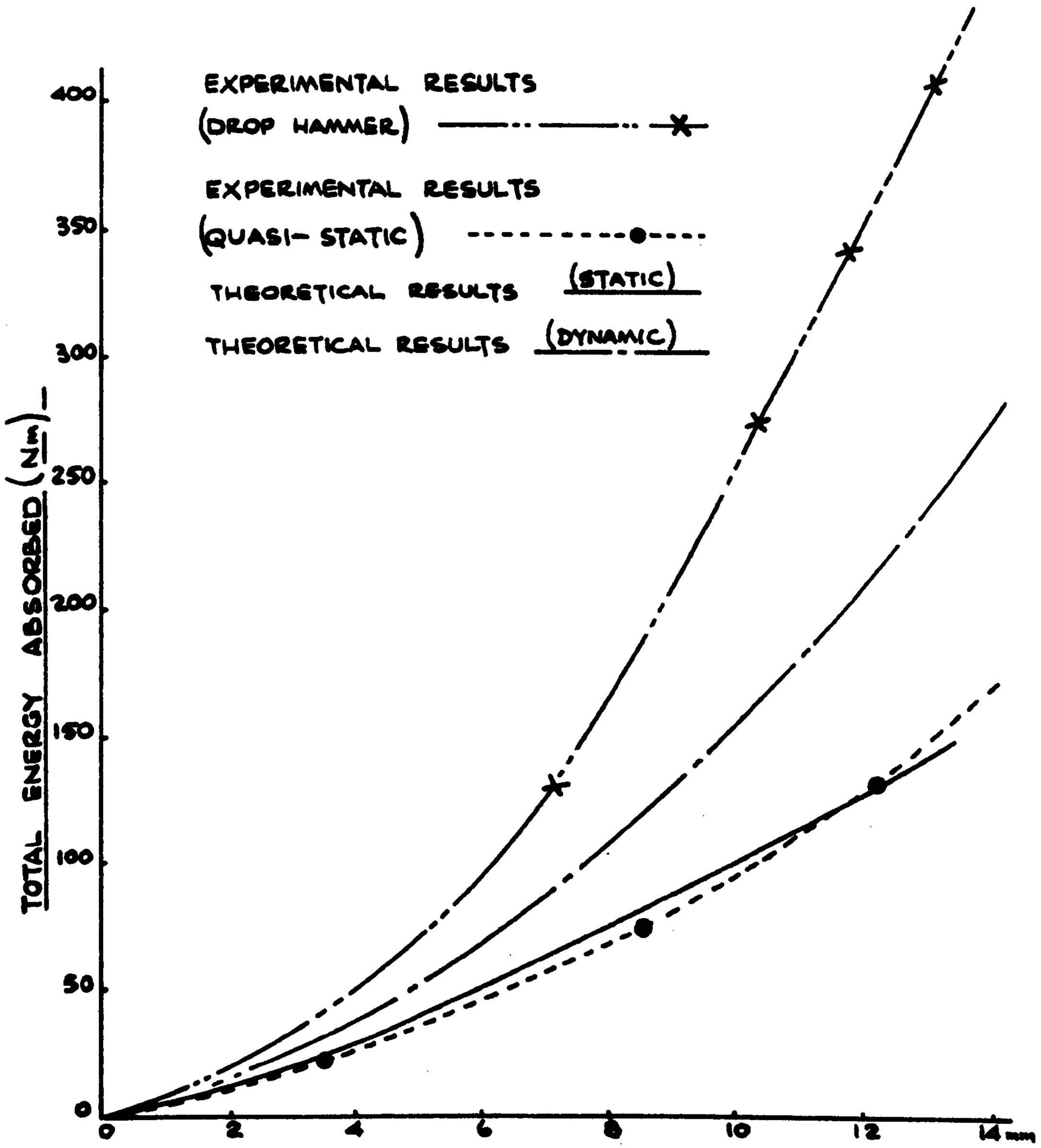

TOTAL DISPLACEMENT $x_0 + x_1$

TOTAL ENERGY ABSORBED v. TOTAL DISPLACEMENT.

FIG. 101

THEORETICAL / EXPERIMENTAL CURVES

BOSS DIA = 18mm Y = 17 N/mm²

EXPERIMENTAL RESULTS
(DROP HAMMER) ——···——···—×—

EXPERIMENTAL RESULTS
(QUASI-STATIC) ----------●----

THEORETICAL RESULTS ——————— (STATIC)

THEORETICAL RESULTS ——·—— (DYNAMIC)

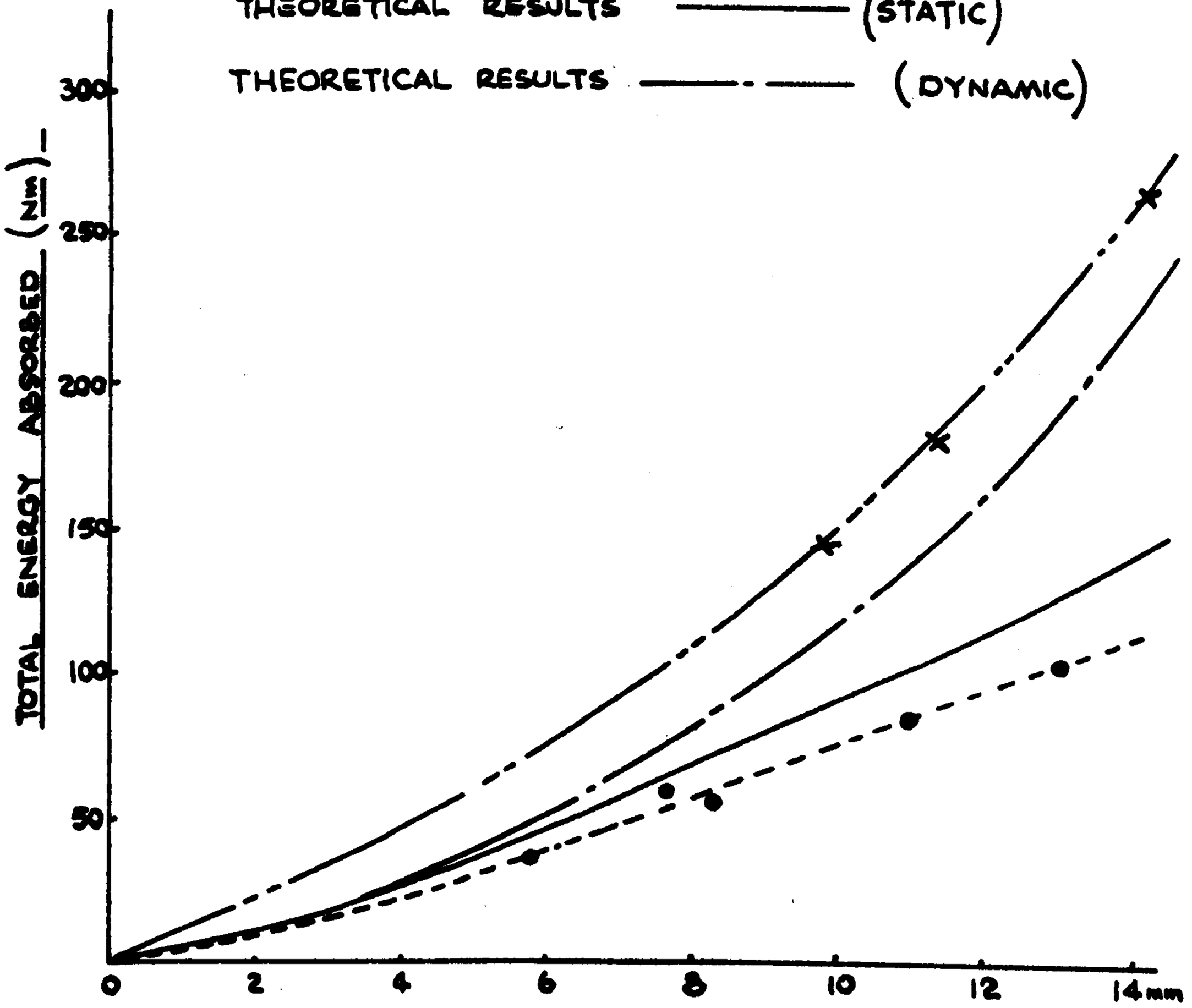

TOTAL DISPLACEMENT $x_0 + x_1$

TOTAL ENERGY ABSORBED v. TOTAL DISPLACEMENT.

FIG.102

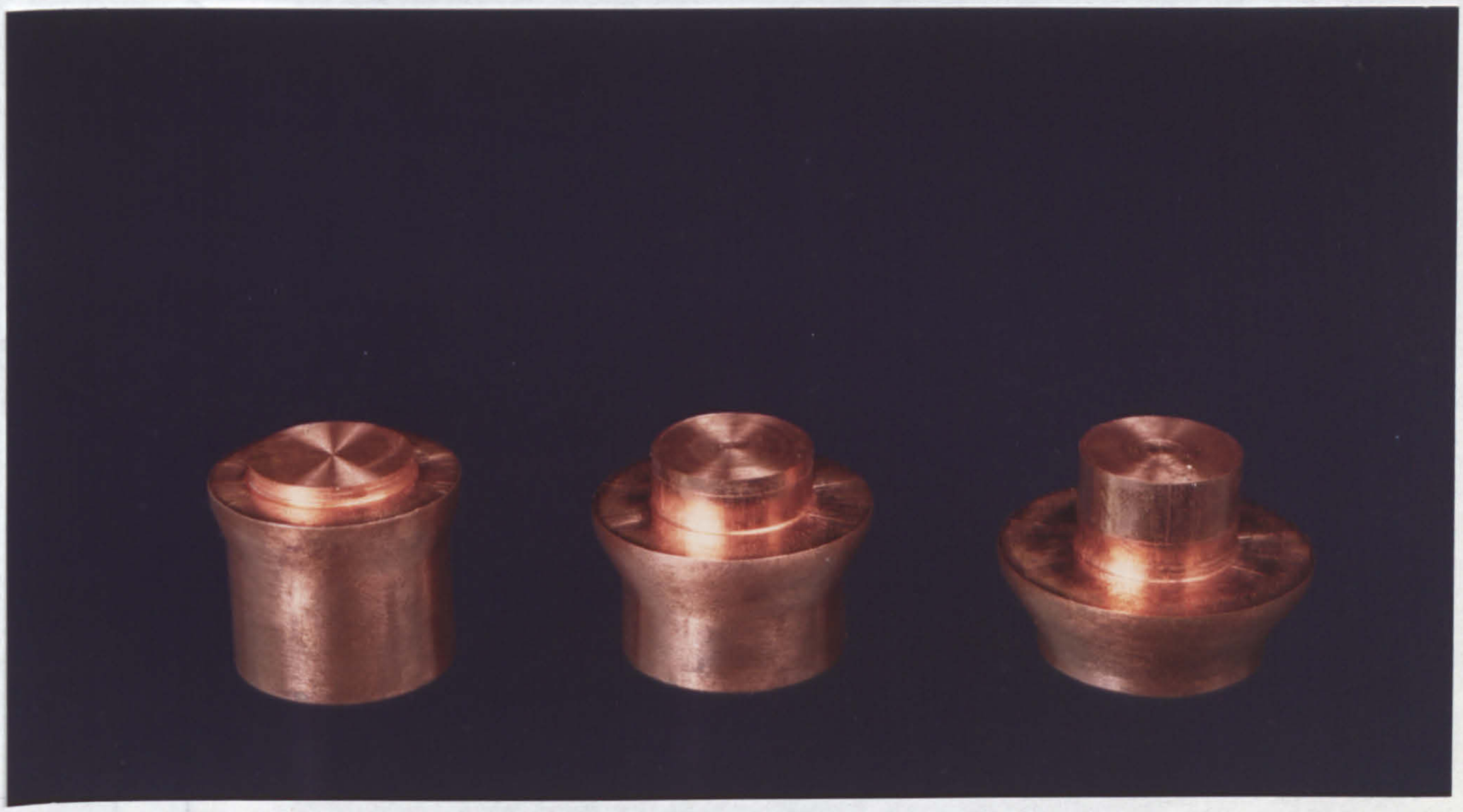

DISPLACEMENT MODE COPPER BILLETS

FIG. 103.

EXPERIMENTAL / THEORETICAL RESULTS

DOUBLE ENDED EXTRUSION $D_c = 18mm$ $L_o = 24mm$ $Y = 17 N/mm^2$

THEORY BASED ON TEST PIECE $L_o = 12mm$
(SINGLE ENDED EXTRUSION)

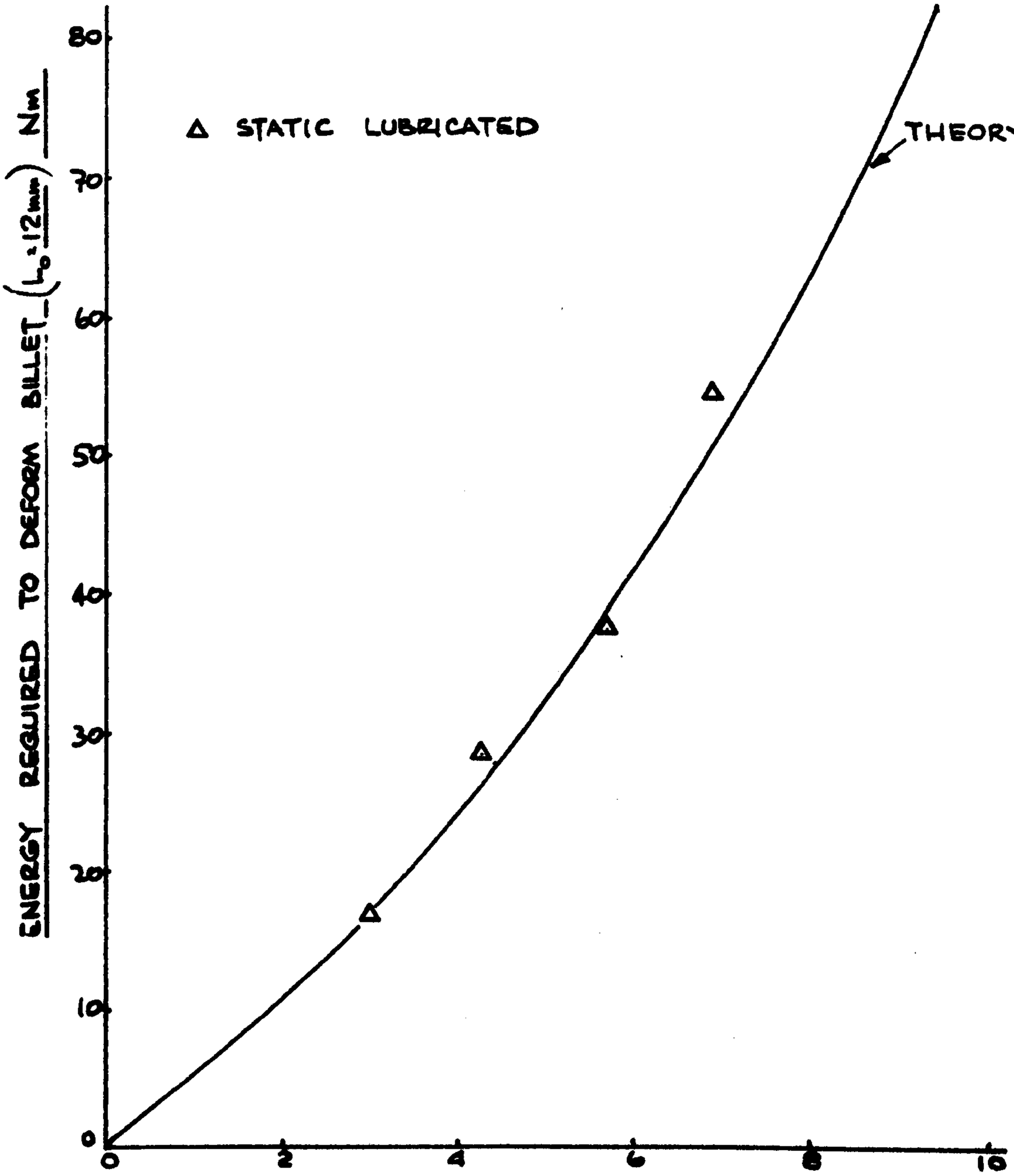

ENERGY v. DISPLACEMENT

FIG. 104.

EXPERIMENTAL / THEORETICAL RESULTS

DOUBLE ENDED EXTRUSION $D_c = 18$ $L_o = 24$ mm $Y = 17 N/mm^2$

THEORY BASED ON TEST PIECE $L_o = 12$ mm
(SINGLE ENDED EXTRUSION)

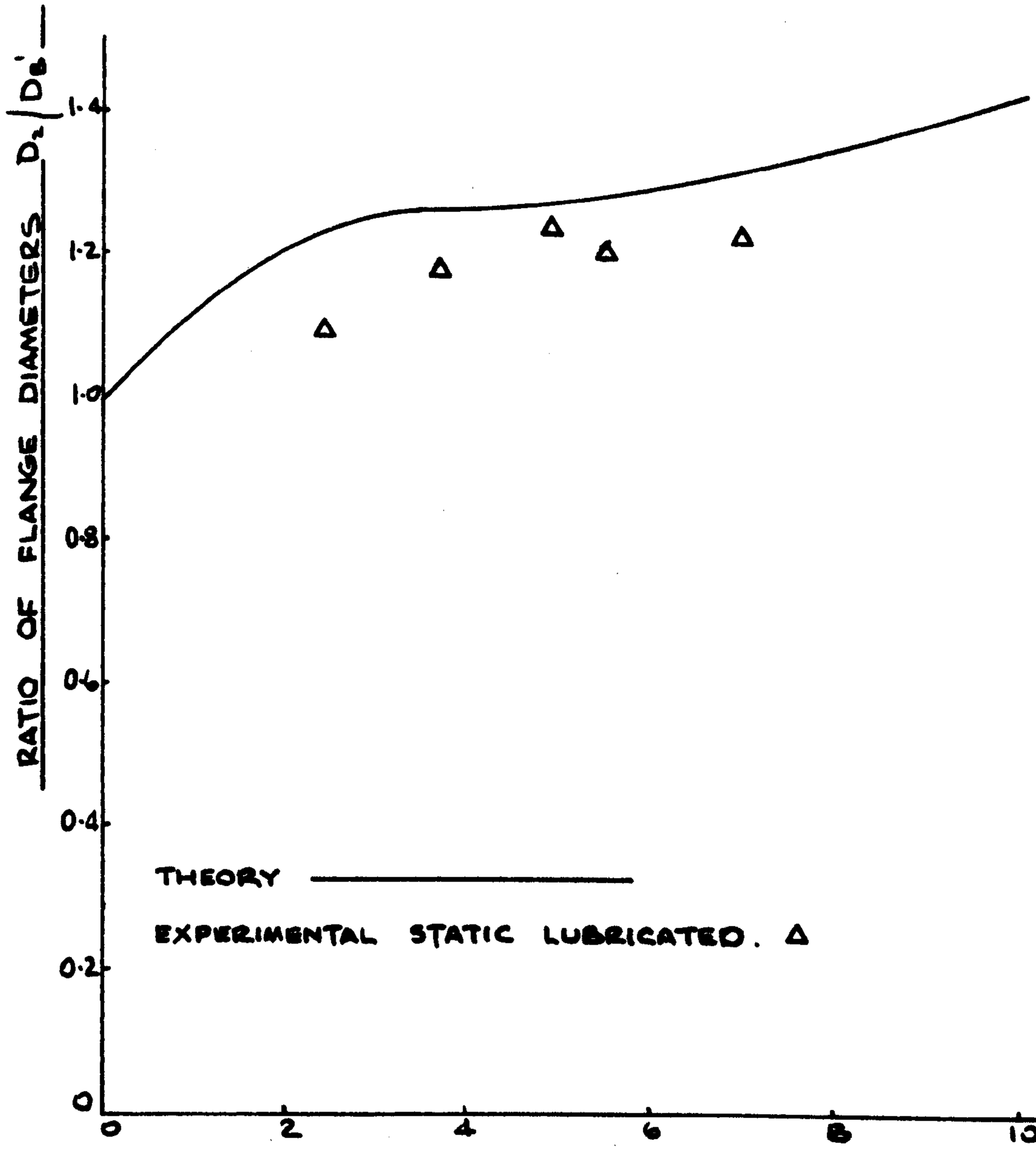

RATIO OF FLANGE DIAMETERS v. TOTAL DISPLACEMENT.

FIG. 105.

EXPERIMENTAL / THEORETICAL RESULTS

DOUBLE ENDED EXTRUSION $D_c = 18mm$ $L_o = 2 \pm mm$ $Y = 17 N/mm^2$

THEORY BASED ON TEST PIECE $L_o = 12mm$
(SINGLE ENDED EXTRUSION)

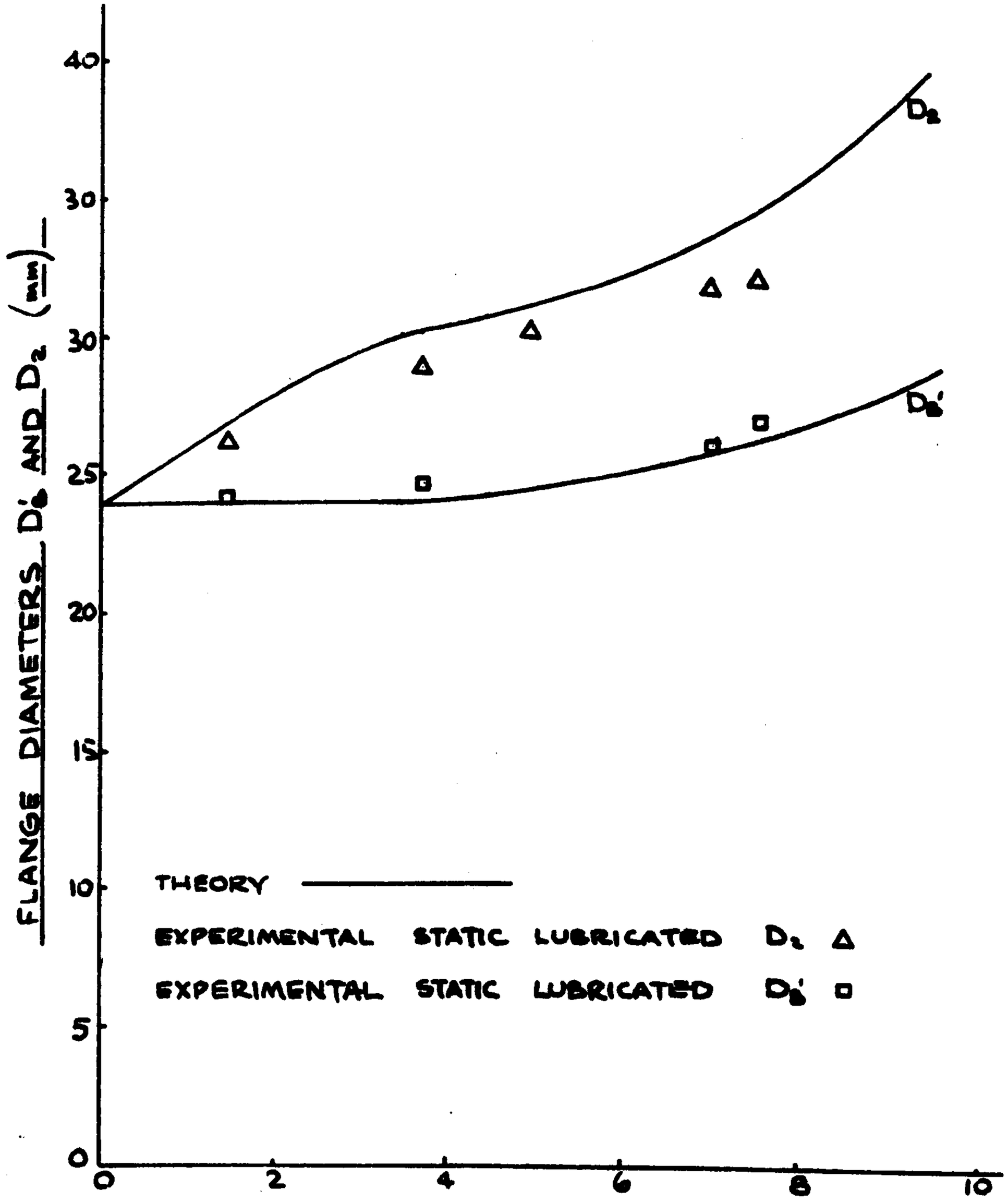

FLANGE DIAMETERS v. DISPLACEMENT.

FIG. 106.

DISPLACEMENT MODE DOUBLE ENDED EXTRUSION

FIG. 107.-

DISPLACEMENT MODE DOUBLE ENDED EXTRUSION

ALUMINIUM COPPER AND LEAD.

FIG. 108.

DOUBLE ENDED EXTRUSION. UNEVEN PROFILE SHOWN IN LEAD AND ALUMINIUM BILLETS.

FIG. 109.

THEORETICAL AND EXPERIMENTAL RESULTS

$m = 1.0$ $L_o = 24$ mm

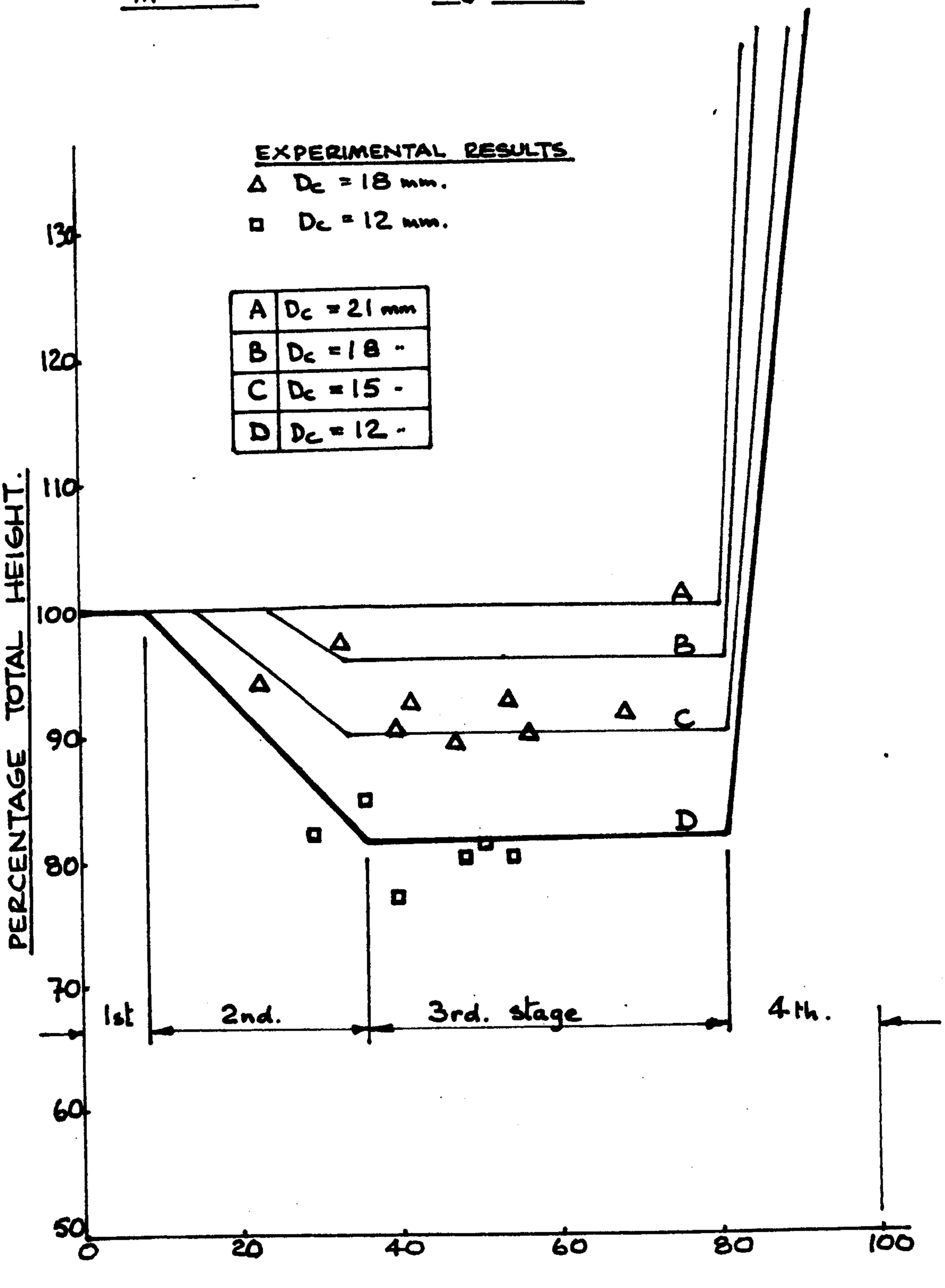

PERCENTAGE TOTAL HEIGHT v PERCENTAGE DEFORMATION

FIG 110

THEORETICAL RESULTS

$m = 0.5$ $L_g = 24$ mm

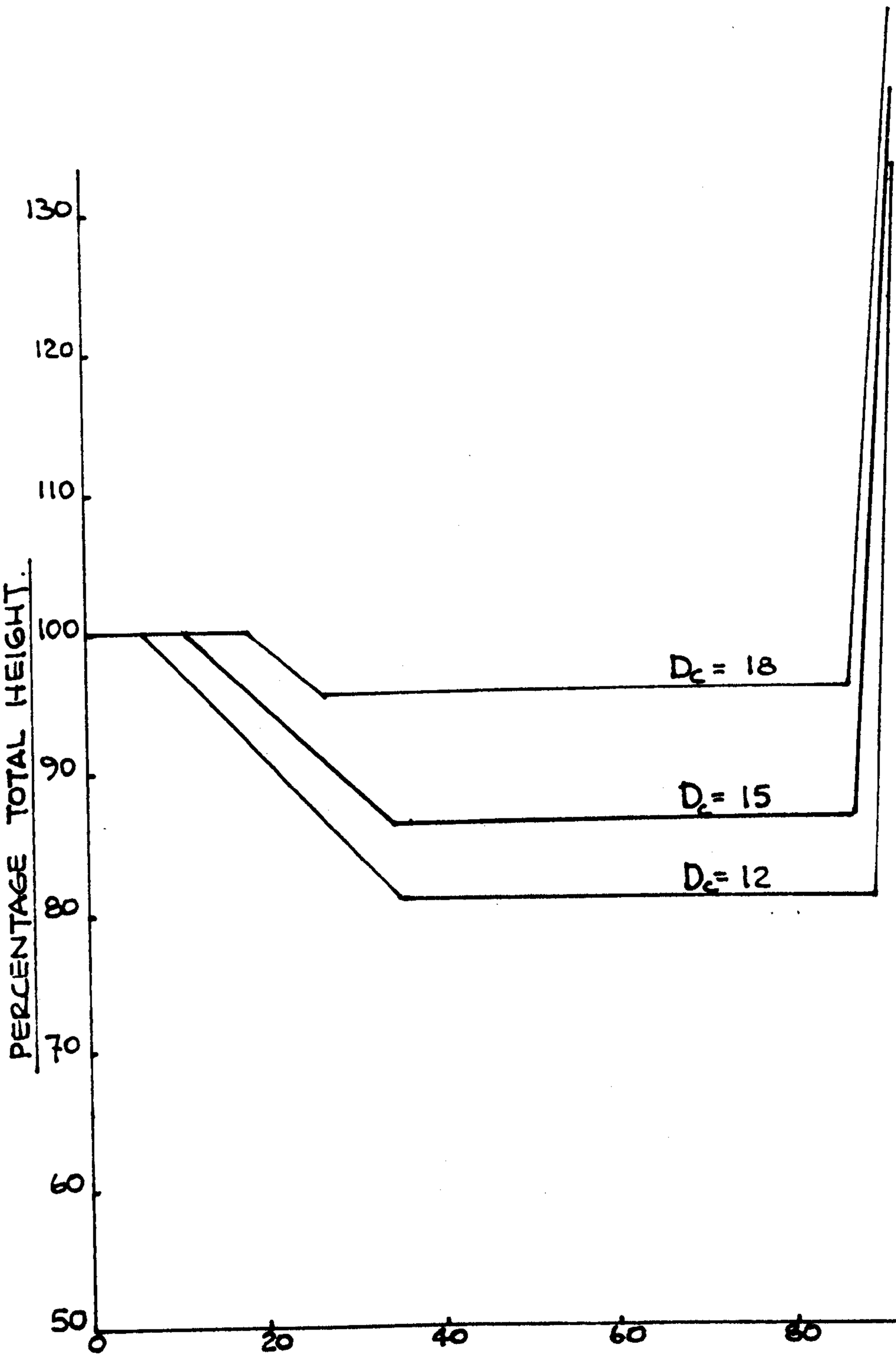

PERCENTAGE DEFORMATION

PERCENTAGE TOTAL HEIGHT v. PERCENTAGE DEFORMATION.

FIG. 111

THEORETICAL AND EXPERIMENTAL RESULTS.

$D_c = 12$ mm $L_o = 24$ mm

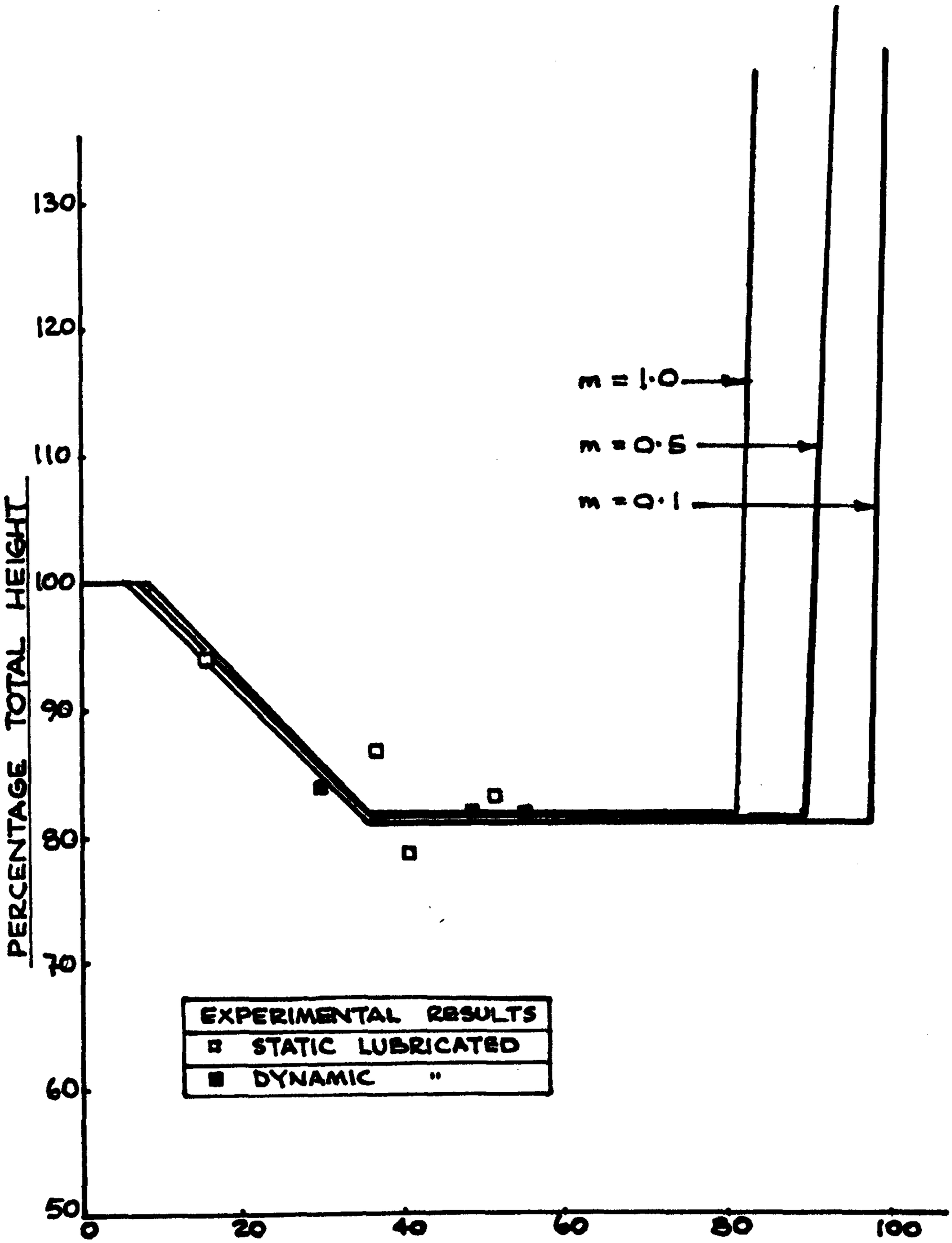

PERCENTAGE TOTAL HEIGHT v PERCENTAGE DEFORMATION

FIG 112

THEORETICAL AND EXPERIMENTAL RESULTS

D_c = 12 mm

L_o = 24 mm

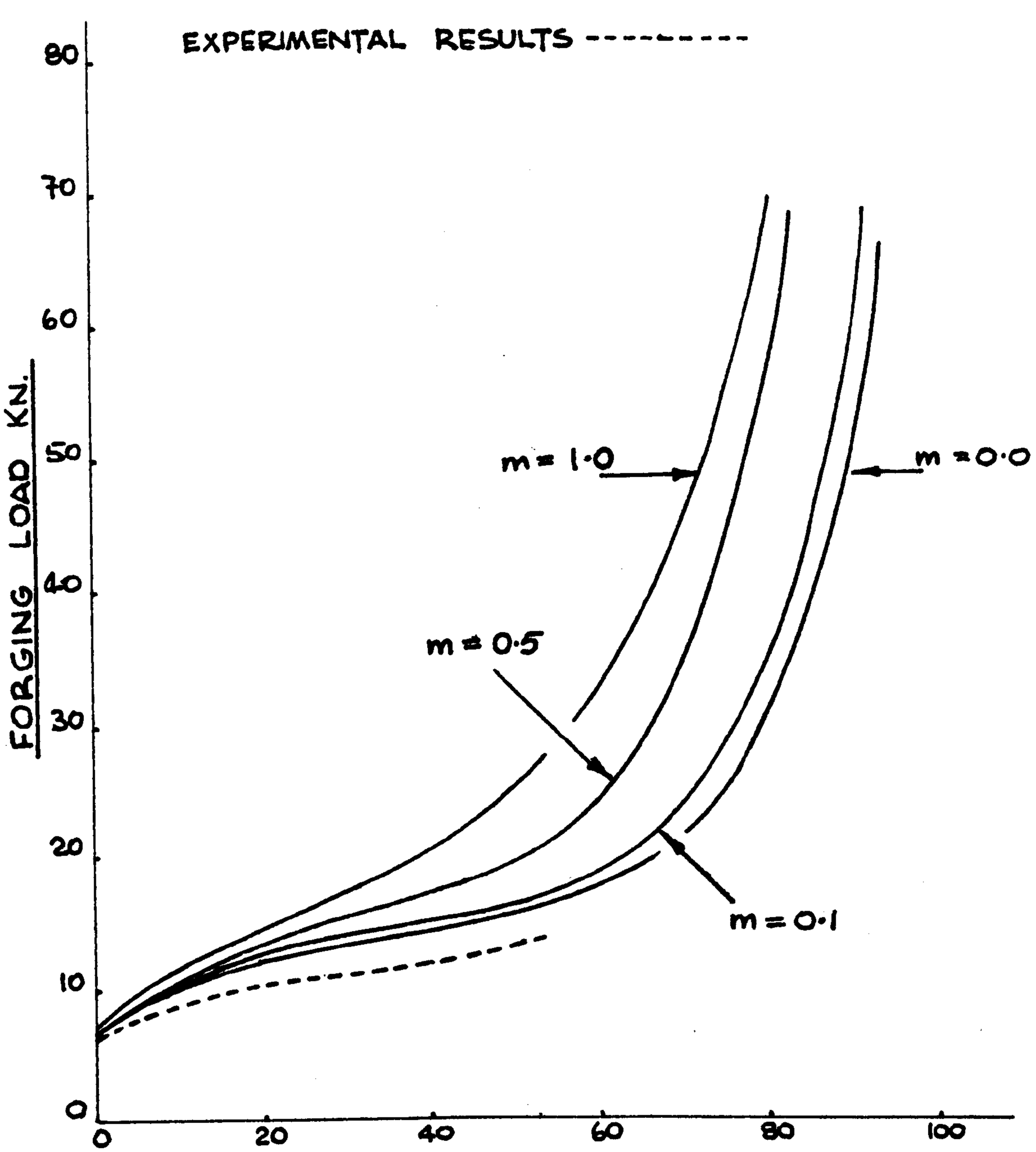

FORGING LOAD v. PERCENTAGE DEFORMATION

FIG 113.

CHAPTER 7

CONCLUSIONS AND SUGGESTIONS FOR FURTHER WORK

7.1 Conclusions

The laboratory drop hammer proved to be an effective means of providing variable impact velocities required for dynamic extrusion forging.

Despite the short forging impact time, less than 10 msec, there was no difficulty in storing, digitally, load/time and displacement time data for later analysis.

When the deformation mode of the billet was not obscured by dies the high speed camera proved very useful for recording the change in shape of the billet.

Lead is an ideal material for simulating the hot-working of steel the one drawback being the difficulty of preparing 'deformed' test pieces so that their grain flow can be observed.

For both simple upsetting and closed die forging, inclusion of the strain rate sensitivity effect in the analysis (numerical technique) greatly improved the accuracy in predicting the load, energy requirements and deformation profiles.

In extrusion forging the deformation profile of the billet is very much influenced by the billet to boss diameter ratios as well as the length of the billet.

The boss height obtainable for a given billet diameter is dependent on the diameter of the boss.

The theory developed provides a useful tool for

predicting the deformation profile of extrusion forged specimens with reasonable accuracy, formed under both dynamic and static conditions. This is one of the most important aspects of the present work which the works of references (61) and (62) did not deal with at all. The forging load predictions agree closely with those obtained from the static tests and also with those obtained from dynamic tests when modified flow properties of the material are incorporated in the theory.

The deformation profile of the billet under extrusion forging conditions appears to be independent of material property, especially the tapering effect, until the fourth stage commences.

7.1.1 The Effect of Friction

It has been seen that the radial flow of metal within a die cavity will be restrained by friction. The extent to which this will occur will depend upon the type of lubricant used and the surface finish of the die. Also, as the metal flow resembles that of a liquid rather than a solid, the influence of friction is more when the metal is flowing through a thin section than through a thick section. The flow situation is further complicated by the fact that the channel through which the metal has to flow is constantly changing due to the relative movement of the dies. From the tests conducted friction was found to modify the shape of the deformed billet

and to increase the energy required for unit displacement.

With the extrusion forging of axisymmetrical shapes friction can have a considerable effect on the amount of metal actually extruded, particularly when large percentage displacements occur; the higher the coefficient of friction, the earlier the fourth deformation mode will occur.

7.1.2 The Effect of Strain Rate

If the material being formed is a rigid-perfectly plastic and non rate sensitive material then the rate at which it is deformed will not affect the forces involved, apart from the material inertia effect. But many materials are rate sensitive in that the faster they are deformed the greater the force required to produce the deformation. This has been clearly demonstrated in the drop hammer tests where the high initial strain rates, 400 sec^{-1} maximum, can double the forces that would be required for quasi-static tests.

7.2 Suggestions for Further Work

7.2.1 The Equipment

Providing bolt-on sections to increase the mass of the tup would widen the range of tests and would provide more energy capacity.

The die cavity could be modified to include different draft angles and corner radii.

7.2.2 Experimental Work

It would be useful to undertake another series of tests to examine further the existing analysis. Possible tests are: Dynamic and quasi-static tests on billets of different materials and different lengths at room temperature:

(a) single ended extrusion forging to include deformation under fourth mode,

(b) double ended extrusion forging with identical and unequal boss diameters.

Similar tests with steel at hot forging temperatures, would provide useful data to compare with the existing analysis.

7.2.3 The Analysis

Modification of the existing analysis to include the effect of material inertia and strain rate should greatly improve the correlation between theoretical and experimental results. This applies particularly to the dynamic tests on strain-rate sensitive materials. The existing analysis can be used for 'double ended' extrusion of cylindrical billets, where the boss diameters are identical. A further modification to embrace boss diameters of unequal size would widen the application of the analysis.

REFERENCES

1. T.A. SCHEY 'Principles of forging design IITR1 review for the American Iron and Steel Inst.

2. A. GELEJI 'Forge equipment, rolling mills and accessories' Akademiai Kiado, Budapest 1967

3. T. ALTAN and R.J. FIORENTINO 'Prediction of loads and stresses in closed-die forging J of Eng for Industry May 1971

4. Technical handbook on forging and drop forging M.V. Storozhev, Moscow 1959

5. L.G. DRABING 'Forging production seminar' Published by Alfred Herbert Limited, Coventry 1966

6. S.A. BALOGUN 'Die loads and stresses in press forging' PhD thesis University of Aston Birmingham 1971

7. F. NEUBERGER and S. PANNASCH 'Werkstoffverbrauch beim Gesenkschmieden von Stahl' Fertigungstechnik und Betrieb Vol 12 1962

8. 'Counterblow hammers - type EK-A' Trade publication by Technsinpex Hungary

9. F. NEUBERGER et alia 'Prediction of energy consumption in drop forging' Fertigungstechnik und Betrieb Part 1 January 1960

10. H. MAKELT 'Ermittlung des Kraft - und Arbeitsbedarfs fur das Stauchen und Gesenkschmieden' Werkstatt und Betrieb Part 6 1958

11. DROP FORGING RESEARCH ASSOCIATION MEMTRB CONTRACT KA/72C/327/CB/A72C Annex No 2 LOAD AND ENERGY ESTIMATION IN FORGING Final Report

12. E. SIEBEL 'The Plastic forming of metals' Steel Oct 16 1933 to May 7 1934

13. W. SCHROEDER and D.A. WEBSTER 'Press forging thin sections: effect of friction, area and thickness on pressure required' J App Mechanics September 1949

14. J. FOSTER 'The high speed mechanical forging press' Metal Treatment and Drop Forging December 1963.

15. T.A. DEAN 'The mechanics of flash in drop forging - temperature and speed effects'

16. R.L. DIETRICH and G. ANSEL 'Calculation of press forging pressures and application to magnesium forgings' Trans ASM vol 38 1947

17. S.K. BISWAS and B.W. ROOKS 'Application of a modular approach to estimate load and energy in closed die forging' Proc 15th MTDR Conference, Birmingham, September 1974

18. T. ALTAN et alia 'The use of analytical methods in predicting load and stresses in closed die forging'. A study of themechanics of closed die forging, First report Battelle Mem Inst 1969

19. R.P. McDERMOTT 'An Introduction to the upper bound elemental technique (UBET) as applied to axisymmetric forgings' PhD Thesis Leeds Univ 1974

20. J.D. LUBAHN J. Appl. Physics, 1949, 14, 229

21. H.I. FUSFELD J. Appl. Physics, 1949, 20, 1052

22. H.R. LOW, Jr, and F. GAROFALO, Proc. Soc. Exper. Stress Analysis, 1947, 4, (2), 16.

23. J.E. DORN, P. PIETROKOWSKY, and T.E. TIETZ, Trans. Amer. Inst. Min. Met. Eng., 1950, 188, 933.

24. J.F. ALDER and V.A. PHILLIPS 'The Effect of strain rate and temperature on the resistance of Aluminium, Copper and Steel to compression', J. Inst Metals 1954, 83, 80.

25. H. KUDO 'An upper bound approach to plane strain forging and extrusion', Int. J. Mech Science Vol 1, 1960

26. P. LUDWIK "Elemente der technologischen Mechanik" 1909: Berlin (Springer)

27. L.D. SOKOLOV, Doklady Akad. Nauk S.S.S.R., 1949, 67, 459

28. L.D. SOKOLOV, ibid, 1947, 17, 543

29. L.D. SOKOLOV, ibid, 1948, 18, 93

30. L.D. SOKOLOV, Doklady Akad, Nauk S.S.S.R., 1949, 67, 459

31. L.D. SOKOLOV, ibid, 1950, 70, 839

32. F. SEITZ, A.W. LAWSON and P. MILLER, O.S.R.D. Rep, 1942, (495)(NDRC A41)

33. F. SEITZ, A.W. LAWSON and P. MILLER, ibid, 1942 (619) (NDRC A63)

34. F. SEITZ, ibid, 1942 (1388)(NDRC A174)

35. O.C. SIMPSON, E.L. FIREMAN and J.S. KOEHLER, ibid, 1944 (3330)(NDRC A257)

36. G.H. WINSLOW and W.H. BESSEY, ibid, 1945 (5039)(NRDC A324)

37. D.W. GINNS, J. Inst. Metals, 1937, 61, 61.

38. C.F. ELAM, Proc. Roy. Soc., 1938 [A], 165, 568.

39. P.G. JONES and H.F. MOORE, Proc. Amer. Soc. Test. Mat., 1940, 40, 610

40. R.A.C. SLATER, W. JOHNSON and S.Y. AKU Experiments in the fast upsetting of short pure lead cylinders and a tentative analysis Int. J. Mech. Sci 1968 Int. J. Mech. Sci 10, 143

41. P.M. COOK True stress-strain curves for steel compression at high temperature and strain rates. 1957 Proc. Conf. Prop at high rates of strain, Inst. Mech. Engrs. Paper 2.

42. L.E. MALVERN Experimental studies of strain rate effects and plastic wave propagation in annealed aluminium. Proc. ASME Coll on Behaviour of materials under dynamic loading 1965 p.81.

43. S.K. SAMANTA Resistance to dynamic compression of low carbon steel and alloy steels at elevated temperatures and at high strain rates. 1968 Int. of J. Mech. Sci, 10, 613

44. H. SUZUKI, et al Studies on the flow stress of metals and alloys, Report Institute of Industrial Sciences, Univ. of Tokyo, 1968, Vol 18, No 3

45. S.K. SAMANTA On relating the flow stress of aluminium and copper to strain, strain rate and temperature 1969 Int. J. Mech. Sci, 11, 433

46. S.K. SAMANTA The dynamic compression testing of steel at elevated temperatures. 1970, Proc 11th Int MTDR Conf p.827

47. C.E.N. STURGESS and A.N. BRAMLEY The use of impact-forming device to obtain dynamic stress-strain data. Proc. 11th Int MTDR Conf p.803

48. B. LENGYEL and M MOHITPUR Dynamic stress-strain data to large strains 1972 J. Inst. Metals p 100

49. M. MOHITPUR and B. LENGYEL A method of obtaining isothermal, constant high strain rate stress-strain data, Proc 16th Int MTDR 1975 MTDR Conf p 503

50. G.L. BARAYA, W. JOHNSON and R.A.C. SLATER The dynamic compression of circular cylinders of super-pure aluminium at elevated temperatures 1965 Int. J. Mech. Sci. 7, 621

51. S.C. JAIN and A.N. BRAMLEY Speed and frictional effects in hot forging 1968, Proc. Instn. of Mech Engrs, Vol 182, 78

52. T.A. DEAN The influence of billet inertia and die friction in forging processes - A simple energy approach. 1970, 11th Int. MTDR Conf. p.761

53. R.P. McDERMOTT and A.N. BRAMLEY An elemental upper-bound technique for general use in forging analysis. 1974 Proc. 15th Int. MTDR Conf, p 437.

54. T.A. DEAN The mechanics of flash in drop forging - temperature and speed effect. 1976 Proc. Inst. Mech. Engrs. Vol 190-33/76 p.457.

55. M.S.J. HASHMI and F.B. KLEMZ The effect of friction in simple upsetting of cylindrical billets of elastic-plastic and elastic-strain hardening material: A numerical technique 1976 Proc 17th Int MTDR Conf p 597

56. F.B. KLEMZ and M.S.J. HASHMI Simple upsetting of cylindrical billets: Experimental investigation and theoretical prediction 1977 Proc 18th Int MTDR Conf p 323

57. M.S.J. HASHMI A numerical technique for analysing simple upsetting of cylindrical billets of strain rate sensitive material. 1977 Proc 18th Int MTDR Conf p 27

58. M.S.J. HASHMI and F.B. KLEMZ Closed die forging of axisymmetric shapes from cylindrical billets of strain hardening and strain rate sensitive material: Experimental results and theoretical predictions 1978 Proc 19th Int MTDR Conf p 61

59. J. DANCKERT and T. WANHEIM Model-Material Technique Applied in the Analysis of the Forging of a Specimen of Complicated Shape 1977 Scandinavian Journal of Metallurgy 6 185-190

60. A.T. MALE and M.G. COCKROFT (1964) A method for determination of the coefficient of friction of metals under conditions of bulk plastic deformation. J. Inst. of Metals Vol 93 p 38

61. S.C. JAIN, A.N. BRAMLEY, C.H. LEE and SHIRO KOBYASHI. Theory and Experiment in Extrusion Forging. Proc. 11th Int MTDR Conf 1970 p 1097

62. J.A. NEWNHAM and G.W. ROWE. An analysis of Compound Flow of Metal in a simple extrusion/forging process

63. W. JOHNSON Extrusion through square dies of large reduction. J. Mech. Phys. Solids 4, 191, 1955

APPENDIX 1

QUASI-STATIC COMPRESSION OF A SHORT CYLINDER OF PERFECTLY PLASTIC MATERIAL

If a short circular cylinder of rigid-perfectly plastic material whose height to radius ratio, h/a is less than 3, is compressed between rigid parallel dies at a speed less than 150 m/s then all inertia and wave effects can be neglected.

Let the coefficient of friction between the flat end faces of the cylinders and the dies be μ.

Let the three normal stresses be σ_r, σ_θ and σ_z and assume that they are independent of z and that they are principal stresses.

The equation of equilibrium for an element of the cylinder see Fig. 114, is

$$\frac{\sigma_r - \sigma_\theta}{r} + \frac{\partial \sigma_r}{\partial_r} = - \frac{2\mu\sigma_z}{h} \qquad (1)$$

If volume constancy is assumed then it can be shown that $d\varepsilon_\theta = d\varepsilon_r$, and since the elastic components of strain are negligible by comparison with plastic components then through the Levy-Mises equation, $\sigma_\varepsilon = \sigma_r$ then (1) becomes:

$$\frac{d\sigma_r}{dr} = - \frac{2\mu\sigma_z}{h} \qquad (2)$$

Using Tresca's yield criterion, where σ_r, $\sigma_\theta > \sigma_z$, then

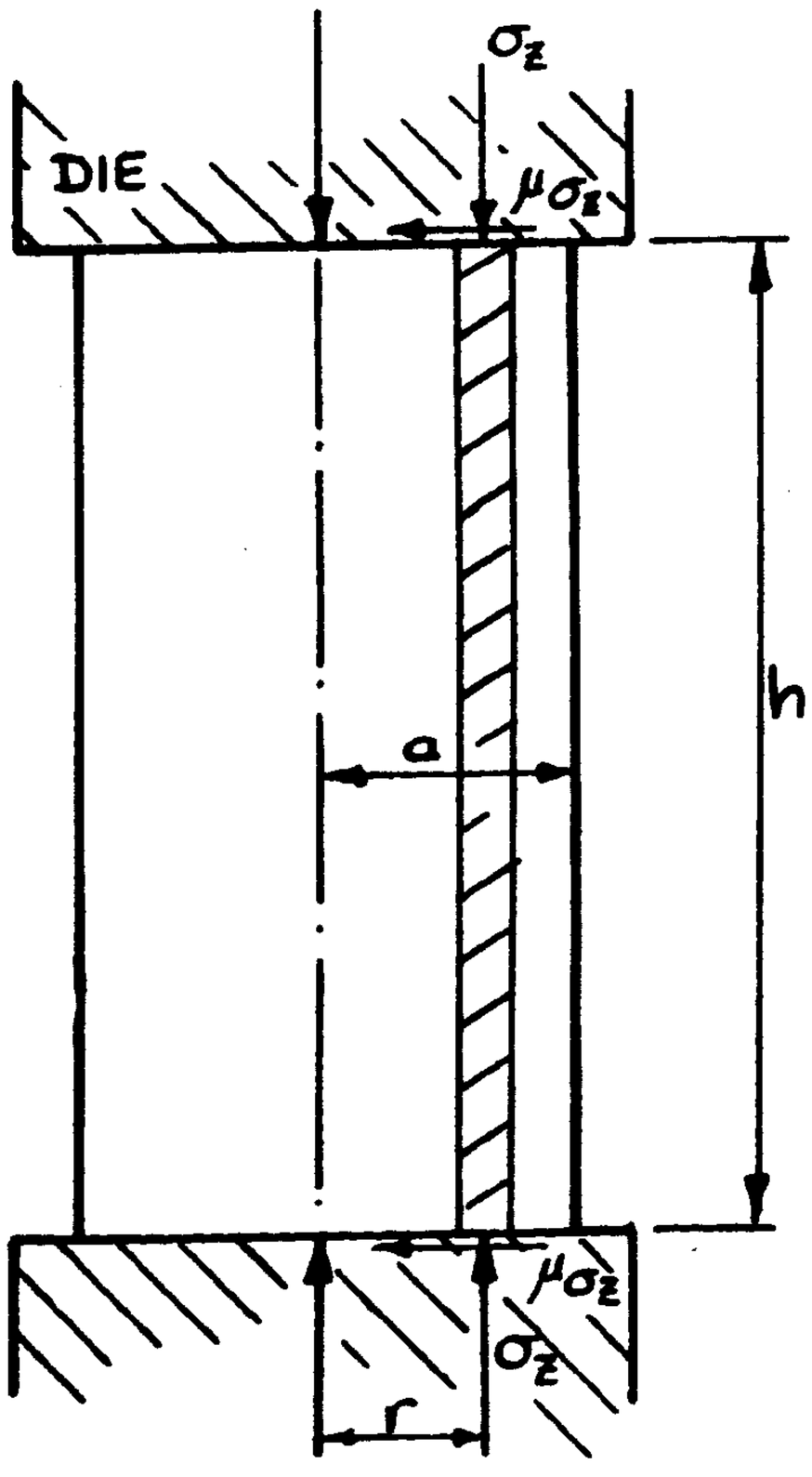

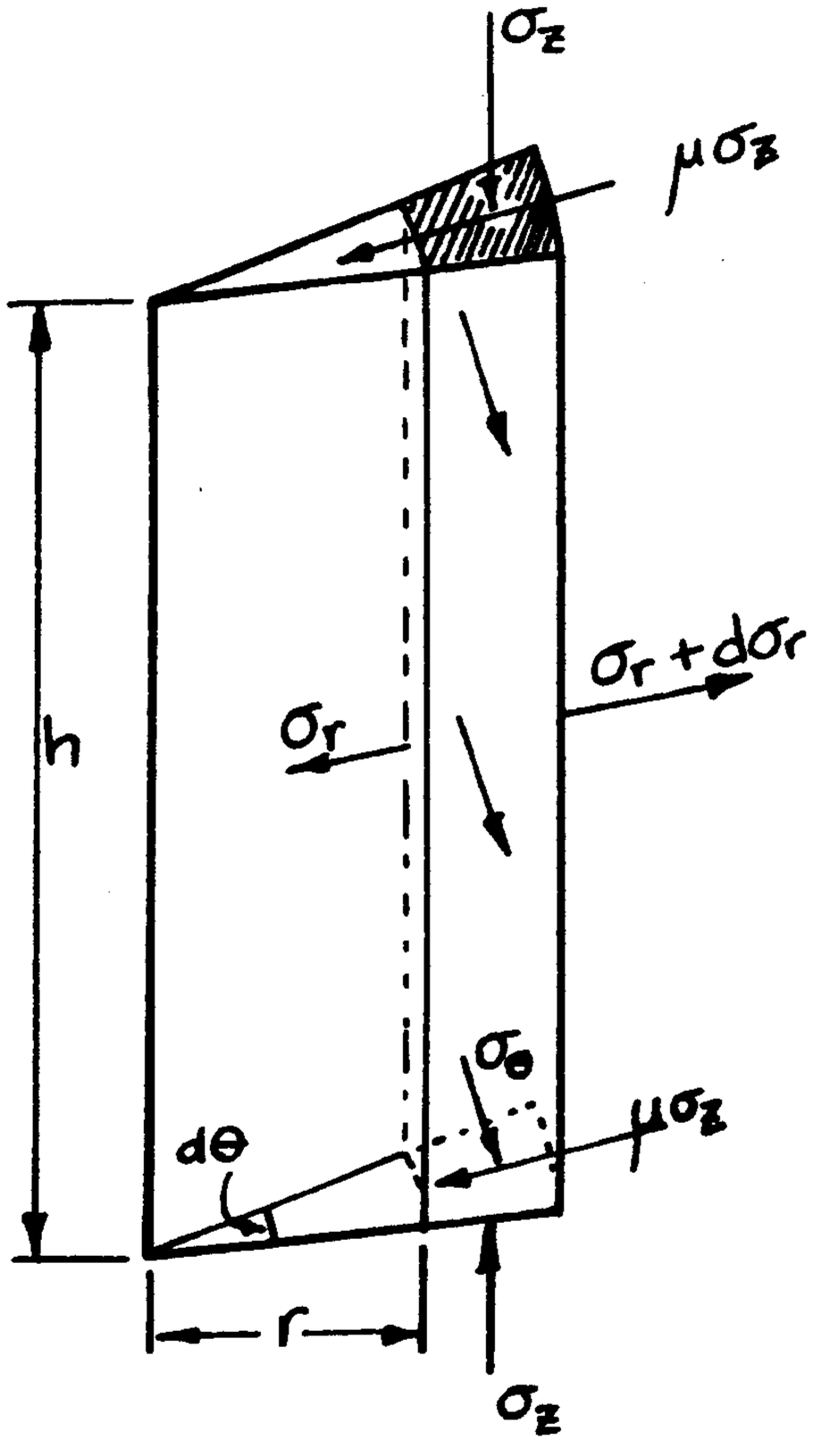

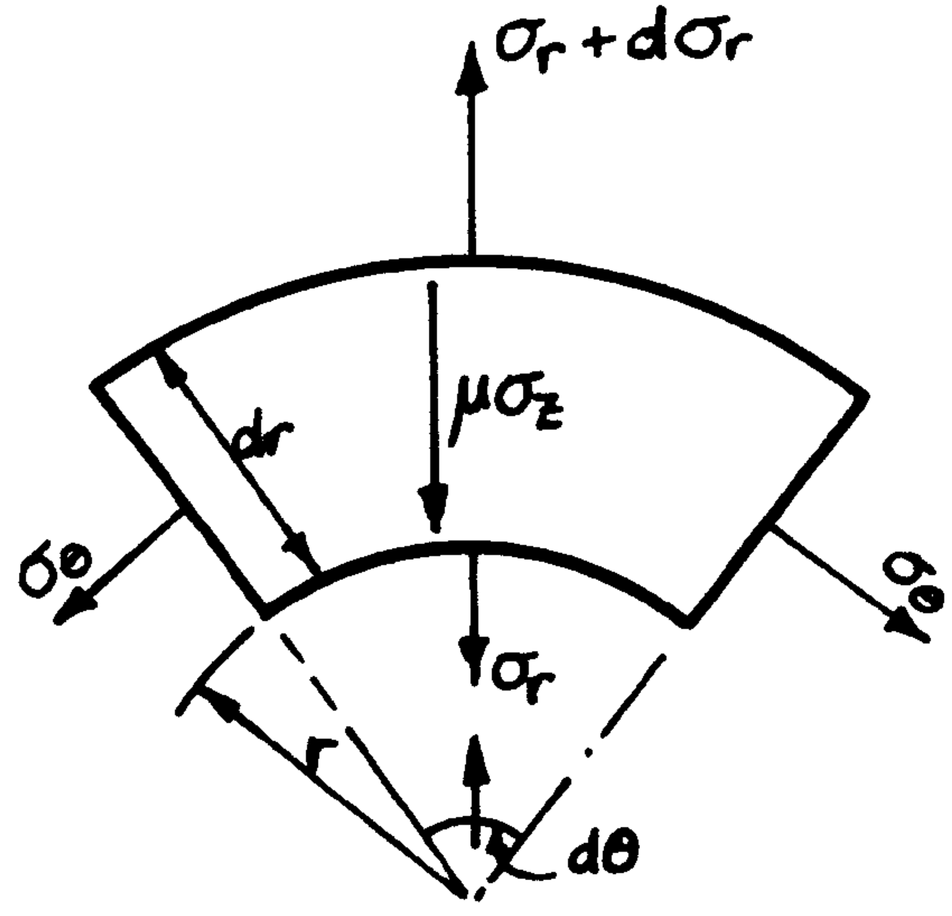

SMALL ELEMENT

FIG.114 QUASI-STATIC COMPRESSION OF A SHORT CYLINDER OF PERFECTLY PLASTIC MATERIAL

$(\sigma_r - \sigma_z) = Y$ or $d\sigma_r = d\sigma_z$, where Y is the uniaxial yield stress of the material. Substituting for $d\sigma_r$ in (2) and integrating

$$\ln\sigma_z = -\frac{2\mu}{h}r + C \qquad (3)$$

at $r = a$, $\sigma_r = 0$ and $\sigma_z = -Y$

equation (3) becomes

$$-\sigma_z = Y\exp[2\mu(a - r)/h]$$

replacing $-\sigma_z$ by p

$$p = Y\exp[2\mu(a - r)/h]$$

and since μ is small

$$p \cong Y\left[1 + \frac{2\mu(a - r)}{h}\right] \qquad (4)$$

APPENDIX 2

FAST COMPRESSION OF A SHORT CYLINDER

To assess the influence of speed in simple compression consider the case of the frictionless compression of a short circular cylinder by an upper die moving at constant speed v, the lower die being at rest.

Fig. 115 shows an upper die descending with speed v; u_r and f_r denote radial speed and acceleration, which are assumed to be independent of z at a given time.

The equation for constancy of volume is,

$$v\pi r^2 = 2\pi r h u_r$$

or
$$u_r = \frac{rv}{2h} \qquad (5)$$

Also

$$f_R = \frac{du_r}{dt} = \frac{\partial r}{\partial t}\frac{v}{2h} + \frac{r}{2h}\frac{\partial v}{\partial t} - \frac{rv}{2h^2}\frac{\partial h}{\partial t}$$

$$= \frac{u_r v}{2h} + \frac{r\dot{v}}{2h} + \frac{rv^2}{2h^2} \quad , \text{ since } \frac{\partial h}{\partial t} = -v$$

and using (5)

$$f_r = \frac{rv^2}{4h^2} + \frac{r\dot{v}}{2h} + \frac{rv^2}{2h^2}$$

$$= \frac{3rv^2}{4h^2} + \frac{r\dot{v}}{2h} \qquad (6)$$

Thus the radial acceleration f_r is $\frac{3rv^2}{4h^2}$ for a constant speed upper die.

The equation of radial motion of an element, see Fig. 115 is

$$d(rd\theta h\sigma_r) - \sigma_\theta hdrd\theta = rd\theta hdr\rho f_r \quad \text{——————} \quad (7)$$

where ρ is the density of the cylinder.

Equation (7) reduces to

$$\frac{\sigma_r - \sigma_\theta}{r} + \frac{\partial \sigma_r}{\partial_r} = \rho f_r$$

Assuming $\sigma_r = \sigma_\theta$ and replacing f_r by $3rv^2/4h^2$ equation (7) becomes

$$\frac{\partial \sigma_r}{\partial_r} = \frac{3\rho v^2 r}{4h^2}$$

or

$$\sigma_r = \frac{3\rho v^2 r^2}{4h^2.2} + C \quad \text{——————} \quad (8)$$

since $\sigma_r = 0$ when $r = a$ equation (8) becomes

$$\sigma_r = \frac{3\rho v^2}{8h^2}(r^2 - a^2)$$

In the absence of acceleration parallel to the axis of the cylinder (if $\dot{v} \neq 0$, then equation (8) should be modified) and using the Tresca yield criterion as

$$\sigma_r - \sigma_z = Y$$

the compressive stress in the dies p, is given by

$$p = -\sigma_z = Y - \sigma_r$$
$$= Y + \frac{3\rho v^2}{8h^2}(a^2 - r^2)$$

A2.3

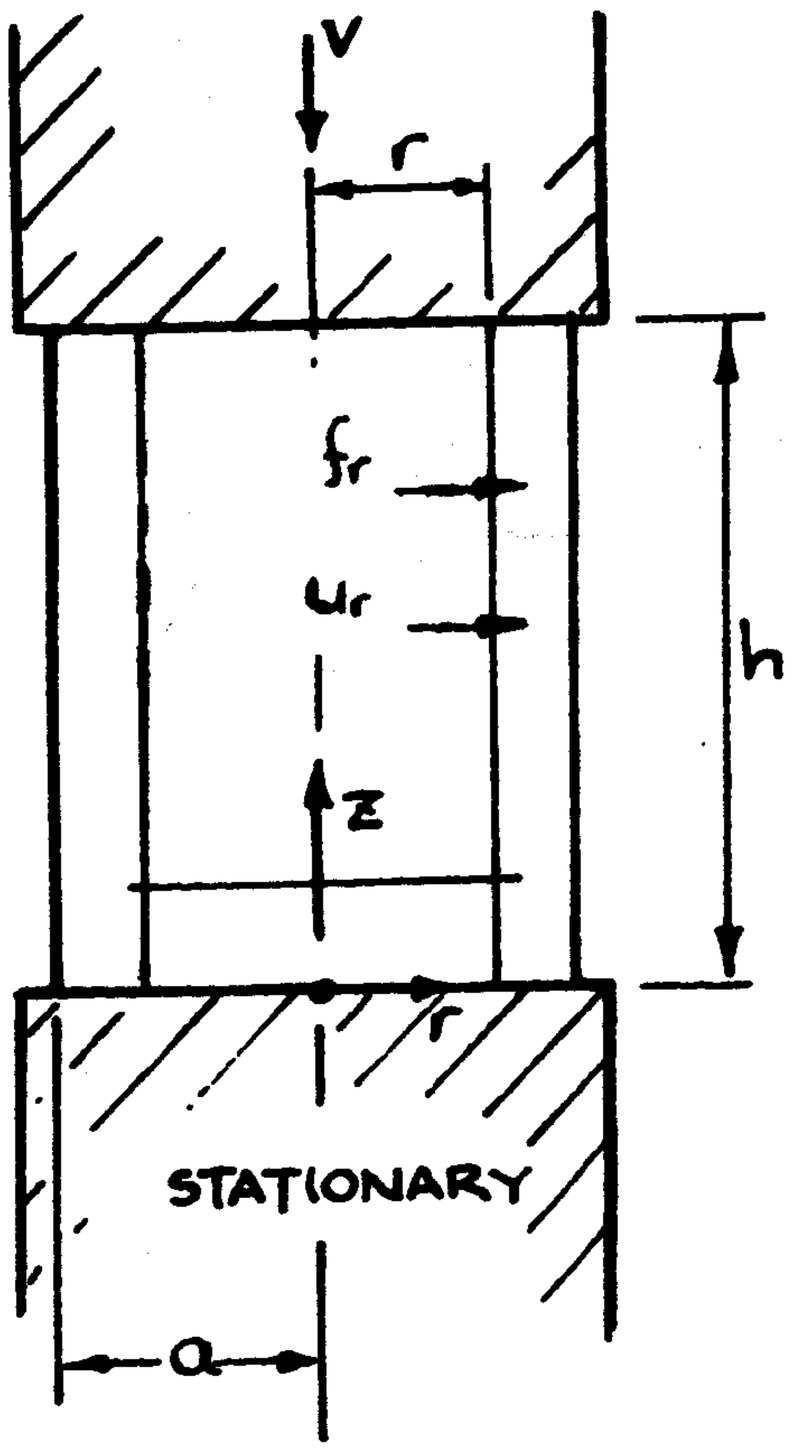

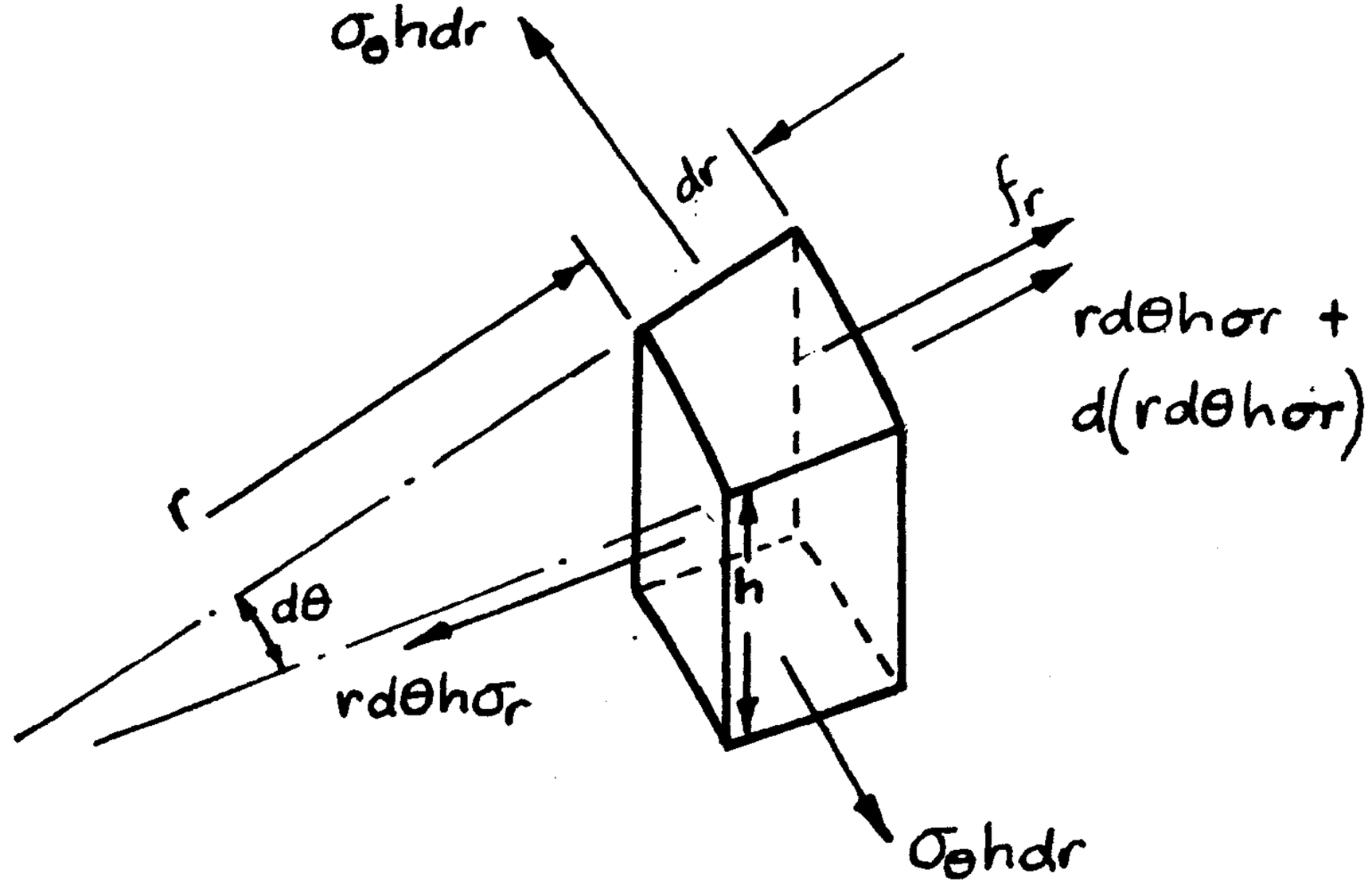

FIG.115 FAST COMPRESSION OF A SHORT CYLINDER

APPENDIX 3

THEORETICAL RESULTS

$D_B = 24$ mm $L_o = 24$ mm $Y = 17$ N/mm^2

$D_c = 18$ mm $x_o = 3.405$

W_p (1ST STAGE) $= 14.22$ Nm.

x mm	W_T Nm	P_2 KN	h_b mm	h_f mm
1.25	32.24	13.81	3.95	19.35
2.5	45.9	13.99	4.50	18.10
3.75	59.86	14.20	5.04	16.85
5.0	74.23	14.47	5.59	15.6
6.25	89.08	14.80	6.14	14.35
7.5	104.62	15.19	6.68	13.1
10.0	138.6	16.26	7.77	10.6
12.0	170.0	17.5	8.65	8.6

THEORETICAL RESULTS

$D_B = 24\,mm$ $L_o = 24\,mm$ $Y = 17\,N/mm^2$

$D_C = 12\,mm$ $x_o = 0.886\,mm$

W_p (1st STAGE) $= 5.22\,Nm$

x mm	W_T Nm	P_2 KN	h_b mm	h_f mm
1.25	17.8	11.29	1.21	21.86
2.5	30.1	11.64	1.53	20.61
3.75	42.9	12.0	1.86	19.36
5.0	56.3	12.44	2.18	18.1
6.25	70.35	12.91	2.5	16.86
7.5	85.23	13.45	2.83	15.6
10.0	11.81	14.7	3.48	13.1
12.0	14.85	16.1	4.0	11.1

THEORETICAL RESULTS

$D_B = 24\,mm$ $L_o = 24\,mm$ $Y = 17\,N/mm^2$

$D_c = 9\,mm$ $x_o = 0.335$

W_p (1ST STAGE) $= 2.31\,Nm$

x mm	W_T Nm	P_2 KN	h_b mm	h_f mm
1.25	13.52	9.98	0.57	22.4
2.5	28.52	10.38	0.81	21.2
3.75	40.62	10.8	1.05	19.9
5.0	53.3	11.27	1.29	18.66
6.25	66.8	11.79	1.52	17.41
7.5	81.12	12.36	1.76	16.16
10.0	11.3	13.7	2.24	13.67
12.0	14.25	15.07	2.61	11.66

THEORETICAL RESULTS

$D_B = 24\,mm$ $L_o = 30\,mm$ $Y = 17\,N/mm^2$

$D_c = 18\,mm$ $x_o = 3.405\,mm$

W_p (1ST STAGE) $= 14.22\,Nm$

x mm	W_T Nm	P_2 KN	h_b mm	h_f mm
1.25	32.6	14.4	3.83	25.35
2.5	46.61	14.54	4.25	24.1
3.75	60.8	14.7	4.67	22.9
5.0	75.27	14.9	5.1	21.6
6.25	90.0	15.1	5.52	20.3
7.5	105.3	15.4	5.94	19.1
10.0	137.43	16.0	6.79	16.6
12.0	146.4	16.7	7.46	14.6

THEORETICAL RESULTS

$D_B = 24mm$ $L_o = 18mm$ $Y = 17 N/mm^2$

$D_C = 18mm$ $x_o = 3.405mm$

W_p (1ST STAGE) $= 14.22 Nm.$

x mm	W_T Nm	P_2 KN	h_b mm	h_f mm
1.25	31.56	12.73	4.17	13.35
2.5	44.61	12.96	4.95	12.1
3.75	58.11	13.27	5.72	10.86
5.0	72.28	13.7	6.49	9.6
6.25	87.43	14.27	7.26	8.35
7.5	104.0	15.04	8.03	7.1
10.0	145.2	17.59	9.57	4.6
12.0	195.77	21.80	10.8	2.6

THEORETICAL RESULTS

$D_B = 24$ mm $L_0 = 18$ mm $Y = 1.7$ N/mm²

$D_C = 9$ mm $x_0 = 0.335$

W_p (1ST STAGE) $= 2.31$ Nm.

x mm	W_T Nm	P_2 KN	h_b mm	h_f mm
1.25	13.6	10.0	0.65	16.4
2.5	25.3	10.58	0.97	15.2
3.75	37.9	11.2	1.29	13.91
5.0	51.44	11.99	1.6	12.66
6.25	66.2	12.7	1.93	11.41
7.5	82.5	13.64	2.24	10.16
10.0	121.4	16.1	2.88	7.66
12.0	162.5	19.0	3.39	5.66

```
10  REM  EXTRUSION FORGING
20  INPUT "BILLET DIAMETER";DB
30  INPUT "BOSS DIAMETER";DC
40  INPUT "BILLET HEIGHT,  FRICTION FACTOR";LO,FM
45  DIM M2(30),M3(30)
47 I = 1
50 PI = 3.1416:YO = 17.
60 D1 =  SQR(DB ↑ 2 + DC ↑ 2):HO = DC / 2.:D3 = D1 - DC:D4 = DB - DC
70 FB = D1 ↑ 2 - DC ↑ 2:FC = DB ↑ 2 - DC ↑ 2:FF = 1. + FM * DB / 6. /
 LO
74 I = 1
80 PO = PI * FC * FF * YO / 4.:P1 = PI * DB ↑ 2 * YO * FF / 4.:P5 = P
1
90  PRINT "D1=";D1;"PO=";PO;"P1=";P1
100  INPUT X
110 WP = PI * YO * FC * (FB * ( LOG (FB) - 1. -  LOG (FC)) + FC) / 8.
 / D
     C
115 WP = WP + PI * YO * FM * (D1 ↑ 2 + DB ↑ 2 - 2. * DC ↑ 2) * (D1 -
DB) /
     16.
120 BC = 2. * (PO + P1) / PI / DC / YO - HO:CC = 4. * WP / PI / DC /
YO
130 XO = ( SQR (BC ↑ 2 + 4. * CC) - BC) / 2.:X1 = XO:ETA = 0:L1 = LO
- XO
140  PRINT "XO=";XO
150  PRINT "2ND MODE STARTS": PRINT
170  INPUT "INCREMENT";DX
180 X1 = X1 + DX
185 DETA =  LOG (L1 / (L1 - DX)):ETA = ETA + DETA
187 CDC = DC *  EXP (DETA / 2.)
190 W1 = PI * FC * (HO + XO) * YO * ( LOG (L1 / (L1 - DX))) / 4.
200 W2 = PI * DC * YO * DX * (HO - HO * DX / 2. / L1) / 2.
```

```
210 W3 = (LO - XO - HO) * PI * DB ↑ 2 * YO * ( LOG (L1 / (L1 - DX)))
/ 4.

215 W4 = PI * DC ↑ 2 * YO * (CDC - DC) / 8.
220 D2 = D3 *  EXP (ETA / 2) + DC:DDB = D4 *  EXP (ETA / 2) + DC
230 WT = PI * YO * (D2 - D1) * (D2 ↑ 2 + D1 ↑ 2 - 2 * DC ↑ 2) / 16. *
 FM
240 WB = PI * YO * (DDB - DB) * (DDB ↑ 2 + DB ↑ 2) / 16. * FM
250 T2W = W1 + W2 + W3 + W4 + WT + WB
260 W1 = PI * FC * LO * YO * DETA / 4.
270 W2 = PI * DC * YO * DX * (L1 - DX / 2.) / 2.
280 T3W = W1 + W2 + WT + WB
290  PRINT " T2W=";T2W;"  T3W=";T3W
310 P4 = PI * DDB ↑ 2 * YO * (0.8 + 3.0 *  LOG (D2 / DC)) / 4.
320  IF T2W > T3W THEN  GOTO 402
325 J = 5
340 S1H = LO - XO - HO
350 H2 = DC * (1. - (X1 - XO) / L1) / 2.
360 S2H = S1H * (L1 - (X1 - XO)) / L1
370 HB = (XO + DC * (X1 - XO) / 2. / (LO - XO))
380 HF = LO - X1
390 HT = HB + HF
392 P2 = T2W / DX
395  PRINT : PRINT " P2= ";P2: PRINT
400  GOTO 500
402 P3 = T3W / DX
405  IF P4 < P3 THEN  GOTO 460
410  PRINT "THIRD STAGE BEGIN"
412  IF J = 5 THEN  GOTO 420
414 HB = XO + DX
```

A4.2

```
416 HF = LO - XO - DX
418 HT = LO
419  GOTO 445
420 HB = HB + DX
430 HF = HF - DX
440 HT = HT
445  PRINT : PRINT "P3=";P3: PRINT
450  GOTO 500
460  PRINT "FOURTH STAGE BEGIN"
461 M2(I) = D2:M3(I) = DDB
462 P4 = PI * M3(I) ↑ 2 * YO * (0.8 + 3 *  LOG (M2(1) / DC)) / 4.0
466 XL = M2(1) ↑ 2 / DC ↑ 2 * X
467  PRINT "DISP VOL=";XL: PRINT
468 HB = HB + XL
469  PRINT "BILLET DIA=";M2(1)
475 I = I + 1
480 HF = HF - DX
490 HT = HB + HF
495  PRINT : PRINT "P4=";P4: PRINT
500  PRINT "BOSS HT= ";HB;" FLANGE HT=";HF;" TOTAL HT=";HT: PRINT
503 PHT = HT * 100 / 24
505  PRINT "PERCENTG TOTAL HT=";PHT: PRINT
510  PRINT " TOTAL COMPN.=";X1 * 100. / LO;" PERCENT": PRINT
520 D1 = D2:DB = DDB
522 L1 = LO - X1
540  PRINT " TYPE'1'TO PEPEAT,'2' TO END"
545  INPUT X
550  IF X = 1 THEN  GOTO 180
560  END
```

A4.3

THE EFFECT OF FRICTION IN SIMPLE UPSETTING OF CYLINDRICAL BILLETS OF ELASTIC-PLASTIC AND ELASTIC-STRAIN HARDENING MATERIAL: A NUMERICAL TECHNIQUE

M. S. J. HASHMI and F. B. KLEMZ
Department of Mechanical and Production Engineering, Sheffield Polytechnic

SUMMARY

This paper describes a numerical technique for analysing simple upsetting of cylindrical billets, which incorporate the effects of interface friction, axial inertia and strain hardening property of the billet material. This method essentially uses a lumped mass model for the actual billet. The procedure amounts to expressing the dynamic force equilibrium equation for each mass point in finite-difference form and relating the displacement of each mass point to the strain in the corresponding link after each time increment. The stress in each link, and hence the axial force, is then calculated from the material stress-strain characteristics which may be elastic-plastic or elastic-strain hardening.

This theoretical approach enables the billet profile, the tup load, and velocity to be determined at any stage during the in-process time. The stress and strain-time history at any point within the billet can also be determined. Three different values of the friction coefficient - 0, 0.25 and 0.5 have been considered.

INTRODUCTION

In recent years high energy rate forming processes have received considerable attention, firstly since it has proved to be an effective method of producing complex components to a high degree of accuracy and secondly, because of difficulties arising from the shortening of tool life caused by the complex forcing function in the die-billet interface. It has been established [1-3] that high rates of forming also enhances the effect of material inertia, strain-rate sensitivity, stress wave propagation and friction in the interface.

A great deal of experimental and theoretical work has already been carried out to investigate various aspects of high energy-rate forming as applied to forging and simple upsetting operations. Comprehensive surveys of previous work appeared in references [1] to [7] and will not be repeated in this paper.

It is, however, worth noting that most of the theoretical methods developed previously have so far contributed towards understanding the in-process variation of the tup load and billet height, often employing complicated and sometimes cumbersome analytical expressions. The authors felt that a simpler theoretical approach, capable of incorporating the material inertia and strain-hardening effect and also the effect of elastic and plastic stress wave propagation could be developed enabling further understanding of the behaviour of the billet during the in-process time.

The present paper describes a numerical technique for analysing simple upsetting of cylindrical billets which incorporates the effects of billet-tup interface friction, radial inertia and strain hardening properties of the billet material. This method essentially uses a lumped mass model for the actual billet and operates on the following assumptions,

(i) the billet could be idealized to be made up of a number of concentrated masses connected to each other by massless links of circular cross-section which possess the same strength properties as the material of the billet,

(ii) the plane sections remain plane throughout the deformation process,

(iii) uniform axial straining occurs within each individual link,

(iv) the frictional stress in the billet-tup interface is proportional to the normal stress in the face of the billet,

(v) the radial expansion of each connecting link is governed by the condition of volume constancy, and

(vi) there is no resistance to radial expansion of any link from the neighbouring link except for the links in contact with the top and the bottom platens in which case interface frictional force resists radial expansion.

The procedure amounts to expressing the dynamic force equilibrium equations for each concentrated mass point in finite-difference form and relating the displacement of each masspoint to the strain in the corresponding link after each time increment. The stress in each link,and hence the axial force,is then determined from the material stress-strain characteristics which may be elastic-plastic or elastic-strain hardening. This theoretical approach enables prediction of the instantaneous and final shape of the billet, the variation in tup load and velocity, and the stress and strain-time history at any point within the billet.

The influence of the frictional force at the billet-die interface was also taken into account considering three different values for the coefficient of friction, μ = 0.0, 0.25 and 0.5.

NOMENCLATURE

A layer area in the cross-section model
E elastic modulus
F external force per unit length
N axial force
R current billet radius
m mass per unit length
Δs link length in the numerical model
Δt time increment
u,v displacement
x,y co-ordinate axis
ε engineering strain
σ stress

Subscripts

i this refers to the masspoint number and the preceeding link
j time position
l refers to the sublayer number
r refers to the layer number

Superscripts

m modified value
t trial value

ANALYSIS

The general equation of motion for an element of the billet, soon after the tup strikes the top face, can be derived by considering the internal and external forces acting on the element as shown in Fig.1(a) and is given by

$$\frac{\partial (N)}{\partial x} + F_x - m\ddot{u} = 0 \qquad (1)$$

where m denotes mass per unit length and (¨) denotes double differentiation with respect to time.

Figure 1(b) shows the lumped parameter model for the element in Fig.1(a) and equation (1) could be written in finite-difference form to correspond to this model. This model replaces the actual billet by a mass-link system. The mass of each element of the billet is represented by a concentrated mass connected to other masses by massless links which can transmit axial force. Under the action of the external and internal forces therefore, the position of each mass in the model identifies the position of the corresponding element of the actual billet.

The finite-difference equation for the element at the ith location of the model in Fig.1(b) is given by

$$N_{i+1} - N_i + F_x\left(\frac{\Delta s_i + \Delta s_{i+1}}{2}\right) - m_i\ddot{u}_i = 0 \qquad (2)$$

Equation (2) as it applies to all the mass points along the billet gives the instantaneous values of $u_{i,j+1}$ for any time t_{j+1} when coupled with the following relationship between the acceleration and displacement in finite-difference notation,

$$u_{i,j+1} = \ddot{u}_{i,j}(\Delta t)^2 + 2u_{i,j} - u_{i,j-1} \qquad (3)$$

The time increment Δt is defined through

$$\Delta t = t_{j+1} - t_j \qquad (4)$$

The change in length of each link is given by the change of location of each mass point and hence the axial strain in each link is obtained. A constitutive relationship is next used to calculate the stress at any section which in turn gives the value of the axial force.

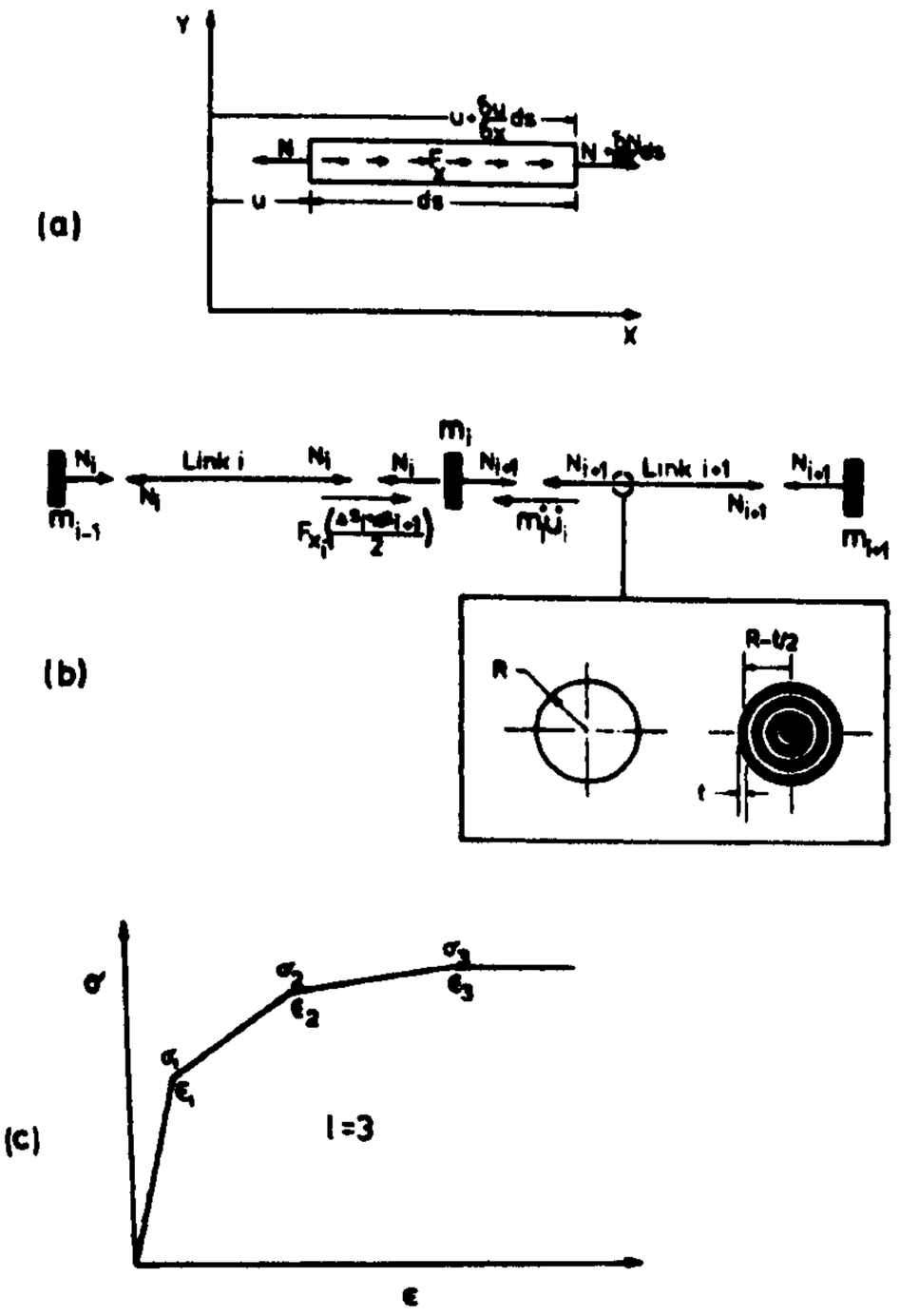

Fig.1. (a) An element of the billet
(b) Equivalent finite-difference model
(c) Approximated polygonal stress-strain diagram

In order to facilitate the calculation of stress which may vary across the cross-section of the billet, it is necessary to idealize the actual cross-section to an equivalent cross-section model which consists of a number of layers across each of which the stress is assumed to be uniform. The circular cross-section of the billet is assumed to consist of n discrete, evenly spaced tubular cross-sectional area layers of material which can carry normal stresses. These layers are considered to be separated by a material which can not carry any normal stress but has infinite shear rigidity.

With this simplified model the stress in the billet can be defined by the individual normal stresses at the n separate layers without having to contravene the assumption that plane sections remain plane throughout the deformation process. The cross-sectional area of each tubular layer can be calculated by equating the fully plastic pure axial load carrying ability, with those of the actual cross-section of the billet. A typical circular section and the corresponding idealized section model are shown in the inset in Fig.1(b).

In order to describe the elastic-plastic stress state in a layer of the section-model further idealization is made and each layer is assumed to consist of sublayers the number of which is determined by the number of positive sloped sides in the approximated polygonal stress-strain diagram shown in Fig.1(c). For example, the polygonal stress-strain diagram for an elastic linearly strain hardening material consists of two positive sloped sides and hence two sublayers to each layer are required. Each sublayer can only carry stresses not exceeding the sublayer yield stress.

The sublayer area $A_{\ell r}$ is related to the layer area A_r by

$$A_{\ell r} = A_r(E_\ell - E_{\ell+1})/E \qquad (5)$$

where

$$E_\ell = \frac{\sigma_\ell - \sigma_{\ell-1}}{\varepsilon_\ell - \varepsilon_{\ell-1}}$$

is the ℓth slope of the polygonal stress-strain diagram, σ_ℓ is the stress and ε_ℓ is the corresponding engineering strain as illustrated in Fig.1(c).

The change in length $\delta(\Delta s)$ of the link Δs_i at time t_j gives the strain increment in each layer of ith link as,

$$\delta\varepsilon_{ir,j} = \frac{\delta(\Delta s)_{i,j}}{\Delta s_{i,o}} \qquad (6)$$

where $\Delta s_{i,o}$ is the original length of the link.

Knowing the sublayer stress $\sigma_{ir\ell,j-1}$ at time t_{j-1}, at the ℓth sublayer of the rth layer at the ith link and the strain increment $\delta\varepsilon_{ir,j}$ at time t_j at the rth layer of the ith link, the sublayer stress $\sigma_{ir\ell,j}$ at time t_j, at the ℓth sublayer is determined as follows.

First a trial value $\sigma^t_{ir\ell,j}$ of the sublayer stress $\sigma_{ir\ell,j}$ is calculated by assuming an elastic path, thus

$$\sigma^t_{ir\ell,j} = \sigma_{ir\ell,j-1} + E\delta\varepsilon_{ir,j} \qquad (7)$$

Once the trial value is calculated, the correct value could be ascertained by using the following conditions: Let $\sigma_{y\ell}$ be the sublayer yield stress and be given by $\sigma_{y\ell} = E\varepsilon_\ell$, where ε_ℓ is the strain defining the ℓth corner of the polygonal stress-strain diagram. Denoting $\sigma_{ir\ell,j}$ as σ_ℓ for convenience,

$$\left.\begin{aligned} &\text{If } -\sigma_{y\ell} \leq \sigma^t_\ell \leq \sigma_{y\ell} \quad \text{then } \sigma_\ell = \sigma^t_\ell \\ &\text{If } \sigma^t_\ell < -\sigma_{y\ell} \quad \text{then } \sigma_\ell = -\sigma_{y\ell} \\ &\text{If } \sigma^t_\ell > \sigma_{y\ell} \quad \text{then } \sigma_\ell = \sigma_{y\ell} \end{aligned}\right\} \qquad (8)$$

This procedure is applied to all sublayers of each layer for all the links.

The values of the sublayer stresses for the links in immediate contact with the tup and the anvil are then modified, to take into account the interface friction, by using the equation,

$$\sigma = \sigma_0[1 + 2\mu(R-r)/h] \ldots\ldots \qquad (9)$$

given in reference [8] where σ_0 is the uniaxial flow stress, h, R and r are the current billet height, outer radius and intermediate radius respectively. Following the terminology applied to the numerical model this equation could be written as

$$\sigma^m_{\ell,j} = \sigma_{\ell,j}[1 + 2\mu(R_i - R_{ir})/h] \qquad (10)$$

where μ is the interface friction coefficient, and $\sigma_{\ell,j}$ is the sublayer stress determined by equations (8). After this modification, the axial forces $N_{i,j}$ in each link are then obtained from the equation,

$$N_{i,j} = \sum_{r=1}^{n} \sum_{\ell=1}^{k} \sigma_{ir\ell,j} A_{\ell,j} \ldots\ldots \qquad (11)$$

where $A_{\ell,j}$ is the current sublayer area.

If the links could be assumed to have the same mass density as the billet, then further modification to the values of the sublayer stresses could be made, to take into account the effect of radial inertia of the billet material, by using the equation

$$\sigma = 3\rho v^2(R^2 - r^2)/8h^2 \qquad (12)$$

given in reference [8], where ρ is the material density, v is the rate of straining, h, R and r are the current billet height, outer radius and intermediate radius respectively. The above equation only applies when the velocity v is constant, a condition which is assumed to be satisfied when deformation of each individual link during very small time interval Δt is considered.

In the present numerical approach the time increment cannot be chosen arbitrarily. The value of the time increment should be less than the time needed for the elastic stress wave to propagate through the length of the link. For detailed information about this method the reader is referred to Ref. [9].

RESULTS AND DISCUSSIONS

To illustrate the effectiveness of the present numerical method, a simple upsetting operation similar to the one considered in reference [3], was chosen. This enabled a direct comparison to be made between the theoretical method presented in reference [3] and the present work in predicting the relationship between axial deformation, tup load and velocity. A billet of 2 in. diameter and 2 in. height and a tup weighing 500 lbf impinging on to it with a velocity of 100 ft/sec was considered. For the elastic-plastic (E-P)$_2$ model the yield stress of 22400 lbf/in^2 and Young's modulus of 10 x 10^6 lbf/in^2 and for the elastic-strain hardening (E-SH) model, the stress-strain characteristics shown in Fig.2(b) were adopted. Three values of the interface friction, μ, equal to zero, 0.25 and 0.5 were considered. The billet in actual loading configuration and its corresponding numerical model is shown in Fig.2(a).

The present method enabled the prediction of the instantaneous shape of the billet, the outer profiles of which were obtained by joining the mid-peripheral points of the thin elements. Fig.3 shows a series of changing profiles of a billet of elastic-plastic material having interface coefficient of friction, μ, equal to (a) zero and (b) 0.5. It is evident from careful inspection of this figure, that with the onset of the process, the deformation begins with the billet increasing in diameter in the area immediately adjacent to the tup. This size change takes the form of a slightly mushroomed profile which soon progresses along the length of the billet and is reflected at the anvil, thus reversing the initial mushroomed shape. The reflected plastic front then progresses upwards and is again reflected at the tup. The billet continues to deform in this manner, alternating the mushroomed shape, until the plastic deformation ceases. The instantaneous profiles for zero interface friction in Fig.3(a) shows no significant barrelling effect which, however, is very much evident in the profiles shown in Fig.3(b) for the interface friction, μ, equal to 0.5.

Fig.4 shows the comparison of the variation in tup velocity with billet deformation for billets of elastic-plastic and elastic-strain hardening material. In both cases the interface friction coefficient of 0.5 was considered. The result predicted in reference [3] for a rigid-plastic material of yield stress

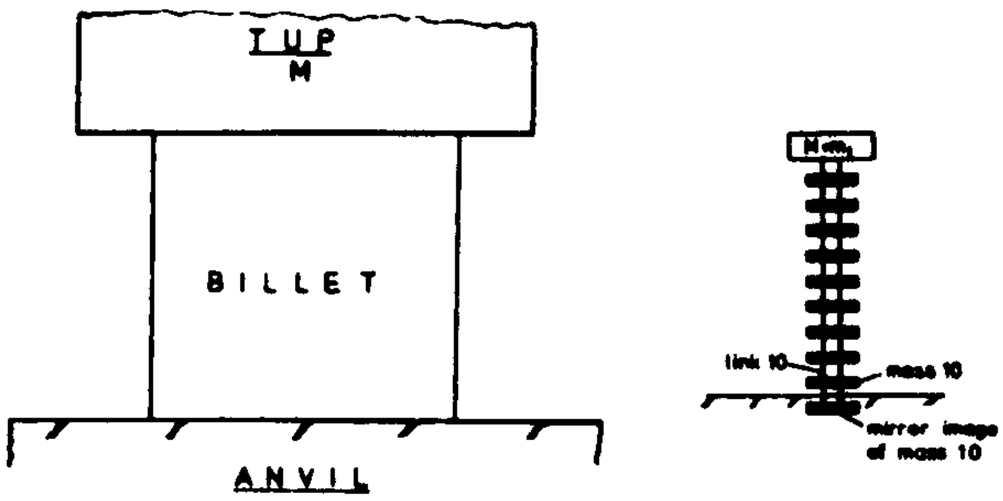

Fig.2. (a) Billet in its actual loading configuration and its corresponding numerical model
(b) Polygonal stress-strain diagrams for E-P and E-SH model

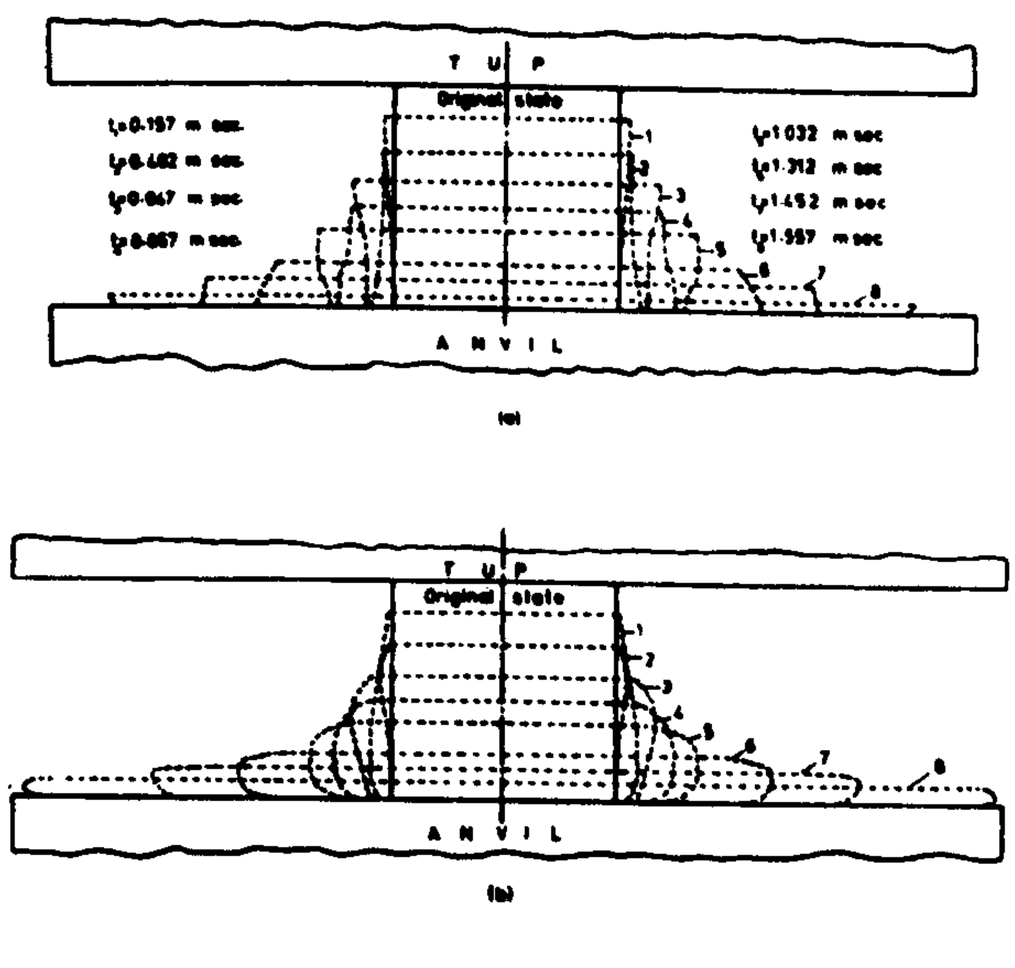

Fig.3. Showing successive deformation pattern of a billet of elastic plastic material
(a) without friction $\mu = 0$
and
(b) with friction, $\mu = 0.5$

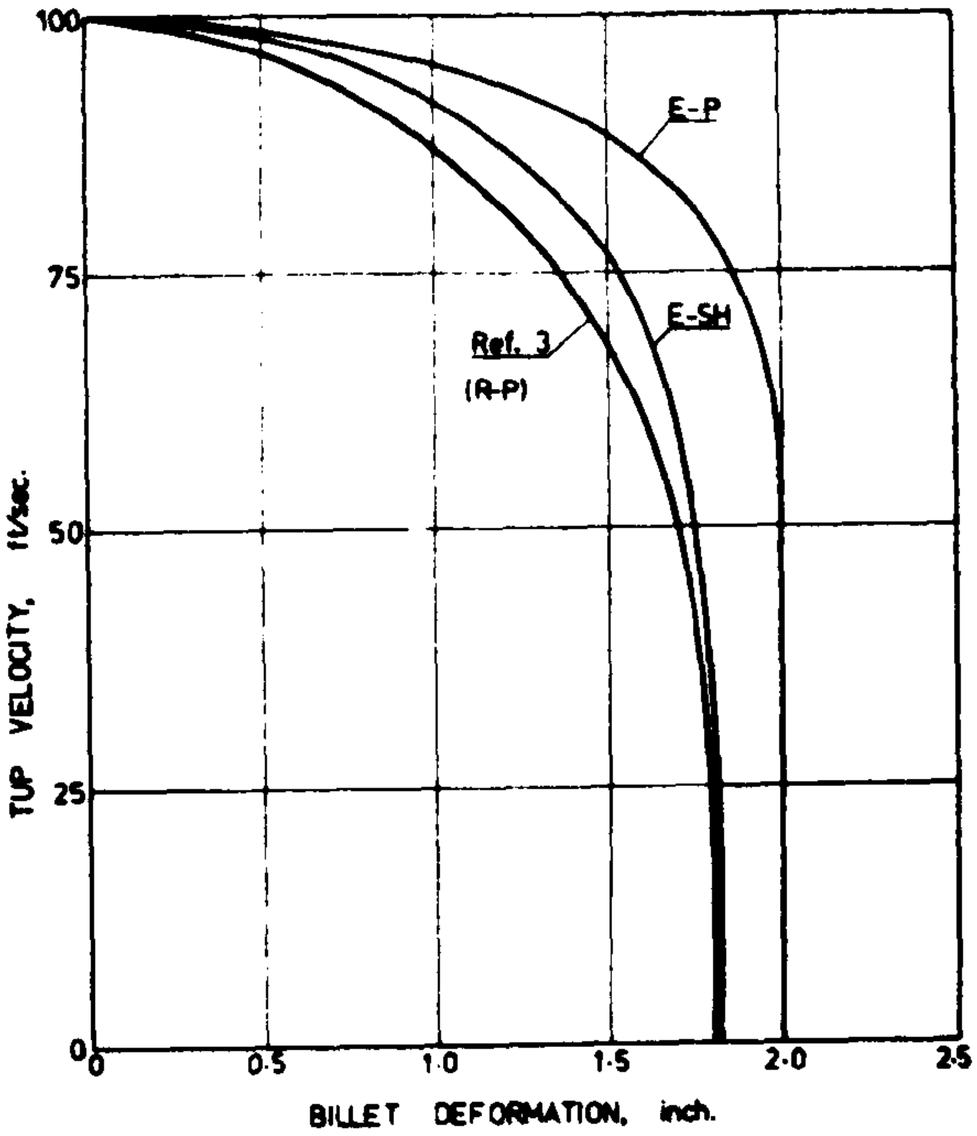

Fig.4. Variation in tup velocity Vs deformation ($\mu = 0.5$)

22400 lbf/in^2 is also included in the same figure for comparison. It is seen that the tup velocity does not change appreciably until near the end of the deformation process, when the velocity decreases quickly. It should be noted, however, that the curve predicted for rigid-plastic material in reference [3]differ considerably from that predicted using the present method.

The variation in tup load during the deformation process is one of the important parameters of interest in an upsetting operation. This is shown in Fig.5 for billets of E-P and E-SH model with friction coefficient of 0.5. A tup-load vs deformation curve from reference [3] for rigid-plastic material is also included in the same figure. The effect of material property on the tup load is clearly evident from this figure. It is seen that a much higher tup-load for a given extent of deformation is predicted in reference [3].

The effect of interface friction on the variation of tup load with deformation for a billet of E-SH material is shown in Fig.6 which shows tup load vs billet deformation curves for coefficients of friction of zero and 0.5. The effect of the material property on the deformation process can be seen from Fig.7 which shows the variation in billet height with in-process time for E-P and E-SH material, in both cases zero interface friction was

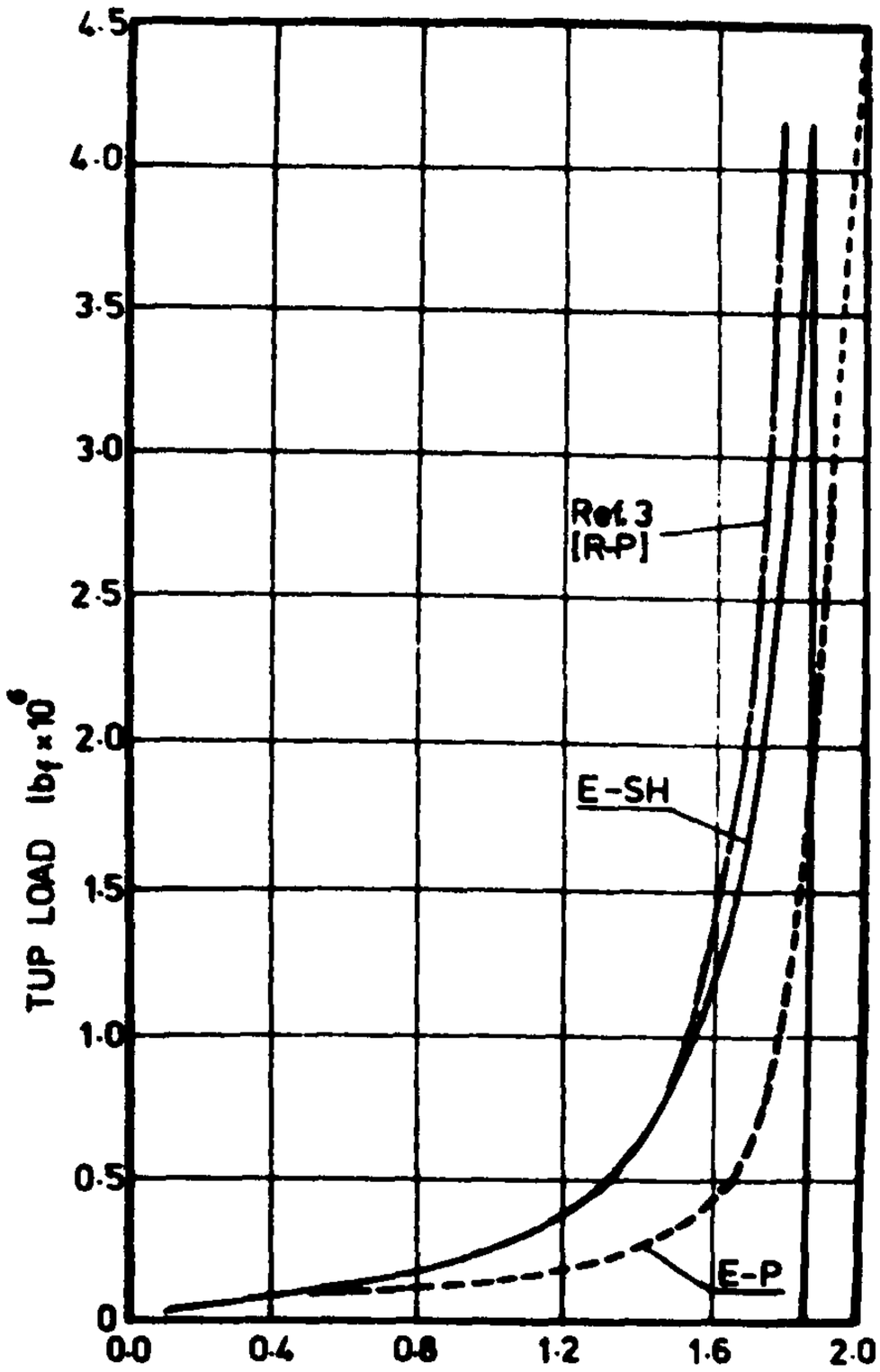

Fig.5. Variation in tup load with deformation ($\mu = 0.5$) showing the effect of billet material properties

considered. Fig.8 compares the rate of consumption of the initial kinetic energy possessed by the tup in deforming billets of E-P and E-SH material having zero interface friction. A more rapid absorption of energy by the E-SH model is clearly evident from this figure. The effect of interface friction on the rate of consumption of tup-energy is demonstrated in Fig.9, which shows percentage kinetic energy absorbed vs billet deformation curves for a billet of E-P material having interface friction of zero, 0.25 and 0.5.

The presence of friction in the tup-billet interface restricts the material at the interface from spreading freely and causes barrelling of the deformed billet. The effect of friction on the extent of spread at the interface for a billet of E-SH material is shown in Fig.10, which shows the percentage change in diameter at the tup-billet interface with billet deformation for interface friction coefficients of zero, 0.25 and 0.5. When friction is present, the restricted material spread at the interface results in

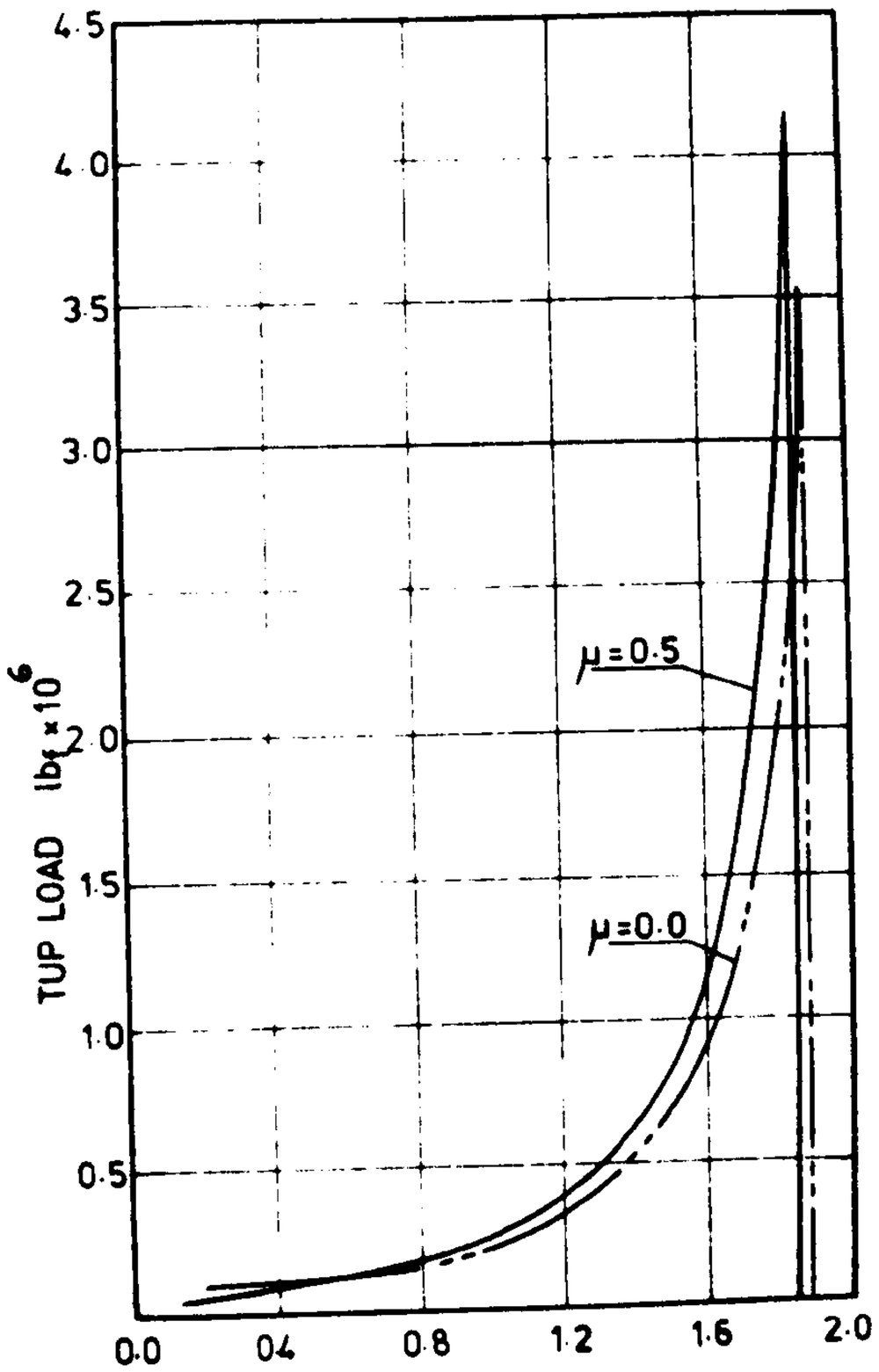

Fig.6. Variation in tup load with deformation (E - SH) showing the effect of interface friction

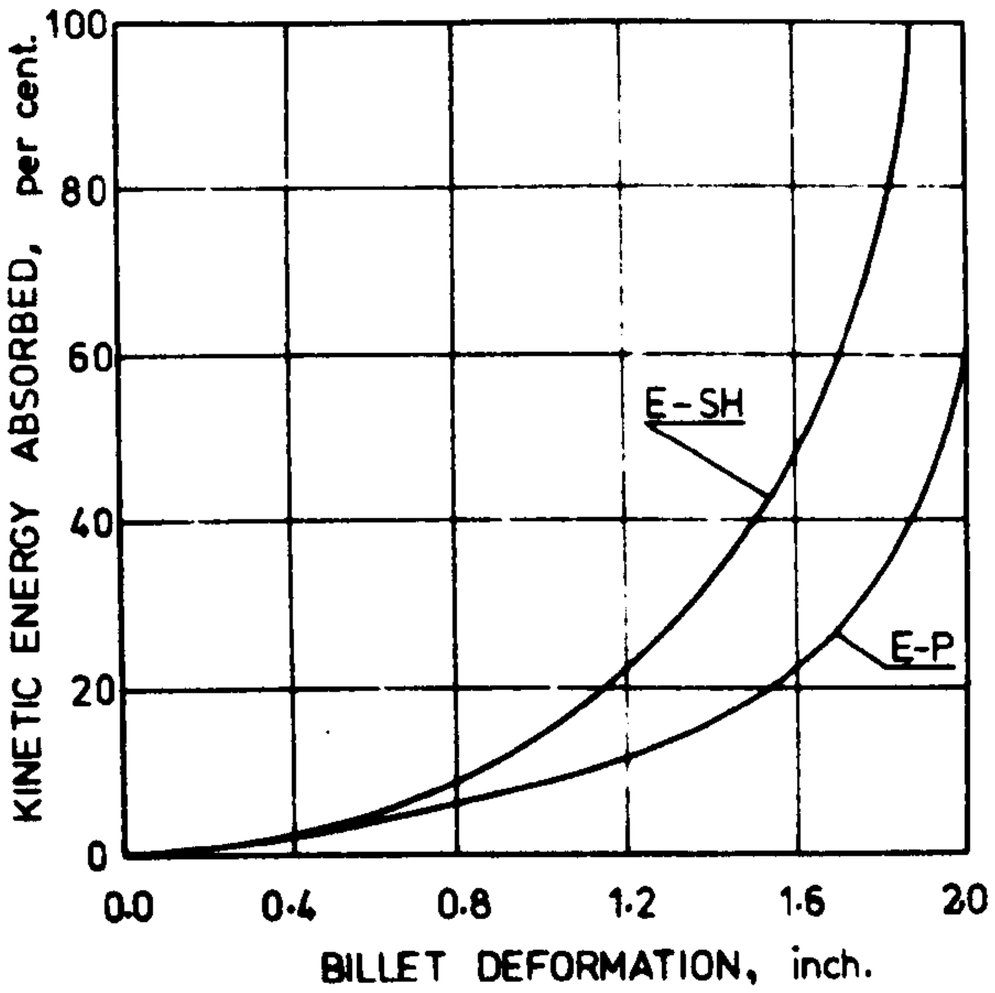

Fig.8. Showing the rate of K.E. absorption with deformation for E-P and E-SH material (μ = 0)

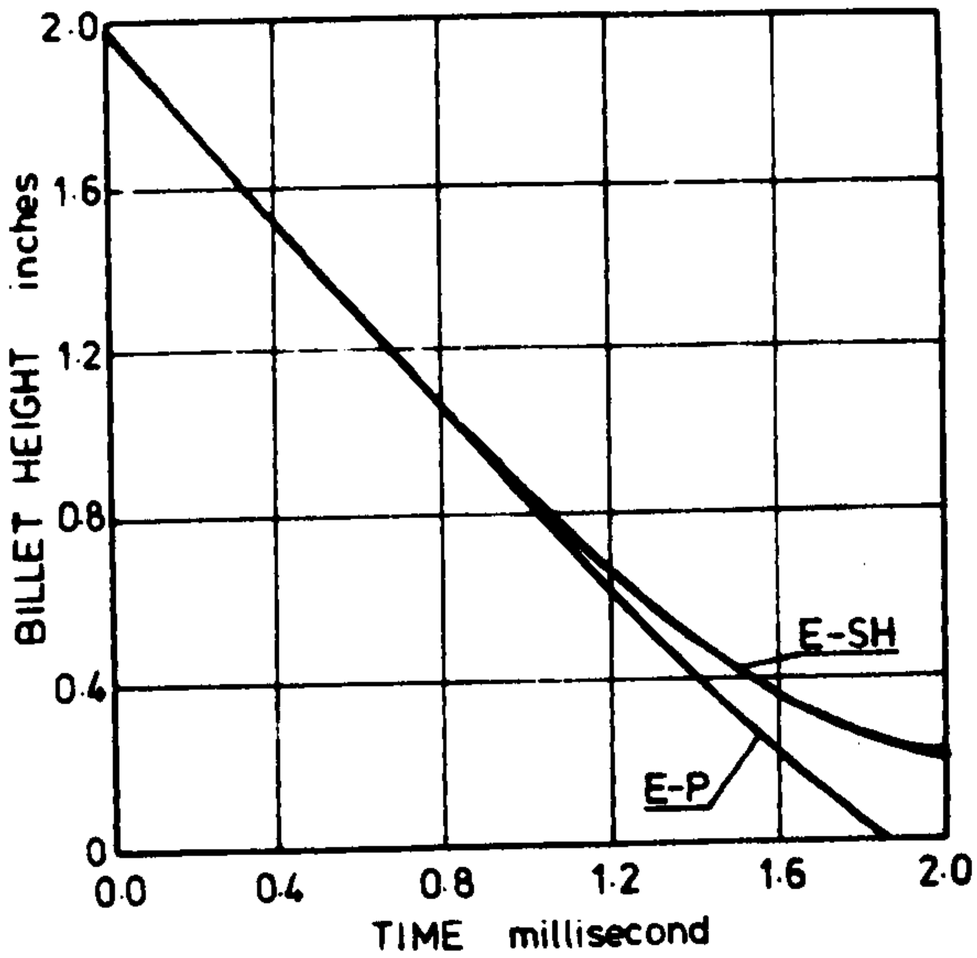

Fig.7. Effect of material property on the time variation of the billet height (μ = 0)

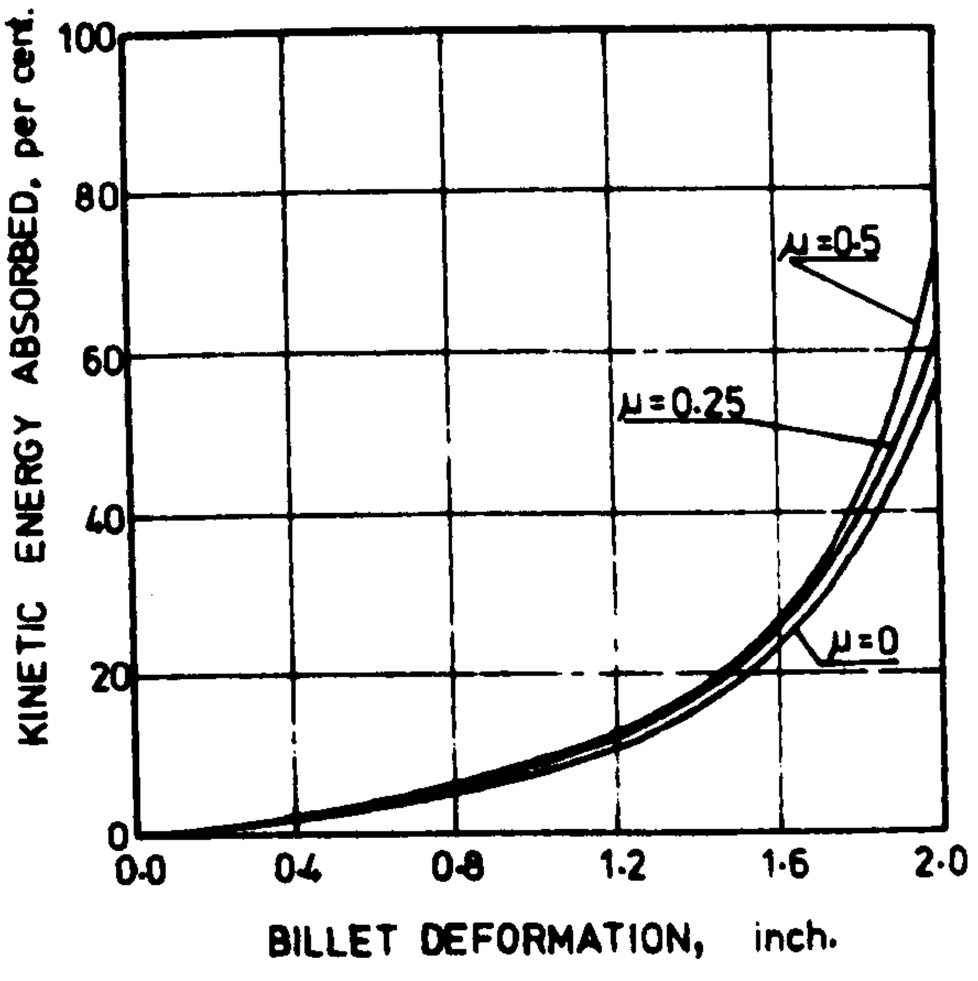

Fig.9. Variation in the kinetic energy absorbed with different values of friction coefficient. (E - SH)

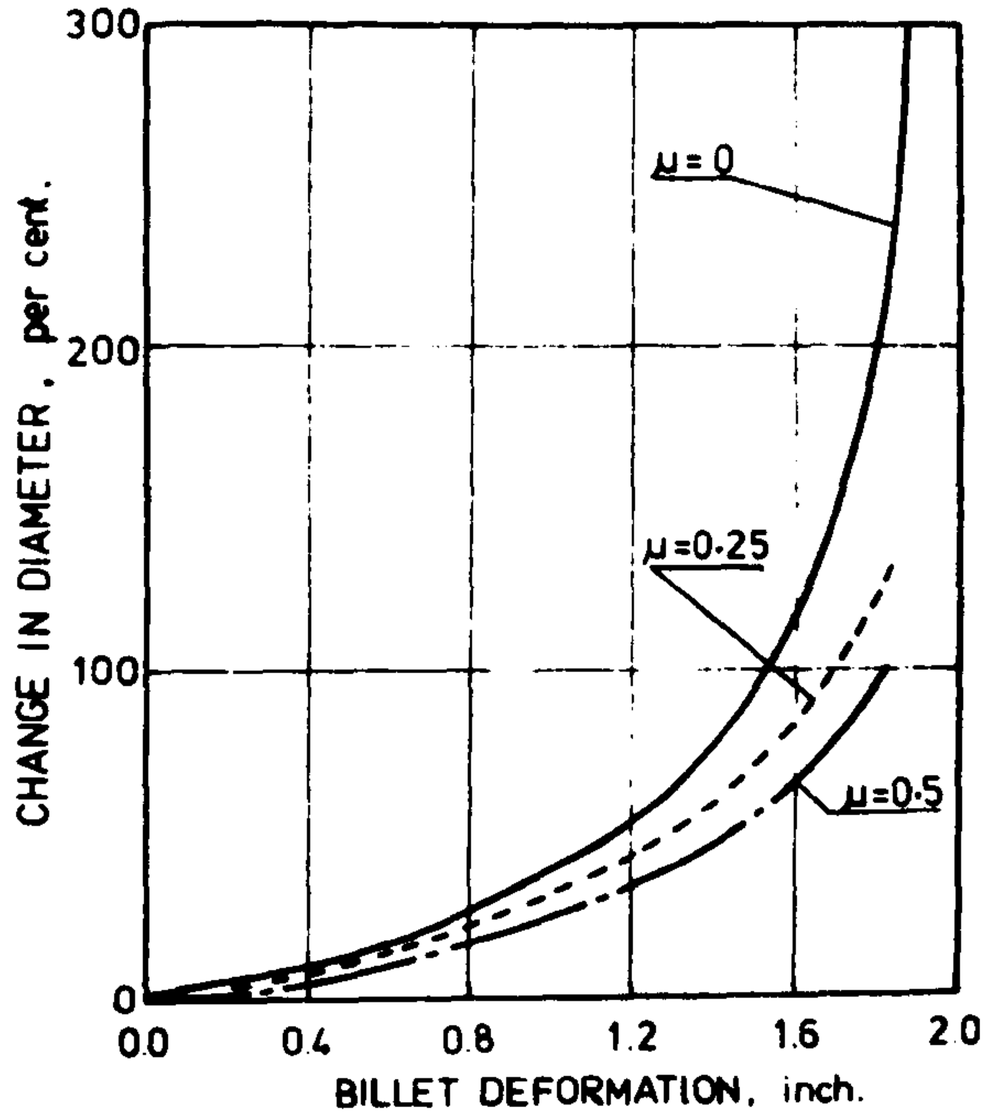

Fig.10. Percentage change in billet diameter at the tup-billet interface with tup displacement (E - SH)

lesser-axial strain to the layer of billet material adjacent to the tup than the layer at mid section. However, equal axial straining within the billet is expected if there is no interface friction. Fig.11 shows the variation in axial strain at the top interface and middle section of a billet of E-SH material during the in-process time for friction coefficients of (a) zero and (b) 0.5.

The radial velocity of the billet material at the top and bottom face was predicted using the present numerical method and is shown in Fig.12 for a billet of E-SH material having zero interface friction. It is evident from this figure that the radial velocity changes with in-process deformation time in a cyclic manner. A phase difference, however, is present between the radial velocity curves for top and bottom face. This could perhaps be explained as the result of the propagation of and reflection of the stress wave fronts in between the tup and the anvil while deformation progresses.

The magnitude of the radial velocity was predicted to reach about four times the initial tup velocity at the final stages of deformation. The radial inertia, however, is found to have insignificant effect on the tup load for the range of tup velocity considered in this work.

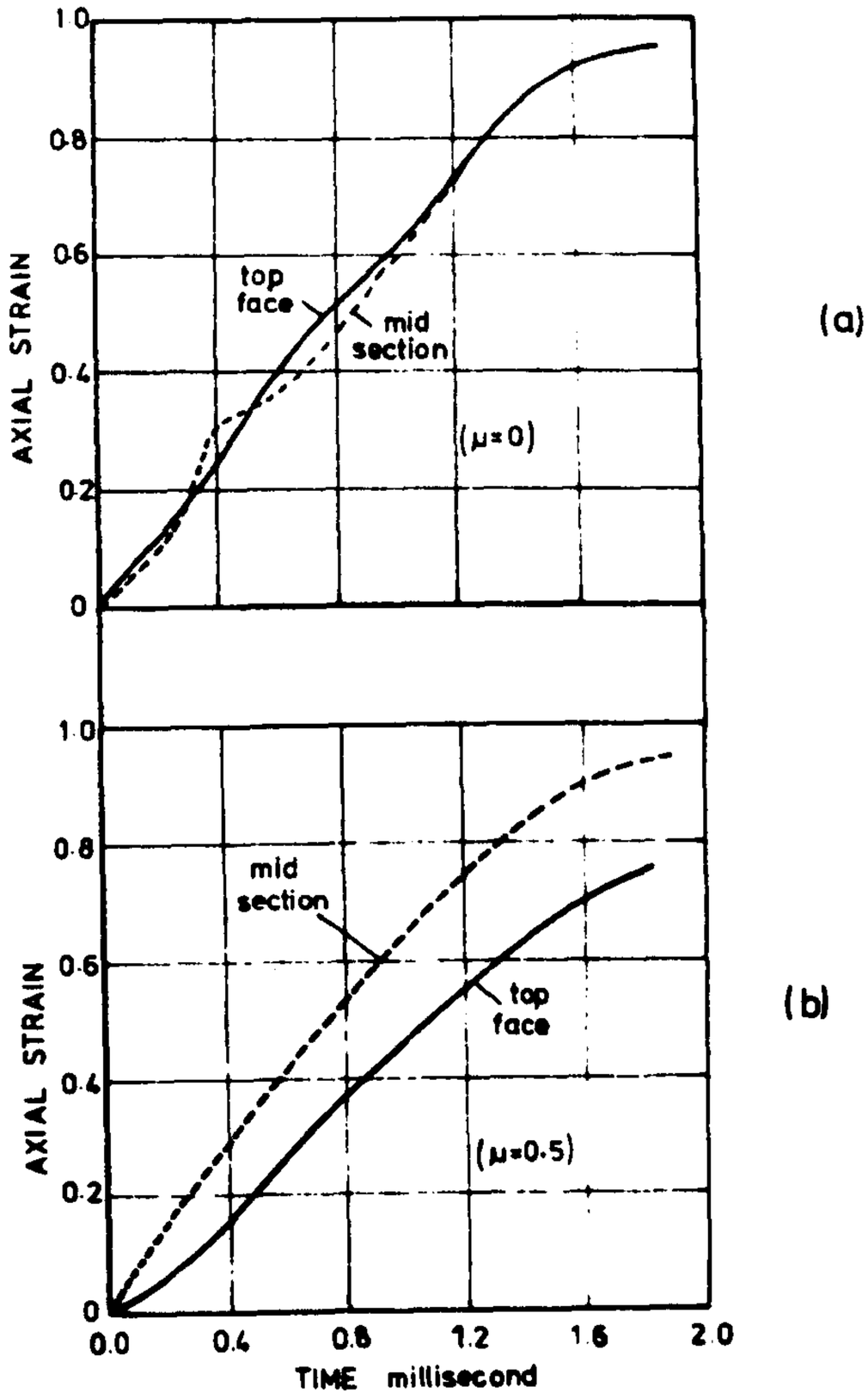

Fig.11. Time variation of the axial strain at the top and middle section (E-SH)

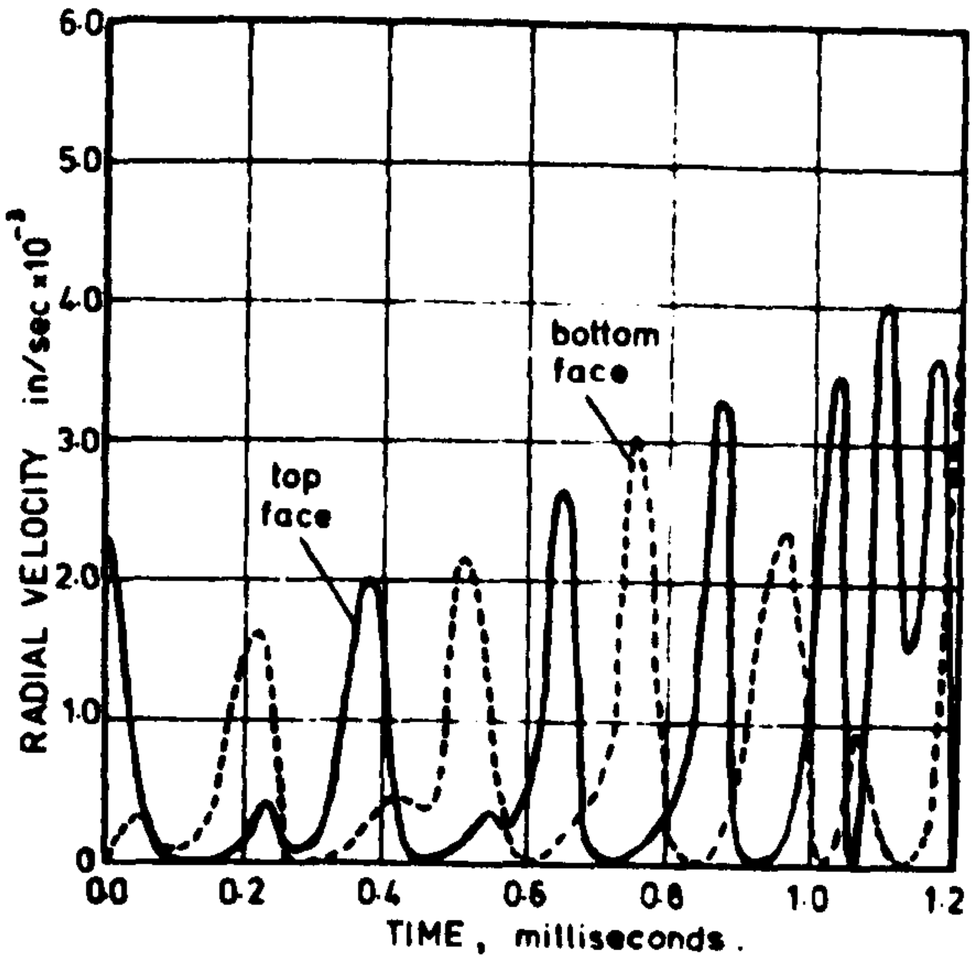

Fig.12. Time variation of the radial velocity of the billet material at the tup and anvil interface of the billet (μ = 0, E-SH)

CONCLUSIONS

The results predicted using the present numerical method compare well with those using other methods [3]. However, further experimental evidence is needed to verify the practical significance of these approaches.

The presence of friction at the tup-billet interface is seen to have considerable effect on the tup load, shape of the deforming billet, and strain and stress distribution during the deformation process.

The present method provides a comprehensive picture of the mechanics of deformation during the upsetting process, thus facilitating the analysis of the behaviour of the billet at any stage during its in-process time.

REFERENCES

1. W.SCHROEDER and D.A.WEBSTER (1949) Press Forging Thin Sections: Effect of Friction, Area and Thickness on Pressures Required. J.App.Mech. p.289

2. J.B.HADDOW (1965) On the Compression of Thin Disc, Int.J.Mech.Sci. 7, p.657

3. H.LIPPMAN (1966) On the Dynamics of Forging, Proc.7th Int.M.T.D.R.Conf. p.53

4. R.A.C.SLATER, W.JOHNSON and S.Y.AKU (1968) Experiments in the Fast Upsetting of Short Pure Lead Cylinders and a Tentative Analysis. Int.J.Mech.Sci. 9. p.169

5. S.K.SAMANTA (1968) Resistance to Dynamic Compression of Low-Carbon Steel and Alloy Steels at Elevated Temperature and at High Strain Rates, Int.J.Mech.Sci. 10, p.613

6. T.A.DEAN (1970) The Influence of Billet Inertia and Die Friction in Forging Processes, Proc.11th Int.M.T.D.R.Conf, p.761

7. C.E.N.STURGESS and A.N.BRAMLEY (1970) The use of Impact-Forming Devices to obtain Dynamic Stress-Strain Data. Proc.11th Int.M.T.D.R. Conf. p.803

8. W.JOHNSON (1972) Impact Strength of Materials, Edward Arnold, London, p.153-154

9. M.S.J.HASHMI (1972) Study of Elastic-Plastic Response of Structures to Dynamic Load. PhD.Thesis, University of Manchester Institute of Science and Technology

SIMPLE UPSETTING OF CYLINDRICAL BILLETS: EXPERIMENTAL INVESTIGATION AND THEORETICAL PREDICTION

F.B. KLEMZ and M.S.J. HASHMI
Department of Mechanical and Production Engineering
Sheffield City Polytechnic, Sheffield

SUMMARY

Experiments were carried out by deforming cylindrical billets under a free falling tup in an experimental drop-hammer unit. Load-time variation was measured experimentally using a load cell incorporated in the anvil. High speed photographs were used to obtain instantaneous and final profiles of the billet and also the data giving tup velocity-time curves after the onset of the deformation process.

In order to study the effect of friction, billets were tested under lubricated and dry condition. Experimental results were then compared with those predicted using a numerical technique (1), incorporating elastic-strain hardening stress-strain characteristics of the billet material obtained from quasi-static compression test.

INTRODUCTION

With the advent of high energy rate forming processes in recent years, considerable effort has been devoted, firstly, to the estimation of the resistance of metals to deformation at high rates of strain and secondly, to the understanding of the complex forcing function which prevails during the deformation process due to material inertia, high strain rate, stress wave propogation and interface friction. To this end simple upsetting of cylindrical billets provided the most convenient and simple means of carrying out experimental as well as analytical studies.

Published literature on the subject shows that most of the experimental studies were aimed at establishing empirical equations of some sort relating dynamic flow stress, strain and strain rate (2-13). A number of other studies have also been carried out putting forward analytical methods for predicting the load-deformation behaviour of billets of material having stress-strain characteristics following one or other of the relations established in earlier studies, some of these incorporated friction and material inertia (16). However, most of these analyses appear to be cumbersome and involve lengthy derivations.

More recently, in reference (1) the authors presented a numerical technique for predicting load and deformation behaviour of a billet of elastic-strain hardening material incorporating interface friction and material inertia. It was also suggested in reference (1) that the billet deforms in a mode dominated by elastic-plastic stress wave propogation through the billet until deformation ceases. This effect was found to be more dominant when interface friction was negligible.

The purpose of this study is to obtain experimental results by carrying out tests on a cylindrical billet and compare with those predicted using the above mentioned numerical technique, thus facilitating verification of its effectiveness. In this study, tests were carried out on commercially pure lead and aluminium alloy cylindrical billets by deforming them under a free falling tup in an experimental drop hammer designed, constructed and instrumented for this purpose. The reason for using lead and aluminium alloy as the billet material is that lead is hot worked at room temperature and is highly strain-rate sensitive. On the other hand aluminium alloy at room temperature is known to be non strain rate sensitive for strains of the order of $10^2 sec^{-1}$. Tests

on billets of these different materials would, hopefully, provide experimental results with and without the influence of strain rate sensitivity. The theoretical prediction for both cases would be without taking strain rate sensitivity into account.

Two types of frictional condition were studied, one, using a paste of graphite in petroleum jelly as lubricant to induce low friction and, the other, without any lubricant to induce dry friction condition. High speed photographs were used to obtain experimental data giving instantaneous billet profiles and tup-displacement-time curves. Elastic strain-hardening stress-strain characteristics of the billet material were obtained from quasi-static compression tests and were incorporated in the numerical technique the details of which are given in reference (1) and will not be repeated in this paper.

EXPERIMENTAL EQUIPMENT AND PROCEDURE

Simple upsetting of commercially pure lead cylindrical billets having diameter of 1.00 in and height of 0.95 in and aluminium alloy cylindrical billets of 0.75 in diameter and 0.75 in height, was performed at room temperature using an experimental drop hammer. The force time variations were obtained by using a hardened tool steel load-cell which was incorporated in the anvil unit of the drop hammer. Output signals generated from the load-cell were fed to a storage oscilloscope through a transient recorder and a built in filter. The traces displayed on the screen were then photographed by means of a Polaroid camera to produce records for further analysis. The tup velocity just before impact was measured using an electronic counter which is activated and stopped by means of a photocell unit which also triggers the oscilloscope.

The energy required to produce plastic deformation of the billet was provided by a tup which could fall freely from any desired height up to a maximum of 15 ft. The mass of the tup was variable but during the present tests it was maintained constant at 35.5 lb. Fig.1. shows a schematic diagram of the lower part of the drop hammer showing the anvil unit, load cell, tup, billet and velocity measuring arrangement. The load cell was calibrated using a 50 tonf compression machine and then incorporated into the anvil unit.

High speed photographs were taken at a speed of 2400 frames/sec using a Hi-cam high speed camera. The processed film was then projected on to a screen using a 16 mm cine-projector with single frame movement facilities and analysed for instantaneous profiles and tup-displacement-time curves.

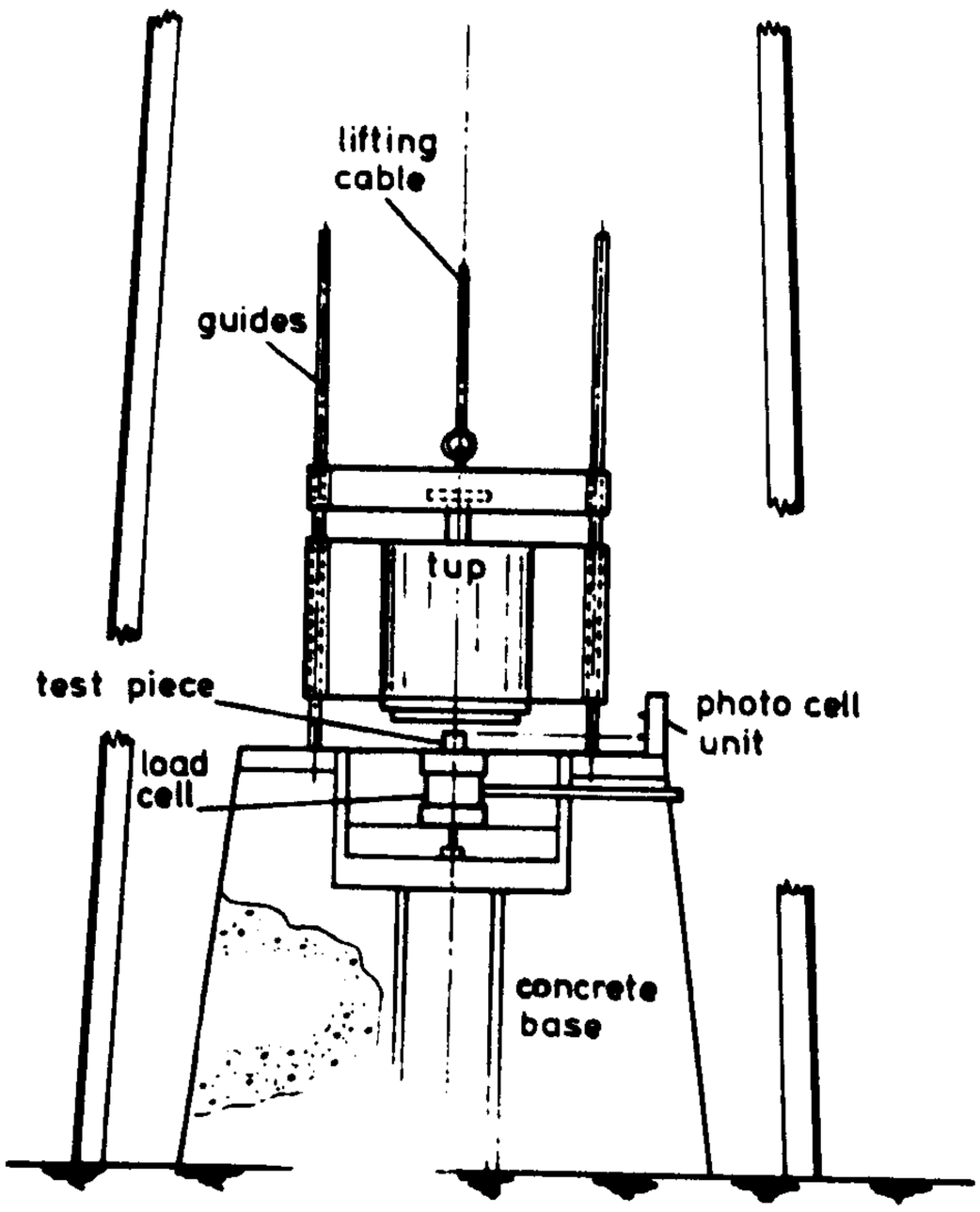

Fig.1. Schematic diagram showing the loading arrangement of the billet.

The lead billets were annealed in boiling water for 30 minutes while the aluminium alloy billets were annealed at 350°C for 15 minutes in an oven before testing.

RESULTS AND DISCUSSIONS

Experimental results were obtained from tests carried out on lead and aluminium alloy billets under lubricated and dry frictional conditions. In all cases the tup weighing 35.5 lbf was allowed to fall freely on to the billet from a height of 15 ft. Experimentally measured tup velocity was found to be 30 ft/sec.

The load-time variation was obtained from the tracings recorded in the oscilloscope. A typical photograph of such a trace for aluminium billet is shown in Fig.2. The distinct kink in the shape of the trace was present in every test with aluminium alloy billets.

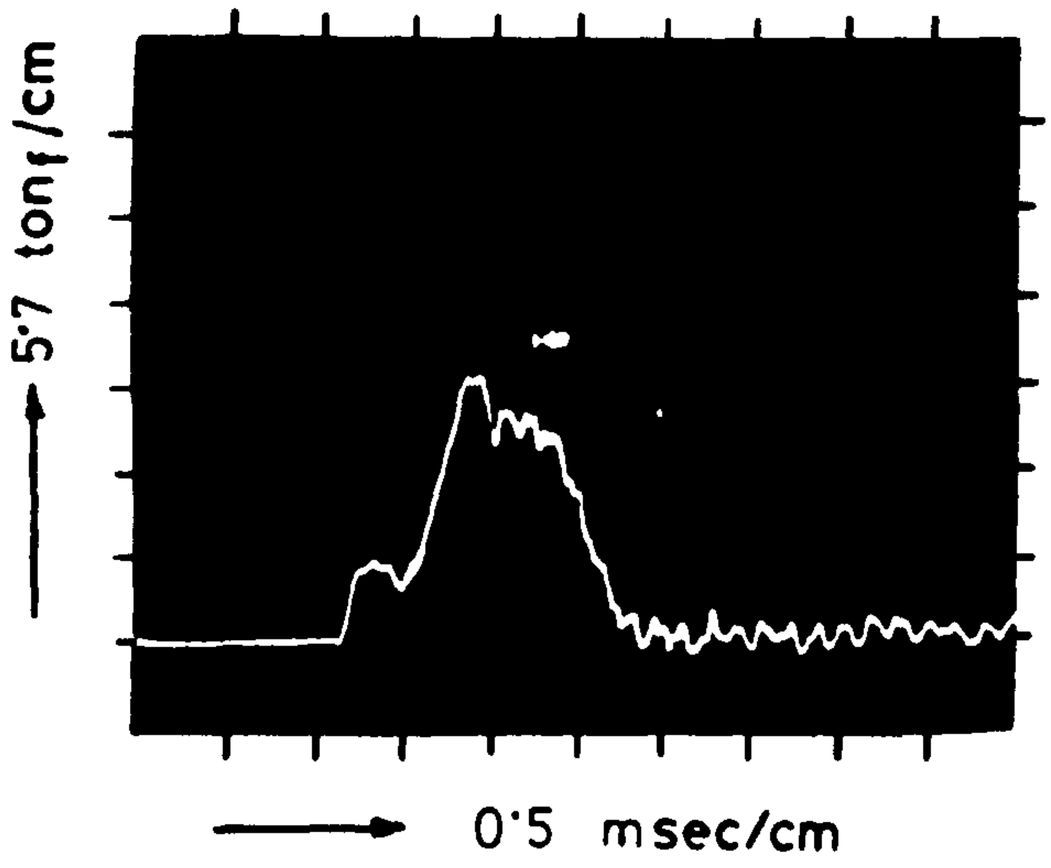

Fig.2. Photograph showing a typical load-time trace for aluminium billet.

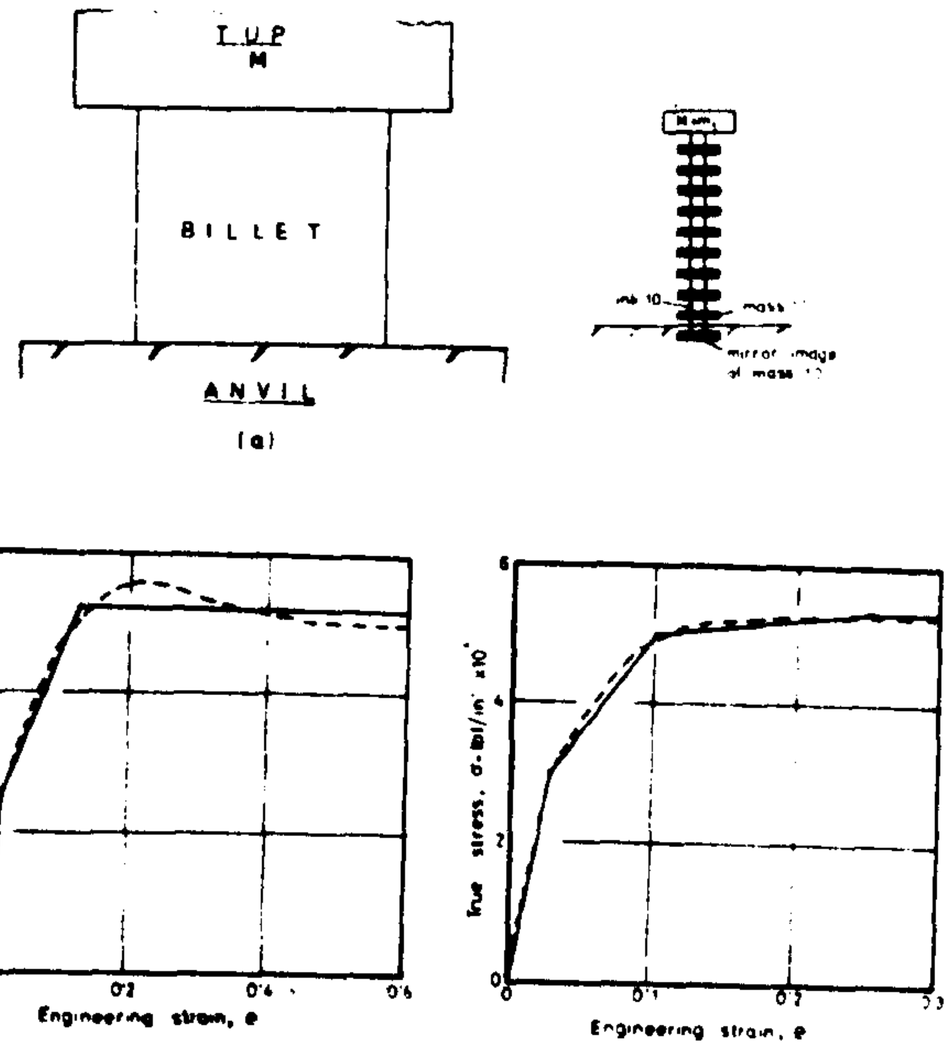

Fig.3a. Actual loading configuration and the corresponding numerical model.

b. Stress-strain characteristics for lead and

c. Stress-strain characteristics for aluminium

Analyses were undertaken for lead and aluminium alloy billets, each loaded under lubricated and dry conditions. The results predicted were then compared with those obtained experimentally. For the lubricated test condition where a paste of graphite in petroleum jelly was used as lubricant, it was assumed in the analysis that a constant frictional coefficient $\mu = 0.06$ existed for both lead and aluminium billets. This value of μ was thought to be a reasonable estimate of what graphite in petroleum jelly would induce. No attempt was made to actually determine frictional coefficient. For dry test conditions the value for $\mu = 0.577$ was incorporated in the analysis for lead billets (15) while for aluminium billets $\mu = 0.18$ was used (14).

The actual loading configuration and its equivalent numerical model, applied to both the lead and aluminium billets, is shown in Fig.3(a). The quasi-statically obtained stress-strain characteristics and their polygonal approximation, as required by the numerical technique, for lead and aluminium used in this study are shown in Fig.3(b) and (c) respectively.

The instantaneous profiles of a lead billet, obtained using high speed photographs, at various instants of time after the onset of the process are shown in Fig.4(a). This test was carried out under lubricated conditions. It is seen that the billet deforms in a manner such that the profile shape remains right cylindrical throughout the deformation process. The theoretically predicted instantaneous profiles for the same billet are shown in Fig.4(b) which shows profile shapes having either upwards or downwards directed slightly tapered sides. Slight barrelling also becomes apparent in the profiles corresponding to higher reductions in billet height.

The instantaneous profiles shown in Fig. 5(a) for a lead billet deformed under dry condition are seen to compare reasonably well with those in Fig.5(b), predicted using a numerical technique. The die load obtained experimentally was plotted in Fig.6(a) and (b) against reduction in billet height measured off the high speed photographs for lead and aluminium billets respectively, both tests carried out under lubricated condition. The theoretically predicted curves are also included in the respective figures for comparisons. It can be seen that for the lead billet a much lower die load is predicted; less than 50% for 60% reduction in billet height. On the other hand the die load predicted for the aluminium alloy billet is comparable with those obtained experimentally, being slightly higher during the initial part of the deformation and slightly lower thereafter.

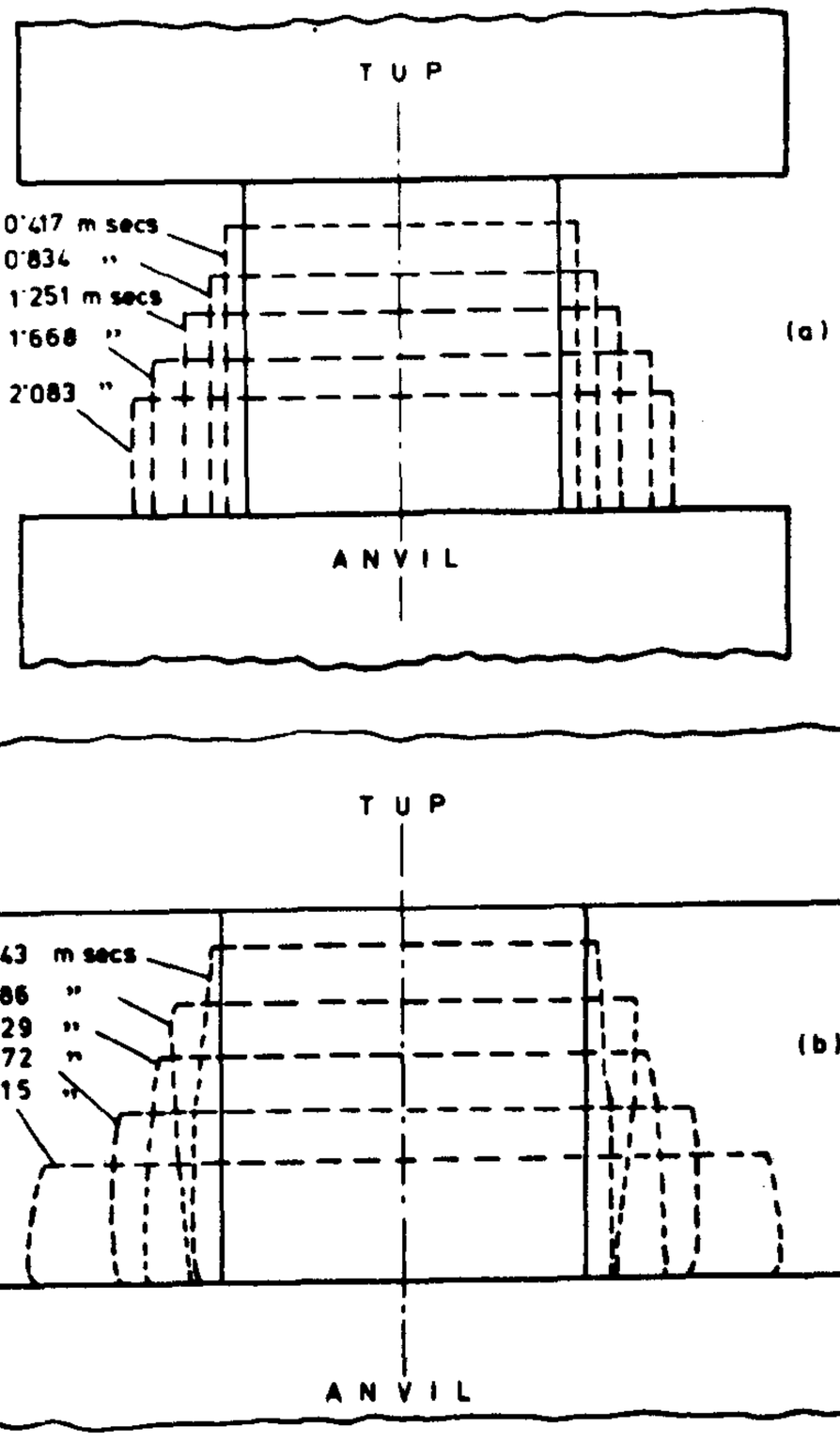

Fig.4a. Showing the instantaneous profiles of a lead billet deformed under lubricated test condition, and

b. Corresponding instantaneous profiles predicted theoretically.

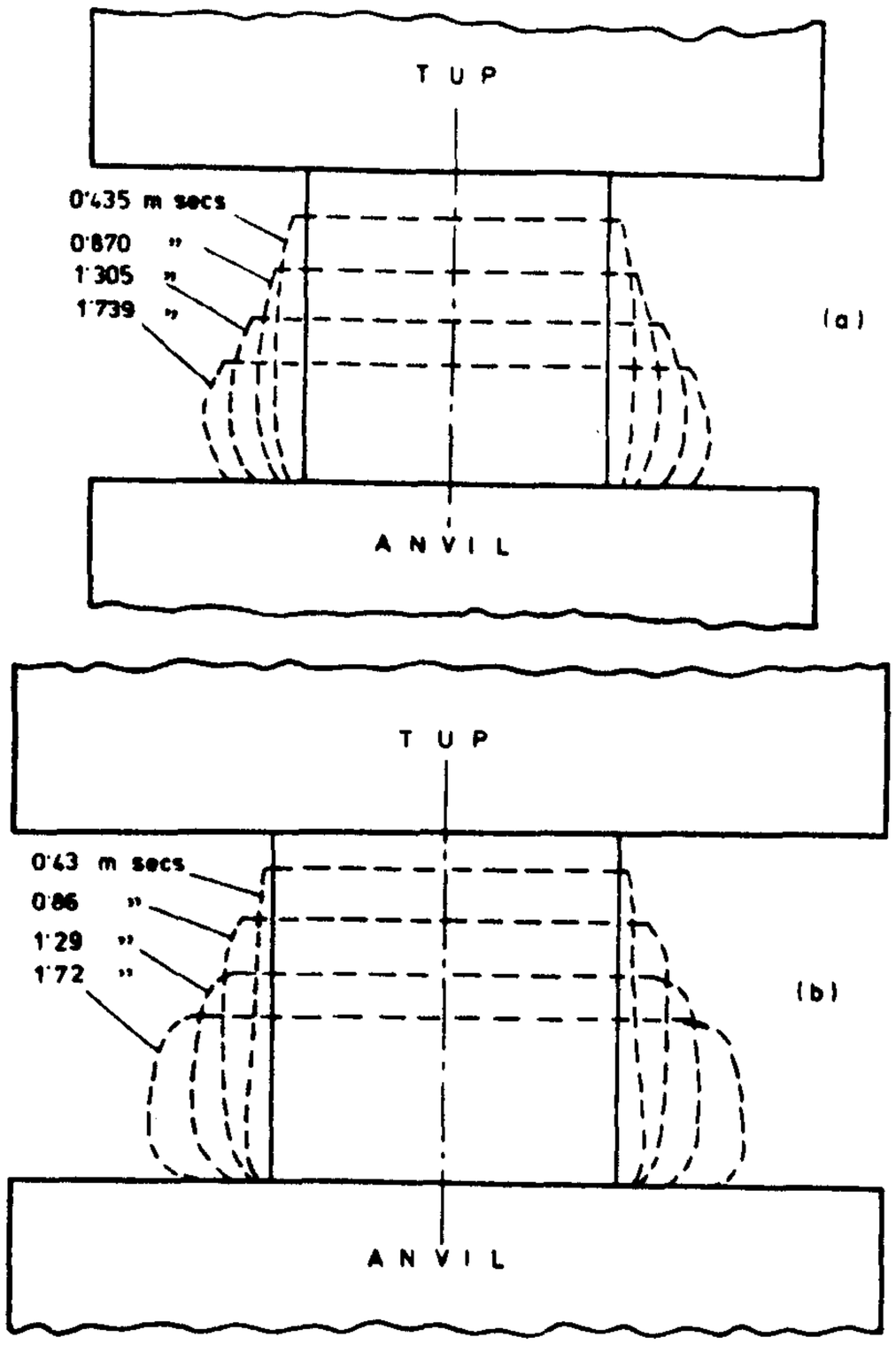

Fig.5a. Showing the instantaneous profiles of a lead billet deformed under dry test condition, and

b. Corresponding instantaneous profiles predicted theoretically.

The prediction of a much lower die load for lead billets points out the inadequacy of the present technique when applied to strain rate sensitive material. For a non strain rate sensitive material this method provides a satisfactory means of predicting load deformation characteristics. In order to compare the effect of end friction the die load /deformation curves obtained experimentally for aluminium billets under lubricated and dry test conditions are plotted in Fig.7. The corresponding predicted curves are also shown in this figure. It is seen that a maximum increase in die load of less than 10% occurs for reductions of billet height of up to 16%. The increase in die load due to friction as predicted using the numerical technique is slightly less than that obtained experimentally.

The increase in friction, when the billet is deformed under dry test conditions, results in increased barrelling of the billet. Fig.8. shows the increase in radii at mid and top section of the aluminum billet. The extent

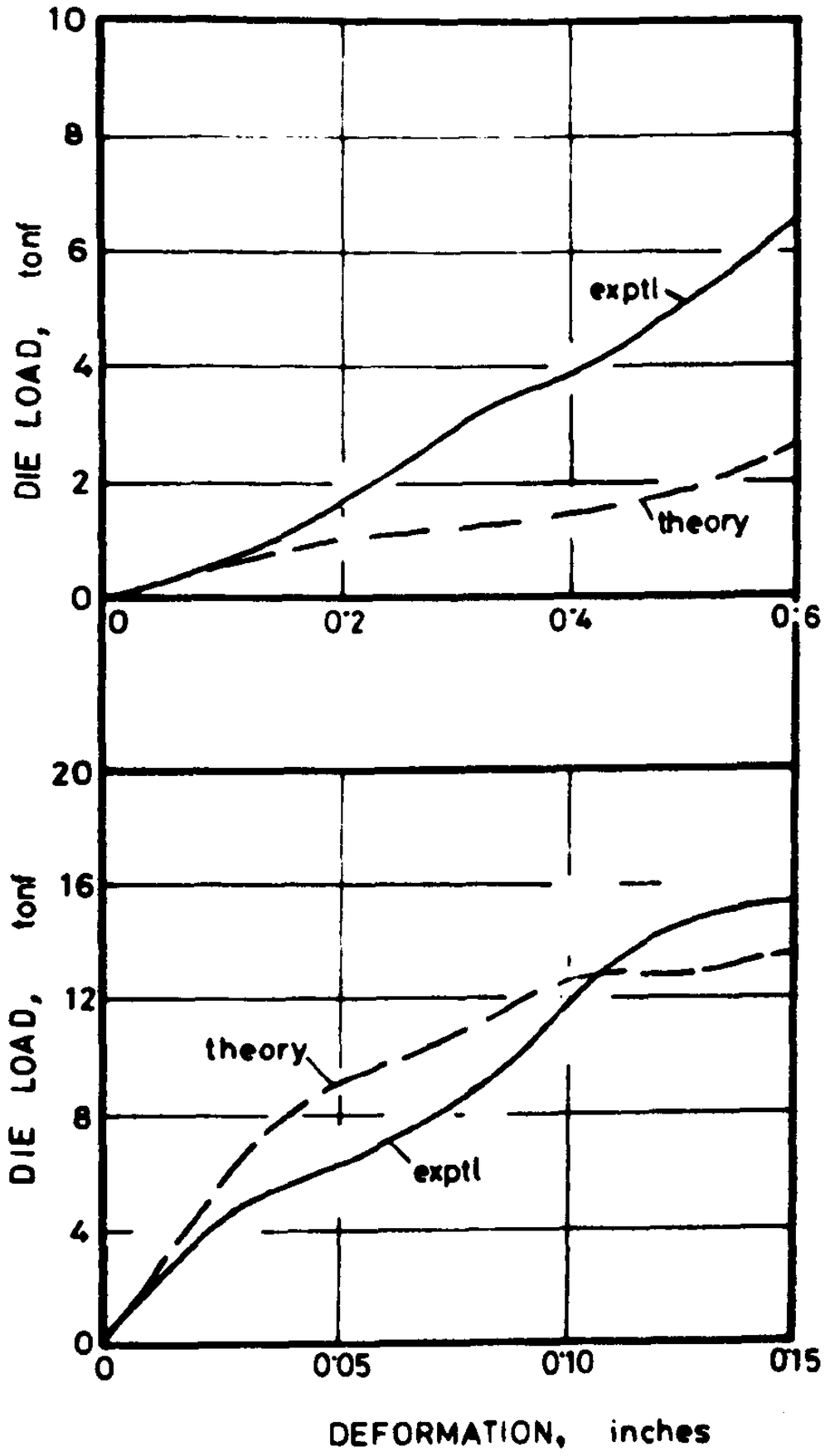

Fig.6. Variation in die load with deformation obtained experimentally and predicted theoretically for (a) lead and (b) aluminium billets deformed under lubricated test condition.

of barrelling can easily be estimated from this figure. The theoretically predicted results suggest slightly less barrelling of the billet.

Tup displacement-time curves were obtained using high speed photographs which upon graphical differentiation gave velocity-time curve and hence kinetic energy of the tup still unused at any time instant during the deformation process.

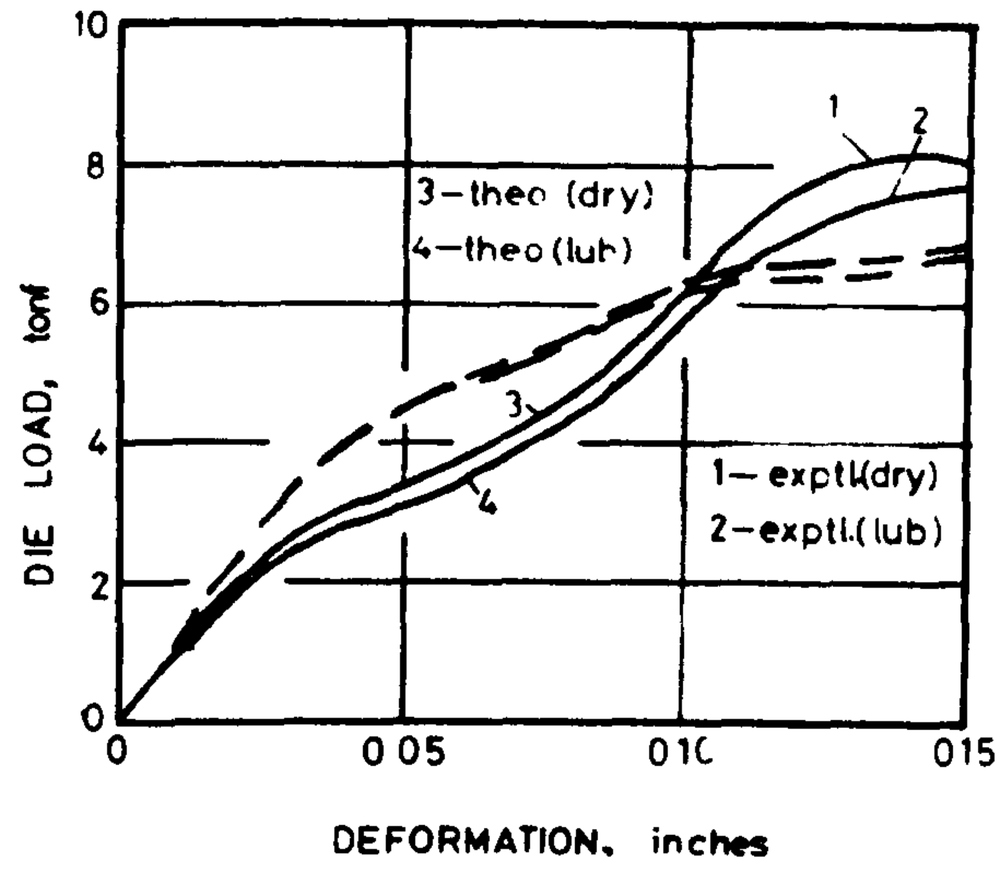

Fig.7. Comparing die load vs. deformation curves for aluminium billet deformed under lubricated and dry test conditions.

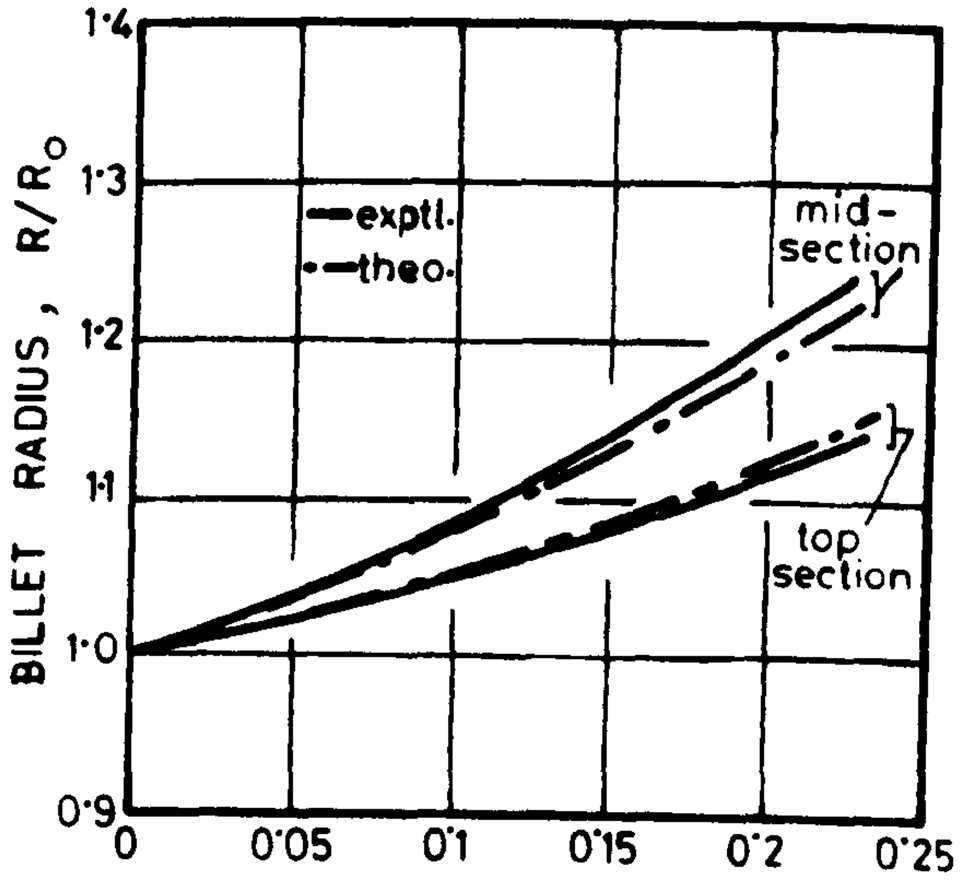

Fig.8. Showing the increase in radius at mid and top section with deformation for aluminium billet under dry test condition.

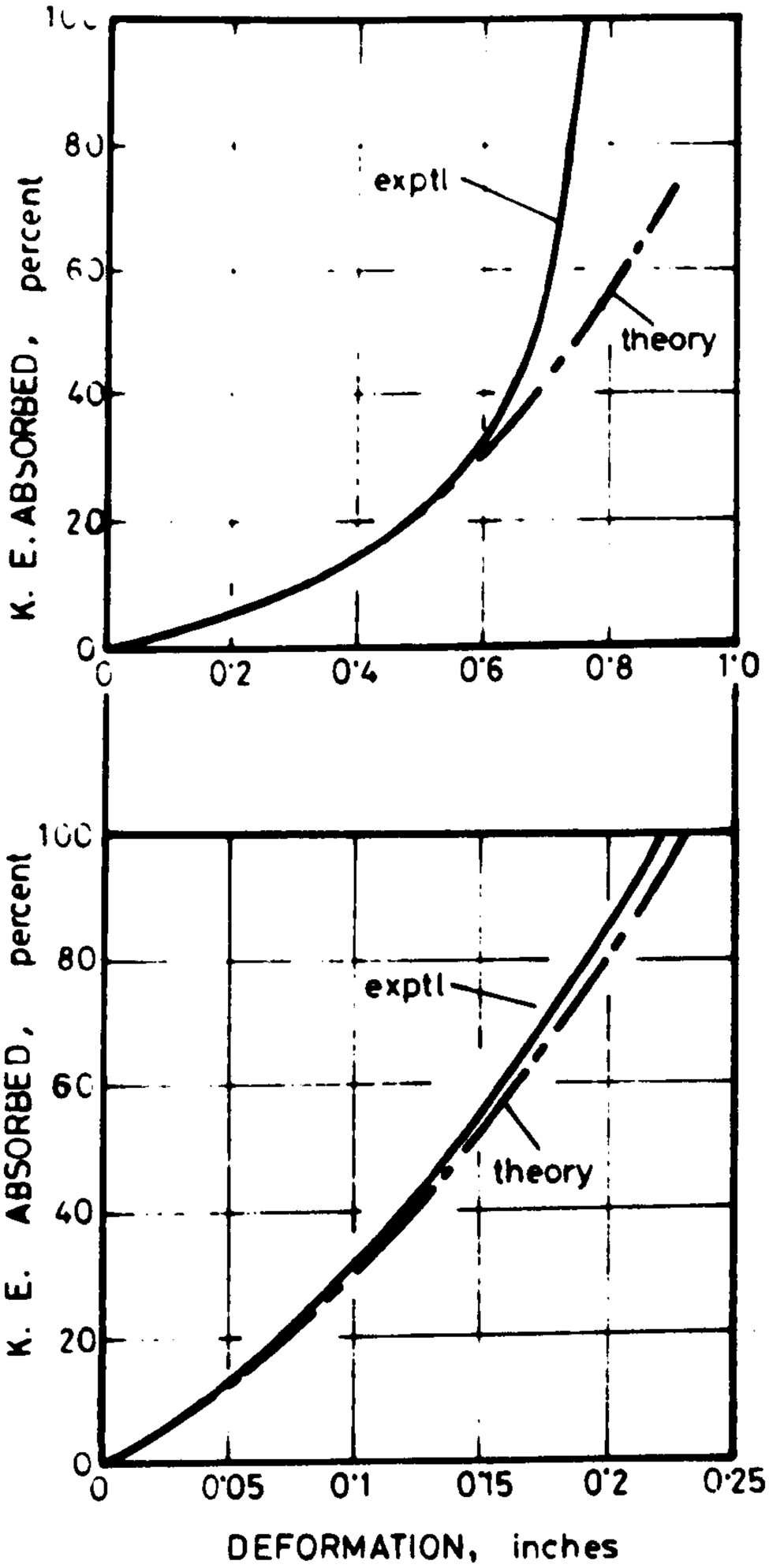

Fig.9. Percent kinetic energy absorbed vs. deformation curves for (a) lead and (b) aluminium billets deformed under lubricated test condition.

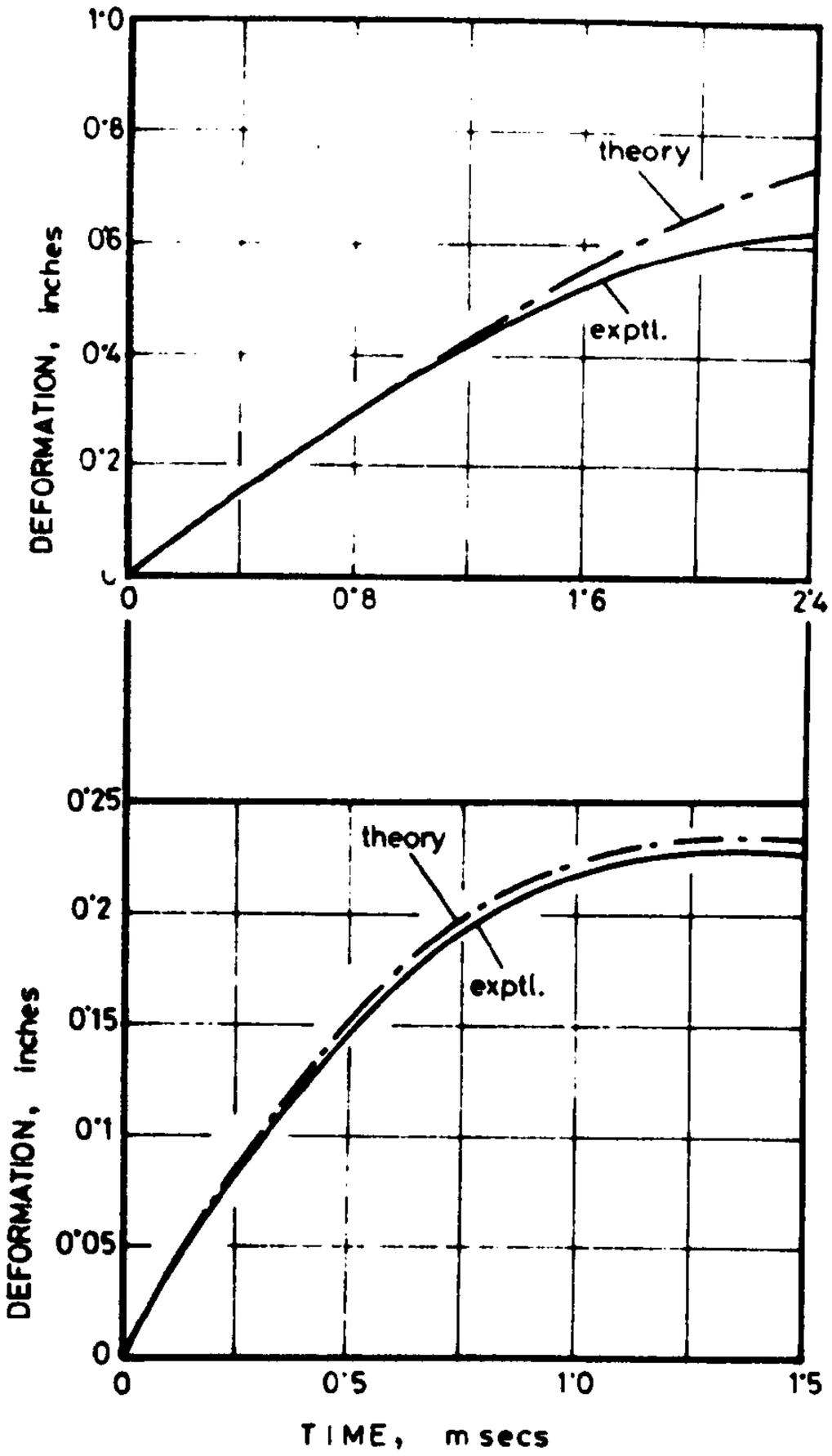

Fig.10. Showing variation in billet height during the in process time for (a) lead and (b) alum inium billets under lubricated test conditions.

Fig.9. shows the variation in percentage kinetic energy absorbed with deformation for (a) lead and (b) aluminium alloy billets both deformed under lubricated test conditions. Tht theoretical curve for the lead billet shows much less energy is required when more than 55%reduction in height is obtained. This is again a gross underestimation of the actual energy requirement. The analysis, by neglecting strain rate sensitivity, assumes low resistance of the billet to deformation and hence predicts less energy requirement for deformation. On the other hand, it is evident from Fig. 9(b), which shows similar kinetic energy vs. deformation curves for the aluminium alloy billet, that there is close agreement between the experimental results of predictions obtained theoretically.

Finally, the deformation vs. time curves for lead and aluminium alloy billets deformed under lubricated test conditions are shown in Fig.10(a) and (b) respectively.

It is seen that the experimental and theoretical correlation is very good for lead billets for up to 55% deformation. For aluminium billet close agreement exists during the whole of the deformation process.

CONCLUSIONS

Experiments were carried out on lead and aluminium alloy billets under a free falling tup. Results obtained from die load measurement and high speed photographs were compared with those predicted using numerical technique outlined in reference (1).

It was shown that the technique is inadequate for predicting load and energy requirements for deforming lead billets, but provide satisfactory predictions for aluminium alloy billets. It is suggested that neglect of strain rate sensitivity in the analysis caused the discrepancy in the results for lead billets.

ACKNOWLEDGEMENTS

The authors gratefully acknowledge the assistance given by Messrs.D.McKay, A.Fletcher and R.M.Wilkinson of the Department of Mechanical and Production Engineering for making, commissioning and instrumenting the drop hammer unit and preparing test specimens. They also express their thanks to Mr.P. Fischer of Visual Aids Unit for his help with high speed photography and reproduction of diagrams. Thanks are also due to Miss J.M.Webster for typing the manuscript.

REFERENCES

1. M.S.J.HASHMI and F.B.KLEMZ (1976). The effect of friction in simple upsetting of cylindrical billets of elastic-plastic and elastic-strain hardening material: A numerical technique. Proc.17th Int.MTDR Conf. p-597

2. J.F. ALDER and K.A.PHILIPS (1954). The effect of strain-rate and temperature on the resistance of aluminium, copper and steel to compression. J.Inst.Metals, 83, p.80.

3. P.M.COOK, (1957). True stress-strain curves for steel compression at high temperature and strain rates. Proc.Conf.Prop at high rates of strain, Inst.Mech.Engrs. Paper 2.

4. L.E.MALVERN, (1965). Experimental Studies of strain rate effects and plastic wave propogation in annealed aluminium. Proc.ASME Coll. on Behaviour of materials under dynamic loading. p-81.

5. R.A.C.SLATER, S.Y.AKU and W.JOHNSON (1968). Experiments in the fast upsetting of short pure lead cylinders and a tentative analysis. Int.J.Mech.Sci. vol 10, p-143.

6. S.K.SAMANTA (1968). Resistance to dynamic compression of low carbon steel and alloy steels at elevated temperatures and at high strain rates. Int.J.Mech.Sci. vol.10. p-613.

7. H.SUZUKI, et al (1968). Studies on the flow stress of metals and alloys, Report.Institute of Industrial Science, University of Tokyo. Vol.18 No.3.

8. S.K.SAMANTA (1969). On relating the flow stress of aluminium and copper to strain, strain-rate and temperature. Int.J.Mech.Sci.vol. 11, p-433.

9. S.K.SAMANTA (1970). The dynamic compression testing of steels at elevated temperatures. Proc.11th Int.MTDR Conf. p-827.

10. C.E.N.STURGESS and A.N.BRAMLEY. (1970). The use of impact-forming device to obtain dynamic stress-strain data. Proc.11th Int.MTDR. Conf. p-803.

11. B.LENGYEL and M.MOHITPUR (1972) Dynamic stress-strain data to large strains, J.Inst.Metals. 100

12. M.MOHITPUR and B.LENGYEL (1975) A method of obtaining isothermal, constant high strain rate stress-strain data, Proc.16th Int.MTDR Conf. p-503.

13. G.L.BARAYA, W.JOHNSON and R.A.C. SLATER. (1965). The dynamic compression of circular cylinders of superpure aluminium at elevated temperatures. Int.J.Mech.Sci. Vol.7. p-621.

14. A.T.MALE and M.G.COCKROFT (1964) A method for determination of the coefficient of friction of metals under conditions of bulk plastic deformation. J.Inst. of Metals. Vol.93. p-38.

15. S.C.JAIN and A.N.BRAMLEY. (1968) Speed and frictional effects in hot forging. Proc.Instn.of Mech.Engrs. Vol.182 p-783.

16. T.A.DEAN (1970). The influence of billet inertia and die friction in forging processes - A simple energy approach. 11th Int.MTDR.Conf. p-761

A5.15

CLOSED DIE FORGING OF AXISYMMETRIC SHAPES FROM CYLINDRICAL BILLETS OF STRAIN HARDENING AND STRAIN RATE SENSITIVE MATERIAL: EXPERIMENTAL RESULTS AND THEORETICAL PREDICTIONS

M. S. J. HASHMI and F. B. KLEMZ
Department of Mechanical and Production Engineering, Sheffield City Polytechnic

SUMMARY

Cylindrical lead billets were forged into axisymmetric shapes using dry and lubricated closed dies under a laboratory drop hammer. The experimental results were compared with those predicted theoretically using a numerical technique previously presented by the authors in references (17, 18). In this numerical technique the elastic strain hardening plastic and strain rate sensitive material property of the billet was incorporated. Effects of material inertia and die-billet interface friction on the tup load and product shape were also taken into account.

INTRODUCTION

In recent years a great deal of experimental and theoretical work has been carried out to investigate various aspects of high-energy rate forming in general and closed die forging and simple upsetting processes in particular. Published literature on the subject shows that most of the experimental studies were aimed at establishing dynamic stress-strain characteristics (1 - 12). Some other studies have been carried out putting forward analytical methods for predicting load-deformation behaviour and other aspects in simple upsetting and closed die forging incorporating, in some cases the effects of friction, material inertia and flash (13 - 16). However, almost all of these analyses involved very cumbersome and lengthy derivation in some approximate form.

In references (17, 18) the authors presented a finite-difference numerical technique for predicting load and deformation behaviour in simple upsetting of elastic-strain hardening plastic and strain rate sensitive material. The effects of material inertia and interface friction were also incorporated. In this study experiments were carried out under a laboratory drop hammer, forging cylindrical lead billets into simple axisymmetric shapes using dry and lubricated closed dies. The forging load initial impact velocity and tup-displacement were measured experimentally. The above mentioned numerical technique was then used to theoretically predict the deformation behaviour of the billet incorporating material inertia, strain rate sensitivity and die-billet interface friction. These predicted results were compared with those obtained experimentally. The detailed description of the numerical technique has previously been given in references (17, 18) and hence will not be repeated in this paper.

EXPERIMENTAL EQUIPMENT AND PROCEDURE

Initially, simple upsetting tests were carried out to establish the dynamic stress-strain properties of the lead under consideration. It was found that the lead showed considerable strain hardening effect for strain rates between about 1 to 500 per second, the quasi-statically obtained stress-strain curve showed no such strain hardening effect. Similar observations were also made in reference (4) for pure lead.

These experimentally determined dynamic stress-strain curves were found to fit closely the strain rate sensitivity equation $\sigma = \sigma_1[1 + (\frac{\dot{e} - \dot{e}_1}{D})^{1/p}]$ where σ is the dynamic flow stress corresponding to strain rates, $\dot{e}$ of up to 500 per second and σ_1 is the flow stress corresponding to strain rate $\dot{e}_1$ equal to 1 per second. The constants of strain rate sensitivity D and p were found to be 100 s^{-1} and 0.65 respectively. These experimentally established static and dynamic stress-strain curves are shown in Fig 1.

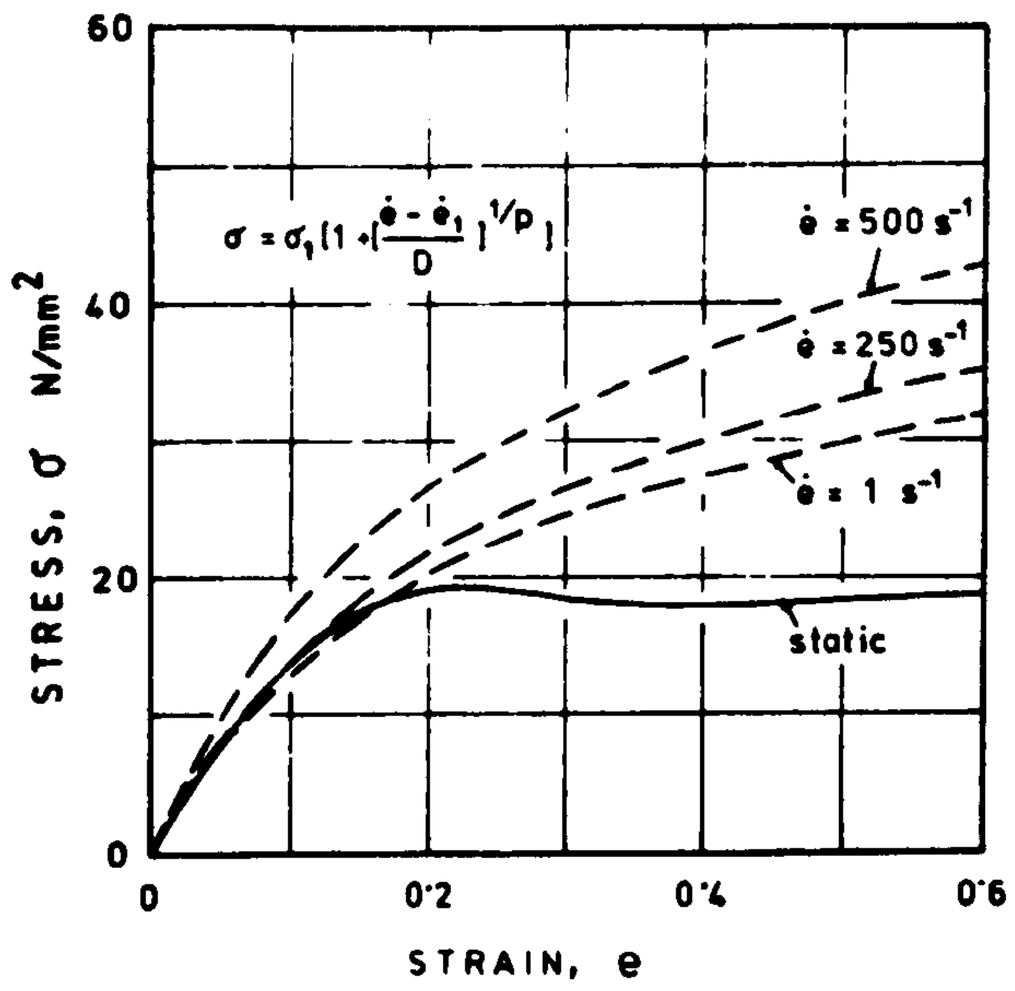

Fig 1 Static and dynamic stress-strain curves for commercially pure lead.

Commercially pure lead cylindrical billets, 24 mm in diameter and 46 mm in height, were forged into axisymmetric shape as shown in Fig 2, using a laboratory drophammer. The schematic diagram in Fig 3 shows the loading arrangement of the billet under the drop hammer. The die-billet assembly was placed on top of the "strain gauge incorporated" tool steel load-cell and the load time trace was recorded using transient recorder CRO and/or a X - Y graph plotter. The tup velocity just before impact and the tup displacement time trace were also recorded simultaneously using transient recorder, photo-cell unit and electronic counters.

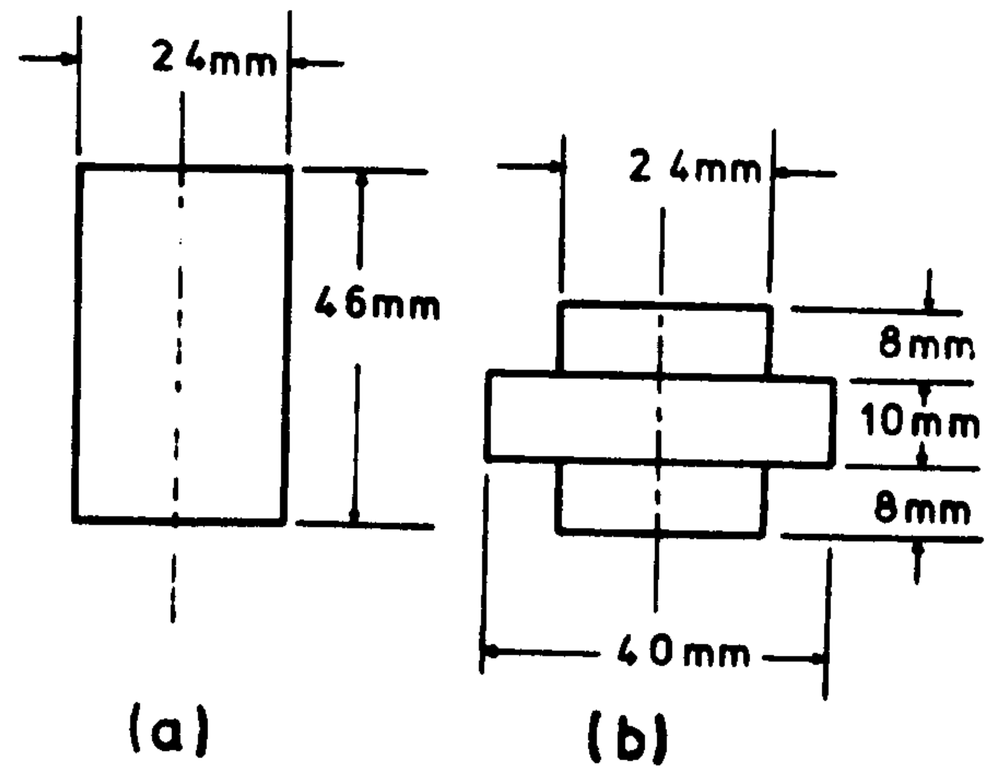

Fig 2 Showing (a) cylindrical lead billet and (b) final deformed shape.

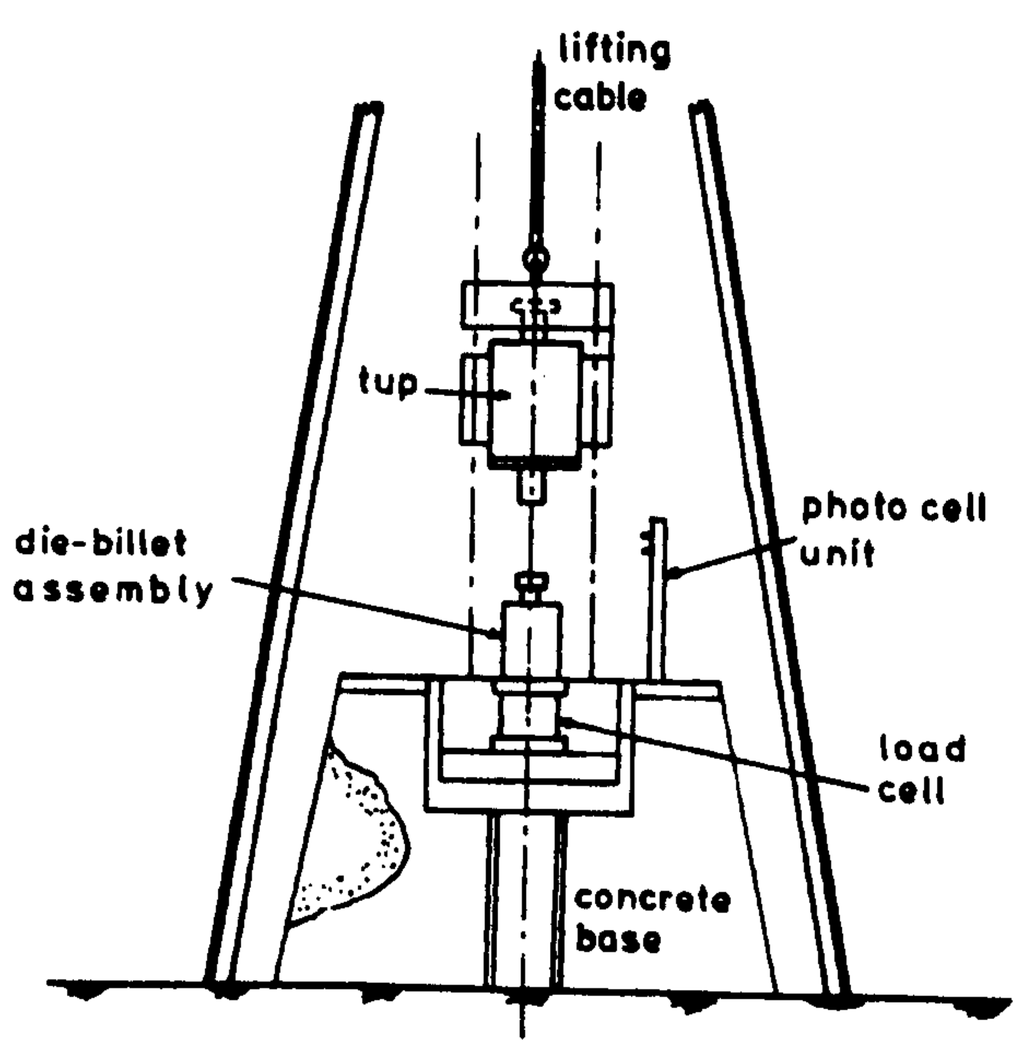

Fig 3 Schematic diagram showing the loading arrangement under the drop hammer.

RESULTS AND DISCUSSION

Experimental results were obtained from forging tests carried out on lead billets under lubricated and dry friction conditions. In both cases the tup of mass 17 Kg was allowed to fall freely on top of the die-billet assembly giving equivalent impact velocity of 9 m/s.

Analysis was undertaken for each loading situation using the numerical technique described in references (17, 18). The stress-strain properties depicted in Fig 1 were incorporated into the analysis. The effects of material inertia and interface friction at the die-billet constraint were also taken into account. The die-load, instantaneous billet profiles, die pressure and strain rate within the billet were predicted theoretically and compared with experimental results where appropriate.

The actual loading configuration of the billet is shown in Fig 4 (a) and the equivalent numerical model is shown in Fig 4 (b). The instantaneous profiles of the billet were predicted theoretically for both the lubricated and dry friction forging conditions. In the analysis, the friction factor for dry friction condition was taken as unity whilst for lubricated condition it was taken as zero along any die-billet interface. For shearing friction within the billet at the die-billet constraint the friction factor was again taken as unity rendering sticking friction. Fig 5 (a) shows theoretically predicted instantaneous profiles at various times during the deformation process for a billet forged under lubricated condition. The instantaneous profiles for a billet forged under dry friction conditions are shown in Fig 5 (b). It was not possible to record the experimental instantaneous profiles due to the nature of the forming process. Therefore, only the corresponding experimentally obtained final profiles are shown in these figures. It is clearly evident that forging under dry friction condition gives rise to considerable barrelling of the billet during the deformation process. This causes the billet material to get into the flash land relatively earlier than under lubricated forging condition.

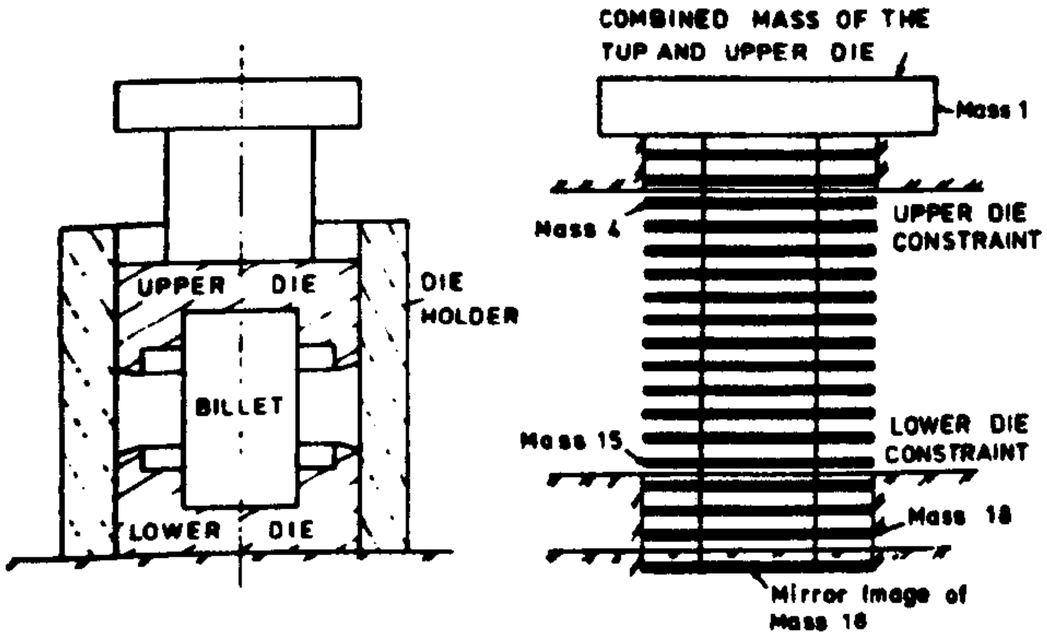

Fig 4 Showing (a) actual loading configuration of the billet and (b) corresponding equivalent numerical model.

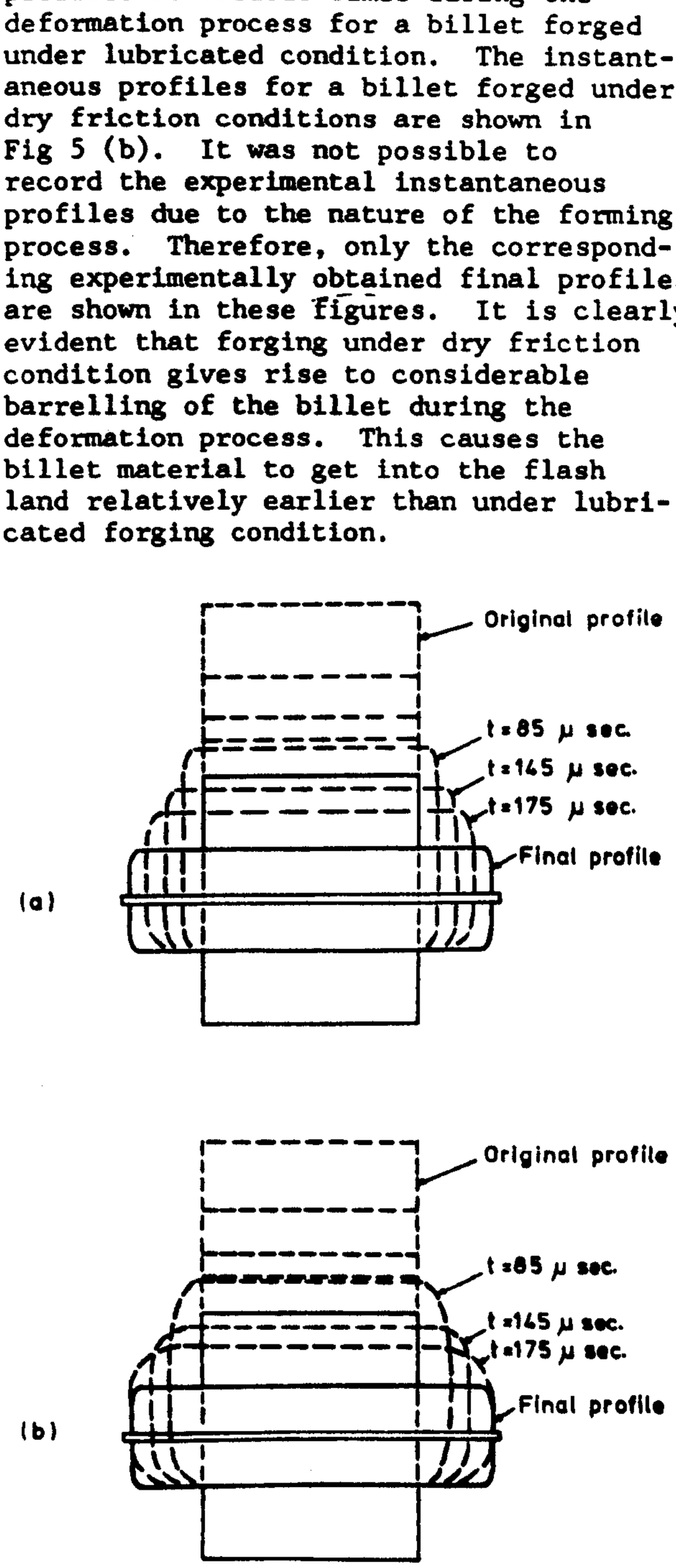

Fig 5 Theoretically predicted instantaneous profiles under (a) lubricated and (b) dry friction condition.

In Fig 6 the variations in forging loads with tup displacement measured experimentally are compared with those predicted theoretically for forging under lubricated and dry friction condition. The effects of strain rate and material inertia on the forging load was found to be significant when the experimentally established dynamic stress-strain properties shown in Fig 3 were incorporated in the analysis. The agreement between the theoretical and experimental forging load under both frictional conditions show close agreement. Fig 6 also shows quasi-static forging load under dry friction condition. This static load is seen to be considerably lower than both the experimental and theoretically predicted dynamic forging loads. This discrepancy may be explained by the apparent strain hardening of lead under consideration under dynamic loading conditions.

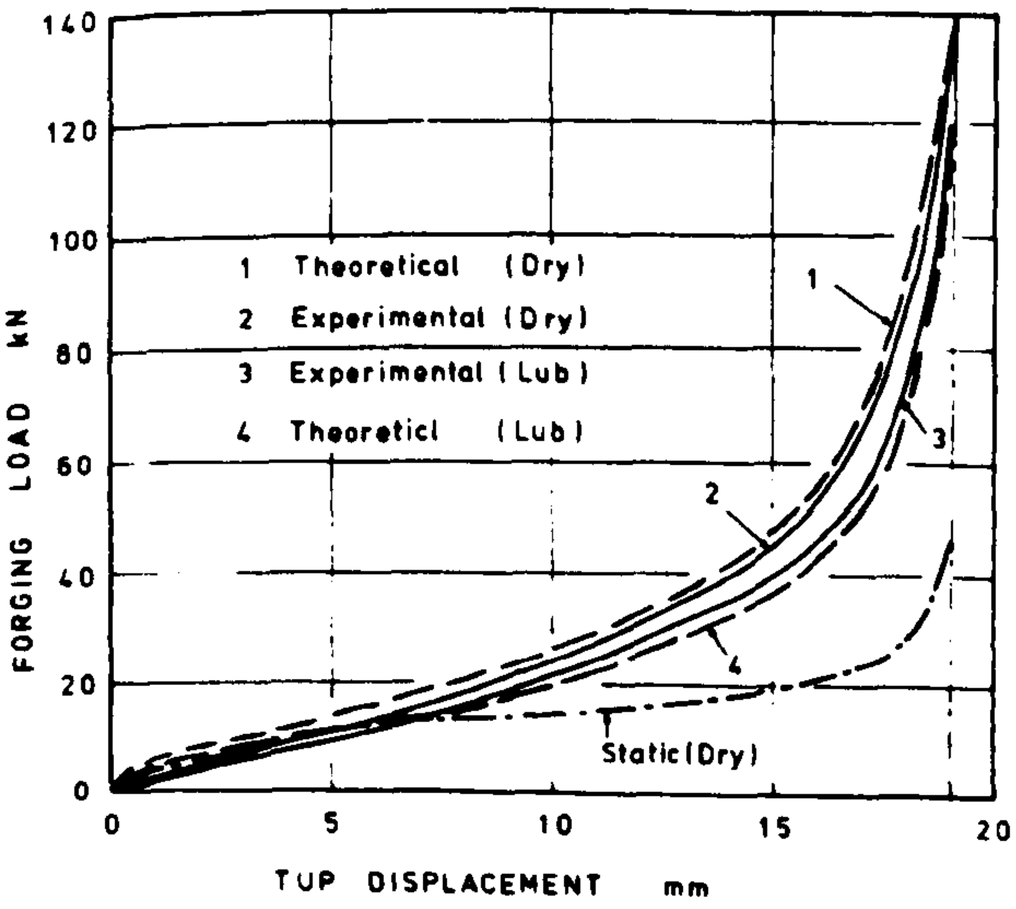

Fig 6 Comparison of experimental and theoretical forging load Vs tup-displacement curves.

The instantaneous profiles in Fig 5 (a) and (b) showed barrelling of the billet in a qualitative manner. In Fig 7 this is shown in a quantitative manner in terms of the variation in the billet radius at mid-section and at the die-billet constraints. It is clearly evident from this figure that forging under dry friction condition causes the billet radius at mid-span to increase at relatively faster rate with deformation than under lubricated forging condition. This may result in appreciable loss of material as flash.

The theoretically predicted variation in strain rate at mid-section and at the section along the die-billet constraint is shown in Fig 8 for lubricated and dry friction conditions. This figure shows that during most of the deformation process the maximum strain rate within

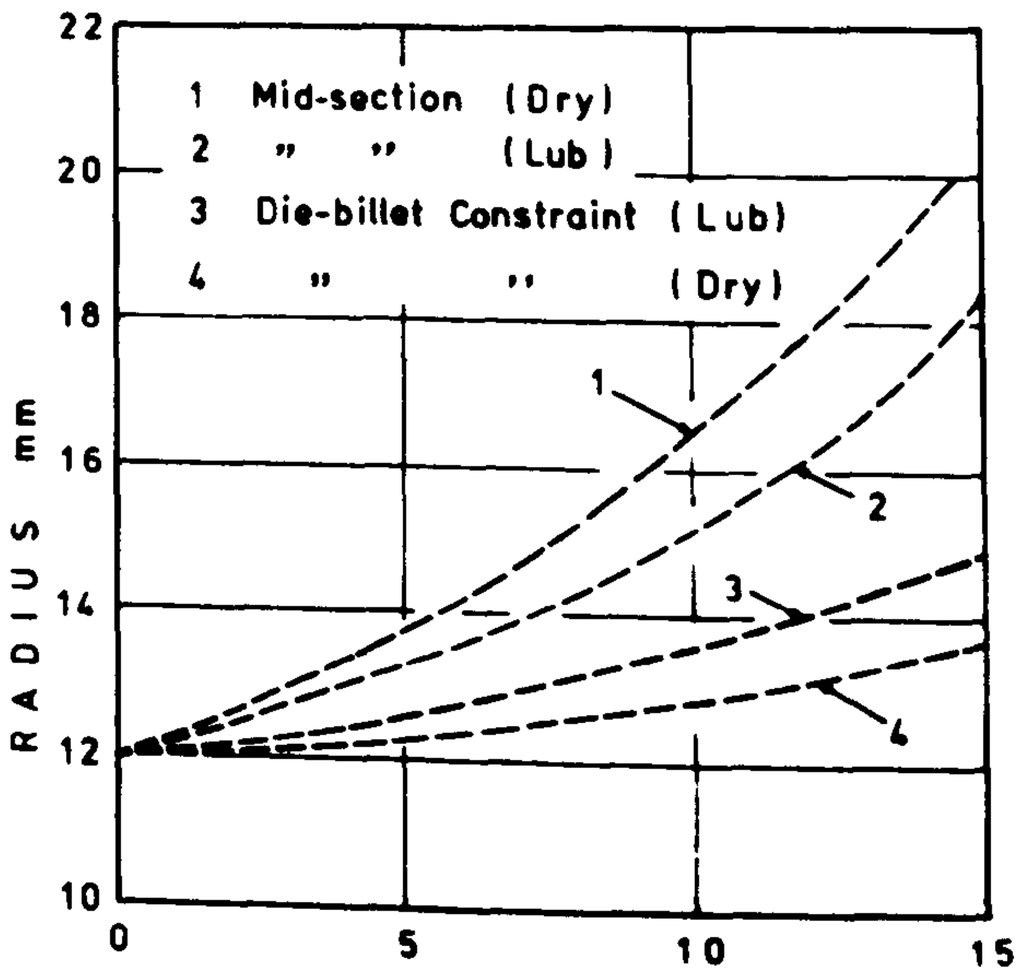

Fig 7 Variation in billet radius with tup-displacement at mid-section and die-billet constraint.

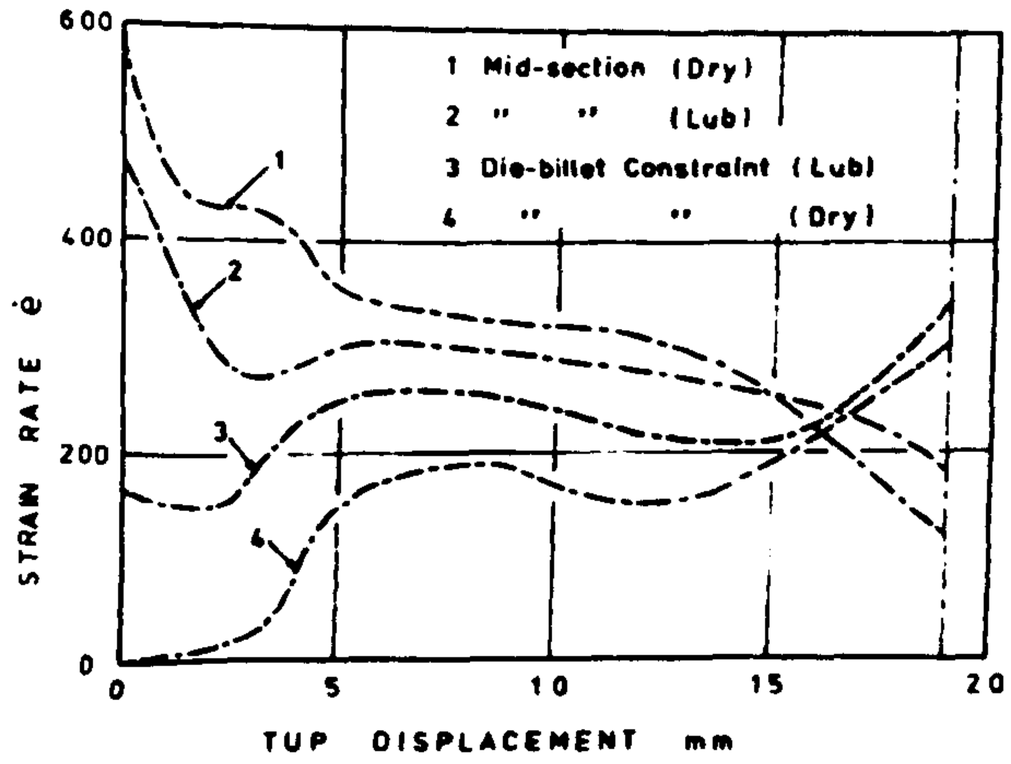

Fig 8 Variation in strain rate with tup-displacement at mid-section and die-billet constraint.

the billet remains below about 350 per second for impact velocity of 9 m/s and hence makes no appreciable difference in the forging load at later stages of deformation.

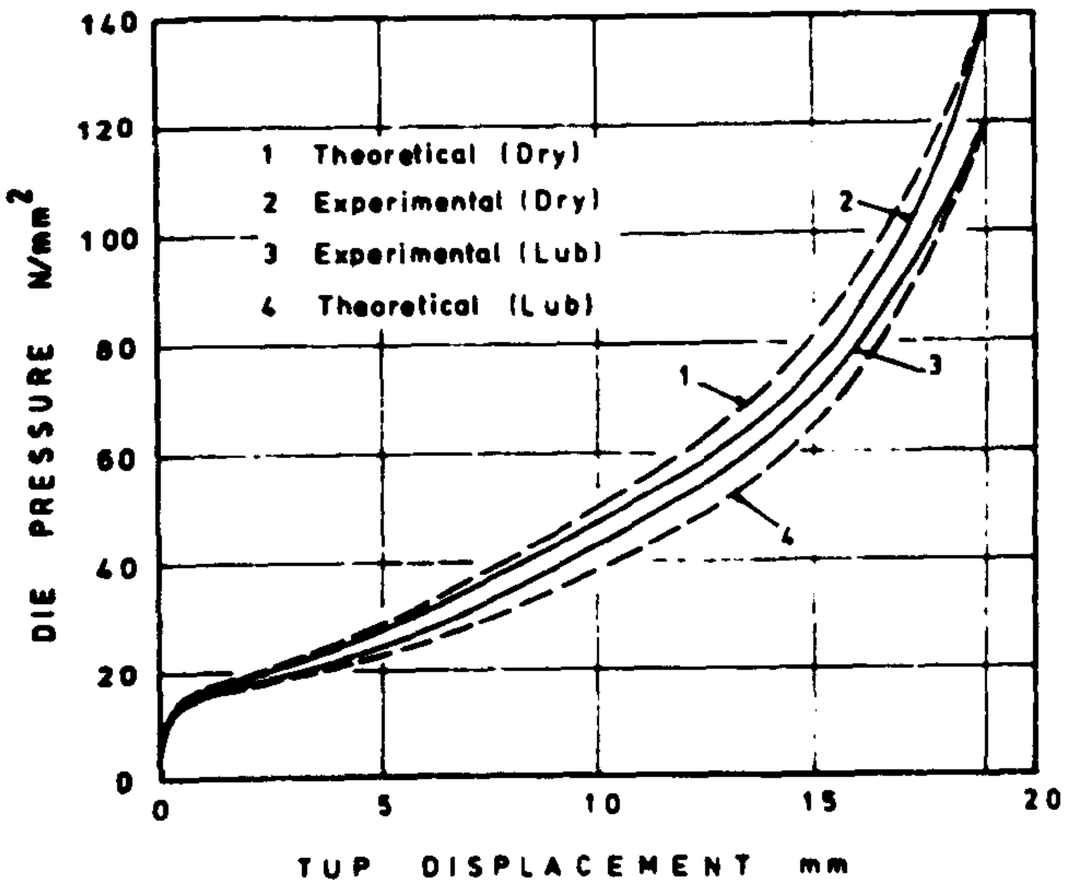

Fig 9 Showing die-pressure Vs tup-displacement curves predicted theoretically and obtained experimentally.

Finally, comparison of the theoretically estimated die pressures with those obtained experimentally as shown in Fig 9 shows close agreement under both forging conditons. It is evident, however, that in the case of dry friction, the theoretically predicted die pressure is slightly greater than that obtained experimentally whilst this trend is reversed in the case of lubricated forging condition. The main reason for this behaviour could be the fact that for dry friction condition the friction factor was taken as unity and for lubricated friction conditions its value was taken as zero in the theoretical calculations.

In actual forging situations it is most unlikely that these limiting frictional conditions were exactly the same, although great care was taken to meet these conditions as closely as possible. "Graphite in petroleum jelly" was used as lubricant for lubricated forging operations.

CONCLUSIONS

Cylindrical lead billets were forged into axisymmetric shapes using closed dies under dry friction and lubricated condition. Experimentally obtained forging loads were compared with those predicted theoretically using a numerical technique previously outlined in references (17, 18). The effects of material inertia and strain rate were incorporated into the analysis and the predicted results showed close agreement with those obtained experimentally.

REFERENCES

1. J.F. ALDER and K A PHILLIPS (1954). The effect of strain-rate and temperature on the resistance of aluminium, copper and steel to compression. J Inst Metals, 83, p 80.

2. P M COOK, (1957). True stress-strain curves for steel compression at high temperature and strain rates. Proc Conf Prop at high rates of strain, Inst Mech Engrs. Paper 2.

3. L E MALVERN, (1965). Experimental Studies of strain rate effects and plastic wave propogation in annealed aluminium. Proc ASME Coll on Behaviour of materials under dynamic loading. P-81.

4. R A C SLATER, S Y AKU and W JOHNSON (1968). Experiments in the fast upsetting of short pure lead cylinders and a tentative analysis. Int J Mech Sci Vol 10, p 143.

5. S K SAMANTA (1968). Resistance to dynamic compression of low carbon steel and alloy steels at elevated temperatures and at high strain rates. Int J Mech Sci, Vol 10, p 613.

6. H SUZUKI, et al (1968). Studies on the flow stress of metals and alloys, Report Institute of Industrial Science, University of Tokyo. Vol 18, No 3.

7. S K SAMANTA (1969). On relating the flow stress of aluminium and copper to strain, strain-rate and temperature. Int J Mech Sci, Vol 11, p 433.

8. S K SAMANTA (1970). The dynamic compression testing of steel at elevated temperatures. Proc 11th Int MTDR Conf, p 827.

9. C E N STURGESS and A N BRAMLEY (1970). The use of impact-forming device to obtain dynamic stress-strain data. Proc 11th Int MTDR Conf, p 803.

10. B LENGYEL and M MOHITPUR (1972). Dynamic stress-strain data to large strains. J Inst Metals, 100.

11. M MOHITPUR and B LENGYEL (1975). A method of obtaining isothermal, constant high strain rate stress-strain data, Proc 16th, Int MTDR Conf, p 503.

12. G L BARAYA, W JOHNSON and R A C SLATER. (1965). The dynamic compression of circular cylinders of super-pure aluminium at elevated temperatures. Int J Mech Sci, Vol 7 p 621.

13. S C JAIN and A N BRAMLEY, (1968). Speed and frictional effects in hot forging. Proc Instn of Mech Engrs, Vol 182, p 783.

14. T A DEAN (1970). The influence of billet inertia and die friction in forging processes - A simple energy approach. 11th Int MTDR Conf, p 761.

15. R P McDERMOTT and A N BRAMLEY (1974). An elemental upper-bound technique for general use in forging analysis. Proc 15th Int MTDR Conf, P 437.

16. T A DEAN (1976). The mechanics of flash in drop forging - temperature and speed effect. Proc Inst Mech Engrs, Vol 190-33/76, p 457.

17. M S J HASHMI and F R KLEMZ (1976). The effect of friction in simple upsetting of cylindrical billets of elastic-plastic and elastic-strain hardening material : A numerical technique. Proc 17th Int MTDR Conf, p 597.

18. M S J HASHMI (1977). A numerical technique for analysing simple upsetting of cylindrical billets of strain rate sensitive material. Proc 18th Int MTDR Conf, p 27.